Владимирский государственный университет

СОВРЕМЕННЫЕ НАНОТЕХНОЛОГИИ И НАНОФОТОНИКА ДЛЯ НАУКИ И ПРОИЗВОДСТВА

Материалы 6-й Международной конференции

9 – 13 ноября 2017

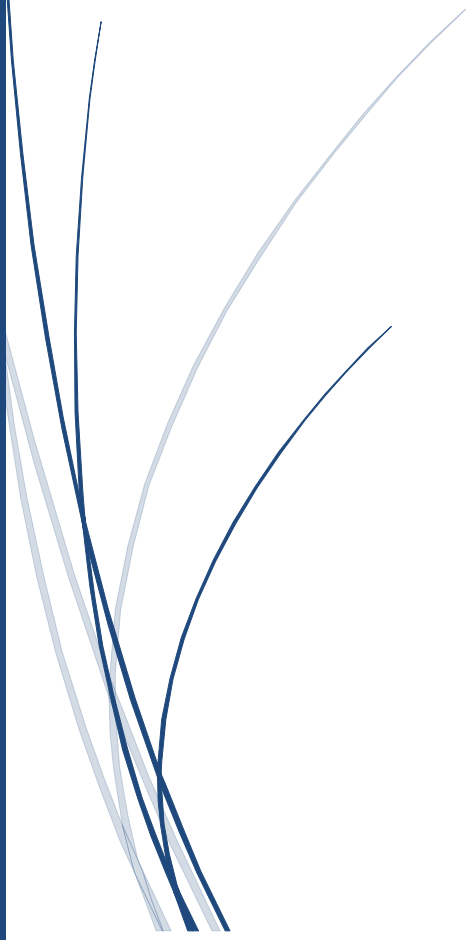

Владимир 2018

Министерство образования и науки Российской Федерации

Федеральное государственное бюджетное образовательное учреждение
высшего образования
«Владимирский государственный университет
имени Александра Григорьевича и Николая Григорьевича Столетовых»

СОВРЕМЕННЫЕ НАНОТЕХНОЛОГИИ И НАНОФОТОНИКА ДЛЯ НАУКИ И ПРОИЗВОДСТВА

Материалы 6-й Международной конференции

9 – 13 ноября 2017 г.,
г. Владимир – г. Суздаль

Электронное издание

Владимир 2018

ISBN 978-5-9984-0751-2

УДК 620.3
ББК 30.6

Издается по решению редакционно-издательского совета ВлГУ

Современные нанотехнологии и нанофотоника для науки и производства : материалы 6-й Междунар. конф. 9 – 13 нояб. 2017 г., г. Владимир – г. Суздаль [Электронный ресурс] / Владим. гос. ун-т им. А. Г. и Н. Г. Столетовых. – Владимир : Изд-во ВлГУ, 2018. – 177 с. – Систем. требования: Intel, AMD от 1,3 ГГц; Windows XP/Vista/7/8/10; Adobe Reader; CD-ROM; 6,5 Мб. – Загл. с титула экрана.

В сборник включены материалы международной конференции, которая состоялась 9 – 13 ноября 2017 года в г. Суздале при поддержке Министерства образования и науки Российской Федерации и Российского фонда фундаментальных исследований. Сборник содержит 62 статьи более 200 авторов на темы: источники терагерцового излучения и их применение, нелинейная оптика и спектроскопия, квантовая и атомная оптика, методы синтеза и диагностики наноматериалов и наноструктур, новые углеродные материалы и их применение, нанофотоника.

Представляет интерес для специалистов в области фотоники и лазерной техники.

УДК 620.3
ББК 30.6

ISBN 978-5-9984-0751-2

CONTENTS

Abstracts 9

PLENARY REPORTS 10

НОВЫЕ ГОРИЗОНТЫ ОПТИКИ СВЕРХКОРОТКИХ ИМПУЛЬСОВ СРЕДНЕГО ИНФРАКРАСНОГО ДИАПАЗОНА Valeriy I. Yudin, Alexey V. Taichenachev, ... 10

VERIFICATION OF THE QUANTUM DIMENSION EFFECTS IN ELECTRICAL CONDUCTIVITY WITH DIFFERENT TOPOLOGY OF LASER-INDUCED THIN-FILM STRUCTURES S. Arakelian, A. Kucherik, S. Kutrovskaya, A. Osipov, A. Istratov, and I. Skryabin 14

APPROACHING TO THE LIMIT OF SPASERS FROM SPP NANOLASERS Tien-Chang Lu*, Yu-Hsun Chou, Kuo-Bin Hong, and Chun-Tse Chang 15

NONLINEAR OPTICS AND SPECTROSCOPY 16

1. THE EFFECT OF MOLECULAR OSCILLATIONS ON ENERGY TRANSFER IN MACROMOLECULAR CHAIN SYSTEMS Chizhov A.V.[1,2], Čevizović D.[3], Galović S.[3] 16

2. TEMPERATURE DEPENDENCE OF TERAHERTZ OPTICAL PROPERTIES OF LBO AND PERSPECTIVES OF APPLICATIONS IN DOWN-CONVERTERS N. A. Nikolaev[1, 2], Yu. M. Andreev[3, 4], N. G. Kononova[5], G. V. Lanskii[3, 4], A. A. Mamrashev[1, 2], V. D. Antsygin[2], K. A. Kokh[5], A. E. Kokh[5] 18

3. ИССЛЕДОВАНИЕ НИЗКОТЕМПЕРАТУРНОЙ ОПТИЧЕСКОЙ ДЕФАЗИРОВКИ В АНСАМБЛЕ ПОЛУПРОВОДНИКОВЫХ КОЛЛОИДНЫХ КВАНТОВЫХ ТОЧЕК CDSE/CDS/ZNS МЕТОДОМ НЕКОГЕРЕНТНОГО ФОТОННОГО ЭХА К.Р. Каримуллин, А.И. Аржанов, А.В. Наумов 19

QUANTUM AND ATOMIC OPTICS 23

4. SPECTROSCOPY OF LASER-COOLED MAGNESIUM IN AN OPTICAL LATTICE N. Jha, S. Rühmann, D. Fim, K. Zipfel, S. Sauer, W. Friesen, W. Ertmer, and E. M. Rasel 23

5. ANALYTICAL SOLUTIONS FOR LIGHT EMISSION INTENSITIES FROM COOPERATIVE ENSEMBLES IN DIELECTRICS Maxim G. Gladush 25

6. HIGH EXTINCTION RATIO INTEGRATED OPTICAL MODULATOR FOR QUANTUM TELECOMMUNICATION SYSTEMS Alexander Tronev[1,2], Mikhail Parfenov[3], Peter Agruzov[1], Igor Ilichev[1] and Aleksandr Shamrai[1,2,3] 26

7. QUANTUM ANTENNAS: DESIGNING STATES FOR FIELD CORRELATIONS I. Karuseichyk[1], A. Mikhalychev[1], D. Mogilevtsev[1], G. Buchs[2], D. L. Boiko[2], G. Ya. Slepyan[3], A. Boag[3] 27

NANOPHOTONICS AND METAMATERIALS 32

8. PLASMONIC NANOLASER AND ITS APPLICATION Pavel Melentiev[1], Alexey Kalmykov[1,2], Anton Gritchenko[1,3], Anton Afanasyev[1], Victor Balykin[1], Alexander Baburin[3,4], Elena Ryzhova[3,4], Ivan Filippov[3,4], Ilya Rodionov[3,4], Igor Nechepurenko[3,5,6], Alexander Dorofeenko[3,5,6], Ilya Ryzhikov[3,5], Alexey Vinogradov[3,5,6] 32

9. THE DEVELOPMENT OF HYBRID PLASMONIC NANOSTRUCTURES FOR MEDICAL APPLICATION Alexey Povolotskiy[1], Anastasia Povolotckaia[2], Alexander Konev[1] 34

10. CHARACTERIZATION OF PATTERNED TEXTURE ON VERTICAL-CAVITY SURFACE-EMITTING LASERS Shen-Che Huang, Ming-Cheng Chen, Tsu-Chi Chang, Kuo-Bin Hong and Tien-Chang Lu 36

11. EFFECT OF ELASTIC DEFORMATION ON THE DISPERSION OF ELECTROMAGNETIC EXCITATIONS IN A CHAIN OF MICROCAVITIES Vladimir Rumyantsev[1], Stanislav Fedorov[1], Konstantin Gumennik[1], Oleksiy Roslyak[2] 37

12. MAGNETIC FIELD CONTROL OF THE POLARITON SPIN DYNAMICS E. S. Sedov,[1,2] A. V. Kavokin[3,2,4] 41

13. OPTICAL PROPERTIES OF β-BBO AND POTENTIAL FOR THZ APPLICATIONS N. A. Nikolaev[1, 2], Yu. M. Andreev[3, 4], T. B. Bekker[5], G. V. Lanskii[3, 4], V. A. Svetlichnyi[1, 4], A. A. Mamrashev[1, 2], D. M. Ezhov[4], V. D. Antsygin[2], A. E. Kokh[5], K. A. Kokh[5] 44

14. FORMATION OF NONCLASSICAL STATES OF LOCALIZED PLASMONS IN THE SPASER SYSTEMS CONTROLLED BY EXTERNAL MAGNETIC FIELD A.V. Shesterikov, S.N. Karpov, M.Yu. Gubin, A. V. Prokhorov 45

15. NONLINEAR BIFURCATION DIAGRAMS OF THE CURRENT STATES OF MICROCAVITY EXCITON-POLARITONS IN THE LATTICE Igor Chestnov[1], Alexey Yulin[2] and Oleg Egorov[3] 48

16. INTERRELATION OF THE SUBWAVE GOLD FILM'S MORPHOLOGY ON SILICON AND THE EFFICIENCY OF THE SECOND OPTICAL HARMONIC GENERATION UNDER ULTRAHIGH VACUUM CONDITIONS Sinko A.S., Aksenov V.N., Kozlov I.S., Ozheredov I.A., Shkurinov A.P. 50*

THE METHODS OF SYNTHESIS AND DIAGNOSTICS OF NANOMATERIALS AND NANOSTRUCTURE 54

17. SIMULATION OF SUBPICOSECOND MULTI-PULSE LASER ABLATION OF METALS Povarnitsyn Mikhail 54

18. ЛАЗЕРНАЯ ПЕЧАТЬ ХИРАЛЬНЫХ ПЛАЗМОННЫХ НАНОСТРУЙ ВИХРЕВЫМИ ПУЧКАМИ Сюбаев С.А. 56

19. ИССЛЕДОВАНИЕ СВОЙСТВ И РАЗРАБТКА СЕНСОРОВ НА ОСНОВЕ ПЛЕНОК ГРАФЕНА, ВЫРАЩЕННЫХ МЕТОДОМ ТЕРМОДЕСТРУКЦИИ ПОВЕРХНОСТИ ПОЛУИЗОЛИРУЮЩЕГО SIC (0001) А.А. Лебедев[1,2], В.Ю. Давыдов[1], С.П.Лебедев[1,2], А.Н. Смирнов[1], В.С. Левицкий[1], И.А. Елисеев[1,4], С.Н. Новиков[3,4], Д.Ю. Усачев[4], А.Г. Рыбкин[4] О.Ю. Вилков[4], Ю.Н. Макаров[5,6] 61

20. СТРУКТУРА ПЛАВАЮЩИХ МОНОСЛОЕВ И ПЛЕНОК ЛЕНГМЮРА-ШЕФФЕРА ГОЛЬМИЕВОГО КОМПЛЕКСА СМЕШАННО-ЗАМЕЩЕННОГО ПРОИЗВОДНОГО ФТАЛОЦИАНИНА Казак А.В.[1,2], Усольцева Н.В.[1], Смирнова А.И.[1], Марченкова М.А.[2,3], Терещенко Е.Ю.[2], Якунин С.Н.[3], Рогачев А.В.[3,5], Ковальчук М.В.[2,3,4] 64

21. ИЗГОТОВЛЕНИЕ ПОРИСТЫХ НАНОСТРУКТУР ДЛЯ УСИЛЕНИЯ СИГНАЛА КОМБИНАЦИОННОГО РАССЕЯНИЯ [1]Мицай Е.В., [1]Сюбаев С.А, [1,2]Кучмижак А.А. 66

22. METAL-CARBYNE COMPLEXES FOR SERS APPLICATION A. Osipov, A. Kucherik, A. Antipov, S. Kutrovskaya, S. Arakelian 70

23. NEW LASER COMPOSITE CERAMIC Michail Pankov, Sergey Lysenko, Andrew Kanaev, Jury Kopylov, Alexander Antipov, Valery Bulaev 72

POSTERS 73

24. ENERGY STATES OF EXCITONS IN SQUARE QUANTUM WELLS Belov Pavel 73

25. МОДЕЛИРОВАНИЕ ВЛИЯНИЯ ПАРАМЕТРА ПОРЯДКА НА ПРЕДЕЛЬНО КОРОТКИЕ ОПТИЧЕСКИЕ ИМПУЛЬСЫ В ГЕРМАНЕНЕ Конобеева Н.Н. 77

26. THE LASER-INDUCED SYNTHESIS OF LINEAR CARBON CHAINS A. Osipov, S. Arakelian, S. Kutrovskaya and V. Samyshkin 79

27. PHOTON ECHO FROM AN ENSEMBLE OF (IN,GA)AS QUANTUM DOTS Ia.A. Babenko[1], I.A. Yugova[1], S.V. Poltavtsev[1,2], M. Salewski[2], I.A. Akimov[2,3], M. Kamp[4], S. Höfling[4], D.R. Yakovlev[2,3] and M. Bayer[2,3] 80

28. THE EMERGING OF CHROMATICITY OF STEEL SURFACE BY LASER RADIATION A. Burtsev[1,2], O. Butkovsky[1], E. Pritotsky[1,2], A. Pritotskaya[1,2] 84

29. DEVELOPMENT OF DIELECTRIC MULTI-LAYER MIRRORS FOR HIGH-POWER SEMICONDUCTOR LASERS E. Pritotsky, S. Lysenko, M. Pankov, A. Antipov 86

30. ПРОЕКТ ФОТОННОГО АЦП Якушенков Павел 88

31. DETERMINATION OF TEMPERATURE MEASUREMENTS ON THE SURFACE CARBONACEOUS MATERIALS WITH SIMULTANEOUS REGISTRATION OF THE LASER INDUCED PROCESSES S. M. Arakelyan, A.F. Galkin, S. V. Zhirnova, E.L. Shamanskaya 94

32. EXPERIMENTAL STUDY OF THE PARAMETERS OF FILAMENTS IN TRANSPARENT SOLID MEDIA M. A. Tarasova, K.S. Khorkov, D.A. Kochuev, V.G. Prokoshev98

33. MORPHOLOGY, GRANULOMETRIC AND STRUCTURAL PHASE COMPOSITION OF MECHANICALLY SYNTHESIZED COMPOSITE POWDER AL-MG+AL/MWCNTS [1]Aborkin A.V., [1]Sobol`kov A.V., [1]Kireev A.V., [2]Volochko A.T., [2]Izobello A.Yu., [3]Sachkova N.V., [3]Sytschev A.E. 101

34. THZ SPECTROMETERS BASED ON ULTRAFAST LASERS Vasilis Apostolopoulos104

35. ATOMIC-FORCE LITHOGRAPHY FOR PHOTONIC APPLICATIONS A. Kucherik, S. Kutrovskaya, I. Skryabin, A. Shagurina, A. Osipov, I. Chesnov 105

36. MECHANISMS OF LIQUID-PHASE EXFOLIATION OF GRAPHENE V.A. Ilin, K.S. Khorkov, D.A. Kochuyev, V.G. Prokoshev, S.M. Arakelian..... 107

37. РЕНТГЕНОВСКИЙ ЛАЗЕР С λ ~ 13.4 НМ, ОБРАЗОВАННЫЙ ПРИ ВЗАИМОДЕЙСТВИИ НАНОСТРУКТУРИРОВАННОЙ МИШЕНИ ОЛОВА С ИНТЕНСИВНЫМ ЛАЗЕРОМ НАКАЧКИ – ПЕРСПЕКТИВНЫЙ ИСТОЧНИК ИЗЛУЧЕНИЯ ДЛЯ ПРОМЫШЛЕННОЙ НАНОЛИТОГРАФИИ Е. П. Иванова..... 109

38. CONTROL OF PROPAGATION OF SPATIALLY LOCALIZED POLARITON WAVE PACKETS IN A BRAGG MIRROR WITH EMBEDDED QUANTUM WELLS I.E. Sedova,[1] I.Yu. Chestnov,[1] S.M. Arakelian,[1] A.V. Kavokin,[2,3,4] and E.S. Sedov[1,3] 111

39. INTERACTION OF LASER RADIATION WITH TITANIUM IN AIR A.A. Voznesenskaya, A.V. Ivashchenko, D.A. Kochuev, V.G. Prokoshev, K.S. Khorkov 114

40. FEMTOSECOND ERBIUM NONLINEAR FIBER LASER SYSTEM A.A. Lachina, K.S. Khorkov, D.A. Kochuyev, M.N.Gerke, V.G.Prokoshev 116

41. АНАЛИЗ ТЕМПЕРАТУРНОЙ ЗАВИСИМОСТИ СПЕКТРОВ ЛЮМИНЕСЦЕНЦИИ ЖИДКОКРИСТАЛЛИЧЕСКИХ НАНОКОМПОЗИТОВ С КВАНТОВЫМИ ТОЧКАМИ СЕЛЕНИДА КАДМИЯ К.Р. Каримуллин[1,2], М.А. Михайлов[2], М.Г. Георгиева[2], К.А. Магарян[1,2], И.А. Васильева[2] 118

42. THE CW-LASER ABLATION OF RESONANT SILICON NPS IN LIQUID A. Osipov, S. Arakelian, S. Kutrovskaya, and V. Samyshkin..... 122

43. LOCAL REFRACTIVE INDEX MODIFICATION OF OPTICAL FIBER BY FEMTOSECOND LASER RADIATION: INSTALLATION FEATURES A.S. Chernikov, K.S. Khorkov, D.A. Kochuev, V.G. Prokoshev, S.M. Arakelian 124

44. SPATIO-SPECTRAL ANALYSIS OF FLUORESCENCE FROM PROBE ORGANIC MOLECULES TO MEASURE EFFECTIVE VALUES OF THE REFRACTIVE INDEX IN FROZEN FILMS Nina S. Voronova and Yurii E. Lozovik 126

45. THE COLLOIDAL SYSTEMS ON SEMICONDUCTOR NANOPARTICLES A. Kucherik, S. Kutrovskaya, I. Skryabin, S. Arakelian, E. Shamanskaya, S. Zhirnova 127

46. ПЕРЕКЛЮЧЕНИЕ СОСТОЯНИЙ ПРОВОДИМОСТИ МЕТАЛЛИЧЕСКИХ ЛАБИРИНТООБРАЗНЫХ ПЛЁНОК НА ПОРОГЕ ПЕРКОЛЯЦИИ Гущин М.Г., Гладских И.А., Вартанян Т.А. 128

47. DETERMINATION OF THE LOCAL FIELD IN THE NUCLEAR SPIN SYSTEM OF N-TYPE GAAS V.M. Litvyak[1], R.V.Cherbunin[1], K.V. Kavokin[1,2] and V.K. Kalevich[1,2] 133*

48. MATHEMATICAL MODELING OF THINFILMS GROWTH AND CALCULATION OF COEFFICIENTS REFLECTION, TRANSMISSION AND ABSORPTION WAVES Istratov A.V., Gerke M.N. 137

49. STRUCTURAL PHASE COMPOSITION AND EFFECTIVENESS OF GASDYNAMIC SPRAYING OF HYBRID COATINGS BASED ON ALMG2 NANOCRYSTALLINE MATRIX REINFORCED WITH GRAPHENE-LIKE STRUCTURES AND MICRO-SIZE CORUNDUM [1]Aborkin A.V., [1]Sobol`kov A.V., [1]Elkin A.I., [2]Arkhipov V.E.140

50. KINETIC ENERGY DISTRIBUTION OF ALKALI ATOMS DESORBED FROM SOLID SURFACES Tigran Vartanyan, Pavel Petrov 143

51. DETERMINATION OF THE NONLINEAR REFRACTIVE INDEX BY THE Z-SCAN METHOD USING FEMTOSECOND LASER RADIATION M.A. Tarasova, K.S. Khorkov, D.A. Kochuev, V.G. Prokoshev 147

52. PHOTON STATISTICS OF SEMICONDUCTOR MICROCAVITY EXCITON-POLARITONS Timur Khudaiberganov, Igor Chestnov, Sevak Demirchyan 150

53. MATHEMATICAL MODELING OF CONVECTIVE HEATING OF A DROPLET ON A SUBSTRATE Bukharov D., Rybak G., Novikova O. 153

54. INTERACTION OF LASER RADIATION WITH TITANIUM IN A LIQUID HYDROCARBON MEDIUM A.V. Ivashchenko, D.A. Kochuev, K.S. Khorkov, V.G. Prokoshev, S.M. Arakelian 158

55. MODELING OF THE TUNNELING EFFECT IN GRANULATED METALLIC NANOSTRUCTURES Istratov A.V, Kucherik A.O. 160

56. FRACTAL BIMETALLIC THIN FILMS OBTAINED BY DEPOSITION OF A SMALL DROPLETS OF COLLOIDAL NANOPARTICLES [1]A.A. Antipov, [1]D.N. Bukharov,

[1]S.M. Arakelyan, [1]S.V. Kutrovskaya, [1]A.O. Kucherik, [1]A.V. Osipov, [1]A.V.Istratov, [2]T.A. Vartanyan and [3]T.E. Itina..... 163

57. LIGHT PROPAGATION IN TUNABLE EXCITON-POLARITON HYPERBOLIC METAMATERIALS S. Arakelian, A. Kucherik, S. Kutrovskaya, A. Osipov 164

58. HARDWARE-SOFTWARE COMPLEX OF FEMTOSECOND LASER MICROMACHINING R.V. Chkalov, K.S. Khorkov, D.A. Kochuev, V.G. Prokoshev, S.M. Arakelian 166

59. THE METHOD OF SURFACE PLASMON-POLARITON PULSES GENERATION VIA COOPERATIVE EFFECTS IN WAVEGUIDE SPASER A. V. Shesterikov[a], M.Yu. Gubin[a], M. G. Gladush[b], A. V. Prokhorov[a]..... 168

CONFERENCE INFORMATION AND CONCLUSION..... 170

Abstracts

НОВЫЕ ГОРИЗОНТЫ ОПТИКИ СВЕРХКОРОТКИХ ИМПУЛЬСОВ СРЕДНЕГО ИНФРАКРАСНОГО ДИАПАЗОНА

Valeriy I. Yudin, Alexey V. Taichenachev,

Institute of Laser Physics SB RAS, Novosibirsk, Russia

Abstract—We consider some implications of the mass defect on the frequency of atomic transitions. We have found that some well-known frequency shifts (such as gravitational and quadratic Doppler shifts) can be interpreted as consequences of the mass defect, i.e., without the need for the concept of time dilation used in special and general relativity theories. Moreover, we show that the inclusion of the mass defect leads to previously unknown shifts for clocks based on trapped ions.

INTRODUCTION

At the present time, atomic clocks are most precise scientific devices. The principle of operation of these quantum instruments is based on modern methods of laser physics and high-precision spectroscopy. In this way, the unprecedented value of fractional instability and uncertainty at the level of 10^{-18} has already been achieved with the goal of 10^{-19} on the horizon [1]. Frequency measurements at such a level could have a huge influence on further developments in fundamental and applied physics. In particular, we can foresee tests of quantum electrodynamics and cosmological models, searches for drifts of the fundamental constants, new types of chronometric geodesy, and so on (see, for example, review [2]). However, this level of experimental accuracy requires a comparable level of theoretical support, which would account for systematic frequency shifts of atomic transitions due to different physical effects. Thus, modern atomic clocks are also at the point of interweaving different areas of theoretical physics.

In this paper we develop the mass defect concept with respect to atomic clocks. Historically, considerations of the mass defect have been connected with nuclear physics, where the mass defect explains the huge energy emitted due to different nuclear reactions. However, a quite unexpected result is that this effect has a direct relation to frequency standards, where it leads to shifts in the frequencies of atomic transitions.

MASS DEFECT PRODUCED SHIFTS IN ATOMIC CLOCKS

The main idea of our approach is following. Let us consider an arbitrary atomic transition between states $|g\rangle$ and $|e\rangle$ with unperturbed frequency $\omega_0 = (E_e^{(0)} - E_g^{(0)})/\hbar$, where $E_e^{(0)}$ and $E_g^{(0)}$ are the unperturbed energies of the corresponding states (see Fig.1). Using Einstein's famous formula, $E=Mc^2$, which links the mass M and energy E of a particle (c is the speed of light), we can find the rest masses of our particle, M_g and M_e, for the states $|g\rangle$ and $|e\rangle$, respectively: $E_g^{(0)} = M_g c^2$ and $E_e^{(0)} = M_e c^2$. The fact that $M_g \neq M_e$ is the essence of the so-called mass defect. In our case, the connection between M_g and M_e is the following:

$$M_e c^2 = M_g c^2 + \hbar\omega_0 \Rightarrow \quad M_e = M_g + \hbar\omega_0 / c^2 \qquad (1)$$

We show that the relationship (1) allows us to reinterpret some well-known systematic frequency shifts (such as the so-called time dilation effects) [3,4]. Moreover, our approach actually predicts some new shifts previously unconsidered, to our knowledge, in the scientific literature.

GRAVITATIONAL SHIFT.

As the first example, let us show how the mass defect allows us to formulate a very simple explanation of the gravitational redshift even under a classical description of the gravitational field (as classical potential U_G). Indeed, because the potential energy of a particle in a classical gravitational field is equal to the product MU_G (where $U_G<0$), we can write the energy of j-th state $E_j(U_G)$ as:

$$E_j(U_G) = M_j c^2 + M_j U_G = M_j c^2 (1 + U_G / c^2),\ (j = g, e) \qquad (2)$$

Using Eqs.(1) and (2), we find the frequency of the transition $|g\rangle \rightarrow |e\rangle$ in the gravitational field:

$$\omega = \omega_0 (1 + U_G / c^2). \qquad (3)$$

This expression coincides to the leading order of the well-known formula from general relativity theory:

$$\omega = \omega_0 \sqrt{1 + 2U_G / c^2} \approx \omega_0 (1 + U_G / c^2) \qquad (4)$$

in the case of $|U_G|/c^2 << 1$.

We emphasize that the expression (4) was here derived without including the concept of time dilation, which is taken as a basis of Einstein's theory of relativity. Nevertheless, in deriving (4) we have used an equality of gravitational and inertial masses, $M_{grav}=M_{in}$, which is one of the cornerstones of general relativity.

FREQUENCY SHIFTS FOR ATOMS (IONS) TRAPPED IN A CONFINEMENT POTENTIAL.

A second example concerns frequency shifts in the presence of a confinement potential U(**r**), which we take to be the same for both states $|g\rangle$ and $|e\rangle$. Such a situation occurs both for clocks based on neutral atoms in optical lattice and those based on trapped ions. In this case, we have the standard task of quantizing the energy levels with translational degrees of freedom:

$$\hat{H}_j \left| \Psi_j \right\rangle = E_j^{(vib)} \left| \Psi_j \right\rangle,\ \hat{H}_j = \hat{\mathbf{p}}^2 / 2M_j + U(\mathbf{r}), \qquad (5)$$

where Hamiltonian $\hat{H}_j$ and state $|\Psi_j\rangle$ describe the translational motion of the particle in the j-th internal state $|j\rangle$ ($j=g,e$), and **r** is coordinate of atomic center-of-mass. Thus, taking into account the translational motion, the atomic wave function is described by the pair products $|j\rangle \otimes |\Psi_j(\mathbf{r})\rangle$. Because of the mass defect ($M_g \neq M_e$), the energy levels for the lower and upper states differ: $E_g \neq E_e$. Consequently, the frequency ω between corresponding levels of trapped particle is different from the unperturbed frequency, ω_0, with a value $\Delta\omega$ (see Fig.1): $\Delta\omega = \omega - \omega_0 = (E_e - E_g)/\hbar$. Let us now estimate this value. For this purpose, we write the Hamiltonian for upper state $\hat{H}_e$ in the following form:

$$\hat{H}_e = \hat{H}_g + \Delta\hat{H};\ \Delta\hat{H} = \frac{\hat{\mathbf{p}}^2}{2M_e} - \frac{\hat{\mathbf{p}}^2}{2M_g} = -\frac{\hbar\omega_0}{2M_e M_g}\hat{\mathbf{p}}^2, \quad (6)$$

where the operator $\Delta\hat{H}$ can be considered as a small perturbation. In this case, using the standard perturbation theory, energy E_e can be written as a series $E_e=E_e(0)+\Delta E_e(1)+...$, where $E_e(0)=E_g$, and the first correction is determined as the average value $\Delta E_e(1)=\langle\Psi_g|\Delta H/\Psi_g\rangle$. Using Eq. (6) and taking into account $M_g\approx M_e$, we obtain the following estimation of the relative value of shift:

$$\frac{\Delta\omega}{\omega_0}\approx-\frac{1}{2c^2}\frac{\left\langle\Psi_g\left|\hat{\mathbf{p}}^2\right|\Psi_g\right\rangle}{M_g^2}. \qquad (7)$$

We note that this expression coincides with a well-known relativistic correction, which is the quadratic Doppler shift due to the time dilation effect for moving particle [4]. Indeed, at the present time the following explanation is conventionally used. In accordance with special relativity, the tick rate Δt in the moving (with velocity $\mathbf{v}$) coordinate system changes with respect to the tick rate $\Delta t'$ in motionless (laboratory) coordinate system by the law: $\Delta t=\Delta t'(1-\mathbf{v}^2/c^2)^{1/2}$. As a result, an atomic oscillation with eigenfrequency ω_0 is perceived by an external observer to be shifted to $\omega=\omega_0(1-\mathbf{v}^2/c^2)^{1/2}$. In the nonrelativistic limit, ($\mathbf{v}^2/c^2<<1$), we have: $\omega\approx\omega_0(1-\mathbf{v}^2/2c^2)=\omega_0[1-(\mathbf{p}/M)^2/2c^2]$ (where $\mathbf{p}$ is momentum of particle). Then, if we take into account quantum considerations through the replacement $\mathbf{p}\to\hat{\mathbf{p}}=-i\hbar\nabla$, we obtain the expression for frequency shift (7).

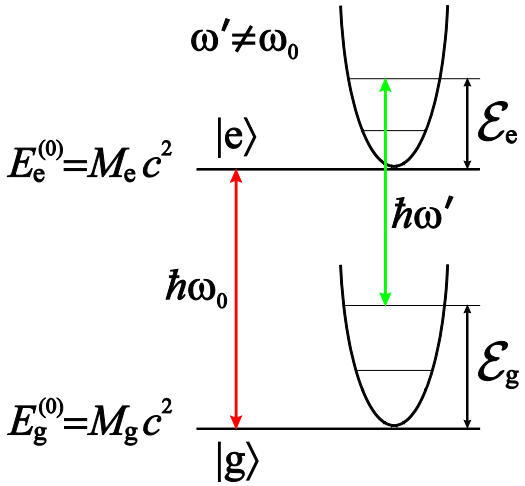

Fig. 1. Schemematic for an atomic transition $|g\rangle\to|e\rangle$. Also shown is the quantization of the energy levels for translational degrees of freedom in a confined potential, $U(\mathbf{r})$, where $\omega\neq\omega_0$ due to the mass defect.

Thus, some well-known systematic shifts, previously interpreted as the time dilation effects in the frame of special and general relativity theories, can be considered as a consequence of the mass defect. Furthermore, our approach has predicted a series of previously unknown shifts for ion clocks related to electric-field sensitivities (as will be shown in our presentation). These results could have importance for high-precision optical atomic clocks.

ACKNOWLEDGMENT

We are thankful for support from the Russian Scientific Foundation (Project No. 16-12-00052) and Ministry of Education and Science of the Russian Federation (Project No. 3.1326.2017).

REFERENCES

1. M. Schioppo, R. C. Brown, W. F. McGrew, N. Hinkley, R. J. Fasano, K. Beloy, T. H. Yoon, G. Milani, D. Nicolodi, J. A. Sherman, N. B. Phillips, C. W. Oates, and A. D. Ludlow, "Ultrastable optical clock with two cold-atom ensembles", Nature Photonics vol. 11, pp.48–52 (2017).
2. A. D. Ludlow, M. M. Boyd, J. Ye, E. Peik, and P. O. Schmidt, "Optical atomic clocks", Rev. Mod. Phys. vol. 87, pp.637 (2015).
3. A. Einstein, Annal. Physik vol. 17, pp.891 (1905).
4. C. W. Chou, D. B. Hume, T. Rosenband, and D. J. Wineland, "Optical Clocks and Relativity", Science vol. 329, pp.1630-1633 (2010).

VERIFICATION OF THE QUANTUM DIMENSION EFFECTS IN ELECTRICAL CONDUCTIVITY WITH DIFFERENT TOPOLOGY OF LASER-INDUCED THIN-FILM STRUCTURES

S. Arakelian*, *A. Kucherik, S. Kutrovskaya, A. Osipov, A. Istratov, and I. Skryabin

Stoletovs Vladimir State University, Gorky Str. 87, Vladimir 600000, Russia

E-mail: arak@vlsu.ru

We studied in both theory and experiment the nanocluster structures of different types (due to topology and composition) taking into account the correlations in nanoparticle-ensemble by quantum states. The problem of high temperature superconductivity due to topological surface structures with localized states (resulting in coupled states on new dimensional principles) has been under our consideration. Dramatic enhancement of electroconductivity (in 4 orders!), observed in our experiments, may be discussed as a real tendency to high temperature superconductivity due to topological peculiarities of nanocluster system. Near-field photoluminescence spectra/optical response in hybrid nanosystems measured by us demonstrated a big efficiency in the nanoantenna respect.

APPROACHING TO THE LIMIT OF SPASERS FROM SPP NANOLASERS

Tien-Chang Lu*, Yu-Hsun Chou, Kuo-Bin Hong, and Chun-Tse Chang

Department of Photonics, College of Electrical and Computer Engineering,
National Chiao Tung University, Tin Ka-Ping Photonics Building,
No.1001, Ta-Hsueh Road, East District, Hsinchu City 30010, Taiwan
+886-3-5131234, timtclu@mail.nctu.edu.tw

Nowadays, the development of nanolaser deals with the manipulation of SPP has attracted the attention to construct ultra-compact integrated optoelectronic devices and systems. The characteristics of SPPs can be determined by the dispersion relation of the device structure, which is influenced by the material's permittivity and structural parameters. One straight forward way to manipulate the dispersion relation of the SPP nanolaser relies on the thickness control of the insulator layer in between the semiconductor and the metal thin film for the Semiconductor/Insulator/Metal (SIM) nanolaser structure, which becomes one of the most popular plasmonic structure to confine the field and against the optical diffraction limit. However, the tailoring range of the dispersion relation was limited by the materials. To investigate the characteristic of SPP nanolaser with huge dispersion difference, we chose the SPP nanolaser with different metals to compare the properties difference between SPP laser operating nearby the SP frequency and the SPP laser operating far away from the SP frequency. For more reliable SPP laser operation, ZnO nanowire provides exciton binding energies larger than thermal energy at room temperature and strong oscillation strength to interact with SPP. Thus, the ZnO nanowire was chosen in our study for stable SPP laser operation under different circumstances. Once the active emitter was chosen to be operated in the near UV range, aluminum and silver are used to properly generate SPPs. Typically, aluminum has a relatively high surface plasmon frequency. The ZnO nanolaser on Al is operated away from the SP frequency, rendering itself operating as a SPP nanolaser. On the other hand, since Ag has an interband transition at 350 nm, the dispersion relation of surface plasmon near 370 nm will be significantly bent, leading to ZnO nanolasers operating approaching the limit of surface plasmon amplification by stimulated emission radiation (SPASER). By investigating richful characteristics of Al- and Ag-based ZnO nanolasers, intriguing phenomena such as the quantum plasmonic effect, ultrafast modulation, strong interaction between the exciton and surface plasmon, and high characteristic temperature operation will be discussed.

NONLINEAR OPTICS AND SPECTROSCOPY

1. THE EFFECT OF MOLECULAR OSCILLATIONS ON ENERGY TRANSFER IN MACROMOLECULAR CHAIN SYSTEMS

Chizhov A.V.[1,2], Čevizović D.[3], Galović S.[3]

[1] *Bogoliubov Laboratory of Theoretical Physics, Joint Institute for Nuclear Research, 141980 Dubna, Russia*
[2] *Dubna State University, 141980 Dubna, Russia*
[3] *Vinča Institute of Nuclear Sciences, 11001 Belgrade, Serbia*
phone: (496) 216-25-33, e-mail: chizhov@theor.jinr.ru

Macromolecular chain systems are of interest from the viewpoint of studying various biological processes and searching possible applications in molecular nanotechnologies. In particular, protein molecules are considered as mediators of the long distance transfer of energy released during the hydrolysis of adenosine triphosphate for photochemical reactions, cross-membrane ion transfer and signal transduction, muscle contraction, cellular mobility [1]. However, at present the mechanism of energy transfer along the chain at long distances without being dissipated or dispersed is not yet clearly understood.

According to recent research [2], in protein macromolecules and other macromolecular chains, due to the interaction of a vibronic excitation with the collective oscillations of the macromolecular, there appears a phenomenon of self-trapping of the vibron. It results in creation of the dressed polaron states. As a consequence, the properties of the self-trapping vibron state may be quite different compared with the properties of the bare vibronic excitation. In fact, it was found that there exist certain values of the system parameters (critical values) for which the polaron state might abruptly change from weakly dressed to heavy dressed, practically localized, vibron state [3]. It was also found that the critical values of the system parameters are temperature dependent, and for some biological structures may belong to room temperature interval. This fact may significantly affect to the mechanism of the vibron motion through the macromolecular chain.

For a theoretical description of such processes, a modified Holstein's polaron model for molecular crystals is proposed. The system under the consideration describes the behavior of a single vibron excited on some structural element of the macromolecule chain system, whose physical properties are affected by the collective oscillations of the macromolecular chain (phonons). The vibronic excitation is supposed to be able to move within the system from one to some other structural element by a hopping mechanism due to the dipole-dipole interaction between the corresponding peptide groups of the macromolecular chains [4]. In order to examine under

which conditions dressed vibronic excitations form dynamically stable eigenstates of the system, we employ the partial-dressing method by using the modified Lang–Firsov unitary transformation. The influence of collective oscillations of the macromolecular chain on polaron properties and, in particular, on the degree of dressing is taken into account in the mean-field approach. As probable states of such collective oscillations, the state of thermal equilibrium at a certain temperature and the multimode squeezed vacuum state are considered.

We demonstrate that in the non-adiabatic regime the degree of dressing as a function of the coupling constants and characteristics of the phonon state continuously increases reflecting the smooth transition of the slightly dressed, practically free vibron, to a heavily dressed one, i.e. small polaron. As "adiabaticity" rises, this transition becomes increasingly steeper, and finally, in the adiabatic limit, a discontinuous "jump" of the degree of dressing is observed. The interchain coupling manifests itself through the increase of the effective adiabatic parameter of the system.

Thus, we studied the influence of the intra- and interchain couplings as well as the state of the chain collective oscillations on the properties of the small polarons in the system composed of coupled infinite parallel molecular chains. For that purpose we employed the variational treatment based on the modified Lang–Firsov transformation. It was shown that for certain values of the model parameters a polaron crossover occurs, in which there is a sharp change in the migration nature of a vibron from practically free to a heavy quasiparticle "dressed" by a phonon cloud.

The work was supported by the bilateral project between Serbian Ministry of Education and Science and JINR, Dubna "Theory of Condensed Matter".

REFERENCES

1. A.S. Davydov, *Biology And Quantum Mechanics* (Naukova Dumka, Kiev, 1979).
2. D. Čevizović, S. Galović, A. Reshetnyak, Z. Ivić. *Chin. Phys*. B **22**, 060501 (2013).
3. P. Hamm and G. P. Tsironis. *Phys. Rev*. B **78**, 092301 (2008).
4. D. Čevizović, Z. Ivić, S. Galović, A. Reshetnyak, A. Chizhov. *Physica* B **490**, 9 (2016).

2. TEMPERATURE DEPENDENCE OF TERAHERTZ OPTICAL PROPERTIES OF LBO AND PERSPECTIVES OF APPLICATIONS IN DOWN-CONVERTERS

N. A. Nikolaev[1, 2], Yu. M. Andreev[3, 4], N. G. Kononova[5], G. V. Lanskii[3, 4], A. A. Mamrashev[1, 2], V. D. Antsygin[2], K. A. Kokh[5], A. E. Kokh[5]

[1] High Current Electronics Institute SB RAS, 2/3 Akademicheskii Ave., 634055, Tomsk, Russia,;
[2] Institute of Automation and Electrometry SB RAS, 1 Academician Koptyug Ave., 630090, Novosibirsk, Russia;
[3] Institute of Monitoring of Climatic and Ecological Systems SB RAS, 10/3 Akademicheskii Ave., 634055, Tomsk, Russia;
[4] Siberian Physical Technical Institute of Tomsk State University, 1 Novosobornaya Sq., 634050, Tomsk, Russia;
[5] Institute of Geology and Mineralogy SB RAS, 3 Academician Koptyug Ave., 630090, Novosibirsk, Russia.
nazar@iae.nsk.su

Lithium triborate LiB_3O_5 (LBO) crystals are widely used for frequency conversion of the near-IR lasers within main transparency windows. Their optical properties at these wavelengths are well studied. However, very little work has been published on the properties in the terahertz (THz) range. There was a lack of data on the refractive indices dispersions, the absorption coefficients spectra and their temperature dispersions. There are no reports of THz applications. Present work reveals all these topics including the prospects for use LBO crystals as down-converters.

Optically finished samples of flux-grown LBO crystals were studied by THz-TDS. The refractive index dispersions were recorded and then approximated in the form of Sellmeier equations for the temperatures of 300 and 81 K. The phase-matching curves for the IR-THz and THz-THz frequency conversions were calculated. It was found that the absorption coefficients of LBO decrease significantly with cooling to cryogenic temperatures but the overall character of optical properties changes is intricated. Experimental results are discussed in detail considering potential characteristics of THz down-converters.

3. ИССЛЕДОВАНИЕ НИЗКОТЕМПЕРАТУРНОЙ ОПТИЧЕСКОЙ ДЕФАЗИРОВКИ В АНСАМБЛЕ ПОЛУПРОВОДНИКОВЫХ КОЛЛОИДНЫХ КВАНТОВЫХ ТОЧЕК CDSE/CDS/ZNS МЕТОДОМ НЕКОГЕРЕНТНОГО ФОТОННОГО ЭХА

К.Р. Каримуллин, А.И. Аржанов, А.В. Наумов

Институт спектроскопии РАН,
108840, Москва, Троицк
Московский педагогический государственный университет,
119435, Москва
+7(916)556-0937, e-mail: kamil@isan.troitsk.ru

Методы оптической спектроскопии примесного центра широко применяются для изучения физических свойств материалов. Оптические спектры примесных центров чрезвычайно чувствительны к параметрам локального окружения, что дает возможность использовать их для исследования не только спектральных свойств, но и внутренней динамики в разных матрицах [1]. Как правило, в качестве спектральных зондов в подобных исследованиях используют органические молекулы. Альтернативой органическим красителям могли бы стать полупроводниковые нанокристаллы (квантовые точки, КТ).

КТ обладают высокой фотостабильностью, они превосходят по квантовому выходу обычные люминофоры, кроме того существует возможность управления спектром люминесценции за счет изменения размеров точек. Уникальные фотофизические свойства КТ обеспечивают их высокую практическую ценность в таких областях, как органическая фотовольтаика, флуоресцентная наноскопия, квантовая оптика и информатика. Для практического использования материалов на основе КТ в приложениях квантовой оптики необходимо детальное исследование их фотофизических свойств. Отдельный интерес представляют исследования закономерностей распада наведенной поляризации в ансамбле КТ, которые могут быть выполнены методом фотонного эха. Настоящая работа посвящена исследованию низкотемпературной оптической дефазировки в неоднородном ансамбле полупроводниковых коллоидных квантовых точек.

В качестве объекта исследования были выбраны КТ CdSe/CdS/ZnS (пр-во QD-light, Россия). Образцы были приготовлены в виде тонких пленок, высаженных на стеклянные подложки из раствора квантовых точек в толуоле. Для получения однородных по структуре образцов с высокой концентрацией излучающих центров, высокой оптической плотностью и хорошим оптическим качеством были проведены специальные исследования [2]. В результате был создан экспериментальный стенд, позволяющий наносить тонкие и

однородные слои КТ из высококонцентрированного раствора на поверхность стеклянной подложки (подробнее см. [3]).

Экспериментальные данные по фотонному эхо были получены в отделе молекулярной спектроскопии Института спектроскопии Российской академии наук на уникальном спектрометре некогерентного фотонного эха (см., например, [4]). В приготовленных образцах были измерены кривые спада сигналов фотонного эха как при комнатной температуре, так и в диапазоне температур от 4,5 до 50 К (см. рис. 1). Были получены значения времени затухания сигналов фотонного эха и построена температурная зависимость обратного времени оптической дефазировки (квадраты на рис. 1).

По аналогии с работой [5], посвященной эхо-спектроскопии эпитаксиальных квантовых точек, измеренную температурную зависимость мы описали следующим образом:

$$\Gamma = \Gamma_0 + \Gamma_{sample} + AT + \frac{B}{\exp(C/kT) - 1}, \qquad (1)$$

где Γ_0 – естественная ширина спектральной линии; A, B и C – подгоночные параметры. Результат фитирования показан на рис. 1 сплошной линией.

Для сравнения на рисунке приведены значения однородной ширины спектров люминесценции одиночных КТ CdSe/ZnS (кружки), измеренные при T=10 К группой M.G. Bawendi [6].

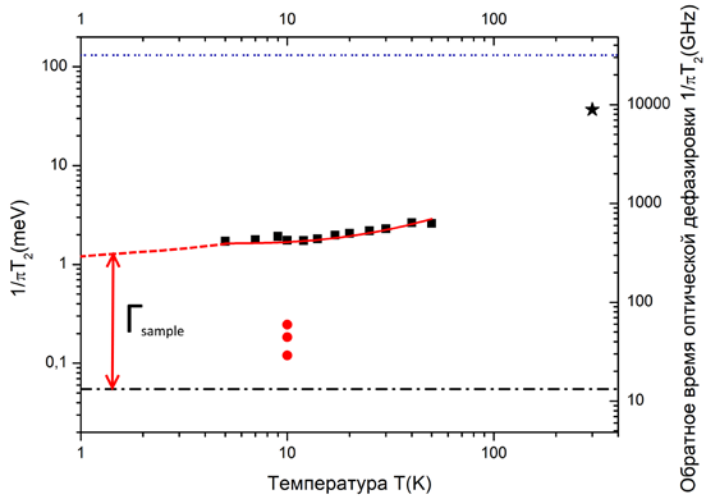

Рис. 1. Температурная зависимость обратного времени оптической дефазировки $1/\pi T_2$, измеренная в ансамбле квантовых точек CdSe/CdS/ZnS. Пояснения см. в тексте.

Значения спектральной ширины, полученные для одиночных КТ, лежат ниже температурной зависимости обратного времени оптической дефазировки, измеренной методом НФЭ. Это может быть связано с тем, что наши измерения проводились в

неоднородном (по размеру и форме) ансамбле КТ, и такая дисперсия приводит к дополнительному спектральному уширению. В верхней части рисунка звездочка соответствует среднему значению ширины спектров люминесценции для одиночных КТ, а пунктирная линия – для ансамбля КТ CdSe/CdS/ZnS, измеренному методами конфокальной люминесцентной спектромикроскопии при комнатной температуре. Штрих-пунктирной линией на рисунке обозначена естественная ширина $\Gamma_0=1/2\pi T_1$ (T_1=12 нс по данным измерения кинетики люминесценции в растворе КТ CdSe/CdS/ZnS в толуоле). Полученные значения обратного времени дефазировки даже при низких температурах характеризуются значительным дополнительным уширением Γ_{sample} относительно естественной ширины.

В отличие от ансамбля примесных молекул органических красителей, для которых время оптической дефазировки T_2 при криогенных температурах составляет величины порядка единиц наносекунд, в случае КТ имеет место быстрая релаксационная динамика с характерными временами порядка сотен фемтосекунд – единиц пикосекунд. Возможные причины столь малых значений времени дефазировки могут быть связаны с неоднородностью структуры самих точек, особенностями внутренней динамики излучающего ядра (например, с эффектом мерцания люминесценции), а также с поверхностными состояниями на оболочках. Кроме того, к ультрабыстрой релаксации в ансамбле могут приводить дисперсия по размеру и сильно-неоднородное локальное окружение квантовых точек.

Работа выполнена в рамках Программы ОФН РАН «Фундаментальная оптическая спектроскопия и ее приложения». К.Р. Каримуллин и А.И. Аржанов благодарят за поддержку грант Президента РФ для молодых ученых – кандидатов наук (проект МК-342.2017.2). Авторы публикации являются членами ведущей научной школы Российской Федерации «Спектроскопия атомов, молекул и конденсированных сред» НШ-7035.2016.2.

Литература

[1] А.В. Наумов // Успехи физ. наук. - 2013. - Т. 183, № 6. - С. 633-652.

[2] К.Р. Каримуллин, А.И. Аржанов, А.В. Наумов // Известия РАН. Серия физическая. - 2017. - Т. 81, № 12. - С. 1581-1586 (в печати).

[3] K.R. Karimullin, M.V. Knyazev, A.I. Arzhanov, L.A. Nurtdinova, A.V. Naumov // J. Physics: Conference Series. - 2017. - V. 859. - Art. No 012010.

[4] M.V. Knyazev, K.R. Karimullin, A.V. Naumov // Physica Status Solidi (RRL). - 2017. - V. 11, No 3 - Art. No 1600414.

[5] G. Moody et al. // Phys. Rev. B. - 2011. - V. 83. - Art. No 115324.

[6] S.A. Empedocles, D.J. Norris, M.G. Bawendi // Phys. Rev. Lett. - 1996. - V. 77. - P. 3873.

4. SPECTROSCOPY OF LASER-COOLED MAGNESIUM IN AN OPTICAL LATTICE

N. Jha, S. Rühmann, D. Fim, K. Zipfel, S. Sauer, W. Friesen, W. Ertmer, and E. M. Rasel

Institut für Quantenoptik
Leibniz Universität Hannover
Hannover, Deutschland
rasel@iqo.uni-hannover.de

Abstract— We present the progress towards the first realization of an optical lattice clock based on the Bosonic 24Mg 1S0 – 3P0 optical transition. We achieve the highest Q-factor for Mg with linewidths below 50 Hz which allows a precise determination of the systematic shifts.

Magnesium possesses all the qualities relevant for an optical frequency standard. The demonstration of Mg optical lattice clock has so far not been possible due to a rather large tunneling induced broadening in the optical lattice trap. In the present work, we report on the improvements in the optical lattice setup to suppress the tunneling induced linewidth broadening to below 50 Hz allowing us to achieve the highest Q-value of 1.6 x 10-13 for the Bosonic Mg.

We interrogate the bosonic atoms trapped in an optical lattice in the Lamb-Dicke regime at trap depths of about fifty times the photon recoil energy. Such a deep optical lattice could be created within an enhancement cavity intertwining the vacuum chamber. This allowed us to more precisely measure the lattice induced AC-Stark shifts. Having suppressed the lattice contributions to the linewidth, we could observe the influence of the probe laser intensity as well as the homogeneous magnetic field on the measured clock transition linewidth. Improvements in the atom loading efficiency to the optical lattice, and an improved normalized detection scheme with higher S/N ratio allowed us to perform spectroscopy at low magnetic and probe laser fields. Following these improvements, we could reduce the linewidth to below 50 Hz. This reduced linewidth allows us to perform more precise determination of various systematic shifts influencing our frequency measurements. We will present these improved systematic shift measurements and the progress towards a frequency measurement against the available frequency standards at PTB via the 73 km long optical fibre link [3]. The spectroscopy laser, stabilized to a high finesse ULE cavity, displays a frequency stability of 4 x 10-16 in 1 second.

This work was supported in part by Deutsche Forschungsgemeinschaft (DFG) within QUEST, Center for Quantum Engineering and Space-Time Research. Moreover we acknowledge

financial support from DFG Research Training Group (Graduiertenkolleg) 1729, the Marie Curie Initial Training Network FACT (ITN-FACT) Program, call FP7-PEOPLE-2013-ITN and the DLR BOOST project.

Acknowledgment

We acknowledge K. Gibble, M. Safranova, U. I. Safranova and S.G. Porsev for the theoretically support. We are immensely grateful to A. Bauch from Physikalisch Technische Bundesanstalt (PTB) for providing the passive H-maser. We also thank O. Prudnikov for helpful discussions.

References

1. A. P. Kulosa, D. Fim, K. H. Zipfel, S. Rühmann, S. Sauer, N. Jha, K. Gibble, W. Ertmer, E. M. Rasel, M. S. Safronova, U. I. Safronova, and S. G. Porsev, Phys. Rev. Lett. **115**, 240801 (2015).
2. A. V. Taichenachev, V. I. Yudin, C. W. Oates, C. W. Hoyt, Z. W. Barber, and L. Hollberg, Phys. Rev. Lett. **96**, 083001 (2006).
3. A. Pape, O. Terra, J. Friebe, M. Riedmann, T. Wübbena, E. M. Rasel, K. Predehl, T. Legero, B. Lipphardt, H. Schnatz, and G. Grosche, Opt. Exp. **18**, 21477 (2010).

5. ANALYTICAL SOLUTIONS FOR LIGHT EMISSION INTENSITIES FROM COOPERATIVE ENSEMBLES IN DIELECTRICS

Maxim G. Gladush

Institute for Spectroscopy of Russian Academy of Sciences,
Troitsk, Moscow, Russia
e-mail: mglad@isan.troitsk.ru

In this study some spectroscopic properties typical for cooperative ensembles of quantum emitters were calculated analytically and shown to meet the results of numeric simulations as well as some experimental observations. Two selected properties measurable with the use of conventional fluorescence detection systems and instruments were considered. Analytical expressions for fluorescence excitation and fluorescence emission spectra were obtained for a few variants of specific geometries of the light-sample interaction. The exact solutions and the approximate compact formulas were derived to give plots of either excitation or emission wavelengths versus number of fluorescence photons produced by quantum emitters with dipole-dipole interactions. The theory was based on the coupled equations for the emitters and photon density matrices completed with the equation for the emitters-photon correlation operator. The equations were derived from the truncated BBGKY hierarchies written for emitters, host matrix particles, and photons. The analytical solutions describe the marginal cases, i.e. a large ensemble and two closely positioned emitters. The results of this study may be applied in experiments to detect position configuration in the system of two emitters and the strength of their dipole-dipole interaction. In the dependence obtained for the fluorescence excitation spectrum, two mechanisms in cooperative absorption of incident light were shown to contribute to the maximums of the measurable curve. The first mechanism represents the absorption of one incident photon when the excitation is distributed between the emitters. The second process reflects the absorption of two photons from the exciting field bringing both particles in their excited states. For each of the considered contributions approximate analytical expressions for the corresponding components of the spectrum were derived. If the interparticle distance is assumed to be less than a quarter of the emission wavelength the exact curve was shown to become the sum of the separated contributions with a very good accuracy.

6. HIGH EXTINCTION RATIO INTEGRATED OPTICAL MODULATOR FOR QUANTUM TELECOMMUNICATION SYSTEMS

Alexander Tronev[1,2], Mikhail Parfenov[3], Peter Agruzov[1], Igor Ilichev[1] and Aleksandr Shamrai[1,2,3]

[1]Ioffe Institute, Polytekhnicheskaya 26, 194021 St.Petersburg, Russia
[2]ITMO University, Kronverksky av. 49, 197101 St.Petersburg, Russia
[3]Peter the Great Saint-Petersburg Polytechnic University, Polytekhnicheskaya 29, 195251 St.Petersburg, Russia
Phone +7 (812)297-7055, e-mail: achamrai@mail.ioffe.ru

Lithium niobate (LN) is one of basic materials of integrated optics used, for example, for electro- and acousto-optical modulators, switches, diffraction gratings, nonlinear optical wavelength converters, and others. After the birth and positioning of quantum information science, lithium niobate waveguide architectures have emerged as one of the key platforms for enabling photonics quantum technologies. This paper is devoted to the Mach-Zehnder (MZ) intensity modulator with improved extinction ratio which is very promising for quantum key distribution, precise sensing, high fidelity signal processing and other applications. A typical extinction ratio of commercially available MZ intensity modulators lies in the range 20 – 30 dB because of finite tolerances of fabrication processes. A high extinction ratio can be achieved by trimming the amplitude balance between the two arms of a MZ modulator. The active trimming with additional electrodes and a corresponding servo loop with a complicated bias control is usually used. We demonstrated that a local micro-size change of refractive index due to photorefractive effect can be effectively used for precise adjustment of the power splitting ratio of waveguide optical splitters and couplers, does not impairs the optical losses and can be efficiently used for the passive trimming of LN MZ modulators. To demonstrate the efficiency of the proposed method the improvement of extinction ratio was performed. The increase of 17 dB (from 30 to 47 dB) with a negligible additional loss was obtained.

7. QUANTUM ANTENNAS: DESIGNING STATES FOR FIELD CORRELATIONS

I. Karuseichyk[1], A. Mikhalychev[1], D. Mogilevtsev[1], G. Buchs[2], D. L. Boiko[2], G. Ya. Slepyan[3], A. Boag[3]

[1]Institute of Physics NASB Minsk 220072 Belarus
[2]CSEM - Centre Suisse d'Electronique et de Microtechnique 2002, Neuchatel, Switzerland
[3]School of Electrical Engineering Tel Aviv University 69978, Israel

+375293545337, ilkarusei@gmail.com

A quantum antenna can shape spatial entanglement of emitted photons originating from entangled states of antennas emitters. In contrast to the classical antenna, the quantum antenna can shape the second and higher order correlations without affecting amplitudes of the field. The shape and directivity of the correlations can be optimized using techniques of quantum state inference. Positive and negative correlated twin-photon, and multi-photon entangled states can be produced from the same antenna for different initial states of emitters.

The radiative properties of the classical antennas are characterized by angular distributions of the radiated field and intensity. For classical radiation, power radiation pattern formed by interference effects is proportional to the squared modulus of the field radiation pattern [1]. However, this simple picture does not hold for non-classical states of emitted radiation. Entanglement of emitters in antennas can lead to collective effects in radiated field, supperradiance and subradiance or intensity values otherwise impossible for the factorized initial state of the antenna emitters [2], quantum nonreciprocity [3], Sub-Rayleigh imaging and superresolution [4, 5], and to superbunching [6]. To be able to use the high-order field correlations, one needs to be able to create and shape them according to desired goals. In this work we suggest a way to design a state of the antenna for shaping the emitted field to provide some desired features of correlation functions in analogy with the procedures of the quantum state reconstruction. By optimizing the second-order correlation function, we show that a twoparticle entangled state of an equispaced linear antenna array allows for producing strongly momentum correlated photons. The same approach works also for multi-particle antenna states.

We consider the quantum antenna model as a set of N identical non-interacting two-level emitters at points $\vec{R}_j$ having dipole moments $\vec{d}$ (see Fig. 1(a)). Omitting the time-dependence common for all emitters, the positive-frequency field operator part giving non-zero contribution to the normally ordered correlation functions and describing the spatial field distribution in the far field zone is

$$\vec{E}(\vec{r}) \propto \sum_{j=1}^{N} \frac{\vec{n} \times [\vec{n} \times \vec{d}]}{|\vec{r}|} \exp\{ i\omega(|\vec{R}_j - \vec{r}|/c)\}\sigma_j^-, \quad (1)$$

where $\sigma_j^- = |-_j><+_j|$ is the lowering operator for the j-th two-level system (TLS) with upper (lower) levels described by the vectors $|\pm_j>$, and $\vec{n}$ is the unit vector from an emitter to the observation point; ω is the TLS transition frequency. Further, we term the right-hand part of Eq.(1) the array factor operator, $A(\vec{r})$. The task of designing the antenna involves determining positions $\vec{R}_j$ and the initial density matrix of the antenna, ρ, so as to achieve the necessary values of the average array operator (array factor) in the given directions or values of simultaneous correlation function of the nth order in the sets of directions $\{\vec{r}_k\}$, $k = 1 \ldots n$:

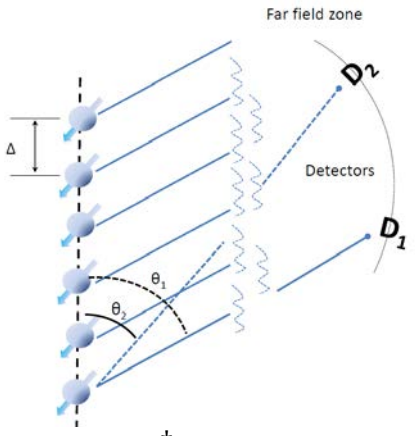

$$G^{(n)}(\vec{r}_1 \ldots \vec{r}_n) = < \left[\prod_{k=1}^{n} A(\vec{r}_k)\right]^{\dagger} \prod_{k=1}^{n} A(\vec{r}_k) >. \quad (2)$$

Fig. 1. The configuration of the equispaced linear antenna. The second-order correlation can be measured by simultaneous counts on the detectors $\boldsymbol{D_1}$ and $\boldsymbol{D_2}$.

The problem of antenna state design can be formulated as a state estimation problem in the following way. We specify a finite number of discrete sets of spatial observation points for which we will perform the antenna design $\{\vec{r}_{k,l}\}$, and re-write Eq.(2) as:

$$p_l = Tr\{\Pi_l \rho\}, \quad \Pi_l \propto \left[\prod_{k=1}^{n} A(\vec{r}_{k,l})\right]^{\dagger} \prod_{k=1}^{n} A(\vec{r}_{k,l}), \quad (3)$$

where the operators Π_l are semi-positive definite and can be considered as elements of a POVM (positive operator valued measure), while p_l can be considered as the set of targeted probabilities.

For illustration of the described method, we consider in some details optimization of the second-order correlation functions in the plane perpendicular to the dipole moments, and give a brief outline of other results. As given by Eq.(3), $G^{(2)}(\theta_1,\theta_2) \propto p(\theta_1,\theta_2) = Tr\{\Pi(\theta_1,\theta_2)\rho\}$, where

$$\Pi(\theta_1,\theta_2) = \sum_{j,m,n,q} \exp\{i\kappa\Delta((j-n)\cos(\theta_1)\}\exp\{i\kappa\Delta(m-q)\cos(\theta_2)\}\sigma_j^+\sigma_m^+\sigma_n^-\sigma_q^-,$$

κ is the wave-number and Δ is the distance between the dipoles; $\theta_{1,2}$ are the angles of the detectors. Let us aim, for example, for the co-directional correlation of emitted photons (i.e., for sharply peaked $G^{(2)}$ corresponding to $\theta_1 = \theta_2$). We consider two-excitation initial states of the antenna described by

$$|\psi>=\sum_{j=2}^{N}\sum_{m=1}^{j-1} c_{jm}\,|+_j,+_m>, \tag{4}$$

where summation is performed over all distinct pairs of indices $(j,m) \in [1,N]$, and the vectors $|+_j,+_m>$ describe the state of excited jth and mth TLSs with all the other TLSs in the lower state. We assume real c_{jm}. In Fig. 2 (a,b), one can see the results of optimization, which was done by minimizing the quadratic distance between the calculated $p(\theta_i,\theta_i;c_{jm})$ and the target (constant) value p_0 for 100 discrete angles θ_i in the range $[0,\pi]$. In Fig. 2(a), one can see that $G^{(2)}$ is sharply peaked around equal angles. The initial state of the antenna allowing to achieve such a correlation is shown in Fig. 2(b).

(a) (b)

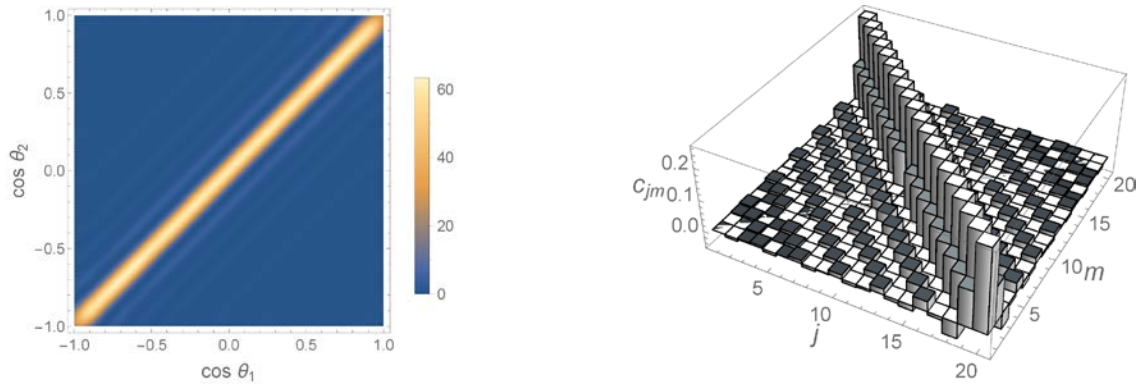

(c) (d)

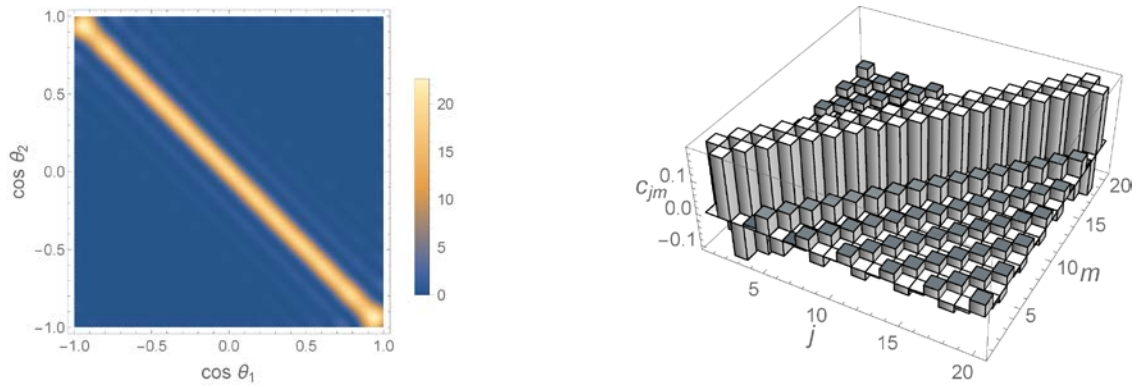

Fig. 2. (a) $\boldsymbol{G^{(2)}(\theta_1, \theta_2)}$ obtained as the result of optimization for generation of two co-direction photons; (b) the state (6) obtained as the results of optimization. For all the panels $\boldsymbol{N = 20}$; $\boldsymbol{\kappa\Delta = 2}$. (c) $\boldsymbol{G^{(2)}(\theta_1, \theta_2)}$ obtained as the result of optimization for generation of two contra-direction photons; (d) the state (6) obtained as the results of optimization. For all the panels $\boldsymbol{N = 20}$; $\boldsymbol{\kappa\Delta = 2}$.

One can also achieve the contra-directional correlation of the emitted photons, i.e. radiation pattern with $G^{(2)}$ sharply peaked around $\theta_2 = \pi - \theta_1$. The optimization results are shown in Fig. 2 (c, d). Strong contra-directional correlation is obvious. As a particular case of both co- and contra-directional emission we have considered also the state with the maximal directivity, when both photons are emitted in the direction, perpendicular to the antenna ($\theta_1 = \theta_2 = \pi/2$). As one would expect, the optimal state is close to the symmetric two-excitation Dicke state ($c_{jm} = const$ for all $j \neq m$).

Moreover, simple linear antenna allows for complete suppression of emission by choosing the state of the antenna. Just by attempt to minimize $G^{(2)}$ anywhere, one can get initial states of the antenna leading to strong field suppression in the far-field zone. Provided $\kappa\Delta < \pi$, such optimization can be successfully done leading to the state shown in Fig. 3.

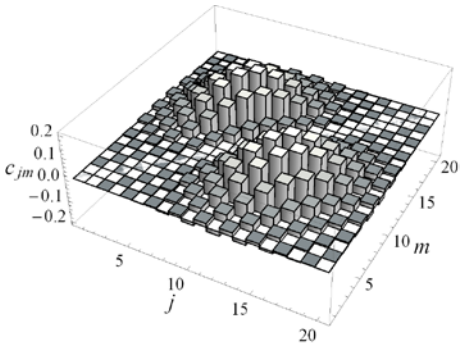

Fig. 3. The "dark" state (6) obtained as the result of optimization for $N = 20$, $\kappa\Delta = 2$.

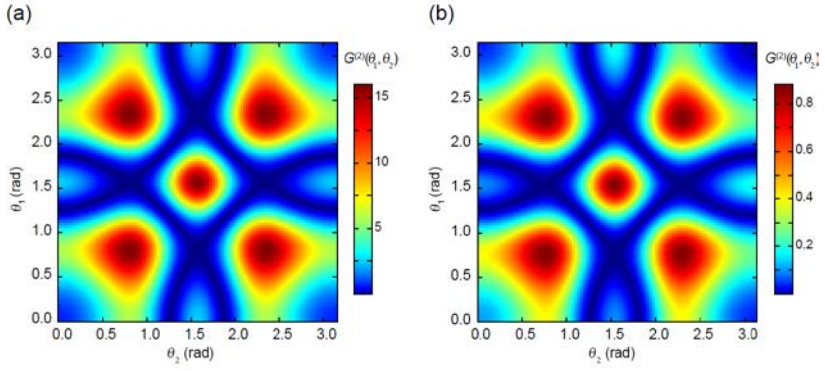

Fig. 4. (a) The quantum and (b) semi-classical $\boldsymbol{G^{(2)}}$ for the initial state giving contra-directional twin-photon correlation and $\boldsymbol{N = 3}$. Both plots are obtained for $\boldsymbol{\kappa\Delta = 4.5}$.

Considering the emitted field in the momentum space, it is possible to prove that the antenna states shown in Figs. 2(b) and 2(d) are entangled in momentum. Similarly, one can show that it is possible to design antenna states with three and more excitations leading to multi-photon

momentum entanglement in the emitted field. Despite the quantum character of the state expected to produce desired spatial patterns of the correlation functions, it is still possible using the appropriately modified semi-classical approach for this purpose and to model our antenna of non-interacting TLS with the semi-classical antenna of interacting TLS capturing the emitted field provided that one can capture dynamics of TLS correlation functions (1) [7,8]. In Fig. 4 the illustration of $G^{(2)}$ spatial patterns is given for quantum (a) and post-semi-classical models (b). Also, the state design can be combined with the geometry design for the antenna for shaping correlations functions, in particular, for reaching high directivity of the emission without the initial Dicke state of the antenna.

We believe that designing state for producing patterned higher-order correlation functions of the emitted field can be of importance for imaging and high-precision sensing, and for designing emitter-field interface for quantum information processing and transfer.

[1] C. A. Balanis, *Antenna theory - Analysis and Design*, John Wiley and Sons, Hoboken, New Jersey, 2005.

[2] R. Wiegner, J. von Zanthier, and G. S. Agarwal, "Quantum-interference-initiated superradiant and subradiant emission from entangled atoms", *Phys. Rev. A*, vol. 84, pp. 023805(1-10), *August* 2011.

[3] G. Y. Slepyan and A. Boag, "Quantum nonreciprocity of nanoscale antenna arrays in timed Dicke states", *Phys. Rev. Lett.*, vol. 111, pp. 023602(1-5), *July* 2013.

[4] A. N. Boto, P. Kok, D. S. Abrams, S. L. Braunstein, C. P. Williams, and J. P. Dowling, "Quantum Interferometric Optical Lithography: Exploiting Entanglement to Beat the Diffraction Limit", *Phys. Rev. Lett.*, vol. 85, pp. 2733-2736, *September* 2000.

[5] http://www.supertwin.eu/

[6] D. Bhatti, J. von Zanthier, and G. S. Agarwal, "Superbunching and Nonclassicality as new Hallmarks of Superradiance", *Scient. Rep.*, vol. 5, pp. 17335(1-8), *December* 2015.

[7] M. G. Benedict (ed.), *Super-radiance: Multiatomic Coherent Emission(Series in Optics and Optoelectronics)*, CRC Press, 1996.

[8] D. L. Boiko and P. P. Vasilâev, "Superradiance dynamics in semiconductor laser diode structures", *Opt. Exp.* vol. 20, pp. 9501-9515, *April* 2012.

8. PLASMONIC NANOLASER AND ITS APPLICATION

Pavel Melentiev[1], Alexey Kalmykov[1,2], Anton Gritchenko[1,3], Anton Afanasyev[1], Victor Balykin[1], Alexander Baburin[3,4], Elena Ryzhova[3,4], Ivan Filippov[3,4], Ilya Rodionov[3,4], Igor Nechepurenko[3,5,6], Alexander Dorofeenko[3,5,6], Ilya Ryzhikov[3,5], Alexey Vinogradov[3,5,6]

[1]Institute of Spectroscopy RAS, Troitsk, Moscow, Russia

[2]National Research University Higher School of Economics, Moscow, Russia

[3]Moscow Institute of Physics and Technology, Dolgoprudny, Russia

[4]Bauman Moscow State Technical University, Moscow, Russia

[5]Institute for Theoretical and Applied Electromagnetics RAS, Moscow, Russia

[6]Dukhov Institute of Automatics, Moscow, Russia

Corresponding authors' emails: melentiev@isan.troitsk.ru

Laser spectroscopy methods are used in many applications where extremely high sensitivity is needed [1]. In such methods, a detected substance (an analyte) being detected is chosen to absorbs light at the lasing wavelength and is placed in the laser cavity. The presence of the analyte and the measurement of its concentration is then accomplished by measuring corresponding dips in the lasing spectrum at absorption wavelengths of analyte.

The dynamics of a plasmonic nanolaser is described by characteristics in a similar way to traditional photonic laser [2,3]. Plasmonic laser intracavity spectroscopy was first proposed theoretically[4], and it was shown that, the use of plasmonic lasers can lead to an increase of up to two orders of magnitude in the efficiency of plasmonic sensors [5]. A number of studies show that addition of an analyte to the plasmonic nanolaser medium result in the modification of the plasmonic nanolaser spectrum [6] or its intensity[7].

We report demonstration of lasing in a *planar plasmonic DFB laser*, extending the idea and implementation of plasmonic DFB lasers reported elsewhere [7, 8]. The plasmonic DFB laser is build using a liquid gain medium and a perforated metallic film. The use of this "flow-through" liquid gain enables possibility of direct introduction of the analyte with maximal sensitivity and multiple operation. The plasmonic laser cavity is characterized by an ultra-low loss (40 cm^{-1}) and little volume of the gain medium (400 nL). Lasing at 630 nm, with a line width of 1.7 nm and directivity of 1.3° is observed. We demonstrate intracavity plasmonic laser spectroscopy using an

analyte concentration down to 70 ppb. We believe that our results open the way to practical developments compact sensors, based on the use of plasmonic nanolasers intracavity spectroscopy.

References

[1] V. Baev, T. Belikova, E. Sviridenkov and A. Suchkov, Zhurnal Eksperimental'noi i Teoreticheskoi Fiziki **74**, 43-56 (1978).

[2] M. Noginov, G. Zhu, A. Belgrave, R. Bakker, V. Shalaev, E. Narimanov, S. Stout, E. Herz, T. Suteewong and U. Wiesner, Nature **460**, 1110 (2009).

[3] M. I. Stockman, Nature Photonics **2**, 327-329 (2008).

[4] Y. E. Lozovik, I. Nechepurenko and A. Dorofeenko, Photonics and Nanostructures-Fundamentals and Applications **21**, 60-66 (2016).

[5] J. Homola, Chemical reviews **108**, 462-493 (2008).

[6] X.-Y. Wang, Y.-L. Wang, S. Wang, B. Li, X.-W. Zhang, L. Dai and R.-M. Ma, Nanophotonics **6**, 472-478 (2017).

[7] R.-M. Ma, S. Ota, Y. Li, S. Yang and X. Zhang, Nature nanotechnology **9**, 600-604 (2014).

[8] X. Meng, J. Liu, A. V. Kildishev and V. M. Shalaev, Laser & Phot. Rev. **8**, 896-903 (2014).

9. THE DEVELOPMENT OF HYBRID PLASMONIC NANOSTRUCTURES FOR MEDICAL APPLICATION

***Alexey Povolotskiy*[1], *Anastasia Povolotckaia*[2], *Alexander Konev*[1]**

[1] *Institute of Chemistry, Saint-Petersburg State University, Saint-Petersburg, Russia*
[2] *Centre for Optical and Laser Materials Research, Research Park, Saint-Petersburg State University, Saint-Petersburg, Russia*

In recent years, a large number of multi-disciplinary research teams having been working on the development and research of new nanomaterials with plasmonic effects that in the near future can be used for effective and minimally invasive treatment of incurable diseases at the moment. It is necessary to create new techniques that allow diagnosis and therapy in cases where standard therapies are ineffective. The development of nanotechnologies and their applications in the biomedical field has led to the appearance of a new discipline, which is widely known as the "Nanomedicine". Nanomedicine offers using the biocompatible nanoparticles with different physical, chemical and biological properties for the diagnosis and treatment. The small size allows to overcome biological barriers, to attach to the cells and to distribute throughout the body via the circulatory system. Progress in Inorganic Chemistry helps to synthesize biocompatible nanoparticles with desired physical and chemical properties. Furthermore, due to advances of surface chemistry, it is possible to modify nanoparticles (NPs) surface for highly specific binding to particular cells. Thus, the biocompatible NPs are the main candidates as the diagnostic and therapeutic agents. With the development of various methods for NPs synthesis one of the most perspective directions is the creation of hybrid nanostructures. The interest in such material, non-uniform in composition and structure, is determined by the new properties, which hybrid materials gain as a result of combination of the original nanocomponents. An important factor here is that in the nanoscale state, many substances acquire new properties. Furthermore, combining the various components in one structure enables not only to obtain a material having the additive properties of the starting components, but in some cases, give the hybrid structure new properties due to the synergistic effect. An example of this synergy effect is the luminescence intensity amplification due to association of fluorescent nanoparticles (quantum dots, nanoparticles with rare earth ions) and plasmonic nanoparticles (Au, Ag etc.).

Currently, fluorescent nanoparticles are widely used for the cancer diagnosis. Under optical excitation (lamp or laser) they exhibit luminescence with a sufficiently large quantum yield. When modifying the surface of fluorescent nanoparticles, they can accumulate in tumor tissues, which allows for optical or fluorescent localization of these tumors boundaries. Despite the progress in the creation of fluorescent nanoparticles, capabilities of diagnostic are limited to the low penetration

depth of optical radiation into the tissues, preventing non-superficial tumor to be detectable. Synthesis of hybrid NPs, consisted of luminescence particles and plasmon NPs, with enhanced luminescence allows to overcome this problem.

Another type of promising hybrid NPs are nanoparticles stabilized by photosensitizers are promising materials for improving its specificity including photodynamic therapy. Porphyrin-functionalized gold nanoparticles demonstrate perspective for their use in photodynamic therapy of cancer. Photoexcitation of porphyrins leads to the formation of cytotoxic singlet oxygen. Two different strategies are applied: the first - porphyrin complexes/gold nanoparticles increase the activity of singlet oxygen formation, partly due to a phase transfer of agent, associated with gold nanoparticles. The second strategy is that the gold nanoparticles are used as carriers of the porphyrins, which are then released into the cancer cells. Hybrid systems of porphyrin/gold nanoparticles have potential applications in various areas of medicine.

10. CHARACTERIZATION OF PATTERNED TEXTURE ON VERTICAL-CAVITY SURFACE-EMITTING LASERS

Shen-Che Huang, Ming-Cheng Chen, Tsu-Chi Chang, Kuo-Bin Hong and Tien-Chang Lu

Department of Photonics, College of Electrical and Computer Engineering, National Chiao Tung University, Tin Ka-Ping Photonics Building, No.1001, Ta-Hsueh Road, East District, Hsinchu City 30010, Taiwan
+886-3-5131234, timtclu@mail.nctu.edu.tw

It's well studied currently that resonances inside the two-dimension symmetric cavity which can sustain either single-mode operation or the directional optical output are confined whispering gallery modes along the circular cavity boundary. In order to increase mode selectivity, a common frequency-dependent feedback mechanism is utilized through optical resonant cavity. Besides, development of mode operation via feedback from a periodicity, or a periodic modulation in the gain of the active medium would offer feedback for enthralling lasing behaviors with much lower threshold. Two-type feedback mechanisms are illustrated as follows: one is the index-coupled structure would mainly enhance the side mode suppression, leading to single-mode operation. The other is a gain-coupled scheme for semiconductor devices has been applied on some semiconductor light emitters such as distributed feedback (DFB) lasers. Based on corresponding follow-up research combining index-coupled and gain-coupled approaches, the effects of a multi-harmonic periodicity has assumed in investigated mode interaction models. These resonances should maintain equal because of the balanced gain and loss. Moreover, vertical-cavity surface-emitting lasers (VCSELs) which could provide small-volume of vertical optical-confined cavity is essential for optical superior performance can be utilized by modifying the surface structures. The lateral mode with modified field distributions of vertical-cavity surface-emitting lasers (VCSELs) is determined by the limited aperture on top surface with symmetrical metal-covered ring. The textured surface on top could modified by etching central hole inside the emission aperture via focused ion beam milling technique. By altering the space from ring edge, we investigated the transverse mode through multiple analyses including near-field optical patterns and angle-resolved electroluminescence observations. We believe this achievement should have an impact on numerous photonic devices and helpful attribution to the proof of concept in solving quantum and simulated annealing problems in the future.

11. EFFECT OF ELASTIC DEFORMATION ON THE DISPERSION OF ELECTROMAGNETIC EXCITATIONS IN A CHAIN OF MICROCAVITIES

Vladimir Rumyantsev[1], Stanislav Fedorov[1], Konstantin Gumennik[1], Oleksiy Roslyak[2]

[1]A.A. Galkin Donetsk Institute for Physics & Engineering, Donetsk, Ukraine
tel.: +380 95 793 1135, e-mail: 380957931135@yandex.ru
[2]Fordham University, New York, USA
oroslyak@fordham.edu

1 Introduction. Results in crystal optics obtained during the past fifty years provide a solid foundation for the progress of modern photonics. Concepts developed in the physics of crystalline solids can potentially be applied to the physics of photonic supercrystals. Recent experiments and theoretical investigations reveal an intense interest for photonic structures and systems of coupled microresonators [1], whose applications include fabrication of clockworks of unprecedented accuracy [2] as well as the sources of coherent irradiation. A number of our recent works have been devoted to photonics of imperfect structures and to dispersion of exciton-like electromagnetic excitations in non-ideal lattices of coupled microresonators [3, 4]. Designing and utilization of novel materials for manufacturing of the sources of coherent irradiation is currently a vast interdisciplinary area, which spans various theoretical and fundamental aspects of laser physics, condensed matter physics, nanotechnology, chemistry as well information science [5, 6]. Physical realization of corresponding devices requires the ability to manipulate the group velocity of propagation of electromagnetic pulses, which is accomplished by the use of the so-called polaritonic crystals. The latter represent a particular type of photonic crystals featured by a strong coupling between quantum excitations in a medium (excitons) and optical fields.

We considered 1D polaritonic crystal as a topologically ordered system – chain of coupled microcavities containing quantum dots. The peculiarities of polariton spectrum in the 1D lattice of microcavities caused by uniform elastic deformation of the structure are considered. It is shown that as a result of elastic deformation of the system it is possible to achieve the necessary changes of its energy structure and optical properties caused by the restructuring of the polariton spectrum.

2 Theoretical background. Basing on the approach developed in Refs. [1,3,4], let us consider electromagnetic excitations in a lattice of microcavities composed of S sublattices. Each of tunnel-coupled microresonators is assumed to possess a single optical mode. Under elastic stress Hamiltonian $\hat{H}(\hat{\varepsilon})$ of resonator-localized electromagnetic excitations is a function of deformation tensor $\hat{\varepsilon}$.

Under assumption that the density of excited states of constituent elements in resonator and atomic systems is a small quantity and within the one-level model and Heitler-London approximation Hamiltonian $\hat{H}\left(\hat{\varepsilon}\right)$ has the form (see Ref. [7]):

$$\hat{H}\left(\hat{\varepsilon}\right)=\sum_{\substack{\mathbf{n},\mathbf{m},\alpha,\beta,\\ \lambda,\sigma}} D^{\lambda\sigma}_{\mathbf{n}\alpha,\mathbf{m}\beta}\left(\hat{\varepsilon}\right)\hat{\Phi}^{+}_{\mathbf{n}\alpha\lambda}\hat{\Phi}_{\mathbf{m}\beta\sigma}=\sum_{\substack{\alpha,\beta,\lambda,\sigma\\ \mathbf{k}}} D^{\lambda\sigma}_{\alpha\beta}\left(\mathbf{k},\hat{\varepsilon}\right)\hat{\Phi}^{+}_{\alpha\lambda}\left(\mathbf{k}\right)\hat{\Phi}_{\beta\sigma}\left(\mathbf{k}\right), \tag{1}$$

where

$$D^{11}_{\mathbf{n}\alpha,\mathbf{m}\beta}\left(\hat{\varepsilon}\right)=\hbar\omega^{at}_{\mathbf{n}\alpha}\delta_{\mathbf{n}\alpha,\mathbf{m}\beta}+V_{\mathbf{n}\alpha,\mathbf{m}\beta}\left(\hat{\varepsilon}\right),\ D^{22}_{\mathbf{n}\alpha,\mathbf{m}\beta}=\hbar\omega^{ph}_{\mathbf{n}\alpha}\delta_{\mathbf{n}\alpha,\mathbf{m}\beta}-A_{\mathbf{n}\alpha,\mathbf{m}\beta}\left(\hat{\varepsilon}\right),$$

$$D^{12}_{\mathbf{n}\alpha,\mathbf{m}\beta}\left(\hat{\varepsilon}\right)=D^{21}_{\mathbf{n}\alpha,\mathbf{m}\beta}\left(\hat{\varepsilon}\right)=g_{\mathbf{n}\alpha}\left(\hat{\varepsilon}\right)\delta_{\mathbf{n}\alpha,\mathbf{m}\beta},\qquad \hat{\Phi}^{\lambda=2}_{\mathbf{n}\alpha}=\hat{\Psi}_{\mathbf{n}\alpha},\ \hat{\Phi}^{\lambda=1}_{\mathbf{n}\alpha}=\hat{B}_{\mathbf{n}\alpha} \tag{2}$$

In Eqs. (1,2) $\omega^{ph}_{\mathbf{n}\alpha}$ is the frequency of the photonic mode localized in the $\mathbf{n}\alpha$-th lattice site (resonator), $\hat{\Psi}^{+}_{\mathbf{n}\alpha},\hat{\Psi}_{\mathbf{n}\alpha}$ are Bose creation and annihilation operators of this mode written in the node representation, $\hbar\omega^{at}_{\mathbf{n}\alpha}$ is excitation energy of a quantum dot in the $\mathbf{n}\alpha$-th lattice site, $\hat{B}_{\mathbf{n}\alpha},\hat{B}^{+}_{\mathbf{n}\alpha}$ are Bose creation and annihilation operators of this excitation, $A_{\mathbf{n}\alpha\mathbf{m}\beta}\left(\hat{\varepsilon}\right)$ is the matrix of resonance interaction, which describes an overlap between optical fields of resonators in the $\mathbf{n}\alpha$-th and $\mathbf{m}\beta$-th lattice sites and hence defines the jump probability of the corresponding electromagnetic excitation, $V_{\mathbf{n}\alpha\mathbf{m}\beta}\left(\hat{\varepsilon}\right)$ is the matrix of resonance interaction between quantum dots embedded in the $\mathbf{n}\alpha$-th and $\mathbf{m}\beta$-th lattice sites, $g_{\mathbf{n}\alpha}\left(\hat{\varepsilon}\right)$ is the matrix of resonance interaction between quantum dot in the $\mathbf{n}\alpha$-th lattice site with electromagnetic field localized at the same site. Values 1 and 2 of indices λ,σ indicate, correspondingly, presence or absence of quantum dots in corresponding cavities.

In the last expression of Eq. (1) (summation over $\mathbf{k}$) matrices $D^{\lambda\sigma}_{\alpha\beta}\left(\mathbf{k},\hat{\varepsilon}\right)$ and $\Phi_{\alpha\lambda}\left(\mathbf{k}\right)$ have the forms $D^{\lambda\sigma}_{\alpha\beta}\left(\mathbf{k},\hat{\varepsilon}\right)=\sum_{\mathbf{m}} D^{\lambda\sigma}_{\mathbf{n}\alpha\mathbf{m}\beta}\left(\hat{\varepsilon}\right)\exp\left[i\mathbf{k}\cdot\left(\mathbf{r}_{\mathbf{n}\alpha}-\mathbf{r}_{\mathbf{m}\beta}\right)\right]$ and $\hat{\Phi}_{\alpha\lambda}\left(\mathbf{k}\right)=\frac{1}{\sqrt{N}}\sum_{\mathbf{n}}\hat{\Phi}_{\mathbf{n}\alpha\lambda}\exp\left(-i\mathbf{k}\cdot\mathbf{r}_{\mathbf{n}\alpha}\right)$ (N is the number of elementary cells in the lattice). Such representation of matrices is possible due to preservation of translation invariance of the system under uniform deformations. Let us not that the wave vector $\mathbf{k}$, which characterizes eigenstates of electromagnetic excitations, varies within the first Brillouin zone. The latter under a uniform deformation is a function of deformation $\hat{\varepsilon}$.

Calculation of eigenvalues of Hamiltonian (1) is carried out by its diagonalization through Bogolyubov-Tyablikov transformation [7]. This yields the following equation for elementary excitation spectrum $\Omega\left(\mathbf{k},\hat{\varepsilon}\right)$:

$$\det\left\|D_{\alpha\beta}^{\lambda\sigma}\left(\mathbf{k},\hat{\varepsilon}\right)-\hbar\Omega\left(\mathbf{k},\hat{\varepsilon}\right)\delta_{\alpha\beta}\delta_{\lambda\sigma}\right\|=0 \tag{3}$$

Below we carry out a detailed investigation of the spectrum and on this basis evaluate a number of related quantities of interest, such as the effective mass of excitations and some others.

3 Results and discussion. It is of substantial interest to investigate electromagnetic excitations in a non-ideal one-dimensional microcavity lattice subjected to a uniform elastic stress. Let us consider a one-sublattice chain of identical cavities with randomly embedded quantum dots of two types, whose concentrations are, correspondingly, $C_C^{(1)}$ and $C_C^{(2)}$. Moreover, these microcavity-resonators are also randomly removed at distances between the nearest neighbors either $a_1\left(\varepsilon\right)$ with concentration $C_T^{(1)}$ or $a_2\left(\varepsilon\right)$ with concentration $C_T^{(2)}$. In order to calculate polaritonic spectrum $\Omega\left(k,\varepsilon\right)$ of such a system we shall adopt the virtual crystal approximation [14,15], which is based on diagonalization of the averaged Hamiltonian (1). This procedure yields a system uniform linear equations, whose solvability condition is formulated as the equality of the following determinant to zero:

$$\left\|\begin{matrix}\hbar\left\langle\omega_n^{at}\left(\varepsilon\right)\right\rangle_C+\left\langle V\left(k,\varepsilon\right)\right\rangle_{C,T}-\hbar\Omega\left(k,\varepsilon\right) & \left\langle g_n\left(\varepsilon\right)\right\rangle_C \\ \left\langle g_n\left(\varepsilon\right)\right\rangle_C & \hbar\omega^{ph}\left(\varepsilon\right)-\left\langle A\left(k,\varepsilon\right)\right\rangle_T-\hbar\Omega\left(k,\varepsilon\right)\end{matrix}\right\|=0 \tag{9}$$

Angular brackets in (9) denote the procedure of configuration averaging of microcavity array over all possible positions of cavities (index “T”) and composition of quantum dots (index “C”).

The numerical calculations were carried out within the nearest-neighbor approximation for the following modeling values of parameters. The frequency of cavity-localized resonance photonic modes was put equal to $\omega^{ph}=2\pi\times387{,}5\,THz\approx2434\cdot10^{12}\,Hz$, the two types of quantum dots were assumed to posses excitation frequencies $\omega_1^{at}=2\pi\cdot191\,THz\approx1200\cdot10^{12}\ Hz$ and $\omega_2^{at}=2\pi\cdot202\,THz\approx1269\cdot10^{12}\ Hz$, whereas $A/2\hbar=8\cdot10^{13}\,Hz$, $V^{11}/2\hbar=1\cdot10^{13}\,Hz$, $V^{22}/\hbar=3\cdot10^{13}\,Hz$, $V^{12}\approx V^{21}=6\cdot10^{13}\,Hz$, $g^{(1)}/\hbar=5\cdot10^{12}\ Hz$, $g^{(2)}/\hbar=1.5\cdot10^{12}\ Hz$ (within the adopted approximation the magnitude of resonance interaction of a quantum dot with electromagnetic field localized at the same cavity is independent of deformation ε), lattice periods are $a_1=3\cdot10^{-6}m$ and $a_2=7\cdot10^{-6}m$. The surfaces, which describe the dispersion dependence of

frequencies $\Omega_{\pm}(k, C_C, C_T, \varepsilon)$ of the considered collective excitations in the microcavity array are plotted in Fig. 1 for concentration values $C_T = 0.6$ and $C_C = 0.3$. It should be remembered that k ranges between $-\frac{\pi}{a_2(\varepsilon)+C_T\left[a_1(\varepsilon)-a_2(\varepsilon)\right]} \le k \le +\frac{\pi}{a_2(\varepsilon)+C_T\left[a_1(\varepsilon)-a_2(\varepsilon)\right]}$.

4 Conclusion. The study of the spectrum of elementary electromagnetic excitations in a binary one-dimensional array of tunnel-coupled microcavities shows that subjecting the system to controlled elastic stress is an effective tool for altering its energy structure and optical properties.

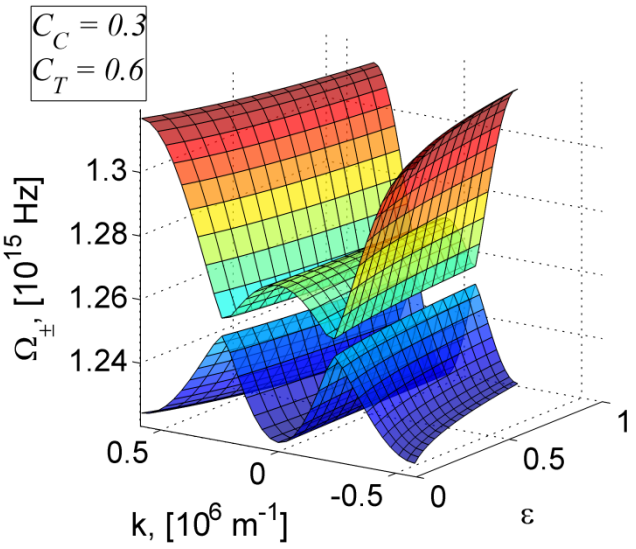

Fig. 1. The dependence of dispersion frequencies $\Omega_{\pm}(k, C_C, C_T, \varepsilon)$ of electromagnetic excitations in a nonideal chain of microcavities on elastic deformation.

The presence of deformation and of structural defects may lead to the in increase of the effective mass of corresponding excitations and therefore to a decrease of their group velocity. The results of numerical calculation performed on the basis of the constructed model contribute to modeling of the new class of functional materials – photonic crystalline system constituted of couple microcavities. Their capabilities include the controllable propagation of electromagnetic excitations.

References

1. A.P. Alodjants, I. O. Barinov, S. M. Arakelian, J Phys B: At. Mol. Opt. Phys **43**, 095502 (2010).
2. D. Hou, B. Ning, J. Wu., Z. Wang. and J. Zhao, Appl Phys Lett **102**, 151104 (2013).

3. V.V. Rumyantsev, S.A. Fedorov, K.V. Gumennyk, M.V. Sychanova, A.V. Kavokin, Nature Sci. Rep. **4,** 6945 (2014).
4. V.V. Rumyantsev, S.A. Fedorov, K.V. Gumennyk, Low Temperature Physics **42**, 447-454 (2016).
5. W. Cai, and V. Shalaev, Optical Metamaterials: Fundamentals and Applications, Springer-Verlag, New York (2010).
6. M. Razeghi., Technology of Quantum Devices, Springer, New York, London (2009).
7. V.M. Agranovich Theory of Excitons. Moscow. Nauka Publishers, 1968.

12. MAGNETIC FIELD CONTROL OF THE POLARITON SPIN DYNAMICS

E. S. Sedov,[1,2] A. V. Kavokin[3,2,4]

[1]Department of Physics and Applied Mathematics, Vladimir State University named after A. G. and N. G. Stoletovs, Gorky Street 87, 600000, Vladimir, Russia

[2]School of Physics and Astronomy, University of Southampton, SO17 1NJ Southampton, United Kingdom

[3]CNR-SPIN, Viale del Politecnico 1, I-00133, Rome, Italy

[4]Spin Optics Laboratory, St. Petersburg State University, Ul'anovskaya 1, Peterhof, St. Petersburg 198504, Russia

Powering the optical communications with their global reach and a vast spectrum of other applications of photonics, new generations of optoelectronic devices and materials have been changing our lives. Polaritonics is the interdisciplinary research area, which is at the heart of modern light technologies and launched at the boundary of laser physics, quantum physics, solid-state physics, quantum information and material science. The main distinguishing feature of Polaritonics is the peculiar composite nature of the subjects of the study, quasiparticles exciton-polaritons. The latter arise from the interaction of light with excitations of a semiconductor medium (excitons). Polaritons combine properties of both their constituents. Due to the presence of a photon component, polaritons can be easily excited retaining the characteristics of the exciting signal. The exciton component provides a wide range of possibilities for controlling the polariton state since excitons are highly sensitive to an external impact of various origins. Polaritons inherit angular momentum projections on the quantum well growth axis of the parent excitons. The bright excitons with the projections ±1 couple with cavity photons of two opposite circular polarizations, σ^+ (right) and σ^- (left), respectively, and form a polariton spin doublet state. This doublet can be described by the pseudospin vector **S** whose behavior in time is governed by the effective magnetic fields of different origin.

In this work, we consider the mechanisms of dynamic control of the polariton pseudospin in semiconductor microcavities through manipulation by properties of excitons under the strong matter-field coupling by an external magnetic field applied in different geometries.

The cavity polariton polarization is mostly dependent on the long-range electron-hole exchange interaction and the polarization splitting of the photonic cavity modes. In particular, the longitudinal-transverse (LT) splitting of the cavity eigenmodes leads to the splitting of linearly polarized polaritons that induces the precession of the pseudospin vector of propagating polaritons. The polariton LT splitting effect can be described as the polariton pseudospin precession around an effective magnetic field applied in the cavity plane [1]. The non-trivial polariton pseudospin dynamics has been revealed in a wide range of experimentally observed effects including the polarization multistability [2], spin switching [3], optical spin Hall effect [4], etc. In the presence of the external magnetic field **B**, the polariton pseudospin dynamics becomes even more complicated.

We consider the pseudospin dynamics of long-living polaritons in a 2D microcavity under the effect of the external magnetic field applied in the Faraday geometry (normally to the cavity plane) [5]. In this geometry, the exciton-polariton energy band structure is enriched with the Zeeman splitting of σ^+ and σ^- polarized polariton states. We reveal the influence of the magnetic field on the interference of ballistic polaritons in the microcavity with the linear gradient of its width as well on the effect of *zitterbewegung*, the jitter of the trajectory of polaritons due to the effect of the LT-splitting.

We demonstrate the direct control of the polariton spin dynamics in the semiconductor cavity through the application of the external magnetic field in the Voigt geometry. The magnetic field acting on spin-resolved electrons and holes gives rise to the mixing of bright and dark exciton states making them interrelated. We show the effect of suppression of the optical spin Hall effect for the polaritons propagating in a given direction by the magnetic field with the chosen magnitude and direction in the 1D geometry. In the 2D geometry we demonstrate deformation of the in-real-space polarization patterns under the in-plane external magnetic field. The considered effects can be described with a simple quasi-analytical nonlinear model for the polariton pseudospin dynamics.

This work was supported by the EPSRC Programme grant on Hybrid Polaritonics No. EP/M025330/1. The work of E.S.S. was supported by the Russian Foundation for Basic Research Grants No. 16-32-60104, No. 15-59-30406, and by the grant of President of Russian Federation for state support of young Russian scientists No. MK-8031.2016.2. A.V.K. acknowledges the partial support from the HORIZON 2020 RISE project CoExAn (Grant No. 644076).

[1] I. A. Shelykh, Y. G. Rubo, & A. V. Kavokin, "*Renormalized dispersion of elementary excitations in spinor polariton condensates*", Superlattices and Microstructures **41**, 313–320 (2007).
[2] Gippius, N. A. *et al.*, "*Polarization Multistability of Cavity Polaritons*", Phys. Rev. Lett. **98**, 236401 (2007).
[2] Amo, A. *et al.*, "*Exciton-polariton spin switches*", Nature Photonics **4**, 361–366 (2010).
[3] Kochereshko, V. P. *et al.*, "*Lasing in Bose-Fermi mixtures*", Sci. Rep. **6**, 20091 (2016).
[4] E. S. Sedov & A. V. Kavokin, "*Artificial gravity effect on spin-polarized exciton-polaritons*", Sci. Rep. **7**, 9797 (2017).

13. OPTICAL PROPERTIES OF β-BBO AND POTENTIAL FOR THZ APPLICATIONS

N. A. Nikolaev[1, 2], Yu. M. Andreev[3, 4], T. B. Bekker[5], G. V. Lanskii[3, 4], V. A. Svetlichnyi[1, 4], A. A. Mamrashev[1, 2], D. M. Ezhov[4], V. D. Antsygin[2], A. E. Kokh[5], K. A. Kokh[5]

[1] High Current Electronics Institute SB RAS, 2/3 Akademicheskii Ave., 634055, Tomsk, Russia,
[2] Institute of Automation and Electrometry SB RAS, 1 Academician Koptyug Ave., 630090, Novosibirsk, Russia
[3] Institute of Monitoring of Climatic and Ecological Systems SB RAS, 10/3 Akademicheskii Ave., 634055, Tomsk, Russia
[4] Siberian Physical Technical Institute of Tomsk State University, 1 Novosobornaya Sq., 634050, Tomsk, Russia
[5] Institute of Geology and Mineralogy SB RAS, 3 Academician Koptyug Ave., 630090, Novosibirsk, Russia
nazar@iae.nsk.su

The anisotropy of optical properties of high quality beta barium borate crystal (β-BaB_2O_4, β-BBO) was studied in the main transparency window by using classic spectroscopic methods and facility, and in the 0.2 – 2 THz range by using THz time-domain spectroscopy. β-BBO crystals were grown by the top-seeded solution technique in a highly resistive furnace with a heat field of 3-fold axis symmetry. At room temperature (RT), absorption coefficient in the maximal transparency window in grown crystals did not exceed 0.05 cm^{-1}. Strong absorption anisotropy was observed in 3 – 5 μm and the THz range. At 1 THz absorption coefficients for *e* and *o* wave were, respectively, 7 cm^{-1} and 21 cm^{-1} at RT; 2 cm^{-1} and 10 cm^{-1} at 81 K. At the most attractive for out-of-door applications range <0.4 THz, absorption coefficient is found to be very low: below 0.2 cm^{-1} at RT and 1 cm^{-1} at 81 K that is favorable for long THz wave generation. Refractive index dispersions measured by THz-TDS were approximated in the form of Sellmeier equations. Birefringence is found quite large for phase matched difference frequency generation (DFG) or down-conversion into the THz range (THz-DFG) under near IR pump at RT and 81 K. Type II (*oe-o* and *eo-o*), and type I (*ee-e*) three wave interactions can be realized at RT. THz-DFG of Nd:YAG laser and KTP OPO can be realized by type II (*oe-o*) three-wave interaction. For selected spectral ranges of femtosecond Ti:Sapphire laser efficient phase matched and group velocity matched optical rectification can be realized by another two types of three wave interactions. Accounting other well-known attractive physical properties of β-BBO crystal, wide application in THz technique can be forecasted.

14. FORMATION OF NONCLASSICAL STATES OF LOCALIZED PLASMONS IN THE SPASER SYSTEMS CONTROLLED BY EXTERNAL MAGNETIC FIELD

A.V. Shesterikov, S.N. Karpov, M.Yu. Gubin, A. V. Prokhorov

Vladimir State University named after Alexander and Nikolay Stoletovs,

87 Gorkogo Str., Vladimir 600000, Russia

*Tel: +7(910)7773068; e-mail: **avprokhorov33@mail.ru***

Quantum dynamics of localized plasmons in spaser systems, consisting of metal nanoparticles and semiconductor quantum dots, are theoretically investigated. Generation of the nonclassical plasmons in the many-particle spaser system with nonlinear plasmon-exciton interaction

is predicted.

Стремительный прогресс последних лет в области нанотехнологий привел к возможности практической реализации принципиально новых устройств генерации и управления параметрами электромагнитного излучения на основе одиночных квантовых излучателей [1], а также высокодобротных микро [2] и нанорезонаторов [3]. На пути миниатюризации подобных устройств ключевым моментом стало создание уникального устройства – нанолазера [4], для описания работы которого потребовалось переформулировать известные условия лазерной генерации на случай субволновых масштабов. В основу такого описания может быть положена модель локализованного спазера [5], в самом простом случае состоящего из связанных ближним полем полупроводниковой квантовой точки (КТ) и металлической наночастицы (НЧ). КТ выступает здесь в качестве эффективной накачки, поскольку в процессе распада имеющихся в ней экситонов происходит возмущение ближнего поля КТ. При соблюдении условий плазмон-экситонного резонанса это возмущение приводит к эффективной передаче энергии от КТ к НЧ и возбуждению локализованных на поверхности НЧ плазмонов [6]. Для целей квантовой обработки информации [7] наибольший интерес связан с массивами нелинейных спазеров, в том числе - цепочечными спазерными моделями, состоящими из большого числа парных НЧ и КТ [8].

В настоящей работе рассматривается возможность управления квантовыми статистическими и корреляционными свойствами генерируемых в многочастичном спазере плазмонов. Для этого, стандартная модель двухчастичного спазера расширяется на случай массива расположенных на малом расстоянии НЧ и КТ, объединенных сильными диполь-

дипольными взаимодействиями. На основе квантования поля НЧ и КТ осуществлен последовательный вывод расширенного гамильтониана Джейнса-Каммингса на случай нелинейных диполь-дипольных плазмон-экситонных взаимодействий в спазерной системе (сборке) в том числе – с учетом двухквантовых процессов распада биэкситонных состояний КТ. Полученные коэффициенты при соответствующих слагаемых гамильтониана являются функциями управляющих параметров системы. Нелинейный режим работы рассматриваемого устройства подразумевает значительную разность в значениях частот плазмонного резонанса в НЧ и энергии экситона в КТ. Тогда, в зависимости от соотношения частот отстроек, размеров нанообъектов и расстояний между ними в системе возможна реализация условий как для эффективной генерации локализованных на НЧ плазмонов с неклассической статистикой, так и перепутанных плазмонов, возникающих под действием внешней волны накачки. Исследовано дополнительное влияние внешнего магнитного поля на процессы двухквантовых переходов при распаде биэкситонных состояний КТ в спазерных системах. Показана возможность управления квантовой кинематикой рассматриваемой системы посредством изменения параметров внешнего магнитного поля.

Рассмотренные в работе процессы могут быть использованы для реализации протоколов квантовой обработки информации с локализованными плазмонами.

Работа выполнена в рамках государственного задания ВлГУ 2017 г. в сфере научной деятельности.

Литература

1. D. Bimberg, N. Kirstaedter, N.N. Ledentsov, Zh.I. Alferov, P.S. Kop'ev, V.M. Ustinov// IEEE Journal of Selected Topics in Quantum Electronics. 1997. V. 3. P.196.

2. М.Л. Городецкий. Оптические микрорезонаторы с гигантской добротностью. – М. Физматлит, 2011, 416 с.

3. E.J.R. Vesseur, R. de Waele, H.J. Lezec, H.A. Atwater, F.J. García de Abajo, and A. Polman// Appl. Phys. Lett. 2008. V.92.P 083110.

4. M.A. Noginov, G. Zhu, A.M. Belgrave, R. Bakker, V.M. Shalaev, E.E. Narimanov, S. Stout , E. Herz, T. Suteewong, and U. Wiesner// Nature. 2009. V. 460. P1110.

5. M.I. Stockman// J. Opt. 2010. V.12.P.024004.

6. А.П. Виноградов, Е.С. Андрианов, А.А. Пухов, А.В. Дорофеенко, А.А. Лисянский// УФН.2012.Т.182.С.1122.

7. G.I. Struchalin, I.A. Pogorelov, S.S. Straupe, K.S. Kravtsov, I.V. Radchenko, and S.P. Kulik// Phys. Rev. A.2016.V. 93.P.012103.

8. S.V. Fedorov, N.N. Rosanov, A.V. Chipouline, and T. Pertsch// J. Opt. Soc. Am. B. 2015. V. 32. P. 824.

15. NONLINEAR BIFURCATION DIAGRAMS OF THE CURRENT STATES OF MICROCAVITY EXCITON-POLARITONS IN THE LATTICE

Igor Chestnov[1], Alexey Yulin[2] and Oleg Egorov[3]

[1]Vladimir State University named after A. G. and N. G. Stoletovs,

Gorkii St. 87, 600000, Vladimir, Russia Federation

[2]ITMO University 197101, Kronverksky pr. 49, St. Petersburg, Russia

[3]Technische Physik, Physikalisches Instität and Wilhelm Conrad Röntgen-Center for Complex Material Systems, Universität Würzburg, Am Hubland, D-97074 Wüzburg, Germany

E-mail: igor_chestnov@mail.ru

Study of the behavior of arranged arrays of interacting quantum particles have long attracted attention of researches working with solid state physics, many-body theories, quantum computing etc. Although the progress in manipulation of cold atoms localized in optical lattices and one-dimensional arrays is rather spectacular the requirement of extremely low temperatures prevents from considering such systems as a convenient tool. On the other hand exciton polaritons formed in semiconductor structures are known to maintain their quantum properties implying formation of the coherent condensate under high (up to room) temperatures.

The interaction of separate polariton condensates was always under special attention. For instance, phase locking and synchronization due to radiative coupling were recently demonstrated in polariton systems [1, 2]. At the same time a number of different techniques allowing to confine polariton quasiparticles in the lattice were developed. They imply microcavity etching [3], deposition of the metal on the surface of microcavity Bragg mirror [4], fabrication of mesa traps [5], surface acoustic waves [6] etc. So, the study of collective coherent properties of polariton condensates in these systems represents an intriguing task for modern polariton physics. In particular, coherent tunnelling of polaritons between neighboring potential wells were intensively investigated experimentally. For instance, besides a conventional in-phase ground state, a spontaneous build-up of anti-phase (π-state) “superfluid” states was observed in both weak-contrast periodical lattices [4, 6] as well as in chains of deep trapping potentials [5].

Several explanations of this phenomenon was proposed recently, which requires accounting for nonequilibrium processes of polariton-polariton interaction [5] or tacking into account dissipative coupling [1, 2]. However as it was shown by some of authors [7] the key properties of periodical chain of polariton condensates can be described in terms of stability of the different states formed from the initial noise during condensation processes. Thus stability analysis provides a basis

for study of dynamical properties of polariton condensate as well as of formation of localized structures and patterns in such systems.

The stability properties of polariton condensates in different geometries including plane two-dimensional microcavity [8, 9], ring-shape structures [10] etc. were investigated previously. However the systems of polaritons in a lattice were out of consideration in this context. Here we provide a comprehensive theoretical study of the nonlinear dynamics of the open-dissipative exciton-polariton condensate in a weak-contrast periodic one-dimensional structures. We consider condensate formed in the semiconductor microcavity by the nonresonant pump which is responsible for the formation of reservoir of incoherent excitons. The influence of the nonlinear exciton-exciton interaction on the system properties were studied in details. It is shown that under certain value of external pump there is a bifurcation of the solution leading to the appearance of a family of essentially nonlinear states. The special feature of these solutions is that its current does not vanish when the quasi-momentum of the state approaches the end of Brillouin zone. The appearance of such current state is accompanied with the formation of energy-loops both at the center and at the end of Brillouin zone.

References

[1] I.L. Aleiner, B.L. Altshuler, and Y.G. Rubo, Phys. Rev. B 85, 121301(R) (2012)

[2] H. Ohadi, R.L. Gregory, T. Freegarde, Y.G. Rubo, A.V. Kavokin, and P.G. Lagoudakis, arXiv:1406.6377 (2014).

[3] T. Jacqmin et al., Phys. Rev. Lett. 112, 116402 (2014).

[4] C. Lai et al., Nature 450, 529 (2007).

[5] K. Winkler et al., Phys. Rev. B 93, 121303(R) (2016).

[6] E.A. Cerda-M´endez et al., Phys. Rev. Lett. 105, 116402 (2010).

[7] A.V. Yulin et al., Phys. Rev. B 94, 054312 (2016).

[8] L.A. Smirnov, D.A. Smirnova, E.A. Ostrovskaya, and Y.S. Kivshar, Phys. Rev. B 89, 235310 (2014).

[9] N. Bobrovska, E.A. Ostrovskaya, and M. Matuszewski, Phys. Rev. B 90, 205304 (2014).

G. Li, M.D. Fraser, A. Yakimenko, E.A. Ostrovskaya, Phys. Rev. B 91, 184518 (2015).

16. INTERRELATION OF THE SUBWAVE GOLD FILM'S MORPHOLOGY ON SILICON AND THE EFFICIENCY OF THE SECOND OPTICAL HARMONIC GENERATION UNDER ULTRAHIGH VACUUM CONDITIONS

Sinko A.S.*, Aksenov V.N., Kozlov I.S., Ozheredov I.A., Shkurinov A.P.

Lomonosov Moscow State University, Moscow, 119991, Russia
*E-mail: Sinko-260395@mail.ru

The research results of second-harmonic generation (SHG) on a clean surface of silicon and thin gold films deposited on it are presented. Silicon (111) samples were studied in the experiments. Special attention was paid to control of the surface cleanness and the effect of this factor on the nonlinear optical conversion efficiency.

Experimental setup

To observe generation of the second-harmonic (SH) on the surface of silicon with thin films, the experimental setup shown in Figure 1 was assembled.

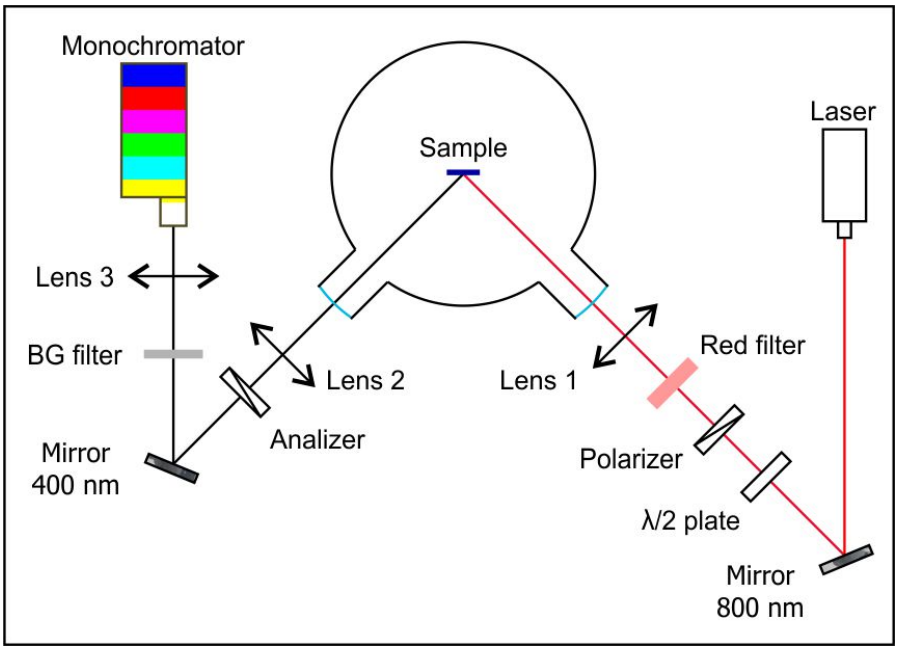

Fig. 1: The scheme of the experimental setup

The sample was placed in a chamber where a vacuum of not worse than 10^{-9} mbar was maintained. The radiation source was a pulsed laser with a wavelength of 805 ± 10 nm, a pulse duration of 100 fs and a repetition rate of 10 MHz, an average power of 50 mW, a peak power of 50 mW. The laser radiation was directed to the sample through the quartz window at an incidence angle of 45°. The reflected radiation of the fundamental frequency and the SH radiation were extracted from the vacuum chamber through the second quartz window. The polarization orientation of the incident radiation could be changed by means of a Glan-Taylor prism and a half-

wave plate. The polarization state of the SH radiation generated on the sample was analyzed with the help of the second Glan-Taylor prism. By means of the optical blue-green (BG) filter only the SH radiation was directed to the spectrograph input to be recorded by a cooled CCD camera.

Results

In this work, three different surface cleaning modes were used:

- Heating to a temperature of several hundred degrees using a helix placed under the sample, through which current was passed. (resistive heating)
- Annealing by direct current passing through a silicon sample. (direct heating)
- Annealing by short high current pulses, so that the sample was heated to an orange glow. (flashing)

A comparison of the SHG efficiency was made between samples that had not undergone special preparation in a vacuum, with samples that had only passed through the first stage of purification, and also with samples that had passed all three stages of purification. The silicon surface quality control was carried out using an Auger spectrometer. The results are shown in Figure 2.

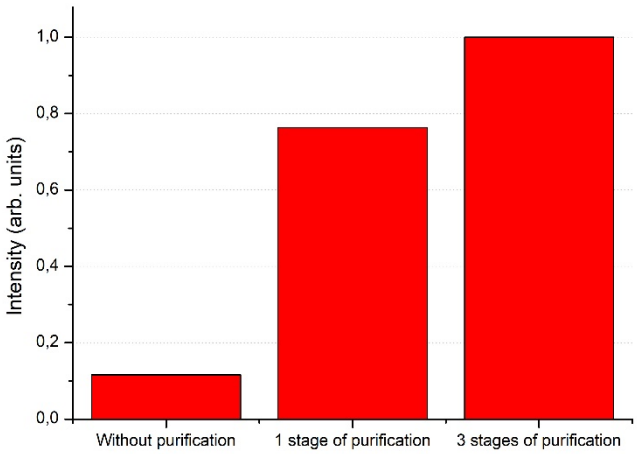

Fig. 2: Comparison of the SH signal in relation to the degree of the silicon surface purification. The normalization was performed on the result for the third stage of purification

From the presented diagram it can be concluded that surface cleaning plays a significant role in the efficiency of SHG.

The next step was to study the generation of SH on thin gold films deposited on the silicon surface. Sputtering was carried out by electron-beam evaporation in an ultrahigh vacuum. The thickness of the film was measured with a quartz thickness sensor. It should be noted that for small thicknesses a gold film on silicon is of an island structure. Therefore, the thickness designation used

in the work is an effective value of the thickness, as if the film lies on the surface as a continuous layer. The film quality was analyzed using an electron and scanning tunneling microscope. The island character was observed for all films made in the work.

The analysis of the gold droplets' size for different films was carried out using a special program for image processing. The images obtained from the electron microscope were analyzed. Figure 3 shows an example of an image for a film with an effective thickness of 10 Å after and before analysis.

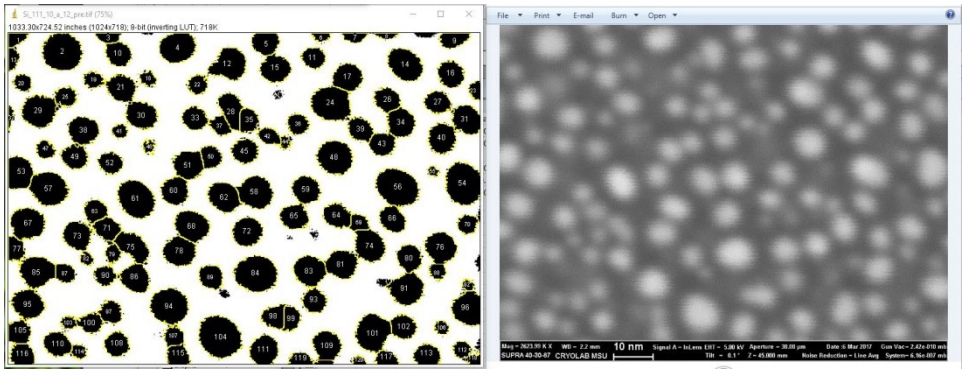

Fig. 3: An example of a program for image processing of film

In the analysis it was assumed that the particles have a spherical or hemispherical shape with approximately the same radius and are located at equal distances. Based on these assumptions and analysis of the obtained images the average droplet diameter was estimated as a function of the effective film thickness.

For each of the studied films, the effective intensity of the SH was calculated. Figure 4 shows the dependence of the SH generation on the film thickness.

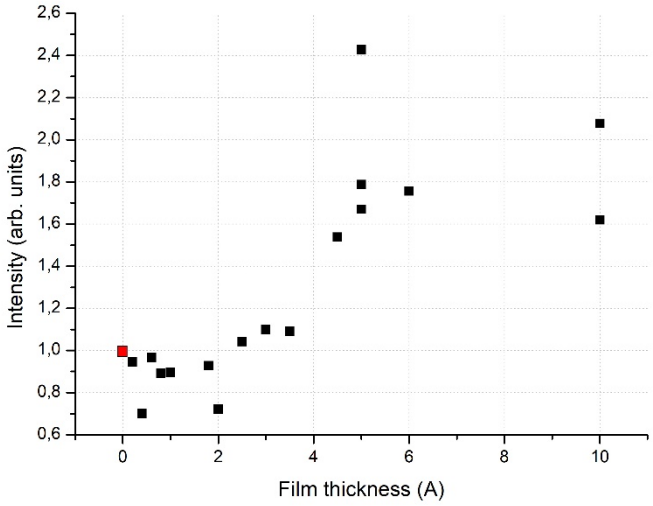

Fig. 4: The efficiency of the SHG as a function of the film thickness. The normalization was

performed on the result for the uncovered silicon

Red color indicates the point corresponding to the signal from uncovered silicon. From the obtained dependence it is well seen that at thicknesses less than 5 Å a slight attenuation of the SH signal is observed in comparison with uncovered silicon, and there's a sharp increase in the SH signal at large thicknesses. Such a dependence can be related to the fact that at an effective thickness of about 5 Å, the shape of the droplet passes through the level of the hemisphere: at smaller thicknesses the droplets have a flatter shape, and at larger they become almost spherical, which can cause a SH amplification due to plasmon resonance.

THE METHODS OF SYNTHESIS AND DIAGNOSTICS OF NANOMATERIALS AND NANOSTRUCTURE

17. SIMULATION OF SUBPICOSECOND MULTI-PULSE LASER ABLATION OF METALS

Povarnitsyn Mikhail

Joint Institute for High Temperatures RAS,
Izhorskaya 13 Bldg 2, Moscow 125412, Russia
Tel. +74954842456, *povar@ihed.ra.ru*

Effectiveness of laser ablation is an important issue in processing of materials. Using a hydrodynamic two-temperature model, we simulate single-, double-, and multi-pulse laser ablation of metal targets. Results of modeling demonstrate that the rate of the multi-pulse ablation increases an order of magnitude in comparison to single-pulse regime, while the repetition rate growth up to several GHz because the material surface does not cool down substantially between successive pulses. To prevent the shielding and suppression effects, previously observed in double-pulse laser irradiation [1], the fluence of each pulse in the burst should have a subthreshold value to avoid the generation of slow moving ablated condensed-phase fragments of matter. Obtained results are in very good agreement with recent experimental findings on ablation by ultrafast bursts of subpicosecond pulses [2]. Laser ablation in single- and double-pulse regimes is presented in Fig. [1].

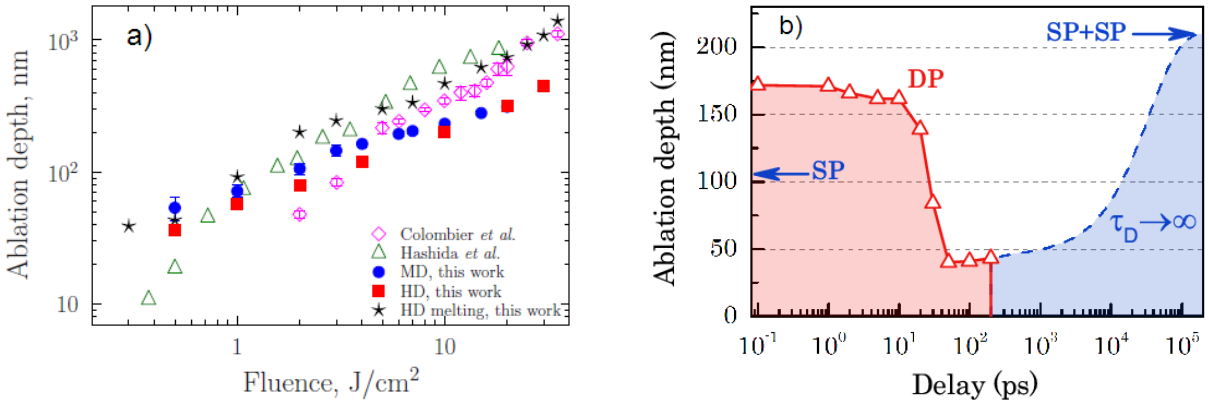

Figure 1. (a) – single-pulse laser ablation of bulk aluminum target as a function of laser fluence; (b) – double-pulse laser ablation of aluminum as a function of inter-pulse delay. The fluence of each pulse is 2 J/cm^2.

[1] M. E. Povarnitsyn, V. B. Fokin, P. R. Levashov, and T. E. Itina, Phys. Rev. B **92**, 174104 (2015).

[2] C. Kerse *et al.*, Nature **537**, 84 (2016).

18. ЛАЗЕРНАЯ ПЕЧАТЬ ХИРАЛЬНЫХ ПЛАЗМОННЫХ НАНОСТРУЙ ВИХРЕВЫМИ ПУЧКАМИ

Сюбаев С.А.

Институт автоматики и процессов управления ДВО РАН, г. Владивосток

+79990590285, trilar@bk.ru

Хиральность является специфичной особенностью, обычно встречающейся в природе у живых организмов почти во всех масштабах. Искусственно изготовленные наноразмерные структуры хиральной формы благодаря уникальным способам взаимодействия с оптическим излучением, обладают такими примечательными свойствами, как круговой дихроизм, усиление нелинейных сигналов, высоконаправленная эмиссия и фотоактивность. Между тем, современные методы создания спиральных наноструктур являются довольно дорогостоящими и с низкой пропускной способностью или ограничивают количество доступных материалов и достижимый размер производимых структур, что в свою очередь инициирует поиск альтернативных подходов. Недавно в ряде работ был продемонстрирован новый альтернативный метод быстрой фабрикации спиральных структур, основанный на использовании оптического излучения и специально разработанных амплитудных-, поляризационных или фазовых пластинок. Более того, было показано, что вихревые лазерные импульсы, обладающие одновременно орбитальным (ОУМ) и спиновым (СУМ) угловым моментом, закручивают временно-расплавленный металл, что приводит к формированию микроструй спиральной формы [1]. Несмотря на потенциал такого прямого и простого в применении метода изготовления хиральных наноструктур до сих пор не продемонстрированы эксперименты, показывающие образование закрученных наноструй различных размеров на поверхности таких перспективных плазмонных материалов, как серебро и золото.

В данной работе впервые детально исследуются процессы взаимодействия наносекундных вихревых лазерных пучков с поверхностью металлических мишеней с целью разработки высокоэффективного и простого лазерного метода печати наноструктур с уникальной спиральной геометрией для последующего использования в задачах создания метаповерхностей с уникальными оптическими свойствами и высокочувствительных плазмонных биосенсоров нового поколения, а также предлагается альтернативное объяснение образования хиральной наноструи на поверхности пленки серебра, основанное на комбинации прямых и закрученных термокапиллярных потоков расплавленного материала, которые инициируются характерным спиральным распределением

интенсивности, возникающем при интерференции падающего “бублик”-образного вихревого пучка и его реплики, отраженной от поверхности расплавленного металла.

Для генерации вихревого пучка излучение из лазерной системы Nd:Yag пропускалось через поляризатор Глана-Тейлора и четвертьволновую пластинку, чтобы сформировать циркулярно-поляризованный пучок, и затем через радиальный поляризационный преобразователь. Затем сгенерированные наносекундные вихревые лазерные импульсы фокусировались на поверхности образца с помощью объективов микроскопа с различной числовой апертурой (NA) (Рис.1). Наконец, топология полученных хиральных наноструктур изучалась с помощью высокоразрешающего сканирующего микроскопа (СЭМ).

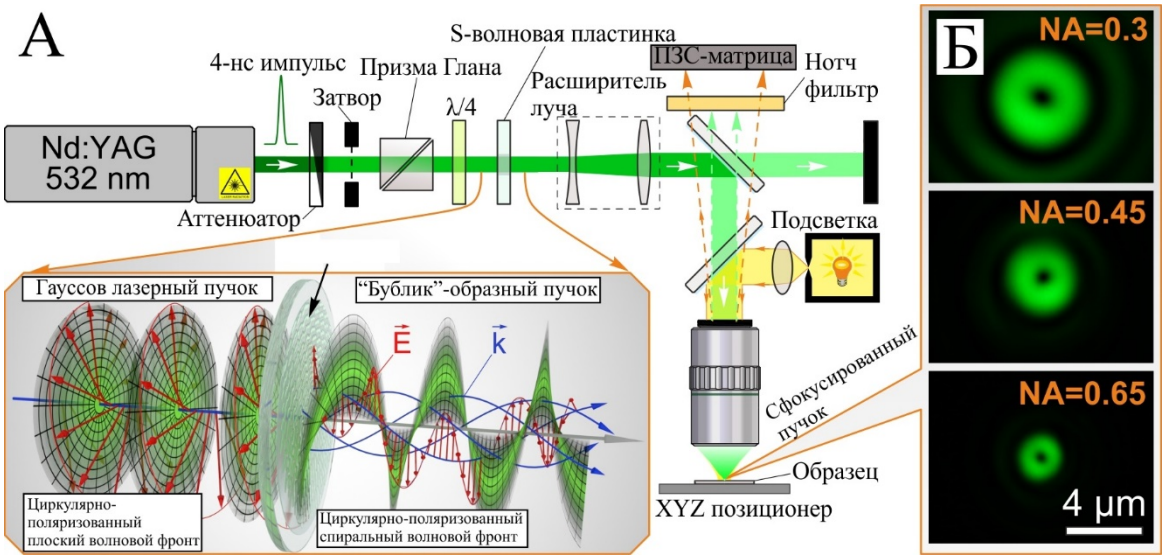

Рисунок 1. (А) Схема экспериментальной установки для наноструктурирования наносекундными вихревыми пучками. (Б) Распределение интенсивности вихревого пучка в фокальной плоскости объективов микроскопа с NA = 0.3 (верхнее изображение), NA = 0.45 (среднее) и NA = 0.65 (нижнее).

Серия СЭМ изображений (рис.2(А) - 2(Г)) иллюстрирует образование и эволюцию закрученных наноструй, полученных при одноимпульсном облучении 500-нм пленки серебра, нанесенной на подложку из кварцевого стекла, наносекундными вихревыми лазерными импульсами, сфокусированными объективом с NA = 0.3. Помимо очевидной спиральной формы полученных наноструй с их закрученной симметрией по часовой стрелке (знак спиральности вихря), которая совпадает с направлением вихревого импульса, процесс их образования, по-видимому, аналогичен тому, как формируются обычные наноструи, получаемые при одноимпульсной абляции благородных металлических пленок импульсами гауссовой формы (нуль-ОУМ). Основные этапы формирования включают (1) накопление расплавленного материала в пространственном центре пучка через термокапиллярные силы

и течения расплава, которые быстро уменьшаются к периферийной части, (2) образование жидкой наноструи, которая подвергается гидродинамической неустойчивости Рэлея-Плато, что приводит к появлению и выбросу расплавленных капель и, наконец, (3) при увеличении энергии импульса, формирование сквозного отверстия (эта стадия не показана на СЭМ-изображениях).

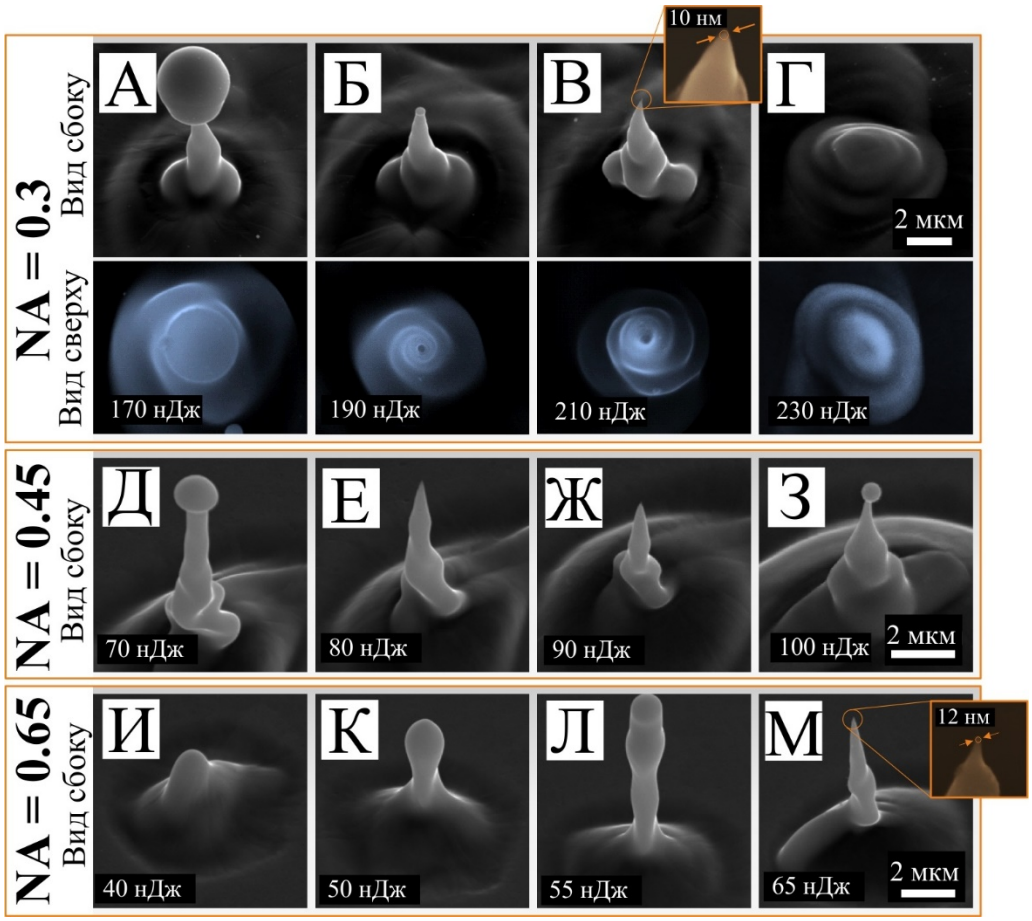

Рисунок 2. (А-Г) Вид сбоку (угол обзора 40°) и вид сверху (в ложном цвете) СЭМ изображений хиральных наноструй, полученных при одноимпульсной абляции 500-нм пленки серебра вихревыми импульсами, сфокусированными объективом с NA = 0.3. Аналогичный вид сбоку (угол обзора 40°) СЭМ изображений, иллюстрирующих закрученные наноструи, полученные на поверхности такой же пленки серебра абляцией одиночными вихрями, сфокусированными объективом с NA = 0.45 (Д-З) и NA = 0.6 (И-М). Энергия импульса в каждом ряду увеличивается слева направо. На вставках к рисункам (В) и (М) показан увеличенный вид наконечника наноструи, указывающий типичные радиусы кривизны

Сходство наших настоящих наблюдений и предыдущего обширного опыта по фабрикации тонкопленочных наноструй с использованием коротких и сверхкоротких лазерных импульсов побуждает нас сравнивать образование не- и хиральных наноигл. В

частности, для почти аналогичного общего механизма, лежащего в основе образования наноструй на поверхности пленки благородного металла и обусловленного температурно-градиентным термокапиллярным потоком расплавленного материала, при облучении вихревым импульсом появляется сильное вращательное движение, скручивающее расплавленный материал в направлении, совпадающем с знаком вихревой спиральности. Спиральный термокапиллярный расплав, протекающий внутри эволюционирующей наноструи и окружающей ее области микровыпуклости, возможно, может происходить из соответствующего характерного спирально-подобного (или более сложного) распределения интенсивности. Для рассматриваемых в этом исследовании пленок благородного металла происхождение такого спирального распределения интенсивности и соответствующего профиля температуры на поверхности металлической пленки можно объяснить в терминах «чисто» оптического процесса, такого как интерференция падающего вихревого пучка с пучком с нулевым ОУМ, имеющим сферический (или более сложный) волновой фронт. Понятно, что появление такой отраженной волны, обеспечивающей желаемую «спиральную» составляющую соответствующего распределения поверхностной интенсивности, может быть связано с переходной наносекундной эволюцией поверхности металлической пленки, которая может быть вызвана ее нагреванием, плавлением и термическим расширением падающим лазерным импульсом в форме “бублика”. Скалярные дифракционные расчеты показывают, что структура вихревого пучка, отраженного от металлической пленки, может быть нарушена при его отражении от пленки, содержащей множественные субмикробные неоднородности со средним размером более 20 нм. В этом случае интерференция падающего вихревого пучка и отраженного спекл-модулированного пучка с нулевым ОУМ создает спирально-подобное распределение интенсивности на поверхности металлической пленки, направление которого совпадает с направлением падающего вихревого пучка (рис.3).

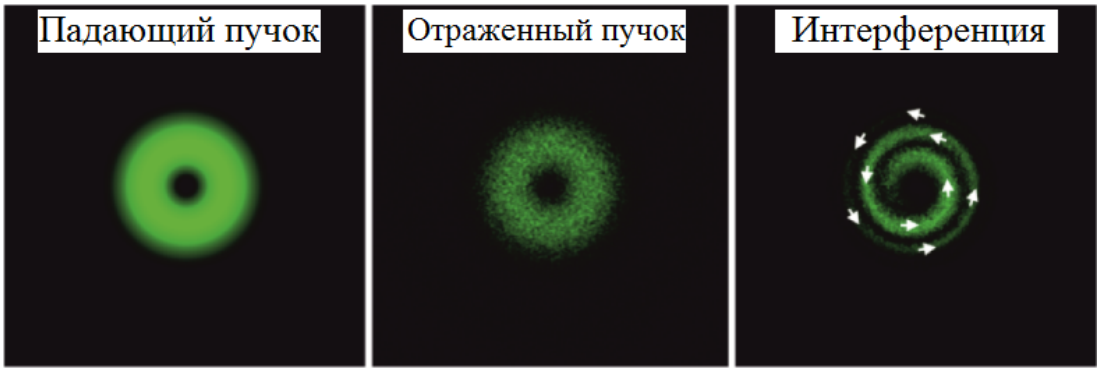

Рисунок 3. Распределения интенсивности сфокусированного падающего вихревого пучка (слева), искаженного пучка, отраженного от шероховатой поверхности металла

(середина) и их интерференционной картины (справа). Белые стрелки на самом правом изображении указывают направление градиента интенсивности, который приводит к появлению «тепловой спирали».

В заключение, в настоящей работе продемонстрировано, что при фокусировке наносекундных лазерных вихрей объективами с высокой числовой апертурой возможно формирование хиральных наноигл варьируемого размера на оптически тонких пленках таких перспективных плазмонных материалов, как серебро и золото. Мы предлагаем альтернативное объяснение формирования хиральной наноиглы на серебряной пленке, основанное на комбинации прямых и закрученных термокапиллярных потоков расплавленного материала, которые вызваны характерным спирально-подобным распределением интенсивности, возникающим при интерференции падающего вихря в форме “бублика” и его реплики, отраженной от поверхности расплавленного металла.

СПИСОК ИСПОЛЬЗОВАННОЙ ЛИТЕРАТУРЫ

1. K. Toyoda, K. Miyamoto, N. Aoki, R. Morita, and T. Omatsu, “Using optical vortex to control the chirality of twisted metal nanostructures,” Nano Lett. 12(7), 3645–3649 (2012).

19. ИССЛЕДОВАНИЕ СВОЙСТВ И РАЗРАБТКА СЕНСОРОВ НА ОСНОВЕ ПЛЕНОК ГРАФЕНА, ВЫРАЩЕННЫХ МЕТОДОМ ТЕРМОДЕСТРУКЦИИ ПОВЕРХНОСТИ ПОЛУИЗОЛИРУЮЩЕГО SIC (0001)

А.А. Лебедев[1,2], В.Ю. Давыдов[1], С.П.Лебедев[1,2], А.Н. Смирнов[1], В.С. Левицкий[1], И.А. Елисеев[1,4], С.Н. Новиков[3,4], Д.Ю. Усачев[4], А.Г. Рыбкин[4] О.Ю. Вилков[4], Ю.Н. Макаров[5,6]

[1]ФТИ им. А.Ф.Иоффе РАН, 194021, С.-Петербург, Россия

[2] Университет ИТМО, 197101, С-Петербург, Кронверкский пр. 49, Россия

[3]Aalto University, Tietotie 3, 02150, Espoo, Finland

[4] СПбГУ, 199034, С.-Петербург, Петергоф, Россия

[5]ГК «Нитридные кристаллы», 194156, С-Петербург, Россия

[6]Nitride Crystals Inc., 181 E Industry Court, Suite B, Deer Park, NY 11729, USA

Одной из самых перспективных технологий синтеза графена, которая позволяет получать высококачественный материал и в тоже время может быть интегрирована в промышленное производство, является термодеструкция поверхности подложек карбида кремния (SiC) [1,2]. В настоящей работе представлены результаты исследований структурных свойств графеновых пленок, выращенных на полярных Si-грани (ориентация поверхности - (0001) подложки карбида кремния с использованием метода термического разложения поверхности кристалла. Также приведены результаты исследований транспортных свойств полученных пленок и параметры сформированных на их основе газовых и биосенсоров.

Формирование графена осуществлялось на высокоомных подложках карбида кремния для того, чтобы исключить влияние проводимости подложки при проведении исследований транспортных свойств Синтез осуществлялся при температуре 1800^{o}C в вакууме и атмосфере инертного газа (Ar). Перед ростом графена проводилось сублимационное травление SiC для удаления дефектного слоя с поверхности. С использованием спектроскопии комбинационного рассеяния света (КРС), атомно-силовой микроскопии, дифракции медленных электронов, рентгеновской фотоэлектронной спектроскопии (РФЭС) и фотоэлектронной спектроскопии с угловым разрешением (ФЭСУР) получена и проанализирована информация о кристаллической и электронной структуре выращенных графеновых слоев (Рис.1–2). Показано, что оптимизация ростовых параметров, выполненная по результатам комплексных исследований, позволила создать надежную технологию роста высококачественных графеновых слоев с толщинами в диапазоне 1–2 монослоя.

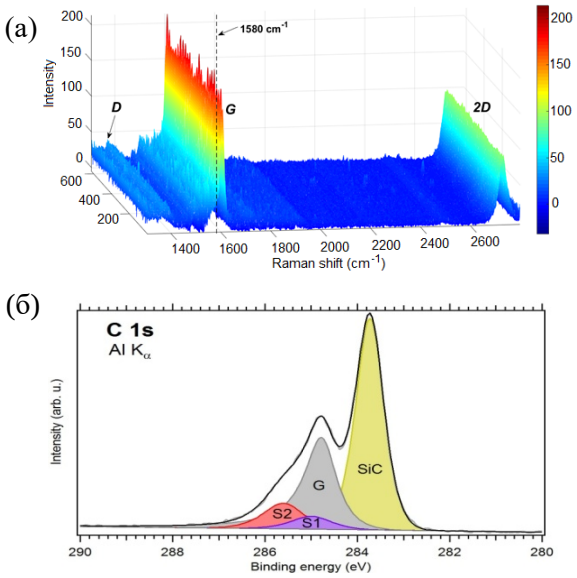

Рис.1. (а) Массив спектров КРС, полученный на площади графеновой пленки размером 12×12 мкм. (б) РФЭС-спектр в области C1s и результат его моделирования (G-графен, S1 и S2 – буферный слой).

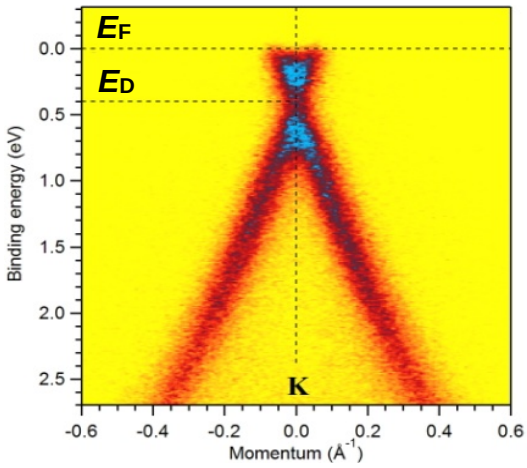

Рис.2. ФЭСУР в окрестности К-точки зоны Бриллюэна. Образец #EG-21, синтезированный на подложке 6H-SiC

Было проведено исследование транспортных свойств пленок методом эффекта Холла. Величина концентрации носителей заряда в исследуемом графене составила 7 x 10^{11} – 1 10^{12} $см^{-2}$, а максимальное значение подвижности электронов приблизилось к 6000 $см^2/(В\ с)$ На основе данных плёнок были изготовлены и протестированы газовые и биосенсоры с рекордной для твердотельных сенсоров чувствительностью [3,4].

В заключении можно сделать вывод о перспективности применения карбида кремния для получения качественных монослойных графеновых пленок с высокой подвижностью электронов. Данные пленки могут найти применение в качестве основы компонентной базы активно развивающейся наноэлектроники.

Список литературы:

1. C. Virojanadara, M. Syväjarvi, R. Yakimova, L. I. Johansson, A. A. Zakharov, and T. Balasubramanian. *Homogeneous large-area graphene layer growth on 6H-SiC(0001).* Phys. Rev. B, 2010, vol. 78, 245403
2. В.Ю.Давыдов, Д.Ю.Усачёв, С.П.Лебедев и др., *Исследование кристаллической и электронной структуры графеновых плёнок, выращенных на 6H-SiC (0001),* ФТП, т 51 (2017) 1118

3. А.А.Лебедев, В.Ю.Давыдов, С.В.Новиков, Д.П.Литвин, Ю.Н.Макаров, В.Б.Климович, М.П.Самойлович, *Биосенсоры на основе графена*, ПЖТФ, т.42, вып.14, стр. 28-35 (2016).
4. S.Novikov, N.Lebedeva, A.Satrapinski, J.Walden, V.Davydov, A.Lebedev, *Graphene based sensor for environmental monitoring of NO_2,* Sensors and Actuators B: Chemical 236, 1054-1060 (2016).

Тезисы подготовлены при финансовой поддержке Министерства образования и науки Российской Федерации (Соглашение № 14.575.21.0148, уникальный номер проекта RFMEFI57517X0148)"

20. СТРУКТУРА ПЛАВАЮЩИХ МОНОСЛОЕВ И ПЛЕНОК ЛЕНГМЮРА-ШЕФФЕРА ГОЛЬМИЕВОГО КОМПЛЕКСА СМЕШАННО-ЗАМЕЩЕННОГО ПРОИЗВОДНОГО ФТАЛОЦИАНИНА

Казак А.В.[1,2], Усольцева Н.В.[1], Смирнова А.И.[1], Марченкова М.А.[2,3], Терещенко Е.Ю.[2], Якунин С.Н.[3], Рогачев А.В.[3,5], Ковальчук М.В.[2,3,4]

[1]НИИ Наноматериалов, Ивановский государственный университет, Иваново, Россия

[2] ФНИЦ «Кристаллография и фотоника» РАН, Москва, Россия

[3]НИЦ «Курчатовский институт», Москва, Россия

[4]Санкт-Петербургский государственный университет, Санкт-Петербург, Россия

[5]Московский институт экономики и математики, национальный исследовательский университет высшей школы экономики, Москва, Россия

Тел.: +7-(4932)-37-08-08, e-mail: alexkazak86@gmail.com

Получение тонкопленочных наноматериалов с контролируемой структурой представляет собой важную фундаментальную задачу, имеющую большое практическое значение для развития наноэлектроники. Мезогенные низкомолекулярные красители донорно-акцепторного типа, являются перспективными органическими материалами для фотовольтаики.

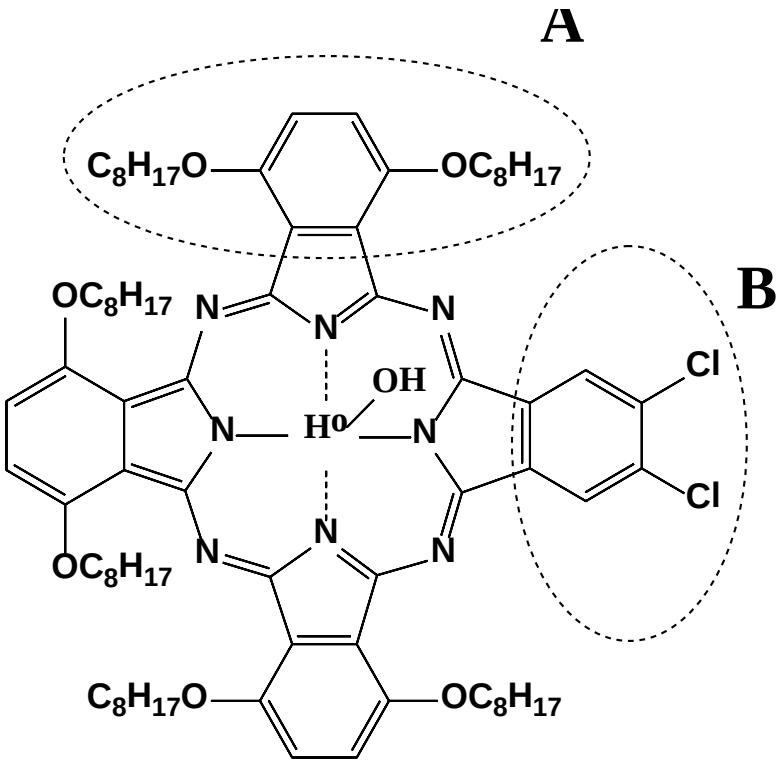

Рис. 1 Структурная формула исследуемого смешанно-замещенного производного фталоцианина

Поэтому в работе была поставлена задача получения тонкопленочных наноматериалов с контролируемой структурой на основе дискотического металлокомплекса смешанно-замещенного производного фталоцианина, содержащего донорные и акцепторные заместители в структуре одной молекулы.

Для достижения поставленной задачи было

проведено комплексное исследование надмолекулярной организации плавающих монослоев и пленок Ленгмюра-Шеффера мезогенного фталоцианина типа A_3B (1,4,8,11,15,18-гексаоктилокси-23,24-дихлор- фталоцианинат гидроксигольмия, рис. 1).

В работе было выполнено моделирование упаковки молекул исследуемого соединения в монослоевых структурах на поверхности воды и рассчитаны параметры элементарной ячейки монослоя. Для исследуемого соединения, если структуру молекулы считать плоской, площадь, приходящаяся на одну молекулу в плотнейшей face-on мономолекулярной упаковке равна 5.6 нм^2. Площадь, приходящаяся на одну молекулу в плотнейшей edge-on мономолекулярной упаковке, равна 2.33 нм^2. В случае вытеснения латеральных заместителей из плоскости макроцикла, площадь, приходящаяся на одну молекулу в плотнейшем face-on монослое, может уменьшаться до 1.6 нм^2.

Методом брюстеровской микроскопии получена визуализация процесса формирования ленгмюровского слоя на поверхности воды и оценен тип формируемых структур (монослой, бислой, полислой).

Методом рентгеновской дифракции в скользящей геометрии установлена надмолекулярная организация ленгмюровских монослоев смешанно-замещенного производного фталоцианина. Определены условия формирования стабильного упорядоченного монослоя: начальная степень покрытия поверхности воды c = 18 %, скорость поджатия барьеров $\nu = 6$ см^2/мин. При данных условиях, начиная с площади $A_{мол} = 3{,}9$ нм^2, приходящейся на одну молекулу соединения и поверхностного давления $\pi = 0{,}4$ мН/м, на границе раздела фаз вода/воздух получали стабильную монослоевую структуру с межплоскостным расстоянием 2.06 нм.

С целью управления надмолекулярной организацией в пленках Ленгмюра-Шеффера путем сравнения структуры плавающих слоев и перенесенных пленок, проводилось исследование структуры тонкопленочных образцов методом электронографии. Были определены параметры элементарной ячейки пленок Ленгмюра-Шеффера: a = 1.65 нм, b = 1.92 нм, $\gamma_1 = 75°$.

Таким образом, результаты структурных исследований в перенесенных пленках находятся в хорошем согласовании с результатами, полученными в Ленгмюровских слоях.

Работа поддержана программой Минобрнауки РФ в рамках государственного задания Ивановскому государственному университету для выполнения научно-исследовательских работ, № 16.1037.2017/ПЧ и частично выполнена при финансовой поддержке РФФИ (грант № 16-03-00883а).

21. ИЗГОТОВЛЕНИЕ ПОРИСТЫХ НАНОСТРУКТУР ДЛЯ УСИЛЕНИЯ СИГНАЛА КОМБИНАЦИОННОГО РАССЕЯНИЯ

[1]Мицай Е.В., [1]Сюбаев С.А, [1,2]Кучмижак А.А.

[1]Институт автоматики и процессов управления ДВО РАН, Владивосток

[2]Дальневосточный федеральный университет, Владивосток

тел. 89940097099, mitsai@dvo.ru

Поверхностно-усиленное комбинационное рассеяние является ультрачувствительным неинвазивным спектроскопическим методом, основанным на безмаркировочном обнаружении различных молекул, размещенных вблизи плазмонных нанотекстурированных металлических подложек[1-3]. Интенсивность характерного комбинационного сигнала, определяющего специфичность колебания отдельных молекул, обычно очень слабая, однако этот сигнал может быть значительно увеличен вблизи нанотекстурированных поверхностей или наноструктур, создающих посредством плазмонов локализованные усиленные электромагнитные поля. С момента первого наблюдения сигнала комбинационного рассеяния от одиночной молекулы[4] были предприняты многочисленные попытки повысить эффективность нанотекстурированных подложек с точки зрения достижения максимального коэффициента усиления внутри одной «горячей точки», а также количества «горячих точек», приходящихся на одну наноструктуру[5-7]. На текущий момент в качестве универсальных подложек для комбинационного рассеяния было изготовлено и исследовано множество нанотекстурированных структур, как правило, имеющих большое отношение поверхности к объему и создающих плотные «горячие точки». В частности, возрастает интерес к пористым материалам, наноструктурам и наночастицам, в которых достигается повышение сигнала комбинационного рассеяния, достаточное для преодоления предела обнаружения одиночной молекулы, независимо от условий возбуждения или обнаружения[8,9].

В настоящей работе изготавливаются микрокольца с контролируемыми геометрическими параметрами и множественными порами, расположенными по окружности, которые обеспечивают сильное ближнепольное усиление падающих электромагнитных волн в видимом и инфракрасном диапазонах, что делает их перспективными для хемо- и биосенсорики. В этом отношении упорядоченные в массив микрокольца можно рассматривать как многофукциональные подложки, обеспечивающие усиление сигналов как фотолюминесценции, так и комбинационного рассеяния от адсорбированных молекул аналита, накачиваемых, как правило, в оптическом диапазоне, при этом давая возможность

использовать диапазон от близкого до среднего ИК для возбуждения в микрокольцах главных дипольных резонансов локализованных плазмонов.

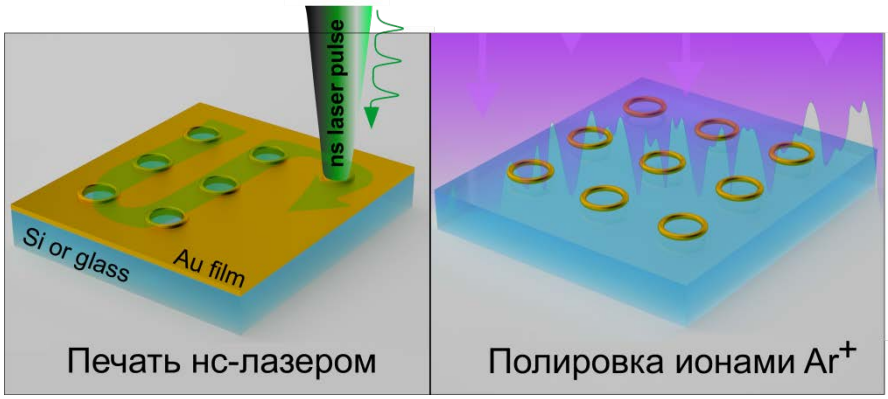

Рис. 1. Двухшаговая процедура производства массива изолированных пористых микроколец

Процедура создания изолированных пористых микроколец включает два этапа, изображенных на Рис. 1. Первый этап заключается в следующем: стеклянная или кремниевая подложка с нанесенным на нее 50-нм слоем золота облучается единичными 7-нс импульсами (532 нм). При определенной энергии импульса в золотой пленке создается отверстие, окруженное гладким затвердевшим кольцом с толщиной в 2.5-3 раза большей, чем исходная толщина пленки. Геометрические параметры микроколец могут быть настроены путем изменения толщины пленки и энергии падающего импульса[10,11]. Второй этап включает в себя удаление необработанных частей пленки с использованием безжидкостного травления при помощи ускоренного пучка ионов аргона при параметрах травления, которые не позволяют пленке расплавиться. Демонстрируется, что дополнительная степень перестраиваемости внутренней структуры полученных микроколец обеспечивается незначительным изменением химического состава металлической пленки в процессе ее магнетронного осаждения в соответствующих средах. Изменение концентрации молекул N_2 в буферном газе определяет размер и плотность создающихся впоследствии нанопор.

Характеристики пористых микроколец исследуются путем измерения сигнала комбинационного рассеяния от самоорганизованного монослоя молекул Родамина 6G и распределения поверхностной интенсивности его основных полос. Типичные спектры комбинационного рассеяния, полученные при помощи слоя красителя Родамина 6G как на гладких, так и на пористых микрорельефах, имеющих почти одинаковый внешний диаметр и толщину стенки, выявляют все основные полосы комбинационного рассеяния, характерные для молекул Родамина 6G, в то время как эти полосы не могут быть обнаружены на стеклянной подложке даже при 10-кратном увеличении времени накопления. Максимальный сигнал комбинационного рассеяния для гладких микроколец достигает

300±60 отсчетов($с^{-1}мВт^{-1}$) и 1550±170 отсчетов($с^{-1}мВт^{-1}$) для пористых микроколец. Средний коэффициент усиления $\approx 10^5$, как сигнал, приходящийся на одну молекулу раствора

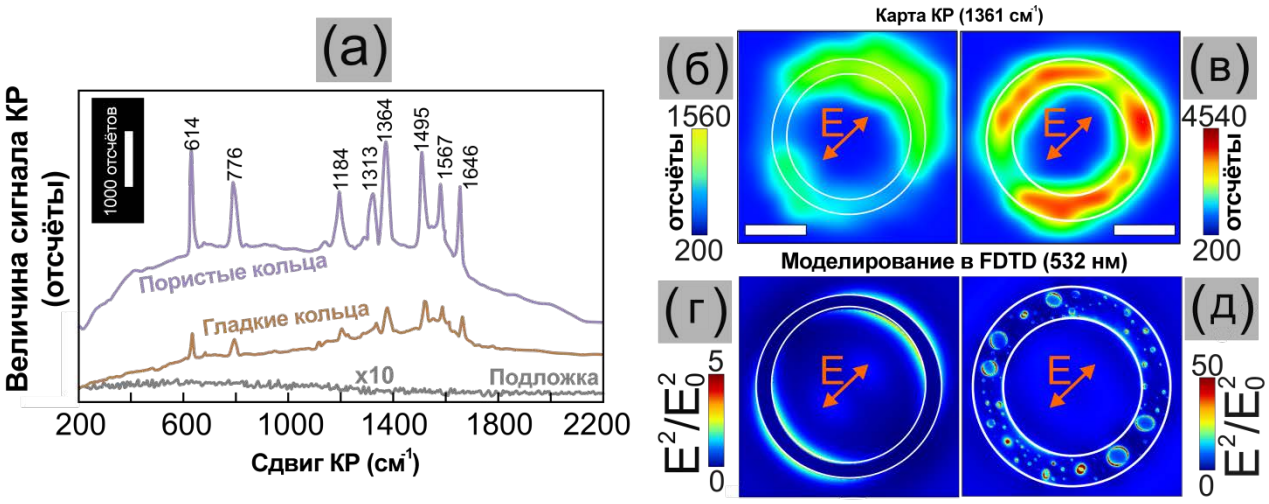

Рис. 2. Спектры комбинационного рассеяния (а) Родамина 6G, измеренные на гладких (коричневая линия) и пористых микрокольцах (фиолетовая линия), а также на стеклянной подложке после полного удаления золотой пленки посредством ионной полировки (серая линия). (б, в) Карты комбинационного рассеяния (для полосы 1361-$см^{-1}$) монослоя молекул Родамина 6G, покрывающего гладкие (б) и пористые микрокольца (в). Эти карты указывают на усиление комбинационного рассеяния согласно распределению амплитуды электрического поля вблизи гладких (г) и пористых микроколец (д), рассчитанных для падающего по нормали линейно-поляризованного 532-нм лазерного излучения. Оранжевые линии указывают направление поляризации. Белые линии показывают реальные размеры микроколец.

Родамина 6G. Это явно указывает на плазмонный вклад в усиление сигнала нежели на концентрационный эффект. Картирование поверхностного распределения интенсивности сигнала комбинационного рассеяния молекул Родамина 6G, покрывающих гладкие микрокольца, показывает положение локальных электромагнитных “горячих точек”, которые, как было установлено, зависят от направления поляризации излучения лазерного источника (Рис. 2(б-д)).

Согласно проведенным расчетам в программе FDTD, такое падающее по нормали линейно-поляризованное 523-нм лазерное излучение обеспечивает низкоэффективное возбуждение стенок гладких микроколец лишь с 5-кратным усилением квадрата амплитуды электрического поля (Рис. 2г). Соответствующие горячие точки, согласно направлению линейной поляризации, распределены неравномерно по окружности кольца, что приводит к

непохожему сигналу комбинационного рассеяния (Рис. 2б). С другой стороны, согласно расчетам, выполненным для пористых микроколец, наноразмерных поверхностные особенности создают множество усиленных электрических полей, однородно распределенных вдоль поверхности микрокольца независимо от направления поляризации (Рис. 2д), в целом коррелируя с полученной картой комбинационного рассеяния (Рис. 2в).

Разработанная процедура лазерной печати и ионно-лучевого травления является универсальным инструментом для изготовления многофункциональных плазмонных структур и метаповерхностей для спектроскопической биоидентификации на основе комбинации схем с поверхностно-усиленным поглощением инфракрасного излучения, комбинационным рассеянием и фотолюминесценцией на одной чувствительной подложке.

1. M. Jahn, S. Patze, I. Hidi, R. Knipper, A. Radu, A. Mühlig, S. Yüksel, V. Peksa, K. Weber, T. Mayerhöfer, D. Cialla-May, and J. Popp, The Analyst 141, 756 (2016).
2. J. Anker, W. Hall, O. Lyandres, N. Shah, J. Zhao, and R. Van Duyne, Nat. Mater. 7, 442 (2008).
3. A. Kuchmizhak, E. Pustovalov, S. Syubaev, O. Vitrik, Y. Kulchin, A. Porfirev, S. Khonina, S. Kudryashov, P. Danilov, and A. Ionin, ACS Appl. Mater. Interfaces 8, 24946 (2016).
4. S. Nie, Science 275, 1102 (1997).
5. X. Wei, Q. Fan, H. Liu, Y. Bai, L. Zhang, H. Zheng, Y. Yin, and C. Gao, Nanoscale 8, 15689 (2016).
6. Y. Yan, A. Radu, W. Rao, H. Wang, G. Chen, K. Weber, D. Wang, D. Cialla-May, J. Popp, and P. Schaaf, Chem. Mater. 28, 7673 (2016).
7. J. Zeng, F. Zhao, M. Li, C. Li, T. Lee, and W. Shih, J. Mater. Chem. C 3, 247 (2015).
8. P. Sahoo, D. Wang, and P. Schaaf, Mater. Res. Express 1, 035018 (2014).
9. S. Ye, F. Benz, M. Wheeler, J. Oram, J. Baumberg, O. Cespedes, H. Christenson, P. Coletta, L. Jeuken, A. Markham, K. Critchley, and S. Evans, Nanoscale 8, 14932 (2016)
10. A. Kuchmizhak, S. Gurbatov, O. Vitrik, Y. Kulchin, V. Milichko, S. Makarov, and S. Kudryashov, Sci. Rep. 6, 19610 (2016).

A. Kuchmizhak, S. Gurbatov, Y. Kulchin, and O. Vitrik, Opt. Commun. 356, 1 (2015).

22. METAL-CARBYNE COMPLEXES FOR SERS APPLICATION

A. Osipov, A. Kucherik, A. Antipov, S. Kutrovskaya, S. Arakelian

A.G. and N.G. Stoletov Vladimir State University
87 Gorki st., Vladimir, Russia, 600000.
E-mail: osipov@vlsu.ru

Abstract

Metal–carbyne materials realize surface-enhanced Raman scattering which has been synthesized by laser irradiation of colloidal systems consisting of carbon and noble metal nanoparticles. The dependence of the Raman scattering intensity of the material composition has been investigated. The possibility of detecting of the Raman spectrum of organic dye Rhodamine 6G was demonstrated.

The creation of new hybrid and composite materials based on carbon structures and metal nanoparticles is the most prospective area of nanotechnology. Carbon quantum dots demonstrate a variation of optical properties depending on the degree of crystallization, size and shape. The amplification of the observed phenomena can be realized by the addition of the noble metal nanoparticles having a plasmon resonant peaks in the visible region of the spectra. The linear carbon chain (carbyne) is the promising carbon material for the creation of the hybrid and composite materials.

Carbyne is an n-type semiconductor with an energy gap up to 0.41 eV, in which electronic transport properties are structurally sensitive. Carbyne has chain of covalently bonded carbon atoms with sp-hybridization of orbitals of two possible types: alternation of n single and triple bonds $(–C{\equiv}C–)_n$, or alternation of n double bonds $(=C=C=)_n$. Optical and electrical properties of carbyne depend on its morphology [1-3]. Thus, the synthesis of carbyne with a variable structure of bonds has a considerable interest not only from a fundamental point of view, but also in the development of new integrated circuits of advanced, next-generation hybrid electronic devices.

The strategy to incorporate metal nanoparticles in a carbon matrix is a great method to integrate the different properties to various materials, enabling to realize multifunctional composites. Such materials may be used in advanced applications like nanobiotecnology, optoelectronics, etc. In particular, a widely used approach is given by the combination of linear carbon chains and metals. In effect, linear carbon chain is the one of the most attractive materials because its unique physicochemical properties and wide potential applications in nanophotonics. The possibility to obtain composites with large visible photoluminescence spectra for optoelectronic devices becomes especially interesting.

In this paper, we report the results of studying the formation of metal–carbyne clusters under laser irradiation of colloidal systems, consisting of shungite carbon and noble-metal nanoparticles. It is shown that this irradiation leads to the formation of clusters, in which metal nanoparticles are interrelated by carbyne chains. The Raman spectra of these structures exhibit SERS and depend significantly on the variation of concentration of metal particles in colloidal system.

The reported study was also supported by the Ministry of Education and Science of the Russian Federation (state project no. 16.5592.2017/VU), RFBR grants # 16-42-330531r_a, #16-32-00759mol_a and by the grant of president of Russian Federation by project MK-3053.2017.2.

23. NEW LASER COMPOSITE CERAMIC

Michail Pankov, Sergey Lysenko, Andrew Kanaev,
Jury Kopylov, Alexander Antipov, Valery Bulaev

FSE "GLP"Raduga", pankov@trassa.org

In the new century, new materials and devices are being created to design promising lasers. One of such materials is laser ceramics that absorbed the best qualities of laser monocrystals and phosphate glasses:

- highly transparent material like glass and like a crystal, has a thermal conductivity of the crystal, which is an order of magnitude greater than that of phosphate glass;

- devices from ceramics can be scaled as well as from phosphate glass up to large sizes, but this can not be done on crystals. Large crystals are difficult to grow for a long time, they have optical inhomogeneities. The refractive index of a crystalline boule on the axis is one, on the periphery of the other. The ceramics made of carefully mixed powders are devoid of this disadvantage;

- ceramics in contrast to phosphate glass and crystal has an increased strength, crack resistance is several times higher than glass and crystal. Laser ceramics are an excellent material for active laser elements.

The quality of ceramics is determined by the profiles of the radiation distribution. With an accurate adjustment of the semiconfocal resonator, the distribution of the main mode is the second harmonic of the Lagher polynomials. This is clearly seen from the two peaks on the radiation distribution when a good quality crystal or ceramic is used as the active element. The presence of smoothed peaks in ceramics allows us to conclude about its quality.

The active laser element with slab geometry from laser ceramics with polished parallel-parallel ends was pumped from one side with 806 nm radiation. As a result, the dependence of the generated power on the pump power was obtained, and the threshold power was 136 W. The differential efficiency of laser generation was 0.68, with a theoretically possible value of 0.72.

POSTERS

24. ENERGY STATES OF EXCITONS IN SQUARE QUANTUM WELLS

Belov Pavel

Saint-Petersburg State University, 198504, St. Petersburg, Ulyanovskaya 1

+79112447085, pavelbelov@gmail.com

Theoretical studies of the exciton states and the radiative decay rate are important for interpretation of the experimental results [1]. Measurements of the radiative decay rate for high-quality quantum wells (QWs) show a variance of the results [2,3] especially for narrow QWs. Meanwhile, the quality of heterostructures is permanently growing and new data on the exciton-light coupling have become available recently [4,5]. These data include the radiative decay rates for the ground and excited states of excitons in QWs.

The analytical description of the exciton states in GaAs-based heterostructures is complicated due to the degenerate valence band. The impact of the QW potential additionally impedes a solution. The problem can be solved approximately only in the limiting cases of very narrow or very wide QWs (L<10 nm and L>150 nm for the GaAs QWs) [1]. On the other hand, recent increase of the computer performance has opened up an opportunity for numerical study of exciton states as well as of the exciton-light coupling. Nevertheless, the numerical solution by the variational method [6,7] is mainly restricted to the exciton ground state. The excited states are difficult to be obtained by the variational method.

In this report, we present a method for a precise numerical solution of the Schrödinger equation for the envelope-function of an exciton in a single square QW of a finite height [8,9]. It makes it possible to calculate the ground and excited energy states. The energy states of the exciton in a single square QW are defined by the three-dimensional equation derived from the Schrödinger equation for the exciton. For description of the degenerate valence band, the spherical approximation of the Luttinger Hamiltonian [10] is used, thus neglecting the corrugation of the valence band. Additionally, the light-hole-heavy-hole mixing is disregarded. This three-dimensional equation for *s*-wave exciton states is given as [8]

$$\left(K - \frac{e^2}{\epsilon\sqrt{\rho^2 + (z_e - z_h)^2}} + V_e(z_e) + V_h(z_h) \right) f(z_e, z_h, \rho) = E_X f(z_e, z_h, \rho),$$

where the kinetic term reads

$$K = -\frac{\hbar^2}{2m_e}\frac{\partial^2}{\partial {z_e}^2} - \frac{\hbar^2}{2m_{hz}}\frac{\partial^2}{\partial {z_h}^2} - \frac{\hbar^2}{2\mu}\left(\frac{\partial^2}{\partial \rho^2} - \frac{1}{\rho}\frac{\partial}{\partial \rho} + \frac{1}{\rho}\right).$$

In the equations, indices *e* and *h* denote the electron and the hole, respectively. The unknown function *f* is related to the three-dimensional wave function φ as [8,9] $\varphi(z_e, z_h, \rho) = f(z_e, z_h, \rho)/\rho$, where $\rho = \sqrt{(x_e - x_h)^2 + (y_e - y_h)^2}$. The potentials $V_{e,h}(z_{e,h})$ are the finite square confinement QW potentials. The term μ is the reduced effective mass in the *xy*-plane, m_{hz} is the hole mass in the *z*-direction. The exciton binding energy, E_b, is defined by the exciton ground state energy, E_X, with respect to the lowest quantum confinement energies of the electron, E_{e1}, and the hole, E_{h1}, in the QW:$E_b = E_{e1} + E_{h1} - E_X$. Energies E_{e1} and E_{h1} are obtained from solution of the corresponding one-dimensional Schrödinger equations for the electron and the hole in the QW.

The exciton-light coupling is usually characterized by the radiative decay rate, Γ_0, which describes the resonance response of an exciton exposed to the electromagnetic excitation. For the exciton in a QW, the radiative decay rate can be given by the expression [1]:

$$\Gamma_0 = \frac{2\pi q}{\hbar \epsilon}\left(\frac{e|p_{cv}|}{m_0 \omega_0}\right)^2 \left| \int_{-\infty}^{\infty} \varphi(z, z, 0)\, e^{iqz} dz \right|^2 .$$

Here $z = z_e = z_h$, $q = \omega\sqrt{\epsilon}/c$ is the light wave vector,ω_0 is the exciton frequency, $|p_{cv}|$ is the matrix element of the momentum operator between the single-electron conduction- and valence-band states.

We have numerically solved the boundary value problem for the three-dimensional partial differential equation and accurately obtained the exciton ground state energy E_X and the wave function. The exponential decrease of the exciton wave function at large values of variables allowed us to impose zero boundary conditions for the function $f(z_e, z_h, \rho)$ at the boundary of some rectangular domain. For discretization, we employed the second-order finite-difference approximation [11,12] of the partial derivatives in three-dimensional equation on the equidistant grids over three variables. The nonzero solution of this homogeneous equation with zero boundary conditions can be found by a diagonalization of the matrix constructed from this equation. A small part of the matrix spectrum was obtained by the Arnoldi algorithm [13]. As a result, we have calculated some lowest eigenvalues of the matrix and the corresponding eigenvectors. Then, the radiative decay rate was calculated using the trapezoidal rule for computing the integral for Γ_0.

The calculations were performed for heavy-hole excitons in the GaAs/$Al_{0.3}Ga_{0.7}As$ heterostructures. In particular, the difference of the gap energies of the heterostructure was modeled as $\Delta E_g = 1087x + 438x^2$ meV; a ratio of potential barriers: $V_e/V_h = 65/35$; the Luttinger parameters are taken to be $\gamma_1 = 6.85$, $\gamma_2 = 2.10$ for GaAs and $\gamma_1 = 3.76$, $\gamma_2 = 0.82$ for AlAs; the

dielectric constant $\epsilon = 12.53$ for GaAs and $\epsilon = 10.06$ for AlAs [7,14]. Masses and dielectric constants for the ternary alloys are obtained by a linear interpolation on *x*.

The energies of the exciton *1s* states and the radiative decay rates in energy units, $\hbar\Gamma_0$, have been calculated for QW widths $L = 20 - 100$ nm. They are shown in Fig.1. The number of exciton states is increased as the QW becomes wider. The ground exciton state takes place for any QW widths. The first excited state initially appears at the minimum QW width of 25 nm with the exciton energy $E_X \approx 7$meV (with respect to E_g). This state can be roughly approximated by the product of three one-dimensional functions. They correspond to the first excited quantum-confined state of the hole, the ground quantum-confined state of the electron and the Coulomb 1s state. For wide QWs, the upper states for QWs of width $L > 80$ nm are difficult to be distinguished and require more precise computations.

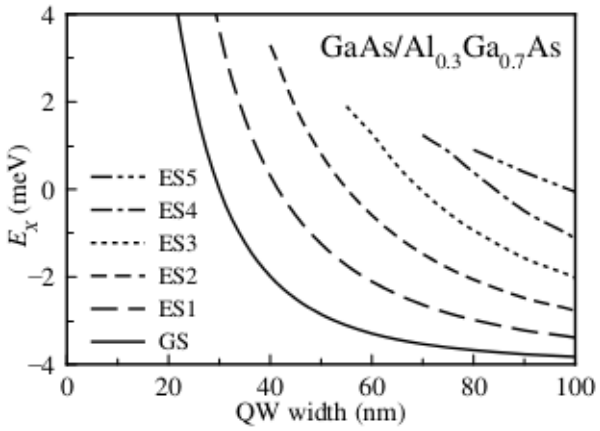

Fig. 1. The energy 1s states of the heavy-hole exciton in QW. The ground state is denoted as GS, ES marks the excited states.

The radiative decay rates in the energy units, $\hbar\Gamma_{0n}$, for the four lowest exciton states, $n = 1 - 4$, have been calculated. The radiative decay rate of the ground state, $\hbar\Gamma_{01}$, is about 37 μeV for QW widths less than 30 nm and grows as further QW becomes wider. The radiative decay rate of the first excited state ($\hbar\Gamma_{02}$) becomes noticeable only for wide QWs. For the upper states and the QWs of width $L \geq 80$ nm, the radiative decay rates seem to be less than 1 μeV. As a result, in the theoretical calculations of Γ_{0n}, it is enough to consider only the ground exciton state, thus to neglect mixing of the states by means of the electric field of the light wave [15]. In experimental studies of the exciton-light coupling in the high-quality heterostructures with GaAs/AlGaAs QWs of corresponding widths, one should observe at least the resonance response of the exciton ground state. The strength of the exciton-light interaction corresponding to the ground state (and upper states) generally decreases as *L* diminishes. That means that the most long-lived exciton in the $GaAs/Al_{0.3}Ga_{0.7}As$ QW is found to be for QW widths $L \leq 30$ nm where $\hbar\Gamma_0$ is smaller. The accurate modeling of exciton states for such QW widths, however, should take into account the discontinuities of the material parameters at the interfaces [9].

The numerical results are consistent with the experimental data for QW width of 20 nm presented in Ref. [8] as well as for QW width of 12 nm given in Ref. [16].

The work is supported by SPbU (grants No. 11.38.213.2014 and No. 11.38.241.2015), RFBR (grants No. 16-02-00245, No. 16-32-00047) and DFG in the frame of Project ICRC TRR

160. The calculations were carried out using the facilities of the SPbU Resource Center “Computational Center of SPbU”.

References

1. E. L. Ivchenko, *Optical spectroscopy of semiconductor nanostructures* (Alpha Science, Harrow, 2005).

2. S. V. Poltavtsev, B. V. Stroganov, Phys. Solid State, **52**, 1899 (2010).

3. S. V. Poltavtsev, Yu. P. Efimov, Yu. K. Dolgikh *et al.* Solid State Commun. **199**, 47 (2014).

4. D. K. Loginov, A. V. Trifonov, and I. V. Ignatiev, Phys. Rev. B **90**, 075306 (2014).

5. A. V. Trifonov, S. N. Korotan, A. S. Kurdyubov *et al.*, Phys. Rev. B **91**, 115307 (2015).

6. D. B. T. Thoai, R. Zimmermann, M. Grundmann, and D. Bimberg, Phys. Rev. B **42**, 5609(R) (1990).

7. B. Gerlach, J. Wüsthoff, M. O. Dzero, and M. A. Smondyrev, Phys. Rev. B **58**, 10568 (1998).

8. E. S. Khramtsov, P. A. Belov, P. S. Grigoryev *et al.*, J. Appl. Phys. **119**, 184301 (2016).

9. P. A. Belov and E. S. Khramtsov, J. Phys.: Conf. Ser. **816**, 012018 (2017).

10. J. M. Luttinger, Phys. Rev. **102**, 1030 (1956).

11. A. A. Samarskii, *The theory of difference schemes* (Nauka, Moscow, 1989).

12. S. Glutsch, *Excitons in low-dimensional semiconductors* (Berlin, Springer, 2004).

13. R. B. Lehoucq, D. C. Sorensen, C. Yang, *ARPACK Users' Guide: Solution of Large-Scale Eigenvalue Problems with Implicitly Restarted Arnoldi Methods* (SIAM, Philadelphia, 1997).

14. I. Vurgaftman, J. R. Meyer and L. R. Ram-Mohan, J. Appl. Phys. **89**, 5815 (2001).

15. M. M. Voronov, E. L. Ivchenko, V. A. Kosobukin and A. N. Poddubny, Phys. Solid State **49**, 1792 (2007).

16. Y. Chen, N. Maharjan, Z. Liu *et al.*, J. Appl. Phys. **121**, 103101 (2017).

25. МОДЕЛИРОВАНИЕ ВЛИЯНИЯ ПАРАМЕТРА ПОРЯДКА НА ПРЕДЕЛЬНО КОРОТКИЕ ОПТИЧЕСКИЕ ИМПУЛЬСЫ В ГЕРМАНЕНЕ

Конобеева Н.Н.

Волгоградский государственный университет, Волгоград

Тел: +79173343160, e-mail: yana_nn@inbox.ru

Целью работы является исследование динамики многомерных предельно коротких оптических импульсов, распространяющихся в германене, а также оценивание влияния параметра порядка на характер их распространения. Актуальность обусловлена тем, что в последние годы наблюдается повышенное внимание исследователей к изучению сильно нелинейных сред. Одним из таких перспективных материалов является германен, состоящий из одного слоя атомов кремния в гексагональной решетке. С другой стороны, не менее сильный интерес вызывают среды с фазовым переходом, т.е. с параметром порядка, благодаря громадным количеством практических приложений. Достаточно сказать, что к таким средам относятся все сегнетоэлектрики и ферромагнетики. Несмотря на огромное количество теоретических и экспериментальных работ по данной тематике остается ряд вопросов, требующих дополнительных исследований. В качестве примера можно привести неравновесную динамику параметра порядка, в том числе в присутствии внешних переменных полей. Решение таких задач должно быть подкреплено и с теоретической точки зрения.

Также стоит отметить, что среды, содержащие германен способны выдержать экстремально сильные электромагнитные поля и, как показано авторами, в них возможно устойчивое распространение локализованных состояний электромагнитного поля - световых пуль. Это, в свою очередь, дает возможность использовать световые пули как для спектроскопии таких сред, так и для процессов, протекающих в них. Учитывая вышеизложенные факты, касающиеся параметра порядка, возникает задача о спектроскопии параметра порядка в средах, содержащих германен.

В настоящей работе построена эволюционная картина распространения двумерных импульсов в германене с параметром порядка. Получена зависимость формы трехмерных предельно коротких оптических импульсов от скорости релаксации параметра порядка, а также от равновесного значения параметра порядка. В результате моделирования удалось остановить, что предельно короткий оптический импульс распространяется с затухающей амплитудой, что вызвано особенностями релаксационной динамики параметра порядка. А

также установлена возможность стабилизации предельно короткого импульса с помощью параметра порядка.

26. THE LASER-INDUCED SYNTHESIS OF LINEAR CARBON CHAINS

A. Osipov, S. Arakelian, S. Kutrovskaya and V. Samyshkin

Stoletovs Vladimir State University, 87 Gorky st., Vladimir 600000, Russia

osipov@vlsu.ru

Synthesis of new carbon form is an actual task of modern nanotechnology. Laser methods for the synthesis of nanostructured carbon allows varying the composition and morphology of the structures obtained according to the experiments conditions. In our experiments, we demonstrate the synthesis of carbyne with the irradiation of the colloidal system obtained during laser ablation of a target schungite in water. The experiments suggest that a change in the conditions of exposure (the exposure time and the energy of the impact) by YAG:Nd laser with a pulse duration of 100 ns leads to the formation of structures with the carbyne structures.

The laser irradiation of the carbon targets allows to realize different ways of the phase transformation solid-liquid-vapor in dependence on the sample heating speed and on the environmental properties [1, 2]. The use of millisecond lasers results in melting of the surface of the target and synthesis of carbyne. During the laser ablation the quazicontinuous regime of laser irradiation allows us to synthesize carbon clusters [3]. The size of carbon clusters depends on power density of the laser radiation. During the laser irradiation in liquid it is possible to obtain special media parameters for carbon modification with different allotropic forms [4]. There are theoretical and experimental results about carbyne synthesis under the nanosecond pulse duration laser radiation, then it results in splitting of graphite layers and formation of linear carbon chains [5].

The reported study was also supported by the Ministry of Education and Science of the Russian Federation (state project no. 16.5592.2017/VU), RFBR grants # 16-42-330531r_a, #16-32-00759 mol_a and by the grant of president of Russian Federation by project MK-3053.2017.2.

References

1. Mel'nichenko V.M., Sladkov A.M., Nikulin Yu.N., Uspekhi khimii, **51**, 736 (1982).
2. Asinovskiy E.I., Kirilin A.V., Kostanovskiy A.V. UFN, **172**, 931 (2002).
3. N. E. Kask, E. G. Leksina, S. V. Michurin and G. M. Fedorov Fractal Nanostructures Arising under the Ablation of Graphite and Silicon by Millisecond-Laser Radiation// Laser Physics, 2008, Vol. 18, No. 6, pp. 762–767.
4. Antpov A.A., Arakelian S.M., Garnov S.V., Kutrovskaya S.V., Kucherik A.O., Nogtev D.S., Osipov A.V. Quantum Electronics, **45**, 731 (2015)

Pan B., Xiao J., Li J., Liu P., Wang C., Yang G. Science Advances, **1**, e1500857 (2015).

27. PHOTON ECHO FROM AN ENSEMBLE OF (IN,GA)AS QUANTUM DOTS

Ia.A. Babenko[1], I.A. Yugova[1], S.V. Poltavtsev[1,2], M. Salewski[2], I.A. Akimov[2,3], M. Kamp[4], S. Höfling[4], D.R. Yakovlev[2,3] and M. Bayer[2,3]

[1] Spin Optics Laboratory, Saint Petersburg, Russia

[2] Experimentelle Physik 2, Technische Universität Dortmund, 44221 Dortmund, Germany

[3] Ioffe Physical-Technical Institute, Russian Academy of Sciences,

194021 St. Petersburg, Russia

[4] Technische Physik, Universität Würzburg, D-97074 Würzburg, Germany

Photon echo from trions and excitons in (In,Ga)As/GaAs quantum dots has been studied theoretically and experimentally. Theoretical analysis allowed us to distinguish photon echo signals from excitons and trions measured in the same range of wavelength using different polarization configurations of laser excitation. The theoretical predictions are in good agreement with the experimental data.

The interaction between material excitations (excitons and trions) in semiconductor nanostructures and light can be very effective due to high oscillator strength of the excitations. Recently it has been found that using the photon echo (PE) technique, one can transfer an information contained in the optical field into a spin system where it is decoupled from the optical field and may persist for a long time [1].

Semiconductor quantum dots (QDs) are considered to be promising for storing an information about the optical excitation since spin relaxation of electrons and holes in these nanostructures is characterized by significantly long times [2]. The inhomogeneity of the QD ensemble and spectral overlap of the exciton and trion transitions hamper investigations and analysis of these structures.

In the present work we describe the theoretical model developed for the photon echo signal from exciton ensemble in (In,Ga)As/GaAs QDs. Theoretical results complemented by the results for trions from Ref. [1] are compared with the experimental data.

We study the dynamics of PE from an ensemble of the (In,Ga)As/GaAs semiconductor QDs excited by the picosecond laser pulses. Several polarization protocols have been used in the experiment: the linear polarization of the optical pulses parallel to the QD axes *x* or *y* (*z*-axis is the structure grows axis) denoted as H and V, respectively, and the linear polarization parallel to the tilted 45^o with respect to the *x*- and *y*-axes (denoted D and X, correspondingly). Transient PE signal was measured using heterodyne detection [4]. Experimental signals measured in different polarization configurations are shown in Fig. 1.

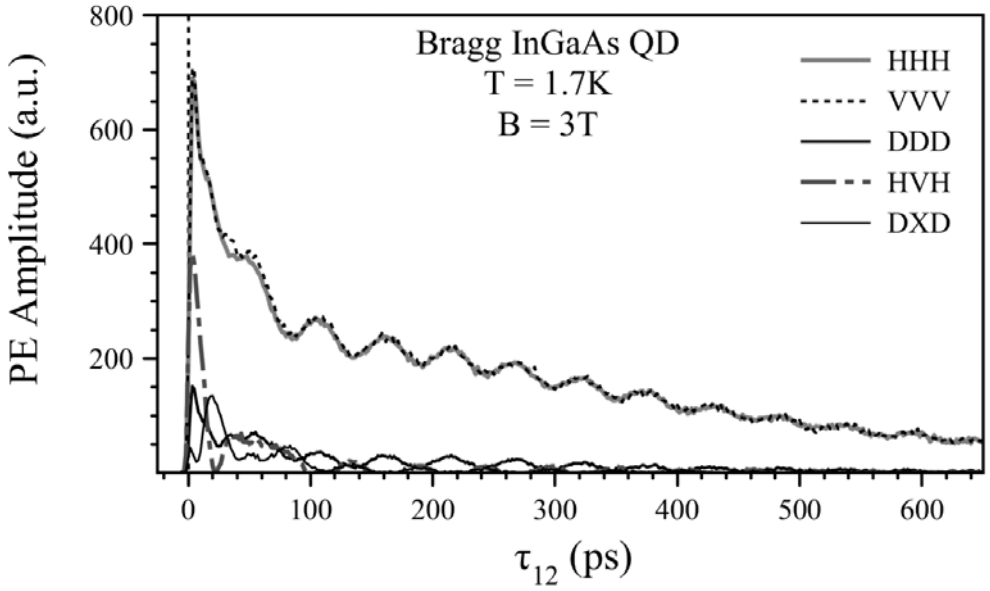

Fig. 1. The delay dependence of the experimental PE signals. Symbols HHH etc. in the legend denote polarization of the first and second pulses and of the detected signal, respectively

The theoretically calculated exciton PE signals for different polarization configurations are described by the following expressions:

$$P_{HHH}^{exc} \propto e^{-\frac{2\tau_{12}}{T_2}}\left[cos^2(\Omega_p\tau_{12}) + \frac{\delta_0^2}{4}\frac{sin^2(\Omega_p\tau_{12})}{\Omega_p^2}\right], \quad (1)$$

$$P_{VVV}^{exc} \propto e^{-\frac{2\tau_{12}}{T_2}}\left[cos^2(\Omega_m\tau_{12}) + \frac{\delta_0^2}{4}\frac{sin^2(\Omega_m\tau_{12})}{\Omega_m^2}\right], \quad (2)$$

$$P_{HVH}^{exc} = P_{VHV}^{exc} = 0, \quad (3)$$

$$P_{DDD}^{exc} \propto \frac{1}{4}e^{-\frac{2\tau_{12}}{T_2}}\left[\left(cos(\Omega_p\tau_{12}) + cos(\Omega_m\tau_{12})\right)^2 + \frac{\delta_0^2}{4}\left(\frac{sin(\Omega_p\tau_{12})}{\Omega_p^2} + \frac{sin(\Omega_m\tau_{12})}{\Omega_m^2}\right)^2\right], \quad (4)$$

$$P_{DXD}^{exc} \propto \frac{1}{4}e^{-\frac{2\tau_{12}}{T_2}}\left[\left(cos(\Omega_p\tau_{12}) - cos(\Omega_m\tau_{12})\right)^2 + \frac{\delta_0^2}{4}\left(\frac{sin(\Omega_p\tau_{12})}{\Omega_p^2} - \frac{sin(\Omega_m\tau_{12})}{\Omega_m^2}\right)^2\right]. \quad (5)$$

Here

$$\Omega_p \equiv \sqrt{\left(\omega_L^e + \omega_L^h\right)^2 + (\delta_0/\hbar)^2},$$

$$\Omega_m \equiv \sqrt{\left(\omega_L^e - \omega_L^h\right)^2 + (\delta_0/\hbar)^2}.$$

In the expressions above ω_L and ω_L^h are electron and hole Larmor precession frequencies respectively, τ_{12} is the delay time between pulses, δ_0 is an isotropic exchange interaction constant, the exponential factor describes relaxation processes after the pulses action. Indices HHH etc. again

denote polarization of the first and second pulses and of the detected PE signal, respectively.

The theoretical trion PE signals for different polarization configurations can be obtained according to the theoretical model provided in Ref. [1]:

$$P_{HHH}^{tr} = P_{VVV}^{tr} \propto \frac{1}{4} e^{-\frac{2\tau_{12}}{T_2}}, \tag{6}$$

$$P_{HVH}^{tr} \propto e^{-\frac{2\tau_{12}}{T_2}} cos\left(\left(\omega_L^e - \omega_L^h\right)\tau_{12}\right), \tag{7}$$

$$P_{VHV}^{tr} \propto e^{-\frac{2\tau_{12}}{T_2}} cos\left(\left(\omega_L^e + \omega_L^h\right)\tau_{12}\right), \tag{8}$$

$$P_{DDD}^{tr} \sim \frac{1}{4} e^{-\frac{2\tau_{12}}{T_2}} \left[cos\left(\left(\omega_L^e - \omega_L^h\right)\tau_{12}\right) + cos\left(\left(\omega_L^e + \omega_L^h\right)\tau_{12}\right) - \right.$$
$$\left. -2\, cos(\omega_L^e\, \tau_{12}) - 2\, cos\left(\omega_L^h\, \tau_{12}\right) - 2\right], \tag{9}$$

$$P_{DXD}^{tr} \sim \frac{1}{4} e^{-\frac{2\tau_{12}}{T_2}} \left[cos\left(\left(\omega_L^e - \omega_L^h\right)\tau_{12}\right) + cos\left(\left(\omega_L^e + \omega_L^h\right)\tau_{12}\right) + \right.$$
$$\left. +2\, cos(\omega_L^e\, \tau_{12}) + 2\, cos\left(\omega_L^h\, \tau_{12}\right) - 2\right], \tag{10}$$

The theoretically obtained dependencies of exciton and trion PE signals calculated for direct and tilted polarizations on time delay are demonstrated in Fig. 2.

Theoretical analysis of the obtained dependencies for excitons (1-5) and of the similar theoretical dependencies for trions (6-10) described in Ref. [1] allows us to propose the polarization protocols of optical excitation to separate experimentally the contributions of the exciton and the trion PE signals. For example, in HHH configuration, the exciton signal has an oscillating character, while the trion signal has a decaying character without any oscillations. For the HVH configuration, the exciton signal is zero, while the trion signal shows cosine-like oscillations.

Similar behavior is observed for the DDD and DXD polarizations when g_h=0 (see expressions 4, 5, 9, 10): the exciton DDD signal is oscillating while the trion DDD signal is decaying; the exciton DXD signal is zero, while the trion DXD signal oscillates.

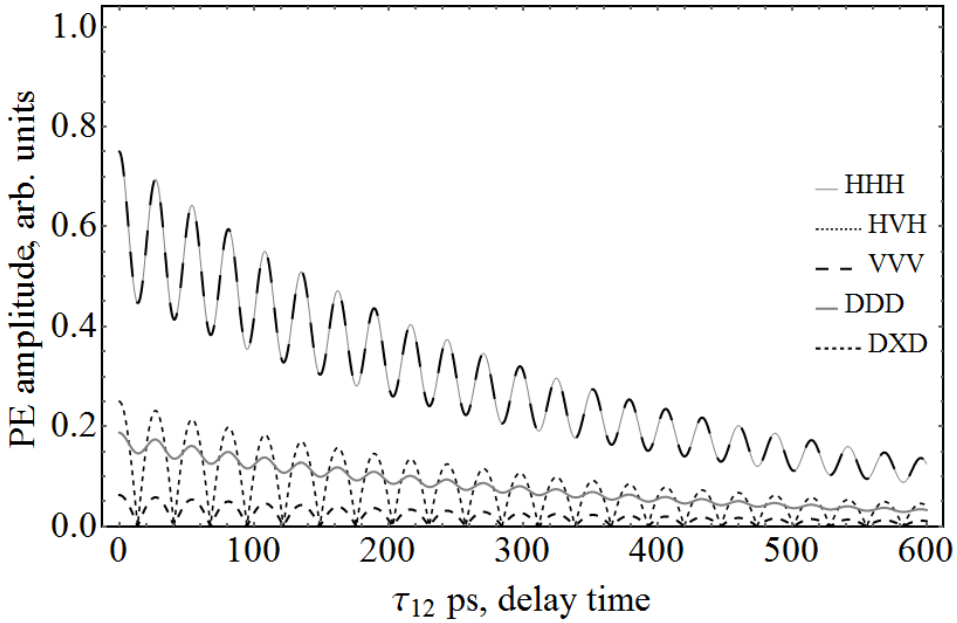

Fig. 2. Theoretically modeled PE signals for excitons and trions in direct and tilted polarization protocols. The thin gray and the black dashed overlapping lines demonstrate the PE signal in the HHH and VVV polarization geometries, the black dotted line demonstrates the PE signal in the HVH geometry, the gray solid line demonstrates PE signal in the HVH geometry, and the black short dashed line demonstrates the PE signal in DXD geometry respectively. The parameters are: electron g-factor $|g_e| = 0.44$, magnetic field $B = 3$ T, the dephasing time $T_2 = 700$ ps, the isotropic exchange interaction constant for excitons is δ_0 and hole g-factor are assumed to be zero. We assume that the fraction of excitons are two times larger than trions

Finally, the theoretical possibility of the experimental separation of the exciton and trion contributions in PE signal by appropriate choice of the exciting pulses polarization configurations have been shown in the present work. The most demonstrative separation of the exciton and trion contributions in the PE signals on the sample with a close to a zero hole g-factor has been analyzed.

This work was carried out in the framework of the joint Russian-Greek project supported by Ministry of Science and Education of Russian Federation (project RFMEFI61617X0085).

[1] L. Langer, S. V. Poltavtsev, I. A. Yugova et al, Nature Photonics 219, 851-857 (2014).

[2] A. Greilich, D. R. Yakovlev, A. Shabaev et al, Science, 313, 341-345 (2006).

[3] S.V. Poltavtsev, M. Salewski M., Yu. V. Kapitonov, et al, Phys. Rev. B 93, 121304(R) (2016).

[4] L. Langer, S. V. Poltavtsev, I. A. Yugova, et al, Phys. Rev. Lett. 109, 157403 (2012).

28. THE EMERGING OF CHROMATICITY OF STEEL SURFACE BY LASER RADIATION

***A. Burtsev*[1,2], *O. Butkovsky*[1], *E. Pritotsky*[1,2], *A. Pritotskaya*[1,2]**

[1]*Vladimir State University named after Alexander and Nikolay Stoletovs, 600000, Russia*

[2]*State Laser Proving Ground "Raduga", 600910, Russia*

Contacts: pritotsky@bk.ru, +7 (900) 474-86-72

The regimes of radiation using nanosecond laser pulses for emerging of chromaticity on stainless steel surface upon laser engraving are studied. Parameters of radiation that correspond to the spectrum of resulting colors on the sample surface are experimentally determined. The spectral analysis of the irradiated area is performed and probe microscopy is used to study the surface relief. Complicated surface relief that results from radiation indicates the contribution of several optical effects responsible for the surface color under laser engraving.

It is known that formation of metal-oxide films leads to coloration [1]. Metal oxide films on metal surfaces are formed owing to the thermal effect of laser radiation. The growth of thin films depends on several parameters of laser radiation and properties of the metal and processed surface. Variations in the parameters of laser radiation make it possible to control the formation of oxide films with variable thickness and, hence, determine the structure and properties of the films.

The width of the groove corresponds to the diameter of the laser spot (about 35 μm). The distance between the grooves is about 45.7 μm and the depth (300–600 nm) is related to the color.

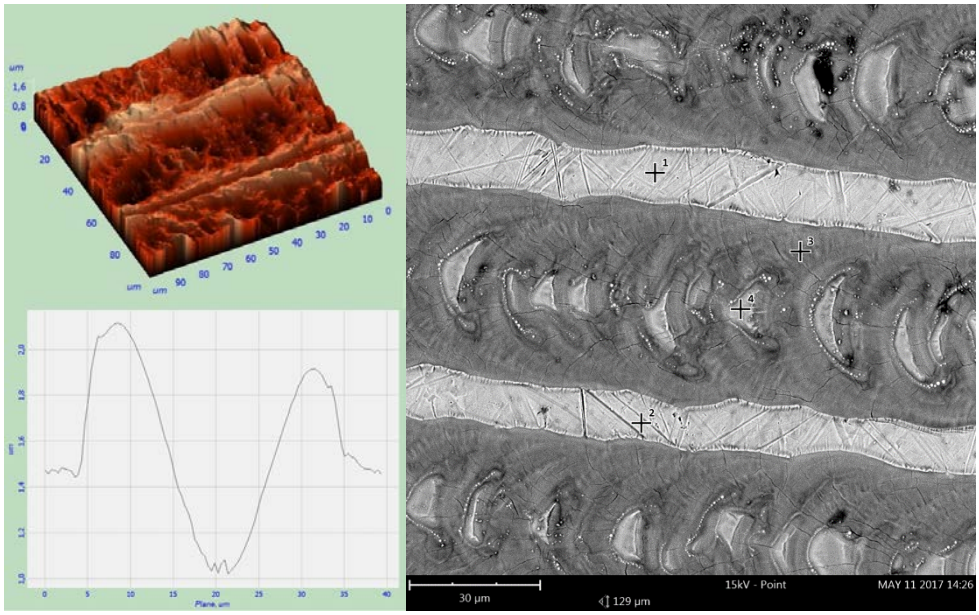

a b

Pic. 1. a) AFM-image of steel surface, b) SEM-image, point number is marking measurement of chemical concentration of O_2 1) 30,3%, 2) 36,8%, 3) 60,2%, 4) 48,8%.

References

1. A. Valiulin, S. Gornyi, Yu. Grechko, M. Patrov, K. Yudin, and B. Yurevich, Fotonika, No. 3, 16 (2007).

29. DEVELOPMENT OF DIELECTRIC MULTI-LAYER MIRRORS FOR HIGH-POWER SEMICONDUCTOR LASERS

E. Pritotsky, S. Lysenko, M. Pankov, A. Antipov

State Laser Proving Ground "Raduga", 600910, Russia

Contacts: pritotsky@trassa.org, +7 (900) 474-86-72

The level of development of science and technology imposes high requirements of quality of metal and dielectric films with different reflection coefficients, transmission and absorption on a certain length of electromagnetic wave. The possibility of receiving the coatings possessing the reproduced spectral characteristics when falling radiation under different angles is defined by the accuracy of calculations and monitoring of evaporation of separate layers and also stability of the modes of sedimentation. Surfaces of the reflecting laser mirrors usually make by methods of ion-plasma or electronic-ray evaporation of a covering on the plane or spherical optical surface of material of a substrate, for example, glasses. It is also possible to weaken reflection from a surface of optical elements the clarifying covering.

The method of calculation of multi-layer coatings with the given optical parameters is developed, simulation of the high-reflecting coatings and their reproduction on a vacuum technology equipment is carried out by method of ion-plasma evaporation. Feature of this method is use of model function of electromagnetic wave in which absorption depends only on coordinate, normal to a surface. Model function corresponds to a situation when the cross sizes of a luminous bundle there are much more than thickness of coatings, and displays the fact that the plane electromagnetic wave, falling on boundary of the section of the environments, refracts and absorbed in the new environment, at the same time its amplitude will change in case of distribution only to depth and will be a constant in the directions of the environments parallel to the plane of the section. Such approach differs from other methods of calculation and allows to create the universal mathematical algorithm for simulation of values of reflection coefficients and passage of multi-layer structures taking into account absorption and oblique falling of light. On the basis of the offered method of calculation the method of non-contact control of thickness of thin films by comparing of the actual and design optical characteristics of separate layers of coatings is offered.

The alignment of dependences of coefficient of passage on wavelength with estimated for the multi-layer mirrors made by an ion-plasma method (number of layers more than 18) at different lengths of waves (410, 532, 630 and 808 nm) is shown. The research of optical properties of samples and comparing with calculated data is conducted. In case of test of mirrors for the ray durability of visible defects it is not revealed at the density of power of laser pulse over 1.5

MW/cm^2. Experimentally the modes of cleaning of a surface of lines of laser diodes, parameters of the compensation layers clarifying, high-reflecting and the protecting covers meeting requirements of minimization of light absorption and stability of the created resonator mirrors when soldering laser diodes to heat exchangers and influence of a powerful laser radiation are defined.

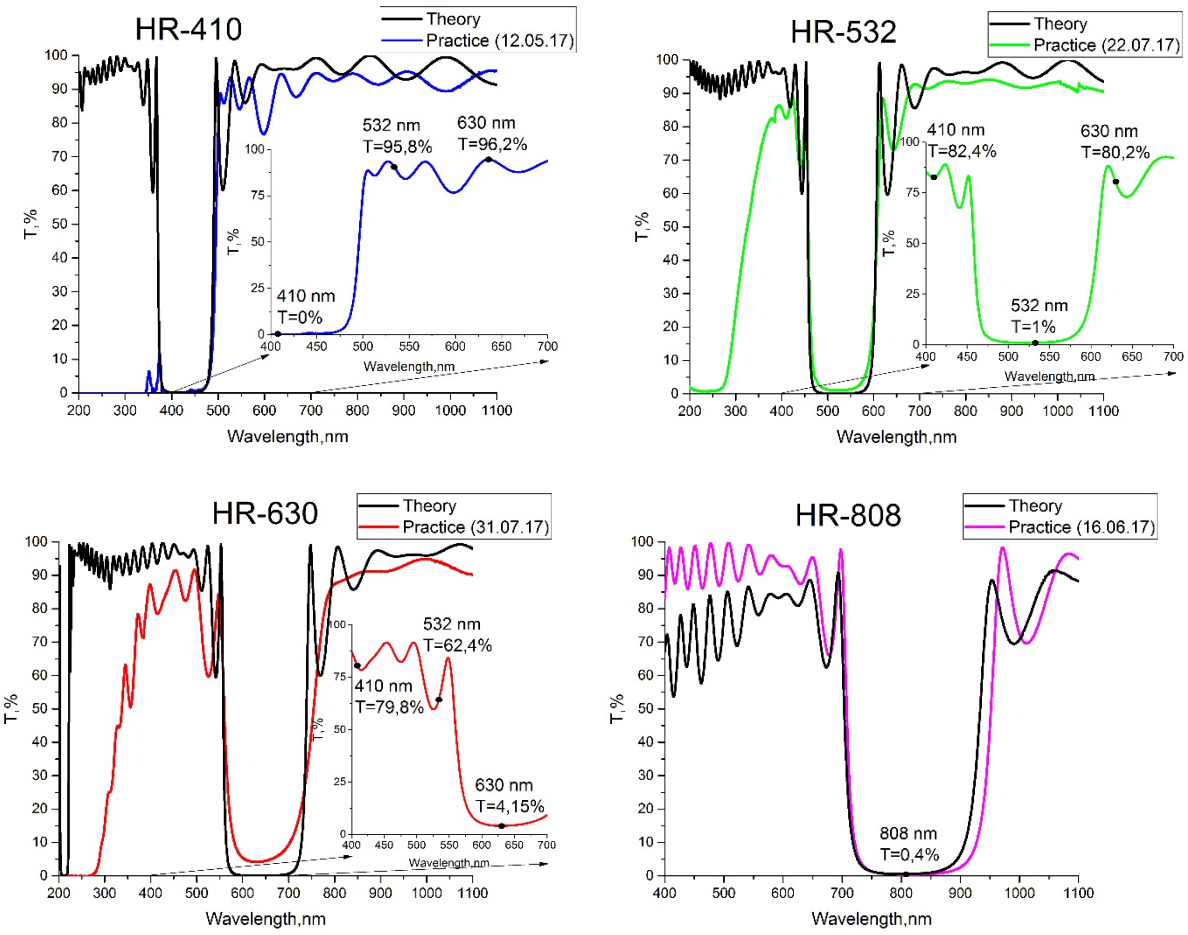

Pic. 1. Comparing of design and actual charts of dependence of energy index on wavelength on the glass K8

The difference of diagrams in the remaining range of lengths of waves is caused by imperfection of technological process, purity of the used targets, vacuum levels in the camera and quality of manual monitoring of processes by the operator. The program for calculation was installed on the controlling computer of vacuum technological system Aspira-150. When finishing the appropriate software and integration into management system of evaporation installation it is possible to automate process of evaporation of multi-layer optical coatings and to increase their utilization properties.

30. ПРОЕКТ ФОТОННОГО АЦП

Якушенков Павел

МФТИ, МИЭТ

loss24680@yandex.ru

Аналого-цифровой преобразователь (АЦП) – это прибор, принимающий аналоговый сигнал и выдающий набор цифр. Суть аналого-цифрового преобразования заключается в дискретизации сигнала во времени и квантовании его по амплитуде или мощности (рис. 1). Дискретизация сигнала обеспечивает не сплошной, а побитовый поток информации, а квантование придает каждому биту одно из дискретных значений (обычно 0 или 1).

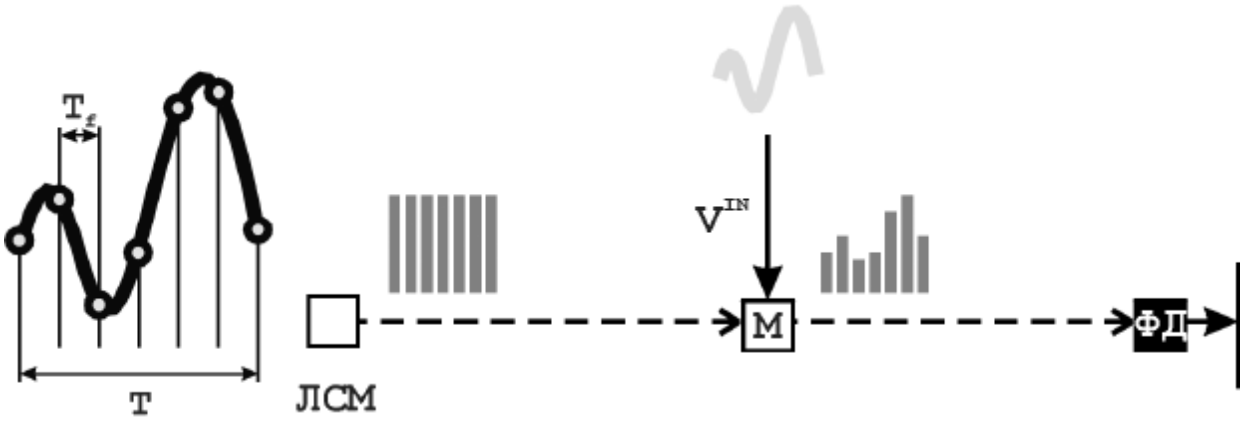

Рис. 1. ЛСМ – генератор импульсов для дискретизации, М – модулятор и ФД – приемник сигнала обеспечивают квантование[1].

Наибольшая частота электронных АЦП, изготавливаемых в России, близка к 500 МГц. Процесс повышения производительности АЦП в настоящее время замедлился, поскольку не удалось снизить флуктуации электронного генератора импульсов, используемого для дискретизации аналогового сигнала, и улучшить быстродействие АЦП. В то же время экспериментально обосновано, что фотонные АЦП (ФАЦП) позволяют на оптической несущей получить значительно более высокую частоту выборки аналогового сигнала, чем это может обеспечить транзисторная электроника. Создание из электрооптических модуляторов фотонного АЦП может обеспечить аналого-цифровое преобразование с частотой порядка 10 ГГц.

Известны различные схемы реализации ФАЦП: с увеличением частоты выборки за счет задержки (рис. 2); с оптическим демультиплексированием сигнала по длине волны в параллельные каналы (рис. 3); с оптическими частотными каналами (рис. 4); ФАЦП с модуляторами с различными длинами электродов для обеспечения нужной передаточной характеристики для обеспечения нужной цифры на выходе (рис. 5), которая так же может

быть обеспечена и отклонением луча из-за нелинейных эффектов и пропусканием его через транспаранты с периодическими щелями и фотодетекторами, настроенными на разные диапазоны, с мультиплексированием и демультиплексированием оптической несущей.

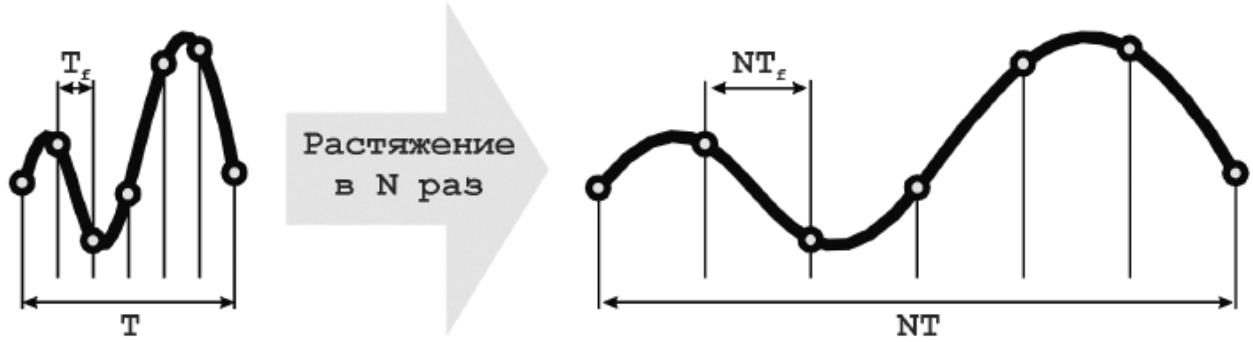

Рис. 2. Возможность увеличения частоты выборки за счет задержки [1].

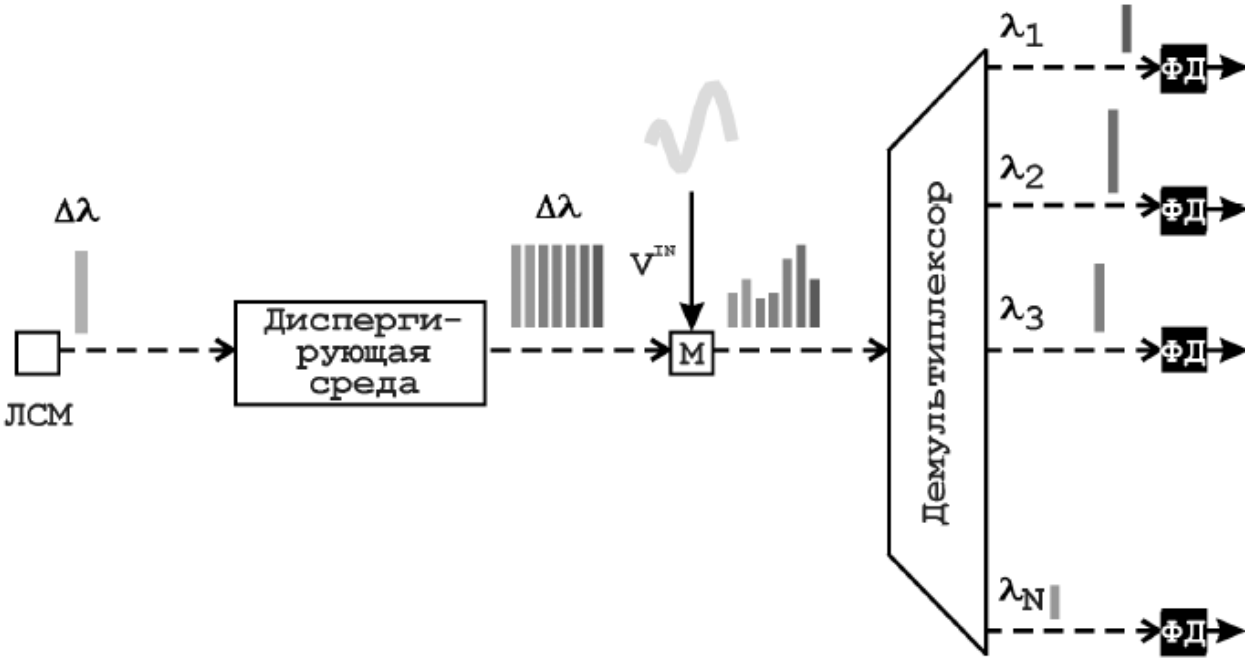

Рис. 3. ФАЦП с демультиплексированием по длине волны в параллельные каналы [1].

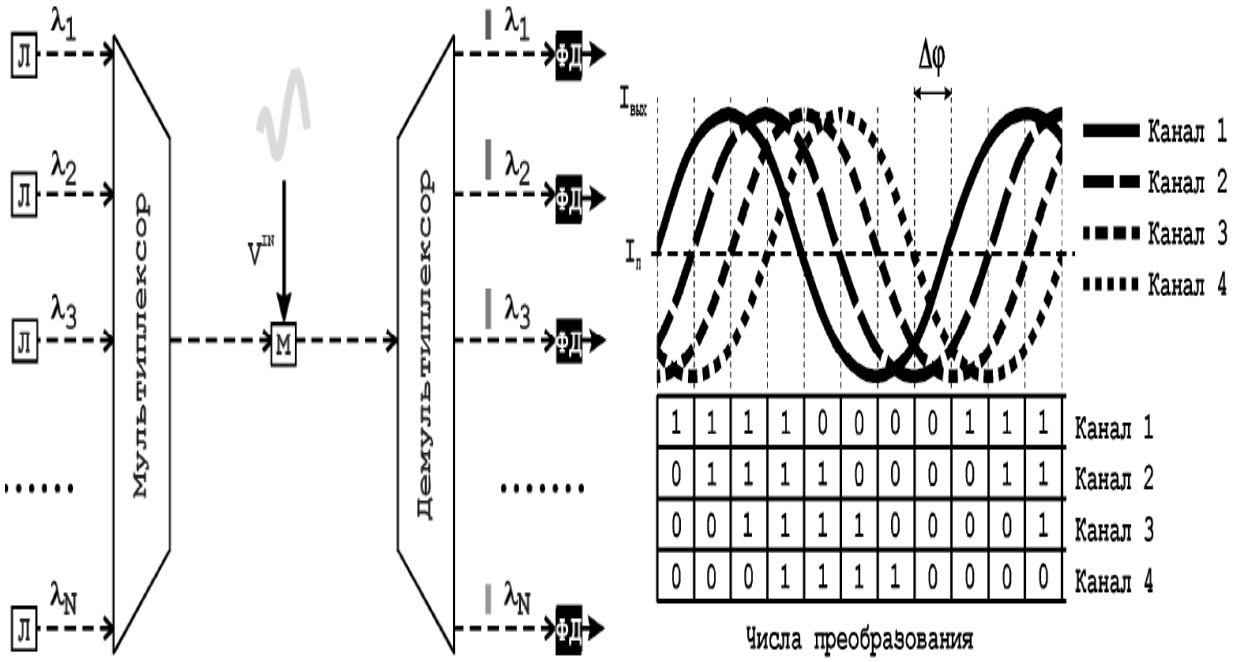

Рис. 4. ФАЦП с оптическими частотными каналами и их передаточная характеристика [1].

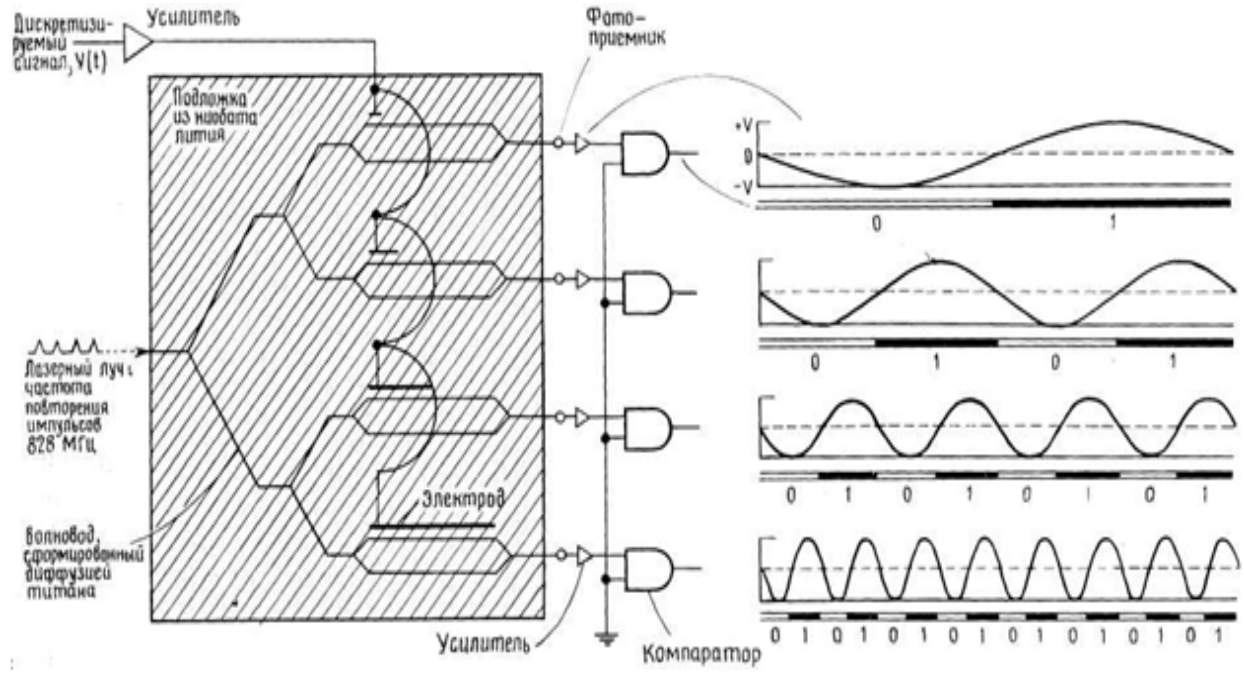

Рис. 5. ФАЦП с модуляторами с различными длинами электродов и их выходные сигналы [3].

Для реализации ФАЦП на фотонной интегральной схеме (ФИС) наиболее оптимальна последняя схема, т. к. в ней используется одна длина волны, количество компонентов в ней минимально, а модуляторы с различными длинами электродов обеспечивают сразу же необходимые выходные характеристики и не надо для этого делать на чипе еще и электронную схему.

ФАЦП на фотонной интегральной схеме

Остановимся на схеме реализации ФАЦП, которую можно будет реализовать на фотонной интегральной схеме (ФИС) в виде одного чипа. Основными элементами чипа являются - импульсный лазер, электрооптический модулятор и фотоприемник, изготовленные на единой схеме в интегральном исполнении (как рис. 5, но с лазером и приемником на той же интегральной схеме).

Для обеспечения быстрого аналого-цифрового преобразования можно использовать быстродействующие импульсные высокочастотные лазеры с частотой импульсов порядка ГГц и быстрые фотоприемники в интегральном исполнении на материалах A_3B_5 для диапазона длин волн в районе 1,55 мкм (популярная в ВОЛС длина волны), изготавливаемые в НПО «Полюс» им. М.Ф.Стельмаха.

Для обеспечения быстрого аналого-цифрового преобразования необходим модулятор с большой частотой переключения, для чего нужно, чтобы быстро перезаряжалась емкость на электродах. Для этого целесообразно использовать материалы с высокой подвижностью, такие, как материалы группы A_3B_5. На сегодняшний день лучшим вариантом электрооптического модулятора является модулятор типа Маха-Цендера (рис. 6). Однако в нашей стране электрооптические модуляторы Маха-Цендера пока делаются только на ниобате лития («ПНППК»), который закупается за границей.

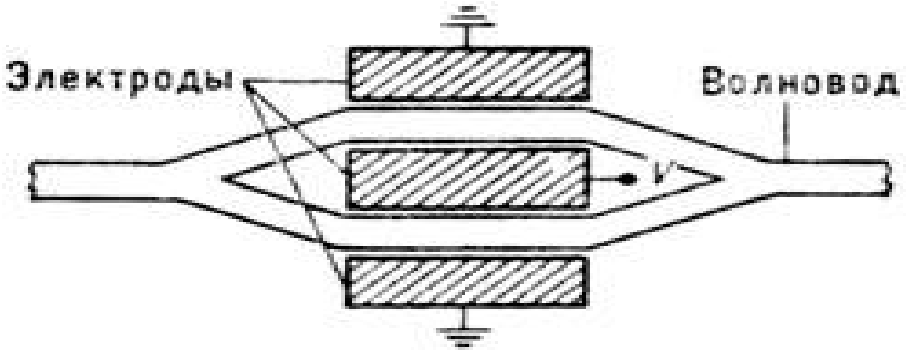

Рис. 6. Электрооптический модулятор типа Маха-Цендера [3].

Для реализации ФАЦП на интегральной схеме необходимо создать электрооптический модулятор типа Маха-Цендера в интегральном исполнении, который можно интегрировать вместе с лазером и фотоприемником и который обеспечит частоту переключения от 10 до 100 ГГц. Гетероструктуры из материалов A_3B_5 можно выращивать, не закупая материалы за границей, а технологические операции с гетероструктурами можно выполнять на существующей технологической базе.

За границей уже делают интегральные электрооптические модуляторы типа Маха-Цендера на InP и GaAs, например Teraxion, Oclaro, aXenics. Более того, уже производятся линейки лазер-модулятор-фотоприемник в интегральном исполнении на единой схеме [2]. Для ФАЦП по сути надо сделать несколько таких параллельных линеек.

Для создания ФАЦП предстоит спроектировать и промоделировать его топологию в САПРе, разработать технологический маршрут для ее реализации, вырастить необходимую гетероструктуру и провести технологические операции согласно маршруту.

В последнее время многие компании стали выпускать САПР для ФИС, например Lumerical, COMSOL, PhoeniX, Optiwave. Для проектирования нами был выбран САПР Lumerical [4]. Эта система совместима с CadenceVirtuoso, на котором проектируется сейчас большинство электронных схем, а так же включает в себя несколькопакетов: FDTDSolutions, в котором можно моделировать различные волноводы, разветвители и другие волноводные структуры из различных материалов; DEVICE, в котором можно моделировать различные приборы; INTERCONNECT для проектирования многих элементов на единой схеме и MODE Solutions в котором можно моделировать плазмонные волноводы, фотонные кристаллы и др. На рис. 7 показан промоделированный в САПР Lumerical простой вариант электрооптического модулятора типа Маха-Цендера.

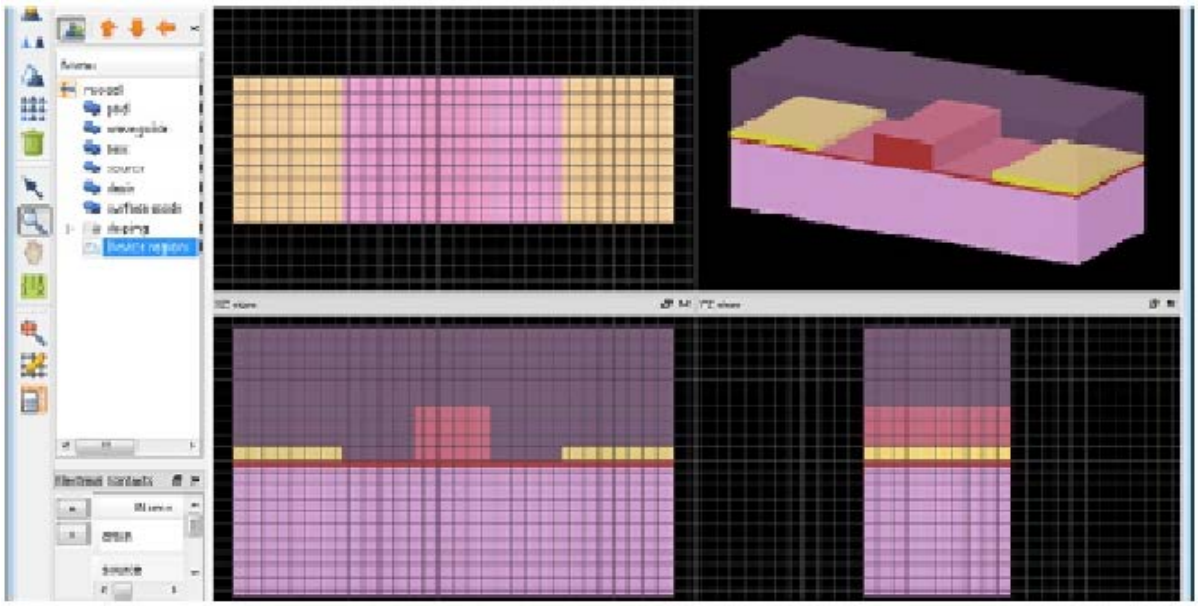

Рис. 7. Электрооптический модулятор типа Маха-Цендера, промоделированный в САПР Lumericle.

После проектирования и моделирования топологии необходимо подобрать нужную гетероструктуру и технологические операции с ней (такие как травление, осаждение, литография, МЛЭ...), которые нужны для реализации ФАЦП.

Для реализации топологии сверхбыстродействующего ФАЦП не обязательно обладать самыми современными в мире технологическими нормами, как Intel (13 нм). Необходимые технологические операции можно выполнить и на имеющимся в России оборудовании (например Corial); ведь Intel нужна такая норма для реализации быстродействующих переключателей - чем меньше длина, тем быстрее переключается транзистор, однако электрооптический модулятор типа Маха-Цендера даже размером до нескольких мм может переключаться со скоростями порядка 10 ГГц.

ЗАКЛЮЧЕНИЕ

Предлагаемый ФАЦП может иметь быстродействие около 10 ГГц. Реализовать топологию ФАЦП на материалах A_3B_5 (вырастить для этого гетероструктуру и провести с ней необходимые технологические операции) можно полностью в России. Имея фотонный АЦП, можно будет разрабатывать цифровые фотонные схемы, включая цифровые оптические процессоры.

Литература:

1. **Р. С. Стариков**Фотонные АЦП - ЗАО «Издательство «Радиотехника», 2015.

2. *'InP-Based Photonic Integrated Circuits', Goldren, 2008.*

3. **Якушенков П. О., Балаклейский Н. С.** Фотонные интегральные схемы. – Сб. докладов6-ой Международной конференции по фотонике и информационной оптике.- М., 02 февраля 2017 г., ННИЯУ «МИФИ» с. 146-148.

4. www.lumerical.com.

31. DETERMINATION OF TEMPERATURE MEASUREMENTS ON THE SURFACE CARBONACEOUS MATERIALS WITH SIMULTANEOUS REGISTRATION OF THE LASER INDUCED PROCESSES

S. M. Arakelyan, A.F. Galkin, S. V. Zhirnova, E.L. Shamanskaya

Vladimir State University, Vladimir
svetlanna_vik@mail.ru

Expansion of technological capabilities of carbonaceous materials is connected with melting. The issue of real time registration of laser induced melting process of glassy carbonis presented in works [1, 2]. Brightness temperature of glassy carbon meltingis determined in work [3].

The purpose of this paper is registrating laser induced processes for surfaces of carbonaceous materials and temperature measurement.

Experimental setup

Samples of glassy carbon and pyrocarbon with carbon content of 99,9% were taken as a targetand were exposed to focused laser radiation. Continuous radiation of the fiber LS-02-T laser (wavelength 1070 nanometers, emitting power changed from 15 to 150 W) was used.

The copper vaporsbrightness amplifier CVL-10 made possible producing up to 16000 optical images laser of affected areaper second, with exposition being up to 20 nanoseconds. To producethe images we installed a 1,3 megapixel matrix CMOS sensor, which allowsinputting 200 images per second. Controller board VS 2001 enabled information transfer to the computer in the form of sequence of frames with the resolution of 1280x1024 pixels when processing and analyzing data.

Temperature was measuredat wavelength of 0,65 μm of a high-temperature micropyrometer of MP-1001. The device enables continuous monitoring of temperatures in the working range from 1500 to 5000 K. The software allows monitoring of stationary temperature inthe graphic form on the monitor screen. Instrumental measurement error for brightness temperatures is no more than ±0,5%.

Fig. 1 shows the scheme of experimental setup.

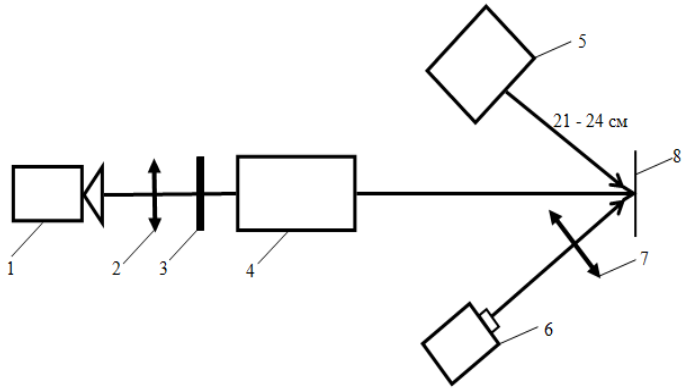

Fig. 1. Experimental scheme:

1 – high-speed camera VS-FAST-NG; 2, 7 – the focusing lenses (with focal lengths 50 mm and 40 mm); 3 – set of light filters (KS-11; ZhS-11; ZhZS-6; SZS-21; ZhS-18; SS-1; NS-1); 4 - the copper vapor amplifier of brightness CVL-10; 5 – MP-1001 micropyrometer; 6 – fiber LS-02-T laser; 8 – sample

ExperimentResults

Fig. 2 represents the diagram of brightness temperature taken by means of a high-temperature micropyrometer of MP-1001 in the process of exposure of glassy carbon surface to continuous laser radiation. Laser radiation power is 120 W. Exposure time is 16 seconds.

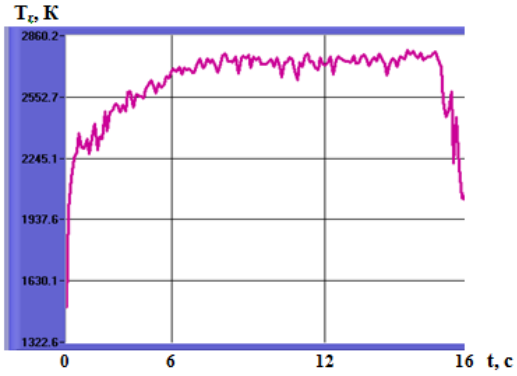

Fig. 2. Brightness temperature of glassy carbon surface

Fig. 3 shows images madewith high-speed digital camera VS-FAST-NG in the course of laser radiation on the surface of glassy carbon, with images being separate frames of video. To show the difference four images of glassy carbon surface are provided: *fig. 3a* – before influence; *fig. 3b* - influence time $\tau_в = 3$ sec; *fig. 3c* – $\tau_в = 12$ sec; fig. *3d* - $\tau_в = 16$ sec. The focusingzone of continuous laser radiation is ~ 0,3 mm, controlled area is ~ 1 mm, the zone of temperaturemeasurement is 0,1 mm. Power of laser radiation is 120 W. Influence time is 16 seconds.

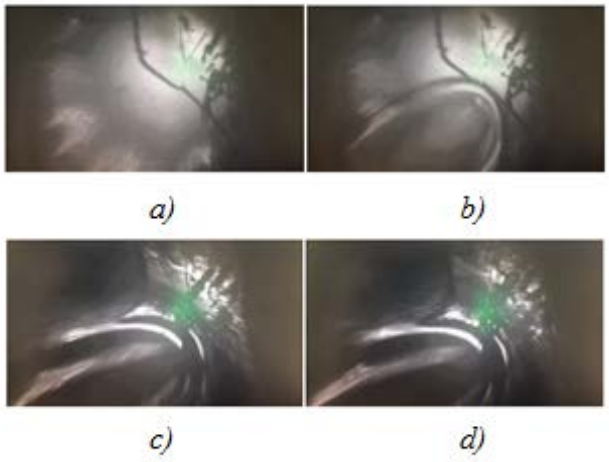

Fig. 3.Surface of a glassy carbonin the course of continuous laser radiation

Wave fronts are clearly visible. Wavelength makes about 0,03-0,04 mm. Melting of glassy carbon is observed at the power of laser radiation of about 70 W which agrees with works [1, 2]. The brightness temperature of glassy carbon melting can beseen on the horizontal part of the diagram (fig. 2) and makes $T_r = 2720 \pm 15$ K.

Fig. 4 shows images taken with high-speed digital camera VS-FAST-NG in the course of laser radiation on the surface of pyrocarbon, the images being frames of video. To show the changes four images of pyrocarbon surface exposed to laser radiation are provided: *fig. 4a* – before influence; *fig. 4b* - $\tau_в = 30$ sec, the power of laser radiation is 75 W; *fig. 4c* - $\tau_в = 60$ sec, the power of laser radiation is 100 W; *fig. 4d* - $\tau_в = 90$ sec, the power of laser radiation is 125 W. The focusingzone of continuous laser radiation is ~ 0,3 mm, controlled areais ~ 1 mm, the zone of temperature measurementis 0,1 mm. Influence time is 90 seconds.

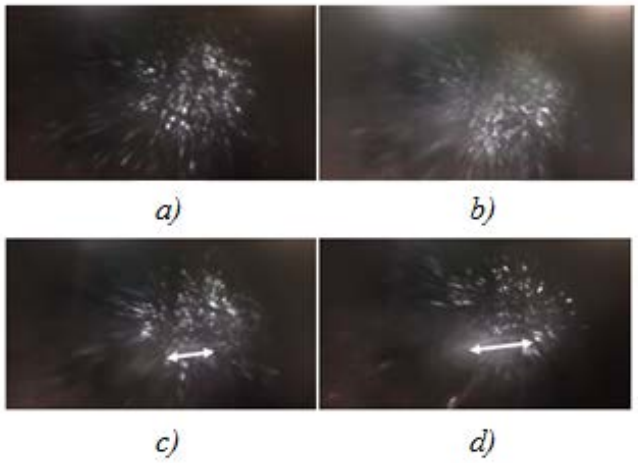

Fig. 4.Surface of pyrocarbon the course of laser radiation

Melting was not observed with different laser exposure modes. The main processes observed are heating and ablyation. Emergence of a cavity is registered at the exposure time of 60 sec and the

power of laser radiation of 100 W *(fig. 4c)*, further increase of exposure time and power of laser radiation *(fig. 4d)* causes the cavity expansion. The brightness temperature of pyrocarbon surface is as follows: T_r = 2383 K *(fig. 4b)*; T_r = 2447 K *(fig. 4c)*; T_r = 2544 K *(fig. 4d)*.

Conclusion

The paper presentsthe design of experiment on registration of laser induced processes on surface of carbonaceous materials with simultaneous measurement of brightness temperature. Brightness temperature of glassy carbon melting due tocontinuous laser radiation is measured using high-temperature micropyrometer and makes 2720 ± 15 K. Wave structures are received, wavelength is estimated. For determination of true meltingtemperature of glassy carbon it is necessary to know the degree of blackness of this material at the melting temperature which is a complex task, requiring further experiments. Melting of a pyrocarbon was not observed with different radiation modes, the main processes being heating and ablyation.

References

1. Abramov D.V., Arakelyan S.M., Galkin A.F., etc. Melting of the carbon heated by the concentrated laser radiation in air with an atmospheric pressure and temperature which isn't exceeding 4000 K//the Letter in ZhETF. - 2006. - t. 8 h, вып 5. - Page 315 – 319.
2. Abramov D.V., Galkin A.F., Zharenova S.V., etc. Visualization of interaction of laser radiation with a surface the uglerodosoderzhashchikh of materials//Works Vladim. the state. un-that. Vyp. 3 Physical and mathematical bases of the industry of nanosystems and materials. – 2007. - Page 20 – 23.
3. S.M. Arakelyan, A.F. Galkin, S.V. Zhirnova, A.V. Osipov "Determination of the brightness temperature of melting of a steklouglerod". Dynamics of Difficult Systems magazine, 2015, t. 9, No. 1, S 48-50.
4. Physical quantities: Reference book / A.P. Babichev, N. A. Babushkina, A.M. Bratkovsky, etc.; under. edition of I.S. Grigoriev, E.3. Meylikhov. - M.: Energoatomizdat, 1991. – 1232 pages – ISBN 5-283-04013-5.

32. EXPERIMENTAL STUDY OF THE PARAMETERS OF FILAMENTS IN TRANSPARENT SOLID MEDIA

M. A. Tarasova, K.S. Khorkov, D.A. Kochuev, V.G. Prokoshev

Department of Physics and Applied Mathematics,
Vladimir State University named after A. G. and N. G. Stoletovs,
87 Gorky, Vladimir, 600000, Russia
E-mail: trsvmargarita@gmail.com

The phenomenon of filamentation of femtosecond laser radiation consists in the spatiotemporal localization of energy in a high–power laser femtosecond pulse under the action of self–focusing in the medium and nonlinearity in a self–induced laser plasma that persists for significant propagation lengths in liquids, gases and solid transparent dielectrics [1]. There are many works devoted to the study of the phenomenon of filamentation and attendant effects [2–5].

In this work, designed and assembled experimental setup for measuring parameters of the filaments. The source of laser radiation was the ytterbium femtosecond laser TETA–10 (wavelength 1029 nm, pulse duration 280 fs, pulse repetition rate 10 kHz, maximum pulse energy 150 μJ). As the sample was used a KU–1 quartz optical glass (5x5x20 mm), which characterized by high transmittance in the UV, visible and near IR spectral ranges [6].

The measurement of filaments, namely the length of the filaments and the intensity distribution in the transverse profile of the beam, was carried out according to the scheme in Fig. 1.

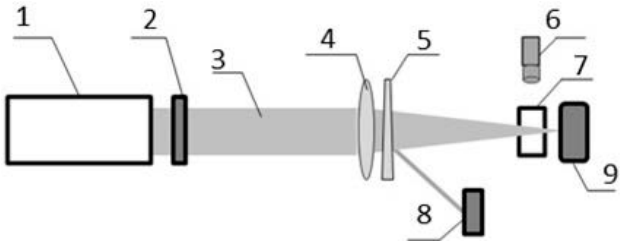

Fig. 1. Scheme measuring the length of filaments: 1 – laser; 2 – polarization attenuator; 3 – femtosecond laser radiation; 4 – spherical lens; 5 – optical wedge; 6 – camera and microobjective; 7 – sample; 8 – photodiode sensor; 9 – spectrometer (Beam Star)

To focus the laser beam was used a spherical lens with a focal length of 150 mm. Behind the sample was installed Beam Star – the device for registering the transverse profile distribution of radiation intensity (Fig. 2).

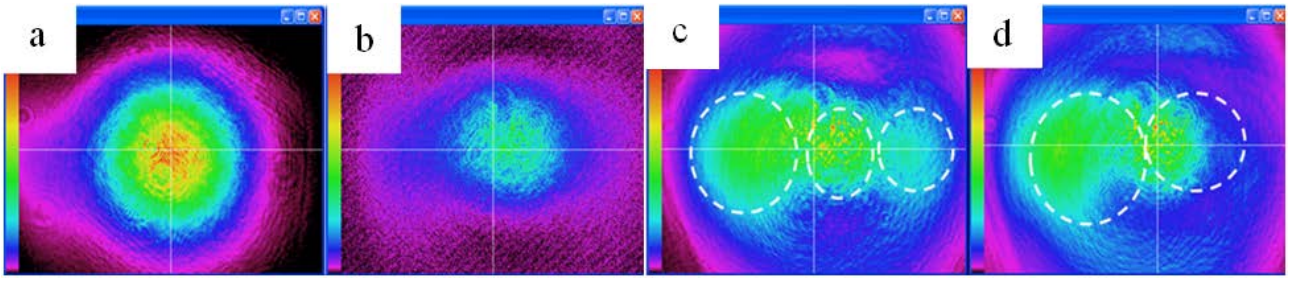

Fig. 2. Distribution of the transverse intensity profile of the laser beam with a power: a) 0,7 mW without sample with a focusing lens; b) 0,7 mW with a sample; c) 4.2 mW; d) 9 mW

Experimentally was established the value of the critical power at which filamentation begins to develop was 5.18 mW. Fig. 2 shows the change of the intensity distribution in the transverse profile of the beam. With increasing power, the length of the filaments also increased, as demonstrated in Fig. 3.

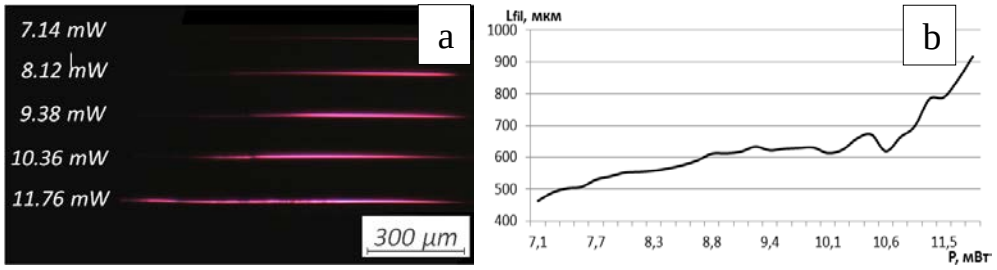

Fig. 3. a) Filamentation in fused quartz of KU–1. Image obtained by the camera. To the left are indicated the values of the radiation power; b) The dependence of the filaments length from the values of the radiation power

Measuring the length of the filaments took place with the help of images obtained from the camera. To calculate values of the filament length were used the measurement standard, with the applied calibration objects of known dimensions, after which occurred a comparison of the size of the filament and the standard. Measurement of filament length was possible with a power gain of 7.14 mW. First of all, this is due to the photosensitivity parameter of the camera used.

The result of the work was measured parameters of the filaments: the length of the filaments, depending on the power of the laser radiation; the intensity distribution in the transverse profile of the beam. Experimentally recorded power value, at which begins to develop filamentation.

This study was performed as a part of the state task VlSU 1106/17 and a grant of the RFBR number 16–32–00760 mol_a.

References

1. *Kosareva O.G.* Filamentation of femtosecond laser radiation in transparent media. Diss. dokt. fiz.–mat. nauk. MSU, Moscow, 2011. 234 p.

2. *Smetanina E.O.* Light bullets and the spectrum of femtosecond laser radiation at filamentation in fused quartz. Diss. kand. fiz.–mat. nauk. MSU, Moscow, 2014. 147 p.
3. *Kandidov V.P., Shlenov S.A., Kosareva O.G.* Filamentation of high–power femtosecond laser radiation // Quantum Electronics. 2009. V. 39. №. 3. P. 205.
4. *Khorkov K.S. et al.* The dynamics of the intensity distribution of the laser radiation in multiple filamentation in transparent medium // Dynamics of difficult systems –XXI century. 2015. V. 9. № 4. P. 23.
5. *Zverev V.A., Krivopustova E.V., Tochilina T.V.* Optical Materials. Part 2. ITMO, St. Petersburg, 2013. 248 p.

33. MORPHOLOGY, GRANULOMETRIC AND STRUCTURAL PHASE COMPOSITION OF MECHANICALLY SYNTHESIZED COMPOSITE POWDER AL-MG+AL/MWCNTS

[1]Aborkin A.V., [1]Sobol`kov A.V., [1]Kireev A.V., [2]Volochko A.T., [2]Izobello A.Yu., [3]Sachkova N.V., [3]Sytschev A.E.

[1]Vladimir State University named after Alexander and Nikolay Stoletovs, Vladimir, Russia
[2]Physical-Engineering Institute, National Academy of Sciences of Belarus, Minsk, Belarus
[3]Merzhanov Institute of Structural Macrokinetics and Materials Science, Russian Academy of Sciences, Chernogolovka, Russia
e-mail: aborkin@vlsu.ru

Creation and study of composite materials reinforced with hybrid carbon structures is a promising trend of scientific researches especially with manufactorins industry demands in parts with improved physical and mechanical properties. Works [1,2] show that using hybrid carbon structures for reinforcement helps gradualy improve tribological behavior of frictionproof babbit coatings.

The objective of this work is to research the influence of microadditions of hybrid carbon structures to morphology, granulometric and structural phase composition of mechanically synthesized composite powders Al-Mg+Al/MWCNTs (Al-Mg+Al/MWCNTs ration changes between 0.05 and 0.3 wt.%).

Initial mixture used consisted of globular granules 1-2 mm in diameter from aluminium alloy AlMg2 with addition of 0.05, 0.15 and 0.3 wt.% of Al/MWCNTs.

Mechanical treatment of the initial mixture was conducted in a globular planetary mill FRITSCH PULVERISETTE 6 using surface-active materials (stearic acid 0.75 wt.%). Milling was conducted using steel balls 8 mm in diameter at the ratio of mixture components to milling bodies 1:20. Mechanical synthesis was conducted at rotation rate 600 rpm during 4.5 hours.

Particle size distribution of synthesized composite powder was measured using MICROSIZER-201C. Structural phase composition of composite powder was performed using X-ray structural analysis. For that purpose a diffractometer D8 ADVANCE was used. Composite powder morphology was examined using ultra high resolution field-emission scanning election microscope ZEISS ULTRA PLUS based on ULTRA 55.

Study of granulometric size composition of composite shows (see pic. 1a) the increase of Al/MWCNTs volume in the mixture from 0.05 to 0.3 wt.% leads to decrease of mediam partice size from 18.7 to 17.6 μm. It should be noted that in all compositions fraction size is less that 10 μm.

Results study of X-ray structural analysis (see pic. 1b) shows that diffraction patterns have similar characteristics. Peaks that correspond to aluminum were noted. At the same time there are

no peaks that correspond to Al/MWCNTs; this is due to small sensibility of X-ray structural method to identifying phases with volume less that 3%.

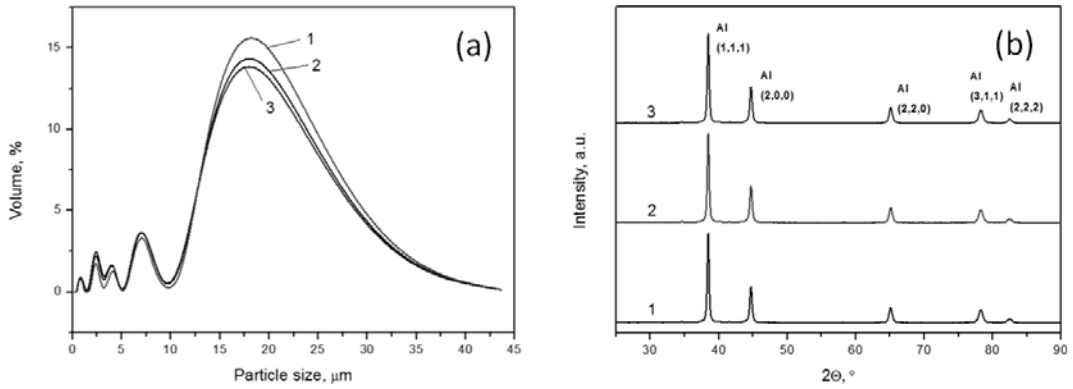

Pic. 1. Granulometric size composition (a) and structural phase (b) composition of composite powders. Numbers identify: 1 – 0.05 wt.%; 2 – 0.15 wt.%; 3 – 0.3 wt.%

Selyakov-Scherrer equation was used to calculate the size of coherent-scattering region. Calculation results show that increase of Al/MWCNTs volume in the mixture leads to decrease the size of coherent-scattering region from 65 to 57 nm.

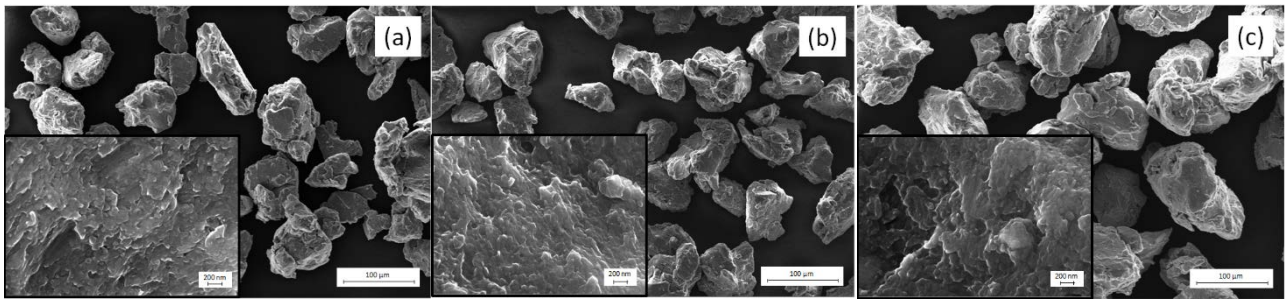

Pic. 2. TEM images of composite powder particles: a – 0.05 wt.%; b – 0.15 wt.%; c – 0.3 wt.%

Pic. 2 shows TEM images of powder particles that characterize it's morphology. At higher resolution on the fracture surface shows micro-crystals which sizes correspond to calculated values of coherent-scattering region. On the surface of powder particles no hybrid carbon structures were detected. This is related to its small concentration and specific formations of powder particles during mechanical synthesis [3].

The reported study was funded by RFBR according to the research project № 17-58-04048

References

[1] Коберник Н.В., Михеев Р.С., Ваганов В.Е., Аборкин А.В. Структура и трибологические свойства антифрикционных покрытий, модифицированных углеродными нанотрубками // Вопросы материаловедения, 2016. № 1(85). С. 60-66.

[2] Aleshin N.P., Kobernik N.V., Mikheev R.S., Vaganov V.E., Reshetnyak V.V., Aborkin A.V. Plasma–Powder Application of Antifrictional Babbitt Coatings Modified by Carbon Nanotubes // Russian Engineering Research, 2016, Vol. 36, No. 1, pp. 46–52.
[3] Aborkin A.V., Evdokimov I.A., Vaganov V.E., Alymov M.I., Abramov D.V., Khor'kov K.S. Influence of Mechanical Activation Mode on Morphology and Phase Composition of Al-2Mg-nC Nanostructured Composite Material // Nanotechnologies in Russia, 2016, Vol. 11, No. 5–6, pp. 297–304.

34. THZ SPECTROMETERS BASED ON ULTRAFAST LASERS

Vasilis Apostolopoulos

Physics and Astronomy, University of Southampton, Southampton, SO171BJ, UK
Vasilis.apostolopoulos@gmail.com

In the Terahertz (THz) laboratories group in the University of Southampton we work on developing novel THz emitters and spectrometers based on the concept of THz time domain spectrometry.

I will present THz emitters based on diffusion currents where terahertz radiation can be generated by ultrafast photo-excitation of carriers in a semiconductor. I will present 2D simulations of the THz generation effect taking into account the diffusion of carriers and the electric field using finite differences time domain simulations. Multiplexed emitter geometries will also be shown such as double-metallic multiple emitters which operate under uniform illumination and are fabricated with periodic Au and Pb structures on GaAs. Terahertz emission in this case originates from diffusion currents and from the different Schottky barrier heights of the chosen metallic pair. I will demonstrate how our large area multiplexed emitters can be used in order to achieve THz focusing.

Finally, I will present our work on the development of Mode-locked Vertical External-Cavity Surface-Emitting Lasers (ML-VECSELs) that have seen advances in pulse energy and peak power thanks to improved power handling techniques and structure designs. The significant increase in gain and intra-cavity power, coupled with the VECSEL's accessible external-cavity, has made the addition of intra-cavity elements for frequency conversion possible even for lossy conversion mechanisms. I will show a gold-patterned Semiconductor Saturable Absorbing Mirror (SESAM) that functions both as a slow saturable absorber in a ML-VECSEL and as an intracavity strip line Photo-Conductive Antenna (PCA) for THz emission. I will describe the design of the strip emitter, and how it performed on a THz-Time Domain Spectrometer based on a ML-Ybfibre laser. I will also show the characterisation of the ML-VECSEL built with the patterned SESAM. Our target is to produce a laser which will perform intra-cavity generation of THz and be the basis for a compact and fast spectrometer.

35. ATOMIC-FORCE LITHOGRAPHY FOR PHOTONIC APPLICATIONS

A. Kucherik, S. Kutrovskaya, I. Skryabin, A. Shagurina, A. Osipov, I. Chesnov

A.G and N.G. Stoletov Vladimir State University
87 Gorki st., Vladimir, Russia, 600000.
E-mail: 11stella@mail.ru

The results of the formation of planar nanostructures with relief, repeating the trajectory of movement of an AFM probe were presented. The parameters affecting their geometric dimensions: height, width, uniformity in the layer, etc. were investigated. The method of induced deposition of silver/golden clusters on the silicon wafer surface p-type in the presence of an external electric field was developed. The possibility of using such structures as hybrid circuits using photoelectronic transducers was discussed.

Noble metals nanostructures such as silver and golden nanoparticles are well known due to their ability of supporting surface plasmon localization at optical frequencies [1-2]. Such optical nonlinear gain effectsare widely used in nanoparticle biological and chemical sensing, surface enhanced Raman scattering or in photoelectric applications. Their spectral response strongly depends on the nature of the metal, the size, the shape and the spatial arrangement of nanoparticles. The precise control of these parameters during fabrication process is the main goal for adjusting the optical properties of such structures in many applications [3].

Among the amount of different notable phenomena appeared in plasmonic structures the effect of the directional propagation of light observed in the silicon-metal interfaces deserves special attention. Such structures could potentially find a promising applications in all-optical information processing devices since it can transmit optical signals. A great number of various methods of fabrication of nanostructures supporting for plasmon resonances on metal-silicon interfaces were recently proposed. Most of them are based on complicated multi-step lithographymethods which can be combined by perforce with different chemical etching techniques, electron beam evaporation and so on. All this procedures demand rather expansive equipment and well optimized technology. In this paper we propose an alternative easy and relatively cheap method of fabrication of metal nanostructures grownon a siliconsubstrate. The main peculiarity of the proposed technique is the ability to control the shape and morphology of the designed structure. The proposed method is based on coating thin layers assembled of silver or golden clusters with a prominent precision accessible by modern possibilities of scanning probe microscopy.

The reported study was also supported by the Ministry of Education and Science of the Russian Federation (state project no. 16.1123.2017/PCh), RFBR grants 16-32-60067 mol_a_dk, and by the grants of president of Russian Federation byprojectsMK-2842.2017.2 and MK-2988.2017.2.

References

1. Antipov A.A., Arakelyan S.M., Vartanyan T.A., et al "Optical properties of nanostructured gold–silver films formed by precipitation of small colloid drops," *Optics and Spectroscopy*, Vol 119, #1, 119-123, 2015.

2. A.B. Evlyukhin and S. I. Bozhevolnyi "Resonant unidirectional and elastic scattering of surface plasmonpolaritons by high refractive index dielectric nanoparticles," *Physical Review B*, Vol 92, #24, 245419, 2015.

3. Arakelyan, S. M., Veiko, V. P., Kutrovskaya, S. V., "Reliable and well-controlled synthesis of noble metal nanoparticles by continuous wave laser ablation in different liquids for deposition of thin films with variable optical properties," *Journal of Nanoparticle Research*, Vol 18, №6, 155, 2016.

36. MECHANISMS OF LIQUID-PHASE EXFOLIATION OF GRAPHENE

V.A. Ilin, K.S. Khorkov, D.A. Kochuyev, V.G. Prokoshev, S.M. Arakelian

Department of Physics and Applied Mathematics,
Vladimir State University named after A. G. and N. G. Stoletovs,
87 Gorky, Vladimir, 600000, Russia
E-mail: viktor33ilin@gmail.com

Graphene is a two-dimensional crystal consisting of carbon atoms arranged in a honeycomb lattice [1]. The concept of "graphene" appeared in 1962, but opening a real graphene was only in 2004, using the method of micromechanical cleavage of graphite. Micromechanical cleavage of graphite was the basic method for producing a graphene in early studies of its properties and was the foundation for a number of new producing techniques, initiating active research in the field of graphene exfoliation.

To date, there are many methods for producing graphene, one of which is the "liquid-phase exfoliation of graphene ". This method is based on the intercalation of foreign atoms or molecules in the interlayer space of graphite. The introduction of impurities weakens the interaction energy between layers by increasing the distance between them. Thus, it becomes possible to further separation into its crystal monolayers. As substances introduction used superficially active substance (SAS) having high interaction energy with the graphene layers, such as, N,N-dimethylacetamide (DMA), g-buthyrolactone (GBL) and other [2].

In paper [3] from N-polymethylpentene and finely divided graphite powder were preparing a suspension, which is then sequentially subjected to ultrasonic treatment and centrifuged. The last stages were used with the aim of obtaining in the solution suspended single-layer graphene sheets, as well as samples composed of small numbers of layers.

One option of the method liquid-phase separation of graphite is an exfoliation of graphene by femtosecond laser irradiation in liquid nitrogen [4]. The freezing of samples with liquid nitrogen is often used in view of the availability of international standard boiling point and small size of nitrogen molecules, which ensures its high fluidity.

At low temperatures the graphite lattice becomes less "plastic" that will probably allow to breaking the interlayer bonds smaller energy contribution at the local heating diffused nitrogen molecules in interlayer spacing .

At immersing graphite sample in liquid nitrogen, the latter as a monolayer liquid penetrates the interlayer distance of graphite planes. The nitrogen molecules penetrate the interplanar spacing in areas with defects (cracks, fractures, layering), as well as the ends of the sample (Fig. 1).

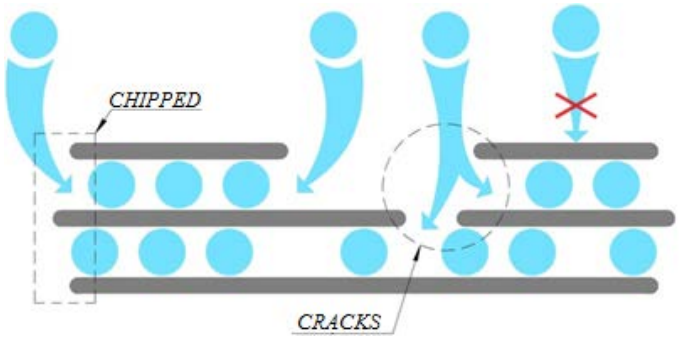

Figure 1. Schematic representation of the process of nitrogen diffusion into interlayer distance of graphite lattice

When the laser output power is insufficient for the processes of laser ablation, photon energy the absorption by a grating of carbon and diffused nitrogen. As a result, laser heating, and consequently, increase of vibration amplitude nitrogen molecules occurs volumetric expansion region occupied nitrogen molecules (transition from liquid to gas). Thereby are breaking the carbon π-bonds, which are weaker σ-bonds, and begin the exfoliation of the graphene structures (Fig. 2).

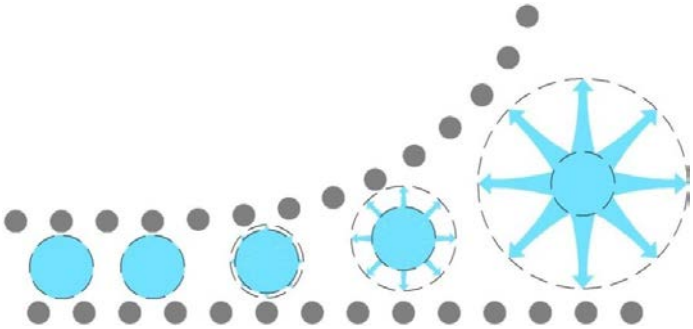

Figure 2. Schematic representation of the exfoliation of graphene as a result of the process thermal heating of the nitrogen

Thus, the general mechanism of exfoliation graphene with femtosecond laser irradiation in liquid nitrogen is detachment of the surface layers of the target in a result of violation of interplanar bonds in the carbon sample due to expansion transition caused to diffuse nitrogen into the gas phase by laser heating.

References

1. *Geim A. K., Novoselov K. S.* // Nature materials, 2007. V. 6. №. 3. P. 183.
2. *Eletskii A.V., Iskandarova I.M., Knizhnik A.A. et al.* // Physics-Uspekhi, 2011. V. 54. №. 3. P.227.
3. *Hernandez Y., Nicolosi V., Lotya M et al.* // Nature. nanotech., 2008. V. 3. №. 9. P. 563.
4. *D. Abramov, S. Arakelian, D. Kochuev et al.* // Nanosystems: Phys. Chem. Math., 2016. V. 1. №. 1. P. 220

37. РЕНТГЕНОВСКИЙ ЛАЗЕР С $\lambda \sim 13.4$ НМ, ОБРАЗОВАННЫЙ ПРИ ВЗАИМОДЕЙСТВИИ НАНОСТРУКТУРИРОВАННОЙ МИШЕНИ ОЛОВА С ИНТЕНСИВНЫМ ЛАЗЕРОМ НАКАЧКИ – ПЕРСПЕКТИВНЫЙ ИСТОЧНИК ИЗЛУЧЕНИЯ ДЛЯ ПРОМЫШЛЕННОЙ НАНОЛИТОГРАФИИ

Е. П. Иванова

Институт спектроскопии РАН, Россия, 108840 г.Троицк, г.Москва
ул. Физическая, 5.
e-mail: eivanova@isan.troitsk.ru

Научно-технические достижения последних лет предопределяют новые направления для нанолитографии следующего поколения - производства и контроля полупроводниковых чипов с размерами < 20 нм - базирующиеся на трех принципиальных разработках.

i) Создание многослойных зеркал для различных диапазонов дальнего ультрафиолета с коэффициентом отражения ≥ 60% [1].

ii) Создание для этих длин волн высокоэффективных рентгеновских лазеров (РЛ) в наноструктурированных мишенях с продольной оптической накачкой. Механизм образования плазмы – ионизация интенсивным оптическим полем. Благодаря чрезвычайно узкой ширине линии $\sim \Delta\lambda/\lambda \leq 10^{-4}$, РЛ могут стать идеальным источником для промышленной нанолитографии (а также для интерферометрии, микроскопии высокого разрешения с использованием зонных пластин Френеля, для голографии и других приложений).

iii) Разработка волоконных лазеров с мощностью порядка сотен кВт и выше, которые используются, в основном, для сварки и резки металлов. Они могут работать в квазинепрерывном и высокочастотных режимах; по мощности, кпд, надежности и совокупности других параметров они на порядок превосходят лазеры киловаттного диапазона на кристаллах YAG, а также CO_2 лазеры. В определенных случаях высокочастотные лазеры могут служить накачкой плазмы для генерации излучения РЛ с высоким энергетическим выходом. Высокий коэффициент конвертации (КК) энергии накачки в энергию РЛ возможен при использовании нано - структурированных мишеней.

В докладе представлена теоретическая модель источника монохроматического излучения с $\lambda \sim 13.4$ нм, предназначенного для промышленной нанолитографии. Необходимый энергетический выход фотонов с $\lambda = 13.4$ нм должен превышать величину ~ 200 Дж/с. Создание высокоэнергетичных источников в указанной области является актуальной проблемой, поскольку именно для этой области разработаны многослойные зеркала с высоким коэффициентом отражения (>60%) [1].

Основа источника – рентгеновский лазер (РЛ) с оптической самонакачкой на переходе $3d^9 4f\ [J=1] - 3d^9 4d[J=1]$ Ni – подобного иона олова (Sn^{22+}). Это относительно новый, малоизученный класс рентгеновских лазеров [2]. Механизм инверсии лазеров с оптической само накачкой обусловлен реабсорбцией (перепоглощением) фотонов в оптически плотной плазме. Экспериментальное изучение РЛ с оптической самонакачкой сопряжено с определенными трудностями:

1) Продолжительность выходящего импульса РЛ не превышает 20 – 30 пс. Накачка плазмы должна производиться ультракоротким моно импульсом с четко заданными параметрами.

2) Наноструктурированная мишень также должна быть приготовлена с заданными параметрами.

Для наблюдения эффективного РЛ - импульса необходим предварительный высокоточный модельный расчет параметров накачки, мишени и плазмы, а также временных характеристик выходящего излучения.

В нашем расчете предполагается, что формирование плазменного шнура происходит при взаимодействии наноструктурированной мишени олова с интенсивным лазером накачки определенной интенсивности, энергии и длительности. Луч накачки направлен вдоль мишени (продольная накачка). Аналогичная схема РЛ в Ni- подобном ксеноне (Xe^{26+}) с λ = 11.3 нм рассматривалась нами в [3], где рабочая область плазмы формировалась в результате взаимодействия лазера накачки с потоком кластеров ксенона.

В докладе обсуждаются: принцип создания наноструктурированной мишени олова, схема экспериментальной установки, параметры накачки. Представлены расчеты коэффициентов усиления и квантовых выходов РЛ с λ = 13.4 нм в оптимальных условиях, необходимых для создания источников ВУФ излучения в промышленной нанолитографии.

ЛИТЕРАТУРА

[1] Stearns D.G., Rosen R.S., Vernon S.P., Multilayer mirror technology for soft projection lithography. *Appl. Opt.* (1993), 32, 6952-6960.

[2] Nilsen J., Dunn J., Osterheld A.L., Li Y. Lasing on the self-photopumped nickel-like 4f $^1P_1$ – 4d $^1P_1$ x-ray transition // *Phys. Rev. A* 1999 V.60 № 4 R2677-80.

[3] Ivanova E.P., X-ray laser near 13.5 and 11.3 nm in Xe^{26+} driven by an intense pump laser interacting with xenon cluster jet as a promising radiation source for nanolithography // *Laser Phys.*, 2017 27 №5 055802-11.

38. CONTROL OF PROPAGATION OF SPATIALLY LOCALIZED POLARITON WAVE PACKETS IN A BRAGG MIRROR WITH EMBEDDED QUANTUM WELLS

***I.E. Sedova*,[1] *I.Yu. Chestnov*,[1] *S.M. Arakelian*,[1] *A.V. Kavokin*,[2,3,4] *and E.S. Sedov*[1,3]**

[1]Department of Physics and Applied Mathematics,

Vladimir State University named after A. G. and N. G. Stoletovs,

Gorky Street 87, 600000, Vladimir, Russia

[2]CNR-SPIN, Viale del Politecnico 1, I-00133, Rome, Italy

[3]School of Physics and Astronomy, University of Southampton,

SO17 1NJ Southampton, United Kingdom

[4]Spin Optics Laboratory, St. Petersburg State University,
Ul'anovskaya 1, Peterhof, St. Petersburg 198504, Russia

Our nowdays' life is largely built on optoelectronic devices. The most of already existing devices operate separately with their optical and electronic parts. We believe that joining together the photonic and electronic parts will substantially change the face of modern optoelectronics make new devices more efficient, targeted and successful. To answer this technological challenge, we resort to methods and approaches of Polaritonics, the interdisciplinary research area which is at the heart of modern optoelectronics and quantum light wave technologies.

Among the most demanded and promising optoelectronic devices are the devices for information storage and processing based on macroscopic manipulation by coherent coupled matter-light states [1]. Cavity quantum electrodynamics, the study of strong coherent interactions of quantized cavity electromagnetic field with matter, provides a versatile platform for this goal. Cavity-QED arrays composed of engineered optical cavity modes and few-level oscillators, e.g. excitons in quantum wells (QWs), may serve as many-body systems for the light manipulation [2]. However, the strength of light-matter coupling in microcavities is limited by the number of QWs embedded in each cavity. To overcome this technological limitation, the concept of Bragg polaritons has been proposed [3,4]. The Bragg polaritons can be created by incorporation of QWs that are holders of excitons periodically throughout a Bragg mirror representing, in fact, a 1D binary photonic crystal. The eigenmodes of the system are an admixture of excitons and Bragg photons.

As a model structure, we consider a GaN/$Al_{0.3}Ga_{0.7}N$ Bragg mirror with embedded narrow $In_{0.12}Ga_{0.88}N$ QWs. By choosing the thicknesses of the layers, we can tune the position and width of the band gaps in a wide energy range. Figure 1(a) demonstrates dispersions of photonic eigenmodes of the pure 1D photonic crystal (without embedded QWs) for three combinations of the parameters: $d_{GaN}\, n_{GaN}=d_{AlGaN}\, n_{AlGaN}$ for the left and right panels and $d_{GaN}\, n_{GaN} \neq d_{AlGaN}\, n_{AlGaN}$ for the middle

panel. The second photonic branch is convex that provides anomalous dispersion. Keeping the convex shape of the dispersion in combination with defocusing nonlinearity one possible to expect the structure supports propagation of spatially localized wave packets that are known to be natural candidates for optical information processing.

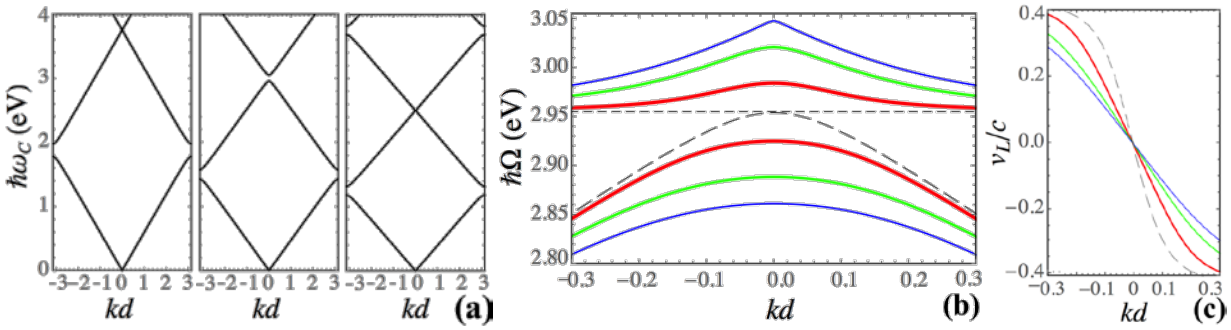

Fig. 1. (a) Energy band gap structure of the empty 1D photonic crystal with different widths of the layers. (b) Dispersion of the UB and LB polariton branches and (c) group velocity of the LB polaritons in dependence the polariton Bloch vector for different values of the exciton-photon coupling. The dashed curves in (b) and (c) and the dashed line in (b) correspond to non-interacting photons and excitons, respectively. The group velocity in (c) is given in units of the speed of light in vacuum.

The presence of periodically arranged QWs significantly changes the band gap structure of the considered system. Exciton-photon coupling results in appearance of new eigenmodes that are not photonic anymore but polaritonic. Figure 1(b) demonstrates dispersions of two polaritonic modes resulting from the coupling of the photonic mode belonging to the second photonic band with the excitonic mode quasi-resonant to the top of the photonic band [5,6]. Both polaritonic branches inherit the convex shape from the photonic dispersion and are suitable for obtaining localized polariton packets in the presence of the repulsive nonlinearity. The lower (LB) and upper (UB) polaritonic branches are separated by the band gap, and the stronger the exciton-photon coupling, the wider the band gap.

Figure 1(c) demonstrates the group velocity of the LB polaritons in dependence of their wave vector for different matter-field coupling strengths. Even at a small change of the wave vector the group velocity can vary in a wide range, from zero to 40 percent of the light speed in vacuum. It is noteworthy that the eigenwaves with positive wave vectors possess a negative group velocity while the eigenwaves with the negative wave vector propagate with the positive group velocity, i.e. the group and phase velocities in the considered structure are anti-parallel [7]. In the work, we demonstrate that the group velocity of the polariton wave packets can be effectively controlled through manipulation by the matter-field coupling strength, herewith the wave packets remain

spatially localized during propagation.

I.E.S. acknowledges support from the grant of the President of Russian Federation for state support of young Russian scientists No. MK-8031.2016.2. I.Yu.Ch. acknowledges funding from RFBR Grant No. 16-32-60102 and from the grant of the President of Russian Federation for state support of young Russian scientists No. MK-2988.2017.2. Work of S.M.A. was supported by the RFBR grant No. 15-59-30406 and the project part of the state task of VlSU No.16.1123.2017/PCh. A.V.K. acknowledges the partial support from the EPSRC Programme grant on Hybrid Polaritonics No. EP/M025330/1 and the HORIZON 2020 RISE project CoExAn (Grant No. 644076). E.S.S. acknowledges support from the RFBR grant No. 16-32-60104.

[1] D. Bruß and G. Leuchs (ed.), *Lectures on Quantum Information* (Wiley-VCH Verlag, Weinheim, Germany, 2007).

[2] M. J. Hartmann, F. G. S. L. Brandao, and M. B. Plenio, "*Effective Spin Systems in Coupled Microcavities*", Phys. Rev. Lett. **99**, 160501 (2007).

[3] S. Faure *et al.*, "*Relaxation and emission of Bragg-mode and cavity-mode polaritons in a ZnO microcavity at room temperature*", Appl. Phys. Lett. **95**, 121102 (2009).

[4] A. Askitopoulos, *et al.*, "*Bragg Polaritons: Strong Coupling and Amplification in an Unfolded Microcavity*", Phys. Rev. Lett. **106**, 076401 (2011).

[5] E. S. Sedov, I. V. Iorsh, S. M. Arakelian, A. P. Alodjants, and A. Kavokin, "*Hyperbolic Metamaterials with Bragg Polaritons*", Phys. Rev. Lett. **114**, 237402 (2015).

[6] E. S. Sedov, E. D. Cherotchenko, S. M. Arakelian, and A. V. Kavokin, "*Light propagation in tunable exciton-polariton one-dimensional photonic crystals*", Phys. Rev. B **94**, 125309 (2016).

[7] P. Jiang, H. Yang, and K. Xie, "*The forward-wave and backward-wave behaviors of electromagnetic waves in two-dimensional photonic crystals*", Optica Applicata **44**, 17 (2014).

39. INTERACTION OF LASER RADIATION WITH TITANIUM IN AIR

A.A. Voznesenskaya, A.V. Ivashchenko, D.A. Kochuev, V.G. Prokoshev, K.S. Khorkov

Department of Physics and Applied Mathematics,
Vladimir State University named after A. G. and N. G. Stoletovs,
87 Gorky, Vladimir, 600000, Russia
E-mail: _b_@mail.ru

At the moment the study of the process of laser ablation of various metals, which is the subject of many works [1-4], is of a great interest for science. The advantage of ablation induced by ultrashort laser pulses (USP) is the absence of heat during processing, which allows to achieve high accuracy. In this work presents the effect of femtosecond laser irradiation on titanium samples in air medium with different modes of action. Changing the power density of laser radiation was achieved by changing the position of the sample plane relative to the focal plane of the lens.

As a used laser source was a femtosecond laser system TETA-10 with the following characteristics: pulse duration ~280 fs, repetition frequency 1-10000 Hz, the average power of 1.5 W, wavelength 1030 nm, focal length of the lens is 50 mm, the beam diameter in the area of beam waist of about 50 μm. Variable parameter during the treatment was the working distance of the focusing lens. Material handling – titanium plate VT1-0 with a thickness of 1 mm, the surface of the sample was polished. The sample was mounted on a motorized 3-coordinate table.

When focusing the laser radiation on the sample surface was observed an intensive formation of laser-induced plasma. On the edges of the cavities present traces the emission of the liquid phase, which was manifested in the formation of characteristic cushion on the edges of the cavity with a height of 10-30 microns, and the "castle" around the cavity where a temperature zone was formed. With the gradual removal of a sample from the area of focus decrease the intensity of plasma, the temperature zone is also decreased, the dynamics of erosion is greatly reduced, which is typical with a sharp drop in the value of the power density. At some removal from the focal plane, there is a process cold laser ablation, erosion surface is less intense than at the location of the sample in the focal plane, but the formation of a temperature zone does not happen, the plasma generation is virtually absent, traces of ejection of the liquid phase were detected, which can speak directly about "cold" processing mechanism.

Thermal processes of laser radiation interaction with matter typical for subnanosecond pulses [5]. The appearance of the zone of thermal influence in the process of laser radiation due to the accumulation of thermal energy near the radiation of exposure due to contact with plasma,

which does not have time to dissipate and cool down to the arrival of the next pulse. An ultrashort laser pulse initiates the formation of a plasma torch, which has a lifetime much greater than the duration of the laser pulse, about few hundreds of nanoseconds [6], so we can talk about laser-plasma treatment. With a large repetition rate of the pulses is "pumping" the plasma torch by laser radiation, laser-induced plasma is becoming the main source of thermal energy in the system, which leads to a pronounced zone of thermal influence and abundant formation of the liquid phase, irrespective of the duration of the laser pulse.

In this work presents a series of experiments of ultrashort laser pulses influence on the surface of titanium, the treatment conditions corresponding to "cold ablation" and the peculiarities of interaction of USP with the surface of titan at different modes of radiation were determined. The experimental results are in good agreement with modern trends of building systems for the "micromachining".

This study was performed as a part of the state task VlSU 1106/17 and a grant of the RFBR number 16-08-01226.

References

1. Ashitkov S.I. et al. Formation of nanostructures under femtosecond laser ablation of metals //Quantum Electronics. – 2015. – V. 45. – №. 6. – P. 547.

2. Abramov D.V. et al. New advantages and challenges for laser-induced nanostructured cluster materials: functional capability for experimental verification of macroscopic quantum phenomena //Laser Physics. – 2014. – V. 24. – №. 7. – P. 074010.

3. Ashitkov S.I. et al. Ablation and nanostructuring of metals by femtosecond laser pulses //Quantum Electronics. – 2014. – V. 44. – №. 6. – P. 535.

4. Abramov D.V. et al. Formation of nanostructured thin-film coatings of titanium under the influence of femtosecond laser radiation in vacuum // Belgorod State University Scientific bulletin Mathematics & Physics. – 2011. – 23. – №. 11. – P. 113.

5. Bulgakov A.V., Bulgakova N.M., Burakov I.M. Nanosized Material Synthesis by Action of High-Power Energy Fluxes on Matter //Novosibirsk: Institute Thermophysics SB RAS. – 2009.

6. Tarasenko N. V., Butsen A. V. Laser synthesis and modification of composite nanoparticles in liquids //Quantum Electronics. – 2010. – V. 40. – №. 11. – P. 986

40. FEMTOSECOND ERBIUM NONLINEAR FIBER LASER SYSTEM

A.A. Lachina, K.S. Khorkov, D.A. Kochuyev, M.N.Gerke, V.G.Prokoshev

Department of Physics and Applied Mathematics,

Vladimir State University named after A. G. and N. G. Stoletovs,

87 Gorky, Vladimir, 600000, Russia

E-mail:lachina.alena@mail.ru

Femtosecond lasers fabricated by conventional scheme have the output pulses repetition frequency (OPRF) 70-100 MHz. However this frequency should be much lower for some applications and be about 1 MHz.

For example, in [1] the fiber laser system with low OPRF is required for carbon-containing films deposition. The same parameters are required for realization of direct writing technology [2].

One can solve the problem of creation of an oscillator with such characteristics in various ways. In the first way the reduced repetition frequency is achieved by decimation of the input high frequency sequence of pulse packet with optical gate. Such method is common used in practice but it's technical realization is complicated an expansive. Another way is increasing of the resonator length. In accordance to formula (1) the resonator length should be about 30 meters to achieve radiation with frequency about 10 MHz.

$$\nu = \frac{\mathrm{c}}{\mathrm{L}}, \qquad (1)$$

where c is light velocity in the medium; L is the resonator length and v is the pulse repetition frequency.

Implementation of this method with volume elements is possible [3] but has no common use due to extreme sensitivity of such long resonator to perturbation effects (vibrations, temperature drift). As for the fiber oscillators, this approach is justified and has common use.

We propose a fiber laser with Er^{3+}-doped active fiber, generating with the wavelength 1550 nm. Getting USP with such a laser is based on passive mode synchronization achieved by compensation of group velocity dispertion (GVD) in passive (negative GVD) and active (positive GVD) fiber parts such way that the total GVD in the resonator is zero. Such compensation is performed automatically in oscillators with high OPRF due to equal length of active and passive parts. Compensation of GVD in long resonators (tens of meters) with low OPRF require special measures. Super doped germanate fiber (about 50 molar percent of GeO_2 in the lightguide) with low mode diameter (about 2.5 mcm at the operating wavelength) is added into the resonator. It provides very high nonlinearity compared to the conventional one mode fiber and high dispersion parameter

100 ps/(nm*km) at the wavelength 1550 nm respectively. That's why it's using leads to positive group velocity dispersion appearance which in turn helps to compensate dispersion and achieve passive mode synchronization in the resonator.

Optical resonator scheme is shown on Fig.1:

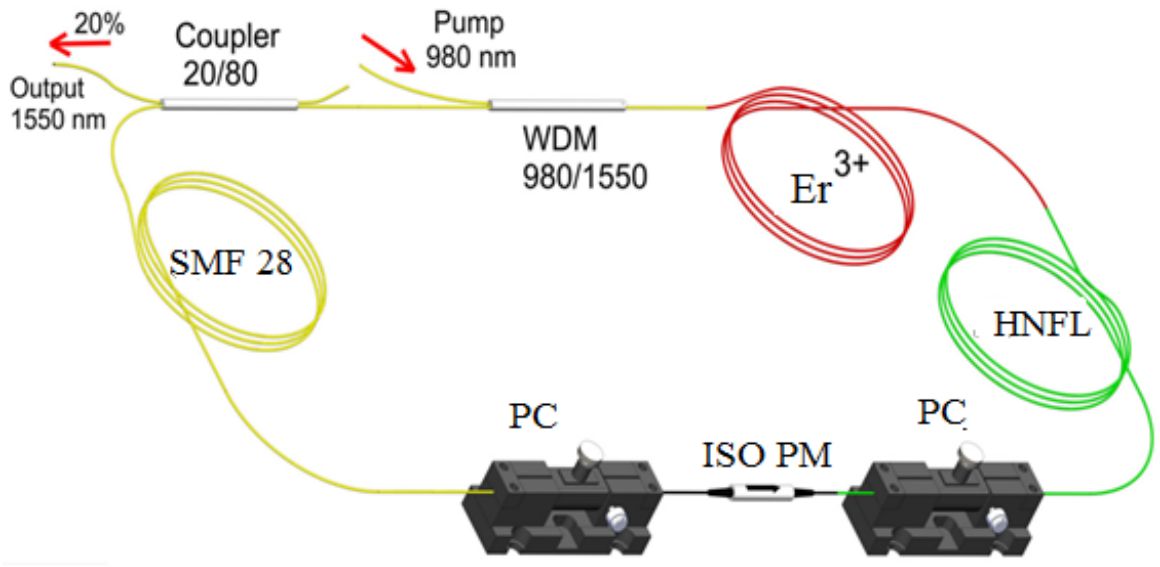

Figure 1. Scheme of a fiber laser with low pulse repitition frequency with nonlinear fiber in the resonator.

As a result of using nonlinear fiber total length of the resonator will be about 50-60 meters which will help to achieve the required OPRF value and increase stability of radiation.

This study was performed as a part of the UMNIK contract number 0033328ГУ/2017.

References

1. *Lachina A., Khorkov K.* // Graphene saturation absorber for fiber laser system, 2016. Materials of the international scientific conference «Lomonosov 2016».
2. Reichman W. // Understanding How Femtosecond Laser Waveguide Fabrication in Glasses. PhD. University of California, 2006.
3. *Cho S., Bouma B., Ippen E., Fujimoto J. //* Low-repetition-rate high-peak-power Kerr-lens mode-locked Ti:Al2O3 laser with a multiple-pass cavity. Optic letters, 1999. Vol. 24, No. 6.

41. АНАЛИЗ ТЕМПЕРАТУРНОЙ ЗАВИСИМОСТИ СПЕКТРОВ ЛЮМИНЕСЦЕНЦИИ ЖИДКОКРИСТАЛЛИЧЕСКИХ НАНОКОМПОЗИТОВ С КВАНТОВЫМИ ТОЧКАМИ СЕЛЕНИДА КАДМИЯ

К.Р. Каримуллин[1,2], М.А. Михайлов[2,1], М.Г. Георгиева[2], К.А. Магарян[1,2], И.А. Васильева[2]

[1]Институт спектроскопии РАН, 108840, Москва, Троицк
[2]Московский педагогический государственный университет, 119435, Москва
+7(916)556-0937, e-mail: kamil@isan.troitsk.ru

Нанокомпозиты, объединяющие в себе свойства полупроводниковых нанокристаллов (квантовых точек, КТ) и материала твердотельной матрицы, в настоящее время широко используются в самых различных областях науки и технологий. На основе материалов с полупроводниковыми коллоидными КТ производят эффективные и экономичные светоизлучающие устройства, разнообразные люминесцирующие покрытия и метки, активные элементы для лазерной генерации. Кроме того, флуоресцентные метки и зонды на основе КТ чрезвычайно востребованы в биологии, медицине и различных методах диагностики в качестве многопараметрических наносенсоров, поскольку их спектральные свойства (например, кинетика люминесценции) существенно определяются параметрами локального поля, зависят от термодинамических параметров системы и внешних полей (см., например [1]). В частности, КТ применяются в качестве температурных сенсоров [2]. Для использования полупроводниковых нанокристаллов в качестве сенсоров температуры необходимо фундаментальное понимание динамических процессов, определяющих фотофизические свойства КТ, и их связи с температурой.

Температурные зависимости спектров поглощения и флуоресценции различных квантовых точек (CdSe, CdS, InAs), помещенных в кристаллические растворы, исследовались экспериментально в ряде работ (см., например, [3-6]). Данная работа посвящена разработке теоретической модели, позволяющей проанализировать перераспределение интенсивности в спектрах флуоресценции нанокомпозитов на основе КТ селенида кадмия (CdSe), выращенных в жидкокристаллических растворах каприлата кадмия (CdC_8) при изменении температуры от 77 до 300 К [5-7] (см. рис. 1).

Для описания наблюдаемых спектров люминесценции была предложена схема энергетических уровней, включающая ряд промежуточных дефектных состояний, и построена система балансных уравнений. В рамках развитого подхода показано, при каких

[1] Посвящается светлой памяти к.ф.-м.н., профессора кафедры теоретической физики им. Э.В. Шпольского Института физики, технологии и информационных систем МПГУ Михаила Анатольевича Михайлова.

условиях формируются полосы люминесценции с определенным числом максимумов. При этом аналогом бесфононной линии поглощения лоренцевской формы в теории Блоха в нашем случае является неоднородно уширенный экситонный пик.

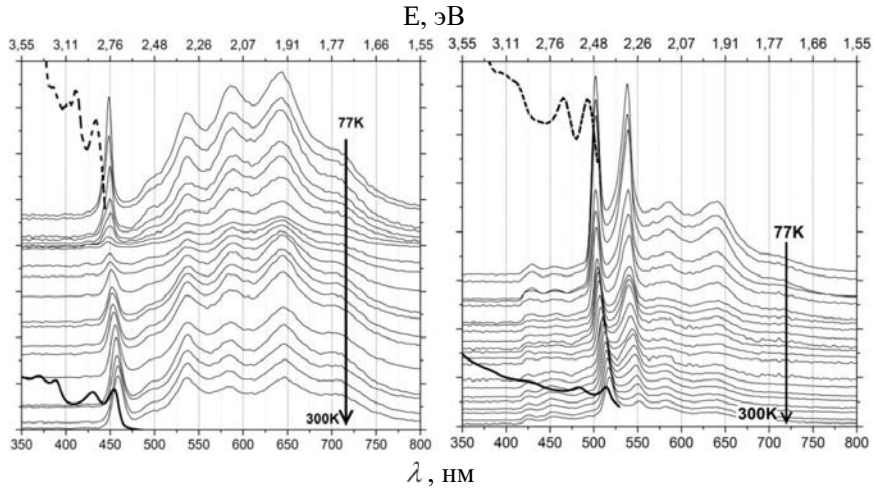

Рис. 1. Спектры флуоресценция (сплошная кривая), поглощения (жирная кривая) и возбуждения флуоресценции (пунктирная кривая) спектров образцов с квантовыми точками CdSe размером 1,8 нм (слева) и 2,3 нм (справа) в диапазоне температур 77 – 300 К.

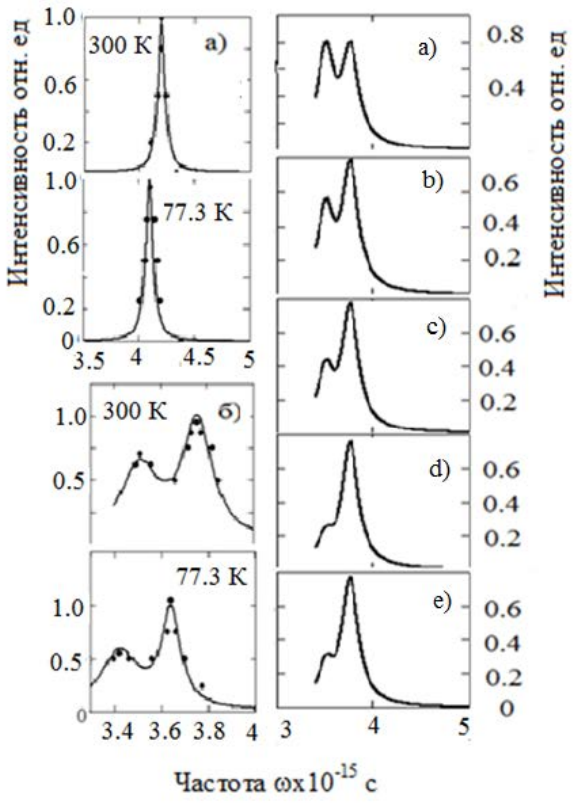

Рис. 2. Рассчитанные полосы люминесценции (сплошные кривые) и экспериментальные данные (точки) [5, 6] для образца с квантовыми точками размером *а)* 1,8 нм и *б)* 2,3 нм (слева). Моделирование перераспределения интенсивности в спектре

люминесценции для образца с КТ размером 2,3 нм при различных значениях скоростей переходов *a) – e)* (справа).

Сравнение с двухуровневым атомом оправдано, поскольку для КТ наблюдаются спектроскопические явления, характерные для двухуровневого атома [8-10], в частности, наблюдаются экситонные линии резонансного поглощения, имеющие лоренцевскую форму [8]. Результаты численного расчета полос люминесценции для КТ CdSe размером 1,8 нм и 2,3 нм при двух различных температурах приведены на рис. 2. Полученные значения свидетельствуют о сильном неоднородном уширении оптических полос, которое практически не зависит от температуры. Мы связываем его с имеющимся разбросом по размерам КТ. Ширина однородных линий люминесценции существенно зависит от температуры, но на фоне сильного неоднородного уширения данный эффект практически не проявляется. При этом заметным образом проявляется уменьшение интегральной интенсивности полос люминесценции и перераспределение интенсивности между пиками люминесценции с одновременным увеличением интенсивности широких полос в длинноволновой области спектра, которые связаны с дефектными состояниями нанокристаллов. Данные эффекты могут быть объяснены на основе предложенных балансных уравнений за счет температурного изменения соответствующих скоростных констант и изменения населенностей уровней. На рис. 3 показана зависимость длины волны максимума экситонных полос люминесценции от температуры. Наблюдаемое смещение может быть обусловлено проявлением экситон-фононного взаимодействия.

Таким образом, в данной работе показано, что развитый подход позволяет описать форму неоднородно уширенных полос поглощения и экситонных полос люминесценции. Введение в схему уровней исследуемой системы двух и более экситонных состояний позволяет на основе балансных уравнений и теории лоренцевской полосы экситонного возбуждения описать перераспределение интенсивности излучения в экситонных спектрах люминесценции при изменении температуры и размеров КТ в исследуемом образце. Необходимо отметить, что уравнения могут быть обобщены для изучения эффектов мерцающей флуоресценции одиночных полупроводниковых нанокристаллов [11]. Показано, что влияние фононов на изучаемую систему приводит к сдвигу полос экситонной люминесценции в красную сторону спектра при повышении температуры. Численный расчет температурной зависимости спектров люминесценции в рамках предложенной модели согласуется с экспериментальными результатами.

Работа выполнена в рамках проекта РНФ № 14-12-01415. К.Р. Каримуллин и К.А. Магарян благодарят за поддержку грант Президента РФ для молодых ученых – кандидатов наук (проект МК-342.2017.2).

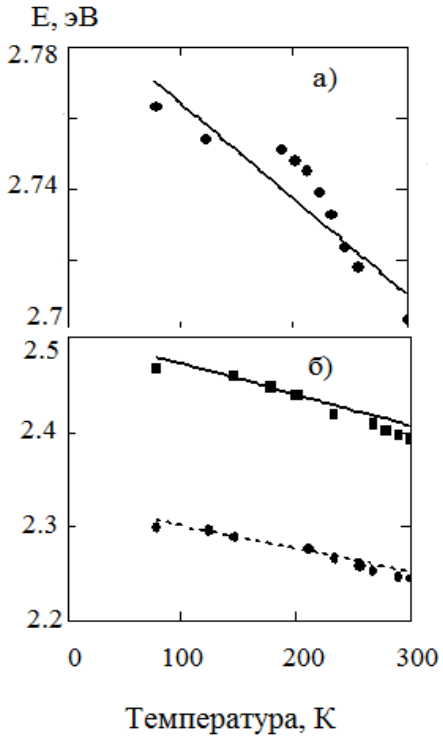

Рис. 3. Экспериментальные данные [5, 6] и результаты расчетов для температурной зависимости положения линий люминесценции для образца с квантовыми точками размером: а) 1,8 нм; б) 2,3 нм.

Литература

[1] A. Aubret et al. // Nanoscale. - 2016. - V. 8, № 4. - P. 2317.

[2] F.J. Zhang et al. // Proc. SPIE. - 2011. - V. 7990. - P. 79900R.

[3] D. Valerini et al. // Phys. Rev. B. - 2005. - V. 71, № 23. - Art. No 235409.

[4] I. Favero et al. // Phys. Rev. B. - 2007. - V. 75, № 7. - Art. No 073308.

[5] K.A. Magarian et al. // J. Phys. Conf. Ser. - 2013. - V. 478. - Art. No 012007.

[6] К.А. Магарян и др. // Изв. РАН. Сер. физ. - 2014. - Т. 78, № 12. - С. 1629.

[7] K.A. Magaryan et al. //J. Lumin. - 2016. - V. 169. - P. 799.

[8] A. Högele et al. // Phys. Rev. Lett. - 2004. - V. 93, № 21. - P. 217401.

[9] M. Kroner et al. // Physica E. - 2008. - V. 40, № 6. - P. 1994.

[10] A. Muller et al. //Phys. Rev. Lett. - 2007. - V. 99, № 18. - P. 187402.

[11] И.С. Осадько // УФН. - 2016. - Т. 186, № 5. - С. 489.

42. THE CW-LASER ABLATION OF RESONANT SILICON NPS IN LIQUID

A. Osipov, S. Arakelian, S. Kutrovskaya, and V. Samyshkin

Stoletovs Vladimir State University
87 Gorky st., Vladimir 600000, Russia
osipov@vlsu.ru

The paper demonstrates that the laser ablation approach can be used for synthesis (with average nanoparticle size control) of silicon nanoparticles supporting strong resonant optical responses in the visible spectral range. Porous and monolithic crystalline silicon targets are considered. The generated colloidal solutions have been used for the formation of one-layered covering composed of silicon nanoparticles. The obtained results may be used for the realization of many functional metasurfaces consisting of randomly distributed resonant nanoparticles.

A huge spectra of photonic applications require silicon nanoparticles [1, 2]. Its optical properties, including resonant responses, are considerably dependent on the size, shape, and crystallization degree [3]. The development of fabrication techniques with controlled nanoparticle parameters is very important. The methods of laser ablation in liquid [3, 4] allow to control the average size and shape of the obtained particles choosing suitable irradiation conditions (pulse duration, energy density etc.). The order deposition of such particles in thin films allows to create metasurfaces for controllable manipulation of the reflection and transmission properties [5,6].

The paper presents results of the silicon nanoparticle synthesis by the continuous laser irradiation of the thin silicon target placed in ethanol. Porous and monolithic silicon targets are considered.

The reported study was also supported by the Ministry of Education and Science of the Russian Federation (state project no. 16.1123.2017/PCh), RFBR grants 16-32-60067 mol_a_dk, and by the grants of president of Russian Federation byprojectsMK-2842.2017.2 and MK-2988.2017.2.

References

[1] U. Zywietz, A.B. Evlyukhin, C. Reinhardt, B.N. Chichkov, Nat. Commun. 5, 3402 (2014)

[2] A.B. Evlyukhin, S.M. Novikov, U. Zywietz, R.L. Eriksen, C. Reinhardt, S.I. Bozhevolnyi, B.N. Chichkov, Nano Lett. 12 (7), 3749 (2012)

[3] D.V. Abramov, A.A. Antipov, S.M. Arakelian, K.S. Khorkov, A.O. Kucherik, S.V. Kutrovskaya, V.G. Prokoshev Laser Phys, 24, 6886356 (2014).

[4] U. Zywietz, C. Reinhardt, A.B. Evlyukhin, T. Birr, B.N. Chichkov, Appl. Phys. A 114, 45 (2014)

[5] U. Zywietz, M.K. Schmidt, A.B. Evlyukhin, C. Reinhardt, J. Aizpurua, B.N. Chichkov, ACS Photonics 2(7), 913 (2015)

[6] A.A. Antipov, S.M. Arakelyan, T.A. Vartanyan, T.E. Itina, S.V. Kutrovskaya, A.O. Kucherik, I.V. Sapegina, Opt Spectrosc. 119 (1), 119 (2015)

43. LOCAL REFRACTIVE INDEX MODIFICATION OF OPTICAL FIBER BY FEMTOSECOND LASER RADIATION: INSTALLATION FEATURES

A.S. Chernikov, K.S. Khorkov, D.A. Kochuev, V.G. Prokoshev, S.M. Arakelian

Department of Physics and Applied Mathematics,

Vladimir State University named after A. G. and N. G. Stoletovs,

87 Gorky, Vladimir, 600000, Russia

E-mail: nacho17x08@gmail.com

Over the past decade methods of the refractive index modification in transparent materials by femtosecond laser pulses rapidly develop. Local changes of refractive index induced by femtosecond pulses used for direct writing of the periodic structures in transparent materials. Fiber Bragg gratings (FBGs) and long-period gratings (LPGs) are one of the most popular optical components have found wide application as sensing elements in sensor devices [1], as spectral filters in fibre lasers [2, 3], etc.

Refractive index modification of the optical fiber by the femtosecond laser pulses is based on energy absorption processes due to nonlinear phenomena such as tunnelling, multiphoton and avalanche ionization [4]. Femtosecond laser technology using to write FBGs in optical fibers without the requirement of material photosensitivity and fabricate optical structures has high thermal stability. The main advantages of the femtosecond writing method is the ability to flexibly change the characteristics of the Bragg grating: the period length and, as a result, the spectral characteristics.

In the experimental setup uses the femtosecond Yb:KGW-laser system producing 280 fs pulses at 1030 nm with repetition rate of 10 kHz. Laser radiation focuses into the fiber by the 50× microscopic objective which has NA 0.42 and working distance of 17 mm.

Optical structures were inscribed in Corning SMF-28e+ fiber (cladding diameter – 125 μm; core diameter - 8.2 μm) without removing the polymer jacket. Schematic drawings of the processing area shown in Fig. 1. To overcome the fabrication limitation imposed by the intrinsic fiber geometry, the optical fiber was placed between glass plates (Fig. 1 a), space between them filled with index-matching immersion liquid so that the surface geometry presented to the path of the incident femtosecond laser beam is flat [4, 5].

In Fig. 1 b the second version of the scheme is shown. In this case, optical fiber stretched and fixed between two guide elements mounted on the side of walls of the cuvette, carrying out input and output of the fiber from the cuvette. The cuvette filled with index-matching immersion liquid whose refractive index is close to refractive index of optical fiber. Microobjective is lowered

into a cuvette with immersion liquid. Laser radiation is focused in the fiber core. The fiber position is adjusted using precision three-axis stage.

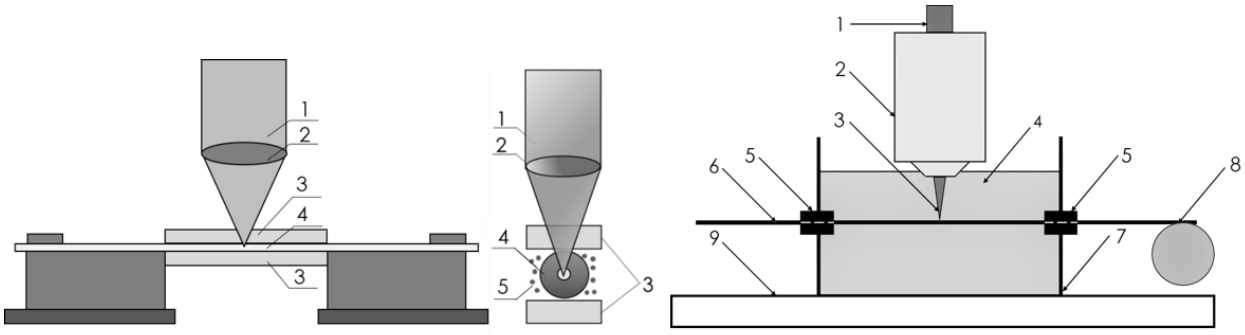

Fig. 1. Schematic drawing of the processing area: a) 1 – femtosecond laser radiation, 2 – focusing optics, 3 – glass plates, 4 – optical fiber, 5 – immersion liquid; b) 1 – femtosecond laser radiation, 2 – microobjective, 3 – focused laser radiation, 4 – immersion liquid, 5 – guide elements, 6 – optical fiber, 7 – cuvette, 8 – stretching roller, 9 – three-axis stage.

Fig. 2 shows microscope images of inscribed structures in fiber core. We have demonstrated that it is possible to inscribe gratings of the refractive index in fiber by femtosecond laser using two different schemes.

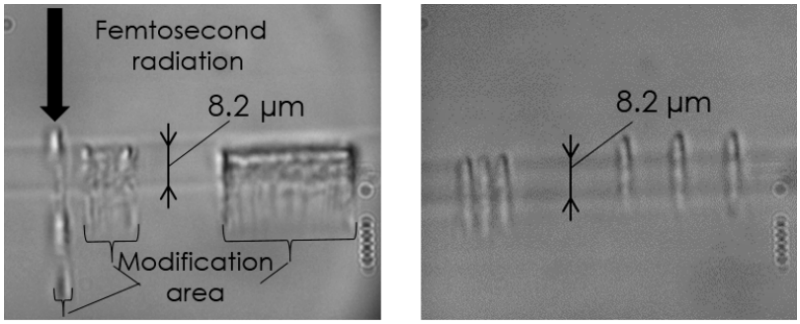

Fig .2. Microscope images of grating structures inscribed

This study was performed as a part of grant of the RFBR number 16-32-00760 mol_a. and program UMNIK contract number 8524GU/2015.

References

1. *Meltz G., Morey W.W., Glenn W.H.* // Optics letters, 1989. V. 14. №. 15. P. 823-825.

2. *Hill K.O., Fujii Y., Johnson D.C. et al* .// Applied physics letters, 1978. V. 32. №. 10. P. 647-649.

3. *Dostovalov A.V., Wolf A.A., Babin S.A.* // Quantum Electronics, 2015. V. 45. №. 3. P. 235-239.

4. *Lai Y., Zhou K., Suqden K., Bennion I.* // Optics express, 2007. V. 15. №. 26. P. 18318-18325.

5. *Chernikov A.S., Khorkov K.S., Bashkirov E.R. et al.* // International Scientific and Technical Conference Fundamental problems of radioelectronics, 2016. V. 1. P. 191-192.

44. SPATIO-SPECTRAL ANALYSIS OF FLUORESCENCE FROM PROBE ORGANIC MOLECULES TO MEASURE EFFECTIVE VALUES OF THE REFRACTIVE INDEX IN FROZEN FILMS

Nina S. Voronova and Yurii E. Lozovik

In the present work, we consider the effects of mirrors curvature on the behavior of the weakly interacting BEC of a 2D photon gas confined in a dye-filled optical microcavity. While the Gross-Pitaevskii description for such systems, akin to the systems of microcavity polaritons, is rather standard, the dependence of the effective photon mass on the distance from the cavity center has not been previously taken into account. The correct description implies the modification of the kinetic term from a simple Laplacian into a mixed derivative of the wave function and the mass. For spherical mirrors, we find corrections to the ground state energy and the photon condensate wave function, which are of the order of L_0/R, where R is the curvature radius of a mirror and L_0 is the cavity width at the center. Following the same idea, we suggest to engineer a cavity with a periodically weakly changing width, which creates a periodic potential for the BEC of photons. We demonstrate that in this case, a weak modulation of the wavefunction leads to anisotropic superfluidity since the superfluid density turns out to be a tensor instead of a scalar.

45. THE COLLOIDAL SYSTEMS ON SEMICONDUCTOR NANOPARTICLES

***A. Kucherik, S. Kutrovskaya, I. Skryabin, S. Arakelian, E. Shamanskaya, S. Zhirnov*a**

A.G and N.G. Stoletov Vladimir State University (VSU), 87 Gorki st., Vladimir, Russia, 600000.
E-mail: 11stella@mail.ru

In this work a method of the laser synthesis of colloidal nanoparticles and the formation of liquid photonic crystals are discussed. Optical properties of the systems depending on the particle concentration, its sizes and shapes were determined.

At present there is the great deal of research related to the application of semiconductor quantum dots having the optical transitions in the visible range of the spectrum. Nowadays more and more attention is paid to nanocrystals of lead chalcogenides (PbS, PbSe, PbTe) – narrow-gap semiconductor compounds with a band gap of 0.41, 0.278 and 0.31 eV at 300 K with transitions, occupying a wide range of near-infrared region of the spectrum (0.8-5 microns) [1-2].

Colloidal quantum dots are the best alternative to conventional various organic and inorganic fluorophores which are good at not only in photostability, but also on the molar extinction coefficient, and having a number of unique photophysical properties. Semiconductor quantum dots located inside complexes with the nanoparticles (NPs) of noble metals or carbon chains can be used in a varied applications such as sensor systems and optoelectronic devices [3-4].

The reported study was also supported by the Ministry of Education and Science of the Russian Federation (state project no.16.1123.2017/PCh), RFBR grants16-32-60067 mol_a_dk, 16-42-330461_r_a.

References

1. Zhang, C.-Y., Yeh, H.-C., Kuroki, M. T., Wang, T.-H., "Single-quantum-dot-based DNA nanosensor," *Nature Materials*, Vol 4, 826–831, 2005.

2. Tian, J., Cao, G., "Semiconductor quantum dot-sensitized solar cells," *Nano Reviews & Experiments*, Vol 4, 22578, 2003.

3. Wood, V., Bulovic, V., "Colloidal quantum dot light-emitting devices," *Nano Reviews & Experiments*, Vol 1, 5202, 2010.

4. Kwak, J., Bae, W. K., Lee, D., Park, I., Lim, J., Park, M., Cho, H., Woo, H., Yoon, D. Y., Char, K., Lee, S., and Lee, C., "Bright and Efficient Full-Color Colloidal Quantum Dot Light-Emitting Diodes Using an Inverted DeviceStructure," *Nano Letters*, Vol 12, № 5, 2362-366, 2012.

46. ПЕРЕКЛЮЧЕНИЕ СОСТОЯНИЙ ПРОВОДИМОСТИ МЕТАЛЛИЧЕСКИХ ЛАБИРИНТООБРАЗНЫХ ПЛЁНОК НА ПОРОГЕ ПЕРКОЛЯЦИИ

Гущин М.Г., Гладских И.А., Вартанян Т.А.

Университет ИТМО, Санкт-Петербург

+7(999)2398596, magusch@gmail.com

Тонкие металлические лабиринтообразные плёнки на пороге перколяции интересны своими уникальными электрическими свойствами. Крайне малое расстояние между наночастицами в плёнке позволяет управлять её проводимостью с помощью приложенного электрического напряжения, что проявляется на вольтамперных характеристиках (ВАХ) в виде резкого, скачкообразного изменения сопротивления. Также можно наблюдать гистерезис ВАХ. Данное исследование металлических лабиринтообразных плёнок интересно в качестве дальнейшего использования их в запоминающих устройствах.

Интерес представляет состояние плёнки в котором отдельные частицы находятся на грани образование связанной системы. Такое состояние, называемое на пороге перколяции, исследовано недостаточно глубоко.

Плёнки на пороге перколяции были получены методом термического вакуумного напыления металлов до образования проводящей плёнки и с последующим отжигом. Напыление металлических плёнок выполнялось в вакуумной установке PVD 75 фирмы Kurt J Lesker при давлении остаточных паров ~10^{-7} Торр на диэлектрические подложки из сапфира или кварца. На диэлектрические подложки перед напылением заранее наносились электроды с шириной 4-6 мм и расстоянием между ними 2-8 мм. Материалы напыления: серебро, золото и медь. В процессе напыления контролировалась скорость напыления и эквивалентная толщина слоя с помощью кварцевых микровесов. Скорость напыления составляла 0,5 Å/с. А с помощью пикоамперметра Keithley 6487 осуществлялся контроль сопротивления напыляемой плёнки, при достижении сопротивления 100 кОм напыление прекращалось. Таким образом получались проводящие металлические плёнки. На рисунке 1 представлена зависимость сопротивления плёнки от эффективной толщины напыления. График показывает форму близкую к экспоненциальной зависимости для всех исследуемых материалов. Эффективная толщина полученных плёнок составила 10 нм для серебра и около 6 нм для золота и меди.

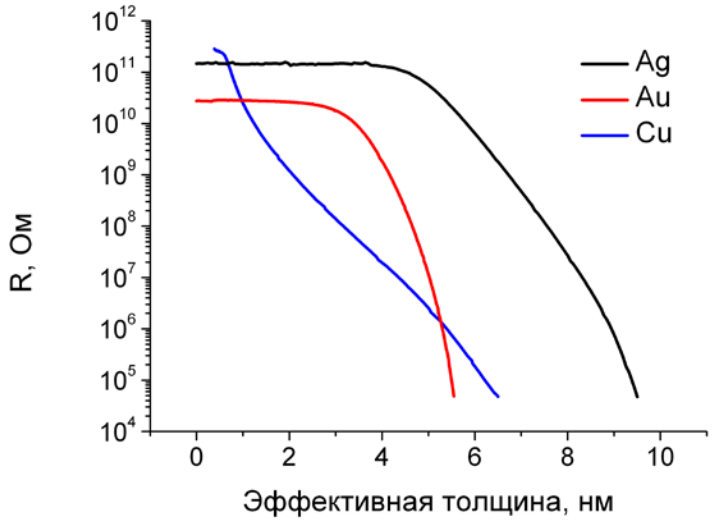

Рисунок 3 Зависимость сопротивления плёнки от эффективной толщины напыления для серебра, золота и меди

Для получения структуры на пороге перколяции после напыления производился термический отжиг, приводящий к разрыву проводящей структуры и образованию отдельных частиц [1]. Такой способ позволяет отчетливо зарегистрировать переход плёнки от проводящей структуры к островковой, что практически невозможно при напылении [2]. Отжиг плёнок осуществлялся при температурах 100-120 °C для серебра, 160-200 °C – золота и 180-220 °C – меди. Отжиг останавливался после достижения сопротивления 100 ГОм, от времени отжига зависит величина порогового напряжения, при котором происходит переключение плёнки из низко проводящего в высоко проводящее состояние. В процессе отжига вначале происходит медленное повышение сопротивления, что вызвано утоньшением мостиков в лабиринтообразной структуре, далее резкий скачок сопротивления при полном разрыве и образования отдельных наночастиц. Процесс образования проводящей лабиринтообразной плёнки был показан ранее [3]. На рисунке 2 представлено СЭМ изображения полученной золотой лабиринтообразной плёнки.

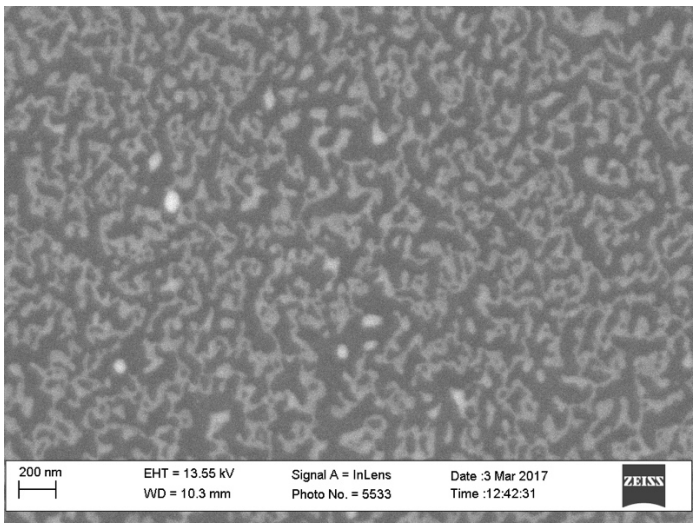

Рисунок 4 СЭМ изображение золотой лабиринтообразной структуры

Полученные структуры имеют особенность в виде наличия двух различных состояний проводимости. В первом состоянии сопротивление плёнки велико и достигает порядка 100 ГОм. При подаче на электроды напряжения больше определённого значения плёнка переключается в низкоомное состояние, в котором порядок сопротивления составляет 100 кОм. Переход плёнки обратно в высокоомное состояние происходит только при подаче напряжения на электроды намного меньшего порогового. Время перехода в начальное состояние лабиринтообразной плёнки намного превышает время переключения плёнки в низкоомное и зависит от её морфологии (расстоянием между наночастицами), для серебра это было исследовано ранее [3,4]. На рисунке 3 представлены ВАХ серебряных, золотых и медных плёнок на пороге перколяции с гистерезисом. Для серебра (рис. 3а) до 8 В плёнка находится в состоянии высокого сопротивления. Смена состоянии плёнки происходит в виде резкого скачка сопротивления при пороговом напряжении 8 В. Таким образом разница сопротивления между состояниями составляет восемь порядков. После ряда последовательных измерений ВАХ пороговое напряжение плёнки снижается для всех металлов.

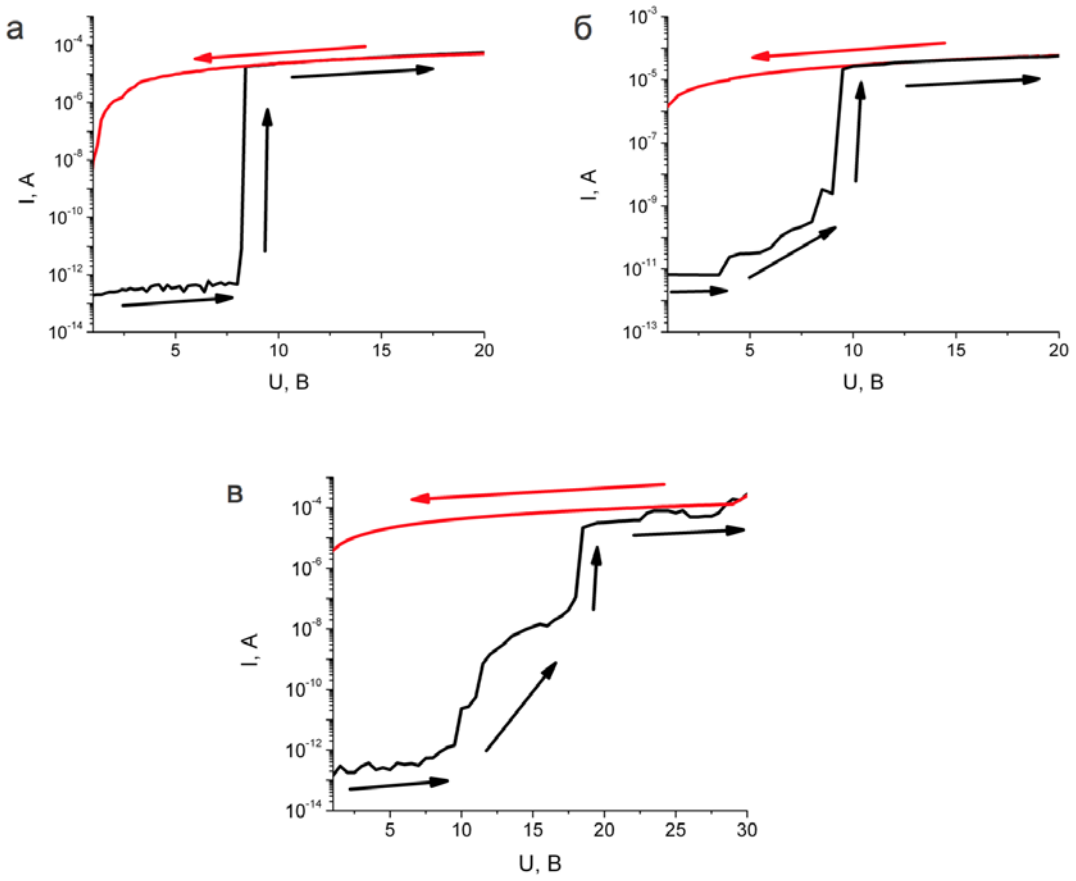

Рисунок 5 Вольтамперные характеристики лабиринтообразных плёнок на пороге перколяции серебра(а), золота(б) и меди(в)

Временные характеристики переключения были получены при помощи осциллографа Rigol DS4052. Характеристики показывали время переключения металлических плёнок при подаче напряжения выше порогового. Измерение сигнала происходило с последовательно включенного резистора и с источника напряжения. Таким образом было получено время переключения плёнок, для серебра составляло около 200 нс, для золота – 2 мкс, для меди – 60 мкс.

Изменение сопротивления на несколько порядков мы заключаем связано с маленькими структурными изменениями при приложенном напряжении. Термический отжиг позволяет образовывать из сформированной непрерывной лабиринтообразной плёнки отдельные наночастицы, расстояние между которыми экстремально мало. Под действием напряжения наночастицы в местах разрыва пленки формируется непрерывная структура с малым сопротивлением.

Работа поддержана Министерством образования и науки РФ (Госзадание № 3.4903.2017/6.7) и РФФИ (№16-32-60028 мол_а_дк и № 16-32-00165 мол_а)

Литература

1. Леонов Н. Б. и др. Эволюция оптических свойств и морфологии тонких металлических пленок в процессах роста и отжига //Оптика и спектроскопия. – 2015. – Т. 119. – №. 3. – С. 458-463.
2. Wagner S., Pundt A. Conduction mechanisms during the growth of Pd thin films: Experiment and model //Physical Review B. – 2008. – Т. 78. – №. 15. – С. 155131
3. Вартанян Т. А. и др. Тонкие структуры и переключение электропроводности в лабиринтных пленках серебра на сапфире //Физика твердого тела. – 2014. – Т. 56. – №. 4. – С. 783-789
4. Wei H., Eilers H. From silver nanoparticles to thin films: Evolution of microstructure and electrical conduction on glass substrates // Journal of Physics and Chemistry of Solids. – 2009. – V. 70. – P. 459–465.

47. DETERMINATION OF THE LOCAL FIELD IN THE NUCLEAR SPIN SYSTEM OF N-TYPE GAAS

V.M. Litvyak[1*], R.V.Cherbunin[1], K.V. Kavokin[1,2] and V.K. Kalevich[1,2]

[1] Spin Optics Laboratory, 1 Ulianovskaya Street, 198504 St. Petersburg, Russia

[2]Ioffe Institute, 26 Politekhnicheskaya Street, 194021 St. Petersburg, Russia

** tel.:89523945719, e-mail: valiok.ok@gmail.com*

The optical polarization of electron spins by circularly polarized light leads to nuclear polarization in semiconductors. The reason of this is a hyperfine interaction between electrons and nuclear spins. Such interaction corresponds to a transfer of angular momentum from electrons to nuclei and also to the appearance of the effective magnetic field created by nuclei on electrons. The nuclear field (Overhauser field) B_N can reach several tesla (B_{N_max}~5.3T for GaAs [1]) and significantly influences the electron spins [1, 2].

In the nuclear spin system (NSS), there is an interaction between neighboring spins that is called dipole-dipole interaction. It is characterized by local field B_L in which nuclear spins precess with Larmor precession period of a few microseconds. This interaction leads to the dipole-dipole relaxation of nuclear angular momentum with characteristic time T_2. During this time a thermodynamic equilibrium is established and the NSS can be characterized by nuclear spin temperature Θ ($\beta=1/\Theta$ – is the reverse spin temperature). This temperature can be significantly different from the lattice temperature during the spin-lattice relaxation time $T_1>>T_2$. In external magnetic field, the energy flow from optically polarized electron into the NSS can change nuclear spin temperature by orders of magnitude [2].

The local field B_L is a very important characteristic of the NSS. Since the dipole-dipole interaction B_L is involved in all processes of interaction of nuclei with electrons and of interaction between nuclear spins in external magnetic fields. Also B_L is responsible for establishing the nuclear spin temperature. So, experimental determination of the magnitude of B_L is important from the point of view of determination of fundamental parameters of the NSS.

Today a lot of research was done about behavior of the electron-nuclear spin system in small external magnetic fields. One of these directions was dedicated to the optical cooling and adiabatic demagnetization of the NSS [3, 4]. This method allows one to obtain low nuclear spin temperature, which reaches 10^{-5} – 10^{-6} K [2]. In this work we have experimentally determined the magnitude of the local field using optical cooling and adiabatic demagnetization of the NSS.

We study n-type GaAs doped by silicon with concentration n~ 10^{15}cm^{-3} at a liquid helium temperature. Samples under study were pumped by circularly polarized light from a semiconductor

laser, and we measured the degree of circular polarization of the luminescence ρ which is proportional to electronic spin < S_z >, z is the direction along excitation beam. For our sample the maximum degree of circular polarization was ρ_{max} = 4%. In the scheme of the detection a photoelastic modulator was used for simultaneous detection of left- and right-circularly polarized photoluminescence (PL). PL was detected by avalanche photodiode and a two-channel photon counter. The geomagnetic fields were compensated by three pairs of Helmholtz coils. Our experiments were conducted in three stages. At the first stage the NSS was prepared in the equilibrium with lattice temperature (optical excitation and magnetic fields turned off). At the second stage the NSS was cooled by circularly polarized light in the longitudinal magnetic field B_z = 100 G during the times equal 10 s and 120 s. This stage corresponds to the energy flow into the NSS that leads to decrease for positive ($B_z \uparrow\uparrow S_z$) or negative ($B_z \uparrow\downarrow S_z$) nuclear spin temperature. After that, B_z turned off adiabatically slowly and at the third stage transverse magnetic field $B_\perp$ was turned on. Electron spins were depolarizing in nuclear field $B_N \sim \beta B_\perp$ and then the NSS warmed up with the spin-lattice relaxation time T_1. Typical experimental curves are presented in figure 1.

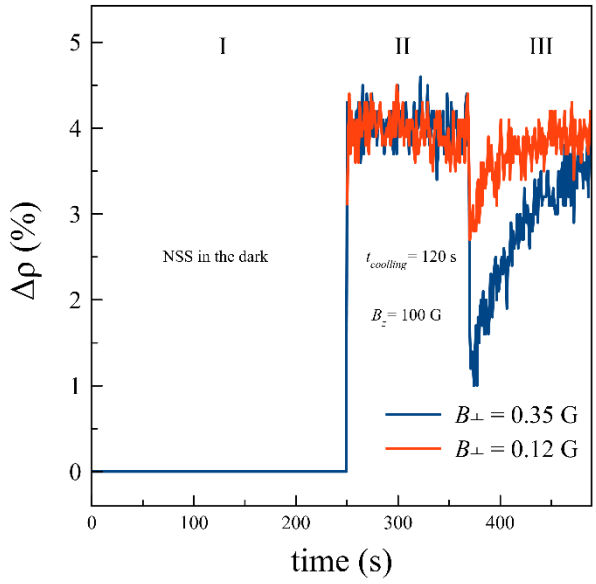

Figure 1. Time dependences of the PL circular polarization in n-GaAs: I) the NSS in the dark during 250 s; II) optical cooling of the NSS in the longitude magnetic field (Bz = 100 G) during 120 s; III) nuclear warm up at transverse magnetic fields equal $B_\perp$ = 0.35 G (blue line) and $B_\perp$ = 0.12 G (red line) during 120 s.

By measuring the difference of degree of circular polarization before and after the switching of magnetic field from longitudinal to transverse we can obtain the value of local field B_L. Degree of circular polarization as a function of transverse magnetic field is defined by the Hanle depolarization curve, eq. (1), which contains the nuclear field B_N, eq. (2):

$$\rho(B_x) = \rho(0) * \frac{B_{1/2}^2}{B_{1/2}^2 + (B_x + B_N)^2} \quad ,$$

$$B_N = b_n \frac{\hbar \gamma_n}{k_b} \frac{I(I+1)}{3} B_x \beta(0) \sqrt{\frac{B_L^2}{B_L^2 + B_x^2}} \quad ,$$

were $\rho(0) = \rho_{max}$; $B_{1/2}$ is the half width of the Hanle curve; $b_n = (16\pi/3)N\mu_0\xi^2/g$, N – nucleus concentration, g - electron g-factor, ξ – characteristic parameter; γ_n is gyromagnetic ration of the nucleus; k_b is Boltzmann constant.

The nuclear field depends on the external magnetic field B_x, x is the transverse direction to the excitation beam, the local field B_L and the inverse spin temperature $\beta(0)$. The value of parameters $\rho(0)$ = 0.04 and $B_{1/2}$ = 10 G were taken from the experiment.

We fit experimental curves (figure 2) by eq. (3) with the adjustable parameters: $\beta(0)$ and B_L^2.

$$\Delta\rho = \rho(0) - \rho(B_x) \; . \qquad (3)$$

Cooling times were 10 and 120 second.

After fitting experimental data, we obtained the values of adjustable parameters:

For 10 s: B_L = 1.48±0.4 G; $\Theta = 1/\beta(0)$ = 3.8±1.5*10^{-5} K.

For 120 s: B_L = 1.48±0.4 G; $\Theta = 1/\beta(0)$ = 0.67±1.5*10^{-5} K.

The value of local field B_L^2 = 2.2±1.0 G^2 determined in our experiments is in a good agreement with the value B_L^2 = 2.1±0.1 G^2, calculated for GaAs by D.Paget [1].

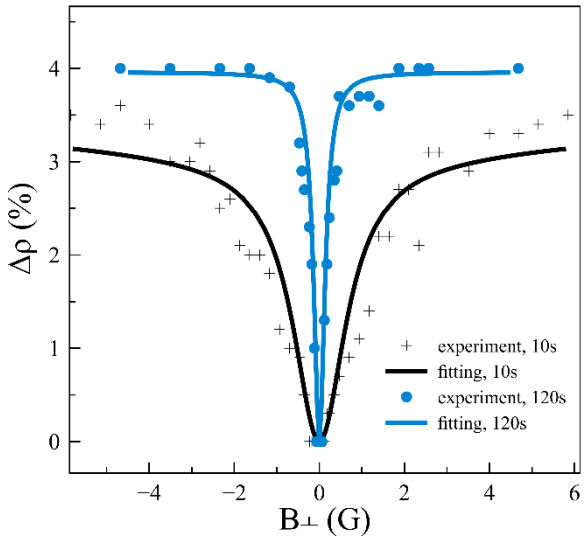

Figure 2. Experimental dependences of $\Delta\rho$ $(B_\perp)$ for cooling times equal 10 s (black crosses) and 120 s (blue dots). Solid lines are obtained by fitting of the experimental data using eq. (3).

In this work we present an experimental method for determination of the local field B_L in the nuclear spin system in n-GaAs with the help of optical cooling and adiabatic demagnetization of the NSS. The obtained value of B_L in *n*-GaAs, measured in weak magnetic fields $B << B_L$, demonstrates a good agreement with the prediction of theory.

This work was carried out in the framework of the joint Russian-Greek project supported by Ministry of Science and Education of Russian Federation (project RFMEFI61617X0085).

References

[1] D. Paget, G. Lampel, B. Sapoval, V.I. Safarov. Low-field electron-nuclear spin coupling in gallium arsenide under optical pumping conditions. Phys.Rev.B. V **15**, 12 (1977).

[2] F. Meier , B.P. Zakharchenya. Optical Orientation. (1984).

[3] V.K. Kalevich, V.D. Kulkov, V.G. Fleisher. Optical cooling of the nuclear spin system of a semiconductor in conjunction with adiabatic demagnetization. Bulletin of Academy of Science of the USSR, Physical Series, V **46**, 70 (1982).

[4] V.K. Kalevich, V.D. Kulkov, V.G. Fleisher. Onset of a nuclear polarization front due to optical spin orientation in a semiconductor. JETP Lett.V **35**, 20 (1982).

48. MATHEMATICAL MODELING OF THINFILMS GROWTH AND CALCULATION OF COEFFICIENTS REFLECTION, TRANSMISSION AND ABSORPTION WAVES

Istratov A.V., Gerke M.N.

e-mail: aleksgreene@gmail.com

The quality of many famous materials can be enhanced by using nanoparticles and atomic processing. Nanotechnology make it possible to create lighter, thinner and stronger composite (mixed, compound) materials.

To study nanostructures, it's important to know not only their mass or arrangement of atoms, but what they consist of. Determine the chemical composition of the samples (i.e. the content atoms of various elements in them) are allowed spectroscopic methods that use various instruments for studying the spectra of radiation, absorption, reflection, scattering.

As is known, ordinary light (visible radiation) is a collection of electromagnetic waves of different lengths (~ 400-760 nm) perceived by the human eye. Our eye perceives different colors not because objects have some abstract property "color", but because they are able to absorb and reflect electromagnetic waves of some length.

The analysis of the spectra of optical transmission and reflection plays a primary role among various methods of investigating quantum-size structures.

The characteristics of a number of optical elements, which include interference coatings, including a metal layer, are significantly influenced by the parameters of thin metal layers (refractive index, main absorption index and thickness). To this group of optical elements are mirrors, both metal and metal-dielectric, attenuating optical filters for a wide spectral range, gradient attenuators (shaders) and metal-dielectric narrow-band filters. The characteristics of each of the listed elements (transmission, reflection) are to some extent influenced by the optical parameters of the metal layers, which in turn depend on the deposited material and the resulting morphology of the sample surface.

The morphology of the surface of thinfilms is one of the most important parameters. That is why there is an increasing interest in the structure of islands, their roughness and thickness. Today, obtaining thinfilms is unthinkable without the use of mathematical modeling, numerical methods and complex programs. In this study, the degree of influence of morphology (particle diameter, number of layers, etc.) on the optical properties of a deposited thinfilm of bimetallic clusters was studied.

For computer modeling of the growth of metal thinfilm, a mathematical model of the "cellular automaton" type was used, which has recently been widely used in modeling processes in nanotechnologies.

For research the optical properties of modeled structures, the Finite Difference Time Domain method (FDTD) was used, which is one of the most popular methods of numerical solution of Maxwell's equations

The main "participants" of the FDTD numerical experiment are material bodies, wave source and detectors.

The medium (material) of objects is described by dielectric permittivity, conductivity, magnetic permeability and magnetic losses. Their default values are (1, 0, 1, 0). Unlike frequency domain methods, the dielectric permittivity of dispersive materials in tabular form cann't be directly replaced by the FDTD scheme. Instead, it can be approximated with the help of several members of Drude or Lorentz in the form:

$$\varepsilon(\omega) = \varepsilon_\infty - \sum_{p=1}^{N_D} \frac{\Delta\varepsilon_p \omega_p^2}{i\omega\gamma_p + \omega^2} + \sum_{p=1}^{N_L} \frac{\Delta\varepsilon_p \omega_p^2}{\omega_p^2 - 2i\omega\gamma_p - \omega^2}$$

The parameters for the Drude and Lorenz constructors are the plasma frequency ω_0 and attenuation γ and the value $\Delta\varepsilon$. The frequency and damping of the plasma are measured in radians per unit time FDTD.

Detectors do not correspond to any real objects, it's understood that they only record the values of fields at some points of computational volume in a file. The values of the fields are already obtained by interpolation by neighboring nodes.

The Total Field/Scattered Field method is used to simulate an infinitely distant plane wave source. It's based on the linearity of Maxwell's equations and the following superposition principle. FDTD difference equations can be independently applied both for the total field and for the incident or scattered fields, which allows us to break the computational volume into the field of the total field and the region of the scattered field. They are separated by a virtual boundary, which serves to generate a plane wave in the region of the total field. The difference equations used to calculate the field components in the grid nodes adjacent to this boundary differ from the original ones by the presence of additional components that take into account the value of the field of the incident wave.

To simulate the departure of a wave from the computational volume to infinity, absorbing boundary conditions are required. One of the best implementations is the use of a thin layer of

special material called the Perfectly Matched Layer (PML) along the boundary. Thus, this material absorbs all waves incident on the boundary of the computational volume, regardless of the angle of incidence. To model infinite periodic structures, periodic boundary conditions are used in one or several directions.

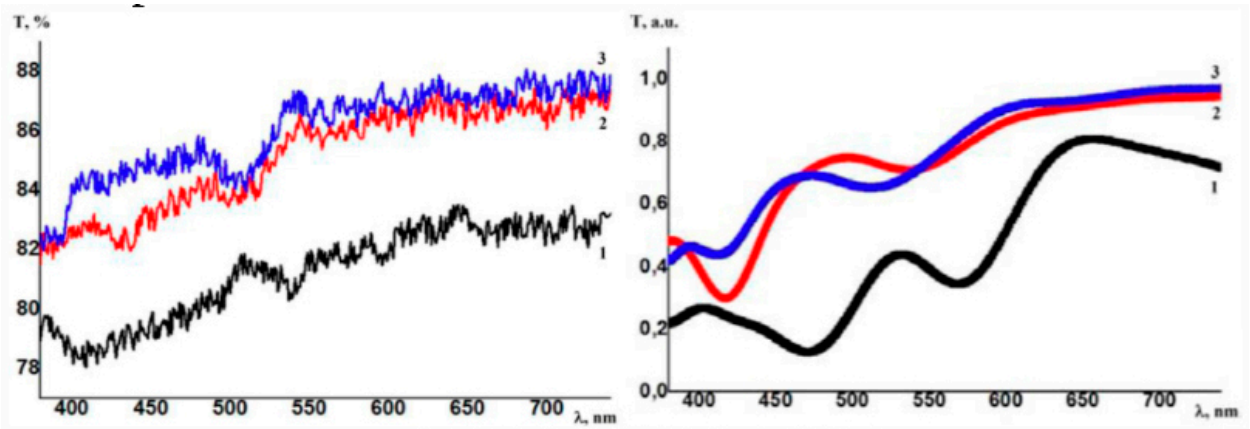

Figure 1 - Transmission spectra of the deposited films:
1 - Au:Ag(1:1) a particle diameter is 50 nm, one layer, the distance between particles is 5 nm;
2 - Au:Ag(1:1) particle diameter is 10 nm and five layers, the distance between particles is 4 nm;
3 - Au:Ag(1:1) particle diameter is 10 nm and five layers, the distance between particles is 2 nm

Figure 1 shows the changes in the optical properties of deposited bimetallic films and the results of modeling the observed optical phenomena using the FDTD method: a plane wave propagates along the Z-axis and automatically calculates the energy flux for the transmitted (T) waves using the data from the detectors. Using the data from the detectors, it's also possible to calculate the coefficients of the reflected (R) waves. Absorption (A) is obtained as A = 1 - R - T.

The calculated transmission spectra are in qualitative agreement with the experimental data.

49. STRUCTURAL PHASE COMPOSITION AND EFFECTIVENESS OF GASDYNAMIC SPRAYING OF HYBRID COATINGS BASED ON ALMG2 NANOCRYSTALLINE MATRIX REINFORCED WITH GRAPHENE-LIKE STRUCTURES AND MICRO-SIZE CORUNDUM

[1]Aborkin A.V., [1]Sobol`kov A.V., [1]Elkin A.I., [2]Arkhipov V.E.

[1]Vladimir State University named after Alexander and Nikolay Stoletovs, Vladimir, Russia
[2] Mechanical Engineering Research Institute, Russian Academy of Sciences, Moscow, Russia
e-mail: aborkin@vlsu.ru

Performance increase posibilites of functional properties of aluminum matrix based composite coating reinforced with only one type of filler are by now almost used up. Creation of hybrid nanocrystalline matrix based coatings reinforced with nano- and micro-sized fillers opens new opportunities of increasing and forming desired complex of working properties of element surfaces of constructions and machine parts.

The objective of this work is to research on the structural phase composition and gasdynamic spray coating of hybrid AlMg2 nanocrystalline matrix based coatings reinforced with graphene-like structures and micro-sized corundum.

Powder for gasdynamic spray coating was manufactured by mechanic synthesis in globular planetary mill during two technological conversions. During the first one a nanocomposite powder AlMg2+1 wt.% graphene-like structures was produced [1]. During the second conversion 10-70 wt.% of corundum was added to the produced nanocomposite powder and treatment was continued under same parameters [2].

The analysis of X-ray diffraction study results of different powder compositions were conducted on Bruker D8 Advance X-ray diffractometer and showed that diffractograms have similar characters. Peaks corresponding to aluminum and corundum were noticed. Calculation of coherent-scattering region performed using Selyakov-Scherrer equation showed that matrix material has a nanocomposite structure (mediam size of crystals ~60 nm).

Manufactured powders were sprayed on mounts from sheets of AlMg2M (120±15 HV) that had a 50 μm thick cladding layer of clean aluminum (45±10 HV) on it's surface. For gasdynamic spraying of manufactured powders a DIMET-404 machine was used. Splaying mode was stationary (point spraying) at the air flow temperature 270°C, exposing time 15 seconds.

After comparing results of powder and manufactured hybrid coatings X-ray diffraction study it cab be stated that during gasdynamic splaying phase composition doesn't change. At the same time there is a 10–20% decrease of half-widths of peaks that correspond to matrix material after

spraying; this proves size increase of coherent-scattering region meaning coarsening of fine structure. Median size of manufactured coatings crystallites was ~85 nm.

Study of hybrid coating manufactured using straying powder consisting 30% volume of corundum that was conducted using electric microscopes (JEM-2010) shows that the coating has nanocrystalline structure. Typical sizes of crystallites visible on TEM images are less that 100 nm. The analysis of those images proves absense of preferred orientation of aluminum particles and it's oxide to each other and orientation dependencies between them. Thin structure analysis shows presense of areas between aluminum crystals that correspond to graphene-like structures (sizes no more than 20 nm) with strongly distorted layers.

Effectiveness of spray coating was based on incremental value of the surface and calculated as a difference of mount mass before and after spraying. The analysis of results shows that the lost effective spraying is at 30% of corundum in the powder mixture. Further increase of corundum leads to decrease of effectivness of gasdynamic spraying.

Studying sections of hybrid coatings shows that during gasdynamic spraying a considerable change of microgeometry of mount's cladding layer is happening; it is determined by deformational and erosive impact of sprayed powder. Increasing the volume of micro-sized particles of corundum in the mixture from 10 to 30% helps increasing the coating thickness produced during the same amount of time 2 times, from 140 to 310 μm. Further increase of corundum volume in the mixture from 35 to 50% leads to decrese of the thickness down to 150 and 40% respectively. With 70 wt.% of corundum in the mixture surface thickness does not exceed 20 μm, in additiong a solid coating is not formed since erosive processes become predominate.

Metallographic examination of sections shows that independently from the corundum composition the formed surfaces are pretty solid with equally distributed particles of corundum (median size 3-5 μm) on the surface thickness. Nevertheless compacting (pressing) cracks can be noticed on the surface; it's lengths descreases with increase of corundum composition from couple hundrends to ten micrometers. Study of «coating – cladding plate» interface shows increase of corundum concentration in that zone; it's related to specific character of surface growth process initiation during gasdynamic spraying on mounts with low firmness and high plasticity.

The reported study was funded by RFBR according to the research project № 16-48-330156.

References

[1] Aborkin A.V., Evdokimov I.A., Vaganov V.E., Alymov M.I., Abramov D.V., Khor'kov K.S. Influence of Mechanical Activation Mode on Morphology and Phase Composition of Al-2Mg-nC

Nanostructured Composite Material // Nanotechnologies in Russia, 2016, Vol. 11, No. 5–6, pp. 297–304.
[2] Khrenov D.S., Sobol’kov A.V., Elkin A.I., Aborkin A.V., Sytschev A.E. Protective Al–2Mg–nC coatings by cold gas-dynamic sputtering: deposition and characterization // Explosive Production of New Materials: Science, Technology, Business, and Innovations — Coimbra: 2016. P. 74-75.

50. KINETIC ENERGY DISTRIBUTION OF ALKALI ATOMS DESORBED FROM SOLID SURFACES

Tigran Vartanyan, Pavel Petrov

ITMO University, Kronverkskiy pr. 49, St. Petersburg 197101
Russian Federation
+7(911)2895606, Tigran.Vartanyan@mail.ru

Adsorption on and desorption from solid surfaces play a crucial role in nature as well as in many technological processes. Despite their importance and many efforts devoted to their studies adsorption-desorption processes are still rather poorly documented. In particular there are few examples of experimentally obtained energies of absorption of atoms on solid surfaces. The difficulties of such measurements are obvious: when the surface number density of adsorbed species is small they are difficult to register, when the surface number density rises the adsorbed species tend to condensate. The way around this problem is to study adsorption on the overheated surface in the dynamic equilibrium with the saturated vapors. Up to now this program was realized only for sodium [1]. In this contribution we repot on the results of our studies of the rubidium adsorption on sapphire.

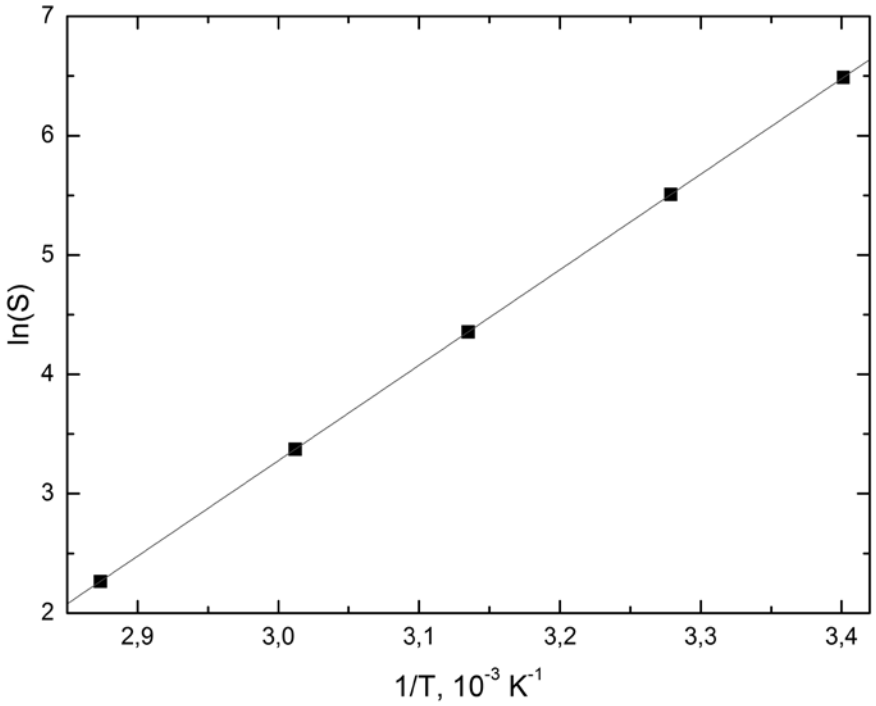

Figure 1. The temperature dependence of the desorption signal (*S*) enables the direct measurements of the adsorption energy. The absolute temperature of the surface (*T*) was varied between 294 and 348 K. The straight line that goes through the experimental points corresponds to

the adsorption energy of 0.7 eV.

In the experiment the surface number density of rubidium atoms adsorbed on sapphire was monitored via laser induced desorption in the time-of-flight measurements setup (fig.2).

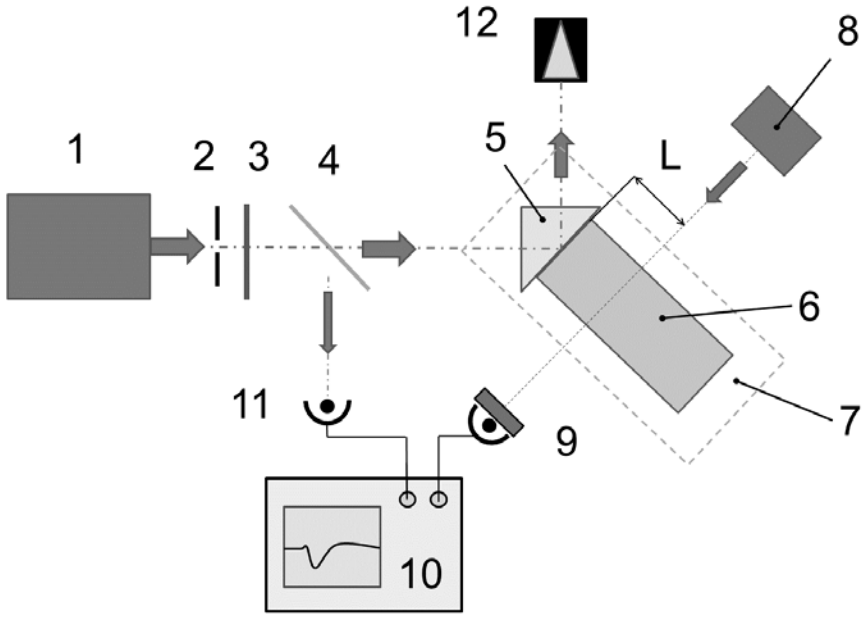

Figure 2. Time of flight measurement setup consists of an optical parametric oscillator (1) pumped by the third harmonic of Nd:YAG laser (not shown), a stop (2), a filter (3), a beamsplitter (4), a prism (5), a Rb sell (6), an oven (7), a diode laser tuned at the Rb atomic line 780 nm, an oscilloscope (10), a photodiode (11) and a trap (12).

We employ the evacuated cell filled with the natural mixture of rubidium isotopes. The construction of the furnace allowed for the independent heating of the sapphire window used as a substrate and the rest of the cell. The surface number density of rubidium atoms was obtained in the range on the substrate temperatures from 21 to 75 °C and fitted to the Boltzmann distribution

$$n=NR\exp(E_{ad}/kT), \qquad (1)$$

where n is the surface number density of the adsorbed atoms, N is the volume concentration of the same atoms, T is the absolute temperature of the cell window used as the substrate for the adsorption, k is the Boltzmann constant, R is the range of the surface potential and E_{ad} is the depth of the surface potential.

This procedure (fig. 1) leaded to the energy of adsorption of rubidium atoms on sapphire surface of 0.7 eV.

Besides the surface number density time-of-flight measurement gave also the velocity distribution of the desorbed atoms $f(v_x,v_y,v_z)$. Let us assume that the distance between the surface and the place where the desorbed atoms are registered is l. When the absorption of the resonance radiation at a particular time t after the 10 ns laser pulse is proportional to the integral over the velocity distribution

$$S(t) \propto \sigma \int_{l/t}^{(l+dz)/t} dv_z \int_{-\lambda\Delta\omega/4\pi}^{\lambda\Delta\omega/4\pi} dv_x \int_{-dy/2t}^{dy/2t} dv_y \, f(v_x, v_y, v_z)$$

Here σ is the absorption cross section at the laser wavelength λ, Δω is the laser spectral bandwidth while *dz* and *dy* stay for the laser beam dimensions in the corresponding directions. An example of time-of-flight spectra obtained in the experiments is shown in fig.3.

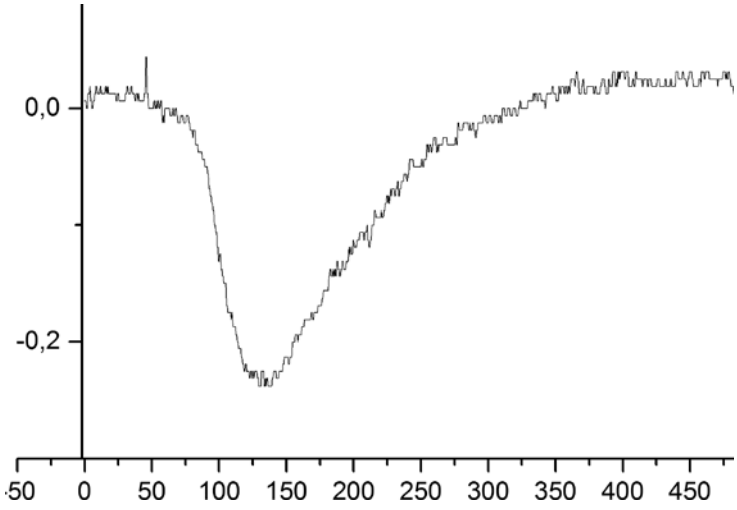

Figure 3. The time-of-flight spectrum of Rb atoms desorbed from sapphire.

These results were used to establish the dependence of the mean kinetic energy of the desorbed atoms on the fluence and the energy of the photons of the desorbing radiation. In the low fluence regime the kinetic energy distribution of the desorbed atoms is independent of the fluence while at higher fluences the mean kinetic energy of the desorbed atoms stats to grow. Contrary to the expectation in the low fluence regime the mean kinetic energy of the desorbed atoms decreases with the increase of the photon energy in the range of 1.3 to 3.0 eV. This counterintuitive behavior may be explained by the opening of new channels of energy relaxation when the photon energy rises.

References

[1] A.M. Bonch-Bruevich, *et al.*, *Proc. SPIE* **3404**, 187, (1998).

51. DETERMINATION OF THE NONLINEAR REFRACTIVE INDEX BY THE Z-SCAN METHOD USING FEMTOSECOND LASER RADIATION

M.A. Tarasova, K.S. Khorkov, D.A. Kochuev, V.G. Prokoshev

Department of Physics and Applied Mathematics,
Vladimir State University named after A. G. and N. G. Stoletovs,
87 Gorky, Vladimir, 600000, Russia
E-mail: trsvmargarita@gmail.com

Currently, nonlinear optics is a dynamically developing field of physics [1–2]. Femtosecond laser radiation has an incomparably greater intensity unlike other radiation sources and reaches up to 10^{14} – 10^{16} W/cm^2. At high intensities of light begin to appear nonlinear effects. The characteristics of the material become variable, depending on the intensity of the incident light, i.e. the medium becomes nonlinear. The dependence of the refractive index of the radiation intensity has the form:

$$n = n_0 + n_2 I\,, \qquad (1)$$

where n_0 – the linear part of the refractive index, n_2 – the nonlinear part of the refractive index, I – the radiation intensity.

Therefore, when using laser radiation, it is important to determine the magnitude of the nonlinear correction to the refractive index. This article is devoted to this problem. Z–scan technique allows determining the magnitude and sign of the nonlinear refractive index n_2 [2].

As the source of laser radiation was used ytterbium femtosecond laser TETA–10 (wavelength 1029 nm, pulse duration 280 fs, pulse repetition rate 10 kHz, maximum pulse energy 150 μJ). A beam of radiation propagating along the z axis was focused by a lens with a focal length of 150 mm. A diaphragm with an aperture of 2 mm was also installed. As the sample used glass KU–1, this was a parallelepiped with the geometrical dimensions 5 x 5 x 20 mm.

The sample was moved along the z–direction of the optical axis with a step of 1 mm. Radiation passed through the sample was recorded by a power meter as a function of the sample position relative to the focal plane. The measurement was started far from the focus, where the transmittance of the diaphragm is relatively constant. Then the sample was moved to focus and further [3].

The measurement result graph is shown in Figure. Based on the obtained power values, we can infer about transmittance of radiation through the sample. The normalization of data is performed according to the values when the transmittance is relatively constant.

The nonlinear refractive index can be determined [4]:

$$n_2 = \frac{\Delta\varphi_0}{kI_o L_{eff}}, \qquad (2)$$

where $\Delta\varphi_0$ – the nonlinear phase shift on the axis with the sample in focus, k – wave number, I_o – the radiation intensity in the focus, L_{eff} – the effective length of the sample.

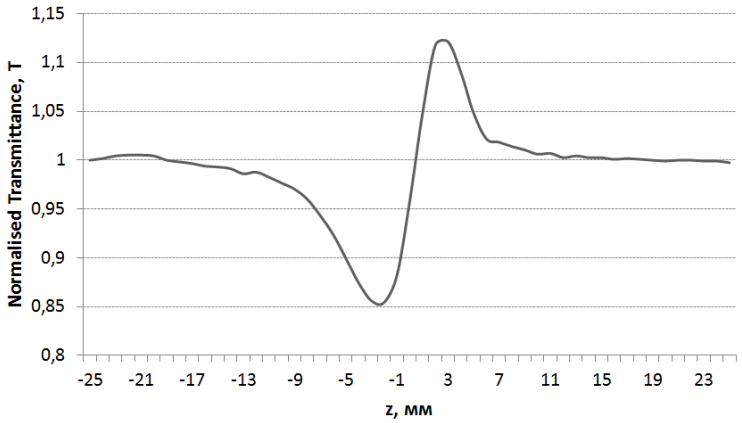

Fig. The graph of the transmittance of laser radiation power (normalized) through the diaphragm from the position of the sample T(z)

Based on the measured values of transmittance of the glass sample obtained a value $n_2 = 1{,}2686 * 10^{-11}\ (m^2/W)$ [5]. However, in the future it is planned to modernize and verify the conducted researches of the nonlinear refractive index. To study the dynamics of changes in the refractive index, is required to conduct a series of experiments with variation of laser radiation power but increasing the power can lead to the destruction of the sample or the formation of waveguide structures.

This study was performed as a part of the state task VlSU 1106/17 and a grant of the RFBR number 16–32–00760 mol_a.

References

1. *Besprozvannykh V.G., Pervadchuk V.P.* Nonlinear optics. Publishing house of Perm state technical University, 2011. 200 p.
2. *Khorkov K.S. et al*. The dynamics of the intensity distribution of the laser radiation in multiple filamentation in transparent medium // Dynamics of difficult systems–XXI century. 2015. V. 9. № 4. P. 23.
3. *Sheik-Bahae M. et al.* Sensitive measurement of optical nonlinearities using a single beam // IEEE journal of quantum electronics. 1990. V. 26. №. 4. P. 760.
4. *Ule E.* Measurement of The Nonlinear Refractive Index by Z–scan Technique // University of Ljubljana, Slovenia. 2015. P. 4.
5. *Tarasova M.A.* Determination of nonlinear refractive index by the method of Z–scanning using

femtosecond laser radiation. The collection of materials of scientific–practical conferences 20 – March 31, 2017. The days of science students, Publisher Vlgu. 2017. P. 423.

52. PHOTON STATISTICS OF SEMICONDUCTOR MICROCAVITY EXCITON-POLARITONS

Timur Khudaiberganov, Igor Chestnov, Sevak Demirchyan

Department of Physics and Applied Mathematics,
Vladimir State University named after A. G. and N. G. Stoletovs,
87 Gorkogo, Vladimir, 600000, Russia
E-mail: thomasheisenberg@mail.ru

Investigation of the quantum properties of light interacting with nonlinear medium represents a fundamental task of modern quantum optics and many-body physics. In such problems statistical properties of light and in particular its fluctuations are of special interest. Nowadays such as engineering of photon sources possessing non-classical statistics are essential in many practically important applications. The properties of light are modified due to the interaction with the medium which is usually considered as classical in the sense that its fluctuations are neglectable. However the influence of the fluctuation of the purely quantum medium represents an intriguing problem. The appropriate candidates for the media which also has a quantum nature but still remains macroscopic and interacts with many photons simultaneously are Bose-Einstein condensates. These exotic states of matter were recently observed both in atomic and solid-state semiconductor structures. While atomic condensates are observed at rather low temperatures the exciton polariton condensates formed in planar semiconductor microcavities can exist at room temperatures in the case of wideband gap semiconductors like GaN and ZnO. Thus semiconductor systems supporting interaction of excitonic states with light inside microcavity represent a robust platform for engineering sources of light with unusual statistical properties.

Here we study the system consisted of a 0D semiconductor microcavity with embedded quantum wells irradiated by a coherent laser field which frequency is close both to photon and exciton resonances of the structure. We performed an analysis of the influence of quantum fluctuations on the properties of exciton polaritons paying special attention to nonlinear interaction between the excitons. Analytical solutions for this problem were found independently using generalized P-function [1] in adiabatic limit [2] and using linearization of a stochastic quantum equation (in c-number). Non-classical statistics (both antibunching and bunching regimes) of photons and excitons were predicted. It has been also demonstrated that the presence of quantum noise leads to metastability [5] of the steady-state solution of the lower branch of bistability [3]. The obtained results could be used in quantum technologies (for example, for constructing of quantum gates) based on continuous quantum variables.

We examined the Hamiltonian describing quantum well excitons strongly coupled to a tightly localized photon mode of a pillar microcavity [4]:

$$H_C = \hbar\omega_{ph} a^+ a + \hbar\omega_{ex} b^+ b + \hbar g\left(a^+ b + b^+ a\right) + \hbar\chi a^{+2} a^2 + i\hbar\left(Ea^+ - E^* a\right), \qquad (1)$$

where a and b are boson annihilation operators of the photons and excitons respectively, $2g$ the Rabi splitting frequency, χ describes the elastic exciton-exciton scattering, E describes the applied pump field, which frequency δ differs from both exciton and photon frequencies. To account for a nonequivalent dissipation rates of the photon and the exciton modes we describe the evolution of the system using master equation approach for density matrix.

It is well known that such system being considered in the mean field limit reveals bistable properties. It means that the steady-state solutions for the photon and the exciton fields are characterized by a couple of stable solutions within the definite range of pumping field intensity [1]. To account for the influence of the quantum noise we use the generalized *P*-representation and solve corresponding Fokker-Planck equation [4].

To analyze the quantum statistic of photons we have evaluated second order coherence function $g_{ph}^{(2)}(\tau) = \dfrac{\left\langle a^+(t)a^+(t+\tau)a(t)a(t+\tau)\right\rangle}{\left\langle a^+(t)a(t)\right\rangle\left\langle a^+(t+\tau)a(t+\tau)\right\rangle}$, which can be represented as $g_{ph}^2 = \dfrac{\left\langle \alpha^{+2}\alpha^2\right\rangle}{\left\langle \alpha^+\alpha\right\rangle^2}$ at zero delay, $\tau = 0$.

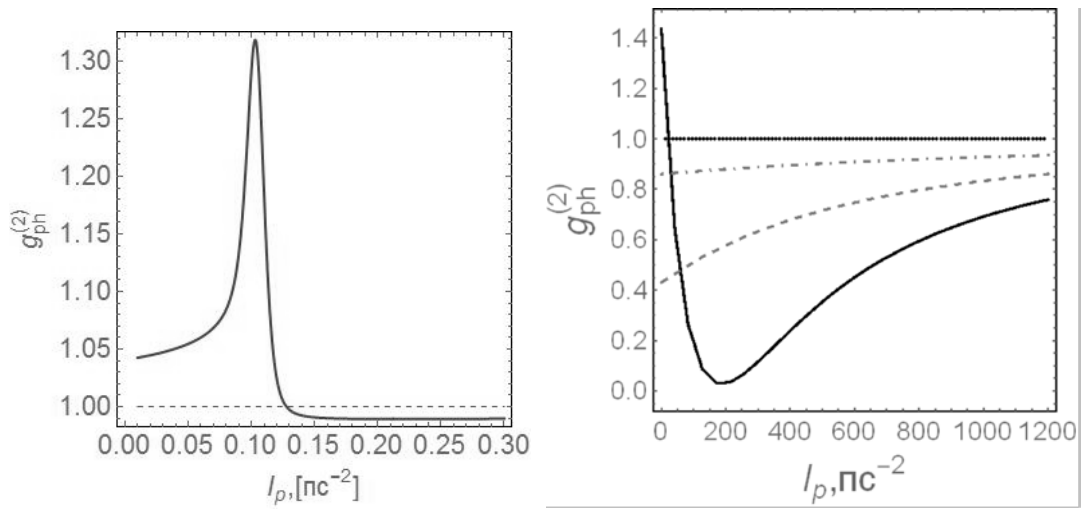

Fig. 1. Second order coherence function of photons versus pump intensity. Left picture corresponds to the presence of bistability for the mean field solutions and is plotted for the following parameters: Δ=-3.104 ps^{-1}, Ω=-4.85 ps^{-1}. Right picture is plotted for the parameters corresponding to the absence of bistability loop. Parameters: solid line – Δ=-0.81 ps^{-1}, Ω=0.73 ps^{-1}; dashed line – Ω=0.6 ps^{-1}; dot-dashed line – Ω=0.3 ps^{-1}.

Fig. 1 shows the calculated second order coherence function of photons versus pump intensity for different values of pump detuning $\Omega = \delta_p - \frac{\omega_{ph} + \omega_{ex}}{2}$ counted form the mean exciton-photon frequency and cavity-exciton detuning $\Delta = \frac{\omega_{ph} - \omega_{ex}}{2}$. This figure clearly demonstrates the presence of bunching and antibunching effects. The peak in the obtained dependence corresponds to the jump of the solutions to the upper branch of bistability loop [3].

References

[10] Drummond P.D, Gardiner C.W. (1980). Generalized P-representations in quantum optics. *Journal of Physics , 3,* pp. 2353–2368

[11] Drummond P.D., McNeil K.J., Walls D.F. (1981). Non-equilibrium transitions in sub/second harmonic generation. *Optica Acta: International Journal of Optics , 25* (2), pp. 211–225

[12] Bass A., Karr J.Ph., Giacobino E. (2004). Polaritonic Bistability in Semiconductor Microcavities. *Physical Review A , 69* (02)

[13] Ciuti C., Savona V., Piermarocchi C., Quattropani A., Schwendimann P. (1998). Role of the exchange of carriers in elastic exciton-exciton scattering in quantum wells. *Physical Review B, 58* (12)

[14] Demirchyan S.S., Khudaiberganov T.A., Chestnov I.Yu., Alodjants A.P. (2017). Quantum fluctuation in the system of exciton polaritons in semiconductor microcavities. *Opticheskii zhurnal* (*Journal of Optical Technology), 84* (2), pp. 10-18

53. MATHEMATICAL MODELING OF CONVECTIVE HEATING OF A DROPLET ON A SUBSTRATE

Bukharov D., Rybak G., Novikova O.

Vladimir State University (VLSU), Vladimir,
buharovdn@gmail.com

The development of methods for managing the architecture of ensembles of micro- and nanoparticles by influencing the processes of their self-assembly in a drying drop of a solution is an urgent task of modern fundamental and applied science. [1]

In recent years, much attention has been paid to the study of thermal processes occurring in drops of liquid on a solid horizontal surface.

Interest in the problem is also stimulated by a wide range of applications, including technologies for embossing coatings, production of micro- and nanostructures, medical diagnostics, and even forecasting the variability of the environment.

Among the main processes in drying drops, it is customary to single out purely hydrodynamic, thermodynamic, diffusion changes in the phase state of the substance at the last stages of drying. [2]

In this connection, it is of interest to model the convection processes in a droplet lying on a solid substrate. As a model approximation, we consider a rectangular layer of a liquid with a temperature gradient, the lower boundary of the liquid has a temperature higher than the upper one.

The process of heating the liquid, accompanied by the appearance of convection, is modeled in the Rayleigh-Benard approximation.

The density of the substance was assumed to be a function of the temperature T. As the unit of length, the thickness h of the layer was chosen, the units of time were the time of vertical diffusion of heat, $\tau_v=h^2/\chi$, χ is the thermal diffusivity coefficient, and the temperature units are the temperature difference between the fluid layers ΔT. The barotropic temperature distribution under the condition of stationarity should be linear in the vertical coordinate z: $T=T_1-\beta z$ is the unperturbed distribution, β is the unperturbed temperature gradient, and T_1 is the temperature at the lower boundary. For an arbitrary T, the temperature perturbation has the form $\Theta = T-T_1 + \beta z$, where p` the pressure perturbation p is its deviation from the distribution corresponding to such a linear temperature profile.

We considered a plane horizontal liquid layer $0 \le z \le h$ (the z axis of the Cartesian coordinate system x, y, z is directed upwards, so that g = {0, 0, - g}). Let us assume that the temperatures of its undeformed upper and lower surfaces are fixed (ie, that the thermal conductivity of the boundaries

of the layer is infinite): $T = T_1$ at $z = 0$, $T = T_2 = T_1 + \Delta T$ for $z = h$, where $\Delta T = \beta h$. This relation determines the condition $\Theta = 0$ on both these boundaries. Each of the surfaces of the layer will be assumed to be either rigid or free, introducing either the fluid adherence condition $v = 0$, or the condition that the vertical component of the velocity and the tangential stresses vanish at that boundary, respectively.

Thus, the problem includes a system of hydrodynamic equations for an incompressible fluid in the Boussinesq approximation in a dimensionless form. [3]

$$\frac{1}{Pr}\left[\frac{\partial v}{\partial t} + (v\nabla v)\right] = -\nabla\pi + \hat{z}Ra\theta + \Delta v,$$
$$\frac{\partial\theta}{\partial t} - v_z + v\nabla\theta = \Delta\theta, \qquad (1)$$
$$div\, v = 0.$$

Here Ra and Pr are the main parameters characterizing the convection regime, called the Rayleigh and Prandtl numbers, respectively, π is the dimensionless form of the quantity $p` / \rho_0$ (ρ_0 is the density value for some appropriately chosen reference temperature T_0), $\widehat{z}$ is the unit vector in the z direction.

The Boussinesq system of equations is solved by the method of the Boltzmann lattice equations (LBM) [4].

The Lattice Boltzmann method approximates flow as the motion of an ensemble of pseudo-particles having a certain distribution function with respect to discrete velocities $f(\mathbf{r}, \mathbf{v}, f)\, d^3\mathbf{r} d^3\mathbf{v}$. The value of $f(x, y, z, v_x, v_y, v_z, t)\, dx\, dy\, dz\, dv_x\, dv_y\, dv_z$ shows the fraction of particles at time t in the cube from x to x + dx, from y to y + dy, from z to z + dz with velocities in the range from v_x to $v_x + dv_x$, from v_y to $v_y + dv_y$, from v_z to $v_z + dv_z$.

The Boltzmann equation is represented in the Batnagar-Gross-Krook approximation (BGK) [5].

$$\frac{\partial f}{\partial t} + \boldsymbol{v}\nabla f + \frac{F}{m}\nabla_v f = -\frac{f - f^{eq}}{\tau}, \quad (2)$$

where F is the external force, m is the mass of the molecule, f^{eq} is the equilibrium distribution function, the Maxwell-Boltzmann distribution, and τ is the relaxation time.

Equations were solved on a uniform grid of spatial coordinates. Assume that there are no external forces. The mass of particles flying from this node in the direction i in a time step is denoted as f_i, then equation (2) is discretized as

$$f_i(r + v_i, t + 1) - f_i(r, t) = -\frac{f - f^{eq}}{\tau}. \qquad (3)$$

Equation (3) decomposes into two components - streaming step and collision step, which are the main steps of the calculation algorithm.

The equation describing the streaming step has the form:

$$f_i(r + v_i, t + 1) - f_i(r, t) = -\frac{f_i - f_i^{eq}}{\tau}. \qquad (4)$$

The equation describing the collision step has the form:

$$f_i(r, t) = \tilde{f}_i(r, t) - \frac{\tilde{f}_i - f_i^{eq}}{\tau}. \qquad (5)$$

Here, $\tilde{f}$ denotes the mass of particles that have come to the node in the direction i, but have not yet collided with the other particles that arrived.

For the sampled rate directions, the mass and macroscopic velocity in each node will be calculated as

$$\rho = \sum_i f_i, \quad \rho u = \sum_i f_i v_i . \qquad (6)$$

Thus, at each step of the calculation algorithm, move the particles flying from the node r in the direction i to the node $r + v_i$. After this, it is necessary to recalculate the masses, velocities, equilibrium distribution functions. Finally, it is necessary to "push" the particles that have flown into the given node-that is, to redistribute the particles along the directions.

Figure 1 shows one iteration of the "streaming / collision" pair. The colored arrows represent the streams of flying molecules. The color intensity encodes the mass of molecules that fly in a given stream, the length of the arrows roughly corresponds to the path traversed by the flow in a time step.

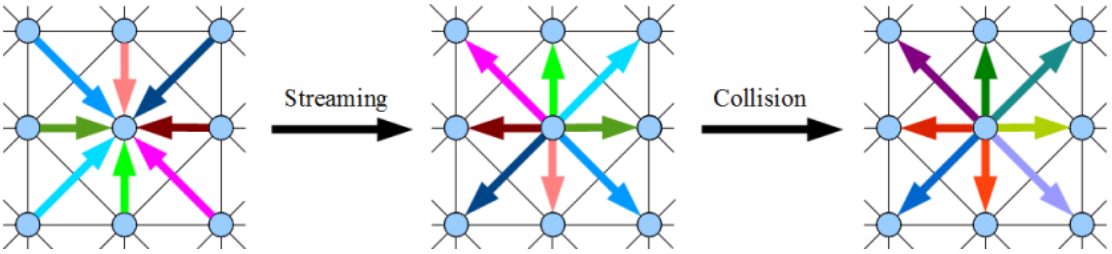

Fig. 1. The step of the computational algorithm

LBM is realized on the lattice D2Q9 (Fig. 2) for the Navier-Stokes equations and D2Q5 lattice for the heat equation [6].

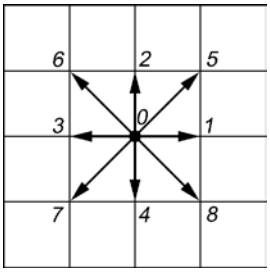

Fig. 2. Possible particle velocity vectors in the Boltzmann lattice equation method for the two-dimensional nine-velocity model D2Q9

The above-mentioned algorithms were used to calculate the velocity and temperature fields for various initial conditions.

The design area was selected in the form of a rectangle measuring 102 by 51 with a grid spacing of 1/48 rel. The initial temperature was calculated as the average from the temperatures of the upper and lower boundaries of the calculated region. The Prandtl number was chosen equal to 1, the Rayleigh number equal to 2000, which corresponds to the conditions for the appearance of the convection phenomenon (Fig.). Below right are the graphs of the temperature and relative velocity fields for the case of heating the lower wall to 5000 C (Fig. 3) and 3000 C (Fig. 4). The temperature field is calculated from the bottom up, the velocity field from the left to the right.

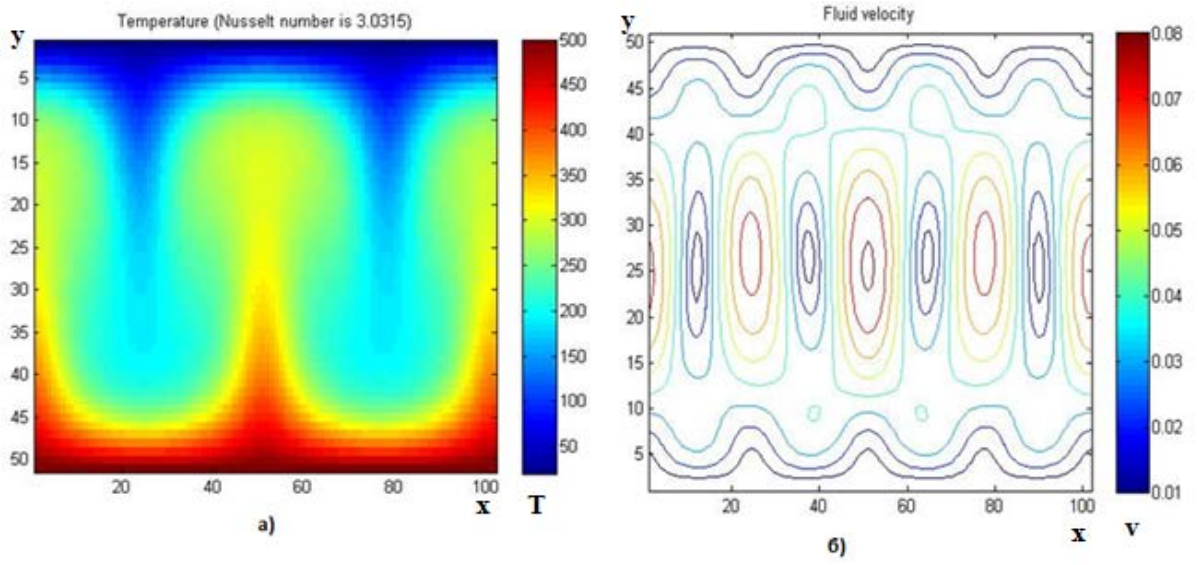

Fig.3. Graphs of the temperature field when the lower boundary is heated to 500 ° C (a) and the velocity field (b)

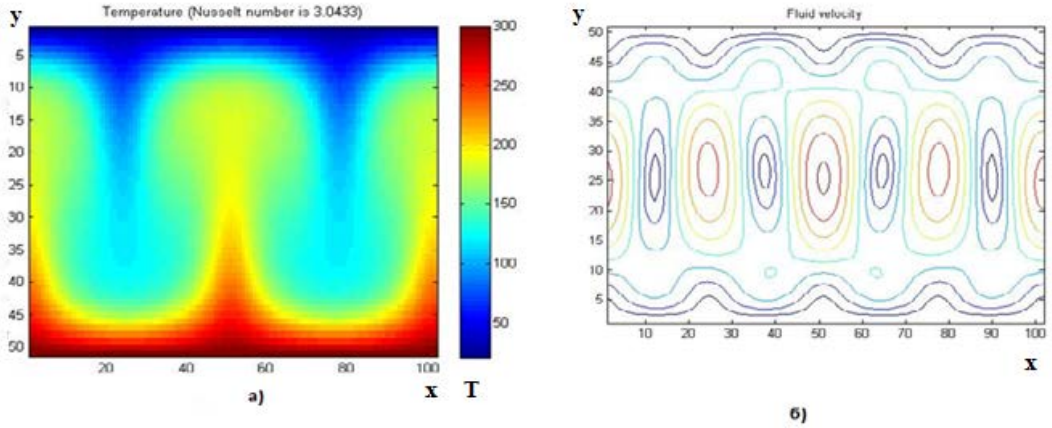

Fig.4. Graphs of the temperature field when the lower boundary is heated to 300 ° C (a) and the velocity field (b)

It was found that there are vortices in the velocity field, which are localized in the center of the computational domain. The central vortices are elongated along the vertical, the nature of the vortices being symmetrical with respect to the horizontal axis. In addition, two central vortices have stretches in the upper right part. Also in the lower part of the calculated region there are two small

vortices, which indicates the presence of instability near the heated substrate. The mathematical model and program can be used to calculate currents at Rayleigh numbers up to 10^5.

The developed mathematical model and the numerical experiments carried out make it possible in the first approximation to reveal the main features of convective processes in a drop.

Bibliogfraphy

1. P.V. Lebedev-Stepanov, R.M. Kadushnnikov etc.
Self-assembly of nanoparticles in the microvolume of a colloidal solution: physics, modeling, experiment / P.V. Lebedev-Stepanov, R.M. Kadushnikov, S.P. Molchanov, A.A. Ivanov, V.P. Mitrokhin, K.O. Vlasov , N.I. Rubin, G.A. Yurasik, V.G. Nazarov, M.V. Alfimov // RUSSIAN NANOTECHNOLOGIES, VOLUME 8, №3 - 4, 2013 p. 5-23.

2. A.V. Kistovich, Yu.D. Chashechkin, V.V. Shabalin Mechanism of formation of an edge roller in a drying drop of a biofluid / Journal of Technical Physics, 2010, Volume 80, №. 4 p. 41-46

3. A.V. Hetling THE FORMATION OF SPATIAL STRUCTURES OF RELAY-BENAR CONVECTION / SUCCESS OF PHYSICAL SCIENCES, Vol. 161, №. 9, 1991

4. Kupershtokh A.L. METHOD OF BOLTZMAN LATTICE EQUATIONS FOR MODELING OF TWO-PHASE SYSTEMS TYPE LIQUID-PAR / COLLECTION OF SCIENTIFIC ARTICLES MODERN SCIENCE №.2 (4), 2010 p. 56-63

5. Xiaoyi He, Li-Shi Luo Theory of the lattice Boltzmann method: From the Boltzmann equation to the lattice Boltzmann equation/ PHYSICAL REVIEW E VOLUME 56, NUMBER 6 DECEMBER 1997

6. A.A. Siner, E.V. Koromyslov, A.M. Sipatov DEVELOPMENT OF THE SOLVENT OF THE BOLTZMAN EQUATION FOR APPLICATION TO ENGINEERING PROBLEMS / Computational Mechanics of Continuous Media. - 2011. - Vol. 4, №. 3. - p. 83-95

54. INTERACTION OF LASER RADIATION WITH TITANIUM IN A LIQUID HYDROCARBON MEDIUM

A.V. Ivashchenko, D.A. Kochuev, K.S. Khorkov, V.G. Prokoshev, S.M. Arakelian

Department of Physics and Applied Mathematics,

Vladimir State University named after A. G. and N. G. Stoletovs,

87 Gorky, Vladimir, 600000, Russia

*E-mail:*_b_@mail.ru

Nowadays the study of laser action on samples in a liquid, which is the subject of many works [1-4], is of great interest for scientists. In this work present results of the impact of femtosecond laser radiation on samples of titanium in the liquid medium. As the laser source was used a femtosecond laser system, the samples material was titanium VT1-0, as the liquid medium was used a hexane. Processing was performed in isolated from the atmospheric air cell with a window for laser radiation input. Variable conditions of the experiment were the scanning speed of the laser beam on the sample surface and depth location of the sample surface in liquid medium. The scanning laser beam was carried out with the help of galvanoscanner at a speed of 0.1-200 mm/s., the thickness of the liquid layer was varied within 1-4 mm.

The main results of this experimental work are the coating of titanium carbide on the surface of the titanium sample and a formation of titanium microspheres containing titanium carbide. Also, as a result of changing modes of treatment, the surface structure was changed. The results of the impact presented in Figure.

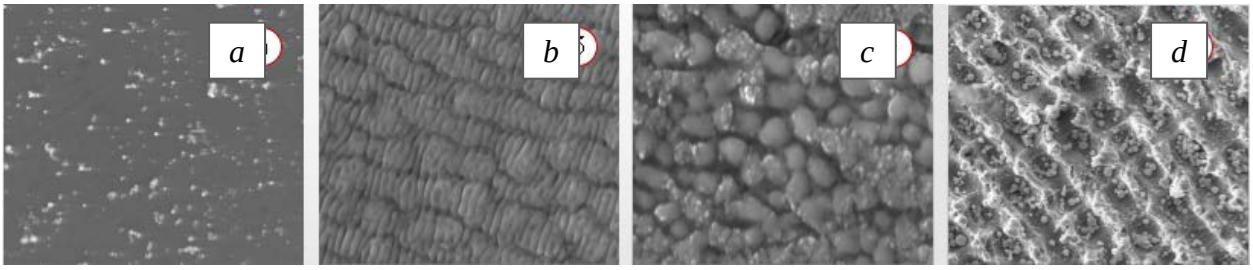

Fig. SEM-images of the dependence of the surface structure of titanium sample from the scanning speed of the laser radiation, mm/sec: a – 200; b – 80; c – 10; d – 0.1

The formation on the surface of the titanium sample coatings of titanium carbide occurs as a result of sorption of free carbon titanium surface exposed to laser radiation, the formation of free carbon occurs as a result of destruction of molecules of hexane in a kind of interaction with laser radiation and ablation products of titan's surface. The absence of carbon in graphite form on the surface due to its acute shortage in view of the excess titanium is capable of forming a chemical

bond. For the formation of microspheres necessary to create conditions abundant emission of the liquid phase as a result of exposure to laser radiation. The size of the microspheres was in the order of 1-3 microns. The presence of a liquid medium, steam-dripping "fog" in the cell formed during the surface treatment of titanium allows receiving microspheres without the effect of "adhesion" between them due to rapid cooling of the surface of the microspheres in mind contact with suspended drops. On the bottom and walls of the cell particles are deposited by being "cold", not able to mate with the surface of the sample, the walls of the cuvette or with each other. In work [5] discusses a similar approach to receive the microspheres as a result of fast cooling. In the study of the received microspheres was observed the formation of crystallites of titanium carbide. Processing was carried out in hexane, it can be assumed that as a result of contact of ablation products with vapors of titanium, a chemical reaction takes place, leading to the formation of the chemical bond of titanium and carbon. In the work [6] describes the interaction of laser radiation with the sample of titanium in the liquid medium, leading to the formation of the chemical bond.

Results, received in this work, can be useful for getting hard protective coatings of titanium products operating in aggressive environments, applications related to additive technologies due to the narrow granulometric composition of the resulting microspheres (1-3 μm), it's high sphericity, and smoothness of the formed surface. This method can also be used for the introduction of carbon to various metal compositions.

This study was performed as a part of the state task VlSU 1106/17 and a grant of the RFBR number16-42-330651.

References

1. *Barmina E. V. et al.* Generation of nanostructures on metals by laser ablation in liquids: new results // Quantum Electronics. 2010. V. 40. №. 11. P. 1012.

2. *Bozon-Verduraz F. et al.* Production of nanoparticles by laser-induced ablation of metals in liquids // Quantum Electronics. 2003. V. 33. №. 8. P. 714.

3. *Yang G. (ed.).* Laser ablation in liquids: principles and applications in the preparation of nanomaterials // CRC Press. 2012. 1192 p.

4. *Yang G.W.* Laser ablation in liquids: applications in the synthesis of nanocrystals // Progress in Materials Science. 2007. V. 52. №. 4. P. 648.

5. *Gordon E. B. et al.* Stability of micron-sized spheres formed by pulsed laser ablation of metals in superfluid helium and water // High Energy Chemistry. 2014. V. 48. №. 3. P. 206.

6. *Shafeev G. A.* Formation of nanoparticles under laser ablation of solids in liquids // Pan Stanford Publishing, Moscow. 2012. P. 327.

55. MODELING OF THE TUNNELING EFFECT IN GRANULATED METALLIC NANOSTRUCTURES

Istratov A.V, Kucherik A.O.

[1]Stoletov Vladimir State University, Vladimir, Russia
e-mail: aleksgreene@gmail.com

The achievements of nanotechnologies are based on fundamentally new scientific knowledge about the nature of the structure materials, and, consequently, fundamentally new technologies and design principles. As the particle size of a substance decreases, its physical and chemical properties can change substantially.

The characteristic dimensions of semiconductor structures at the modern micro- and nanoelectronics are 10^{-7}-10^{-8} m. Such a range of linear dimensions of elements is a fundamental physical barrier behind which all the properties of a solid body, including electrical conductivity, change drastically.

Dimensional effects in solids are a phenomenon observed when the geometric dimensions of an object are comparable with one or other of the lengths that determine the course of physical processes (for example, the mean free path of the charge carrier, the de Broglie wavelength, etc.). Depending on the size of the sample being examined, classical and quantum dimensional effects are distinguished, which can affect practically any properties of the substance. As a rule, for nanometer objects, where the particle sizes are comparable with the de Broglie wavelength of an electron, the quantum size effects determine such properties of matter as heat capacity, electrical conductivity, optical properties, and the like.

The most striking representative of quantum size effects is the tunnel effect, a phenomenon that plays an important role in nanotechnology. The tunnel effect is the microparticle overcoming a potential barrier between two conductors with a small cross-section. Using this effect, you can control the movement of individual electrons. According to the basic principles of quantum mechanics, microparticles (in particular electrons) can pass through an insulator (dielectric) from one conductor to another that is a tunnel transition.

One-electron devices are promising nanoelectronic devices based on the effect of discrete tunneling of individual electrons and providing ultra-low levels of energy consumption at ultra-low operating voltages. The first devices based on the tunnel effect: tunnel diodes, transistors, sensors, thermometers for measuring ultra-low temperatures, and finally, scanning tunneling microscopes, which laid the foundation for modern nanotechnology.

Since physical models of colored plastic balls don’t accurately reflect the real properties of nanoparticles, computer models are usually used in which one can set the real laws of quantum

physics. Based on a powerful mathematical apparatus, computer modeling plays a key role in the development of nanosystems.

To simulate a metallic granular nanostructure with a potential difference applied to the ends, a one-electron mathematical model was used in the form of a three-dimensional stochastic cellular automaton. The metal particles are represented as spheres located on the substrate at a distance S from each other. The electric potential is applied to the ends of the film, and the charge accumulates in the particles until its magnitude is sufficient for making the tunnel by the electrons to the subsequent particles in the direction of the positive potential: this flow of electrons moving in the same direction is electric amperage.

In the Euclidean metric, the distance between the pairs of neighboring particles in question is not the same, therefore, the type of neighborhood (common face, edge or vertex) must be taken into account. A cellular automaton, implemented in the Moore neighborhood in the three-dimensional case. The three-dimensional Moore neighborhood in the simulated space consists of 26 neighboring cubic cells in which the particles are located and which have a current particle with the cell: common faces (6 units) are neighbors of the first order; common ribs (8 units) - neighbors of the second order; common vertices (8 units). Obviously, the distance between the cell centers of the particle in question and the neighboring one, having a common edge, is $\sqrt{2}$ times larger than the distance between the centers of the cells that have a common face. If they have only a common vertex, then the distance between the centers of the given cells will increase by $\sqrt{3}$ times.

This model is implemented in several stages:

1. Modeling of film growth by the method of random deposition;

2. Imposition of periodic boundaries;

3. Transition to physical quantities of the grid dimension;

4. Calculation of the probability of the tunnel effect. The probability is calculated for each pair of particles: the current particle and its nearest neighbor are not more than the third order:

$$P_i = \begin{cases} \dfrac{\operatorname{arcctg}\left(8\cdot\left(\sqrt{n_i}\cdot(S+2\cdot R)-2\cdot R-\dfrac{U\cdot(x_i-x_0)}{\sqrt{n_i}}-\left(\dfrac{q_i-q_0}{e_0}\right)+0.5\right)\right)}{\pi}, \\ 0, \text{ if } \dfrac{q_i}{e_0}=1 \text{ or } \dfrac{q_0}{e_0}=-1 \end{cases}$$

where n_i - the order of the neighborhood of the i-th neighboring particles; S - the distance between the nearest particles along the axes; R - the radius of the deposited particles; U - the voltage at the ends of the simulated thinfilm, collinear with the X-axis; x_0 - the x-coordinate of the current particle center; x_i - the x-coordinate of the i-th neighboring particle center; q_0, q_i - the charges of the particles under consideration; e_0 - the charge of the electron.

The volt-ampere characteristics of the deposited films and the results of modeling the tunnel effect using the model of a stochastic cellular automaton are shown in Figure 1. The main quantitative morphological parameters characterizing the inhomogeneity of thin films: thickness and surface roughness film (standard deviation of the film thickness), particle size (diameter of spheres) and gap (the distance between the particles).

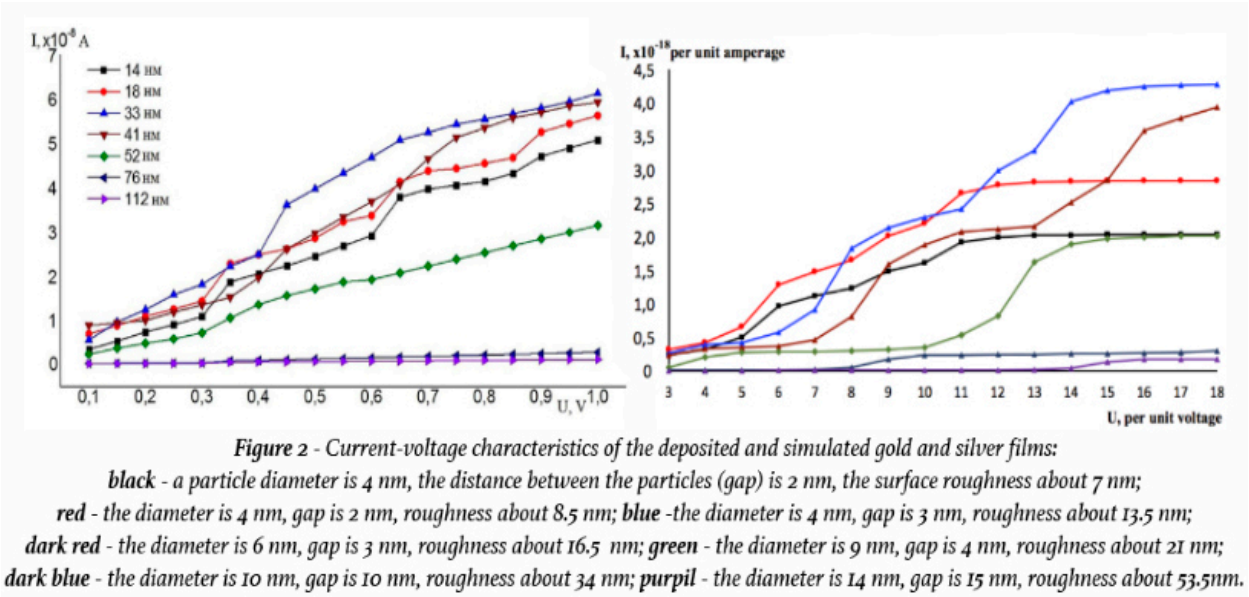

Figure 2 *- Current-voltage characteristics of the deposited and simulated gold and silver films:* ***black*** *- a particle diameter is 4 nm, the distance between the particles (gap) is 2 nm, the surface roughness about 7 nm;* ***red*** *- the diameter is 4 nm, gap is 2 nm, roughness about 8.5 nm;* ***blue*** *-the diameter is 4 nm, gap is 3 nm, roughness about 13.5 nm;* ***dark red*** *- the diameter is 6 nm, gap is 3 nm, roughness about 16.5 nm;* ***green*** *- the diameter is 9 nm, gap is 4 nm, roughness about 21 nm;* ***dark blue*** *- the diameter is 10 nm, gap is 10 nm, roughness about 34 nm;* ***purpil*** *- the diameter is 14 nm, gap is 15 nm, roughness about 53.5nm.*

The calculated volt-ampere characteristics are in qualitative agreement with the experimental one.

The discrepancy in numerical values can be explained by the geometry of the calculation of features: in the model, the particles lie strictly on each other (because of the need to use a computational grid) and a clearly defined interval S.

56. FRACTAL BIMETALLIC THIN FILMS OBTAINED BY DEPOSITION OF A SMALL DROPLETS OF COLLOIDAL NANOPARTICLES

[1]A.A. Antipov, [1]D.N. Bukharov, [1]S.M. Arakelyan, [1]S.V. Kutrovskaya, [1]A.O. Kucherik, [1]A.V. Osipov, [1]A.V.Istratov, [2]T.A. Vartanyan and [3]T.E. Itina

[1]Vladimir State University named after A. G. and N. G. Stoletovs, Vladimir, Russia
[2]ITMO University, St. Petersburg, Russia
[3]Université de Lyon, UJM-Saint-Etienne, CNRS, UMR5516, Laboratoire Hubert Curien, F-42023, Saint-Etienne, France
e-mail: aantipov@vlsu.ru

Abstract

The drop deposition of colloidal nanoparticles was performed from water-based colloidal solutions. The proposed procedure is based on the agglomeration of colloidal particles in laser-assisted evaporation processes. The evaporation process was resulted in the formation of clustered thin films on a glass substrate. In the experiments with bimetallic Au:Ag solutions, the clustered films are grown, the formation of the clustered films with the average height of 100 nm was achieved. Optical properties of the deposited structures were investigated experimentally. It is shown that the obtained films may become transparent and its properties are defined by its morphology.

Efficient synthesis of thin films with controlled optical properties is a key issue in modern photonics. In particular, possibilities of plasmon-assisted light manipulations by using nanoparticles and nanostructures currently attract considerable attention enabling various applications and opening new research area [1]. Drop deposition of the colloidal particles on glass substrate represents, furthermore, a promising solution to this challenging problem. The optical properties of these films are dominated by a set of plasmonic effects and strongly depend not only on the composition of the film but also on its morphology. In the case of the structures composed of nanoparticles, such parameters as spacing and ordering of nanoparticles define the local field enhancement to be observed either for distinct resonance frequencies or in a much wider spectral ranges [2, 3]. Furthermore, if nanoparticle spacing is comparable with its sizes, optical properties of the random structures can considerably differ from that of the ordered ones. In the case of the thin bimetallic films, one can expect even more complicated optical properties [4].

This study was supported by the Ministry of Education and Science of the Russian Federation (state projects nos. 16.5592.2017/VU and 3.4903.2017/VU), RFBR grant number 16-32-60067 mol_a_dk and the grant of president of Russian Federation by project MK-2842.2017.2 .

57. LIGHT PROPAGATION IN TUNABLE EXCITON-POLARITON HYPERBOLIC METAMATERIALS

S. Arakelian, A. Kucherik, S. Kutrovskaya, A. Osipov

Stoletovs Vladimir State University, Gorky Street 87, Vladimir 600000, Russia

kucherik@vlsu.ru

A clear physical model for the quantum states verification in nanocluster structures with jump/tunneling electroconductivity are under study in both theory and experiment. The accent is made on consideration of low-dimensional structures when the structural phase transitions occur and the tendency to high enhancement electroconductivity obtained.

The results give us an opportunity to establish a basis for new physical principles to create the functional elements for the optoelectronics and photonics in hybrid set-up (optics + electrophysics) by the nanocluster technology approach.

We focus our attention on the fact that physical properties of nanocluster/granular systems are very sensitive to the form, size and distance between their composing elements. The phenomena are very well known for any material in general, but to change these parameters and to carry out the stable conditions for ordinary solid state object we need both to put the object under extremal high pressure ($\gtrsim 10^6$ atm) and to work at low (liquid He) temperature range ($\lesssim$30K) [1]. In contrast, the nanocluster structures can be easily modified both in necessary direction and by controlled way in femto- nanophotonics experiments.

In our experiment we use the method of laser-assisted deposition metal particles from colloidal system [2]. For the deposition, we have used ytterbium fiber laser ($\lambda = 1.06$ μ) with a pulse duration of 100 ns, pulse repetition rate of 20 kHz, and a pulse energy up to 1mJ. The diameter of the laser beam in the focal plane was 50 microns. Nanoparticle array formation on the substrate surface was performed by the scanning laser beam along the same direction.

The Volt-Amper characteristics (VAC) of the thin film were measured using a four-probe scheme. The electrical transport properties in analogy with tunnel and quantum correlated states are considered; namely the tunneling/thermal activation effects observed.

The reported study was also supported by the Ministry of Education and Science of the Russian Federation (state project no.16.1123.2017/PCh), RFBR grant 16-42-330461 r_a, President grant for young scientist MK-2842.2017.2.

References

1. Landau L.D., Lifshitz E.M. *Theoretical physics electrodynamics of continuous media*, Vol V, VIII, 2nd Edition, Nauka, Moscow, 1982.

2. Arakelyan, S.M., Veiko, V.P., Kutrovskaya, S.V., Kucherik, A.O., Osipov, A.V., Vartanyan, T.A., Itina, T.E., "Reliable and well-controlled synthesis of noble metal nanoparticles by continuous wave laser ablation in different liquids for deposition of thin films with variable optical properties," *Journal of Nanoparticle Research*, Vol 18, Article ID 155, 2016.

58. HARDWARE-SOFTWARE COMPLEX OF FEMTOSECOND LASER MICROMACHINING

R.V. Chkalov, K.S. Khorkov, D.A. Kochuev, V.G. Prokoshev, S.M. Arakelian

Department of Physics and Applied Mathematics,

Vladimir State University named after A. G. and N. G. Stoletovs

87 Gorky, Vladimir, 600000, Russia

E-mail: j.larenax@gmail.com

The modern experimental processes simultaneously involve a multitude of complex technical and information components, where, in addition to collecting a huge data stream, it is necessary to control various elements of the system according to various algorithms determined by the conditions and nature of the experiment. In connection with the foregoing, there arises the task of combining a set of disparate technical components of a laboratory bench under the operating of a single software, through interaction with which the operator can centrally control all components of the system.

In this paper considered an example of the creation of a control system for a femtosecond laser complex including a number of technical components: various radiation sources, motorized linear and rotary translators, high-speed cameras, measuring and executive modules. The composition of the complex is schematically shown in Figure.

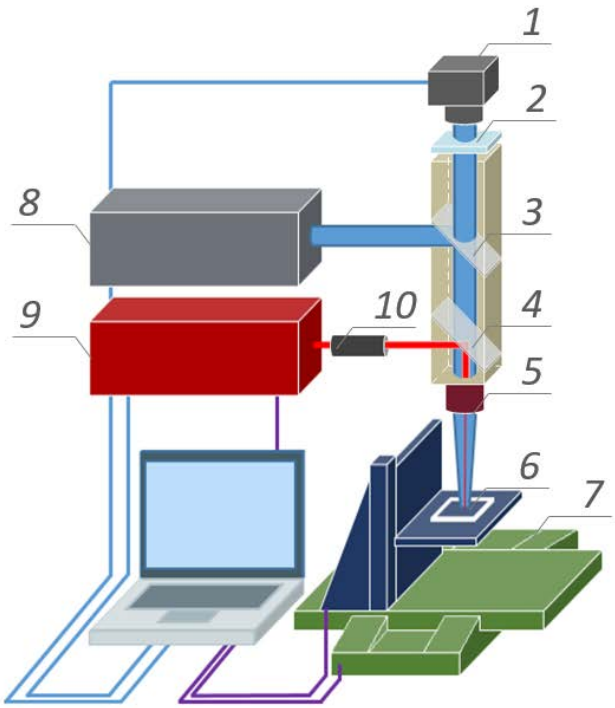

Fig. Experimental setup: 1 – high-speed camera, 2 – light filter, 3 – beam splitter, 4 – dichroic mirror, 5 – focusing lens, 6 – sample/cuvette, 7 – XYZ-coordinate stages system, 8 – backlight, 9 – femtosecond laser, 10 – variable attenuator

Since the task of implementing the control of the presented setup, provided the use of individual software for each complex's element, is extremely difficult and time-consuming, was developed a special software package [1], whose goal is to combine individual technical devices into a single organized and controlled system.

The development of individual software for the designed hardware laser complex made it possible to organize a single centralized control system for the technical components and units of the setup. Being supplemented with its own software, the complex allows to solve the problems of controlled micro- and nanostructuring of surfaces [2-3], the tasks of high-precision local deposition of colloidal complexes [4], to perform precision processing and modification of materials by means of femtosecond laser radiation [5], and also to conduct research of nonlinear processes [6], which makes the developed system a universal tool for solving a wide range of scientific problems.

This study was performed as a part of the state task VlSU 1106/17 and a grant of the RFBR number 16-32-00760 mol_a.

References

1. *Chkalov R., Lokhanov A., Khorkov K., et al.* Programmnoe obespechenie upravleniya kompleksom femtosekundoj lazernoj mikroobrabotki // Certificate of registration of the computer program No. 2017613881 of 04.03.2017.

2. *Abramov D., Arakelian S., Kochuev D., et al.* // Nanosystems: physics, chemistry, mathematics. 2016. V. 7(1). PP. 220-225.

3. *Khorkov K., Abramov D., Kochuev D., et al.* // Physics Procedia. 2016. V. 83. PP. 182-187.

4. *Kucherik, A., Antipov, A., Arakelian, S., et al.* // Proc. IEEE Conf. Laser Optics. Saint Petersburg, 2014.

5. *Chen F., Aldana J. R.* // Laser & Photonics Reviews. 2014. T. 8. No 2. PP. 251-275.

6. *Khorkov K.S., Kochuev D.A., Abramov D.V., et al.* // Proc. IEEE Conf. Laser Optics. Saint Petersburg, 2016. C. R8-52-R8-52..

59. THE METHOD OF SURFACE PLASMON-POLARITON PULSES GENERATION VIA COOPERATIVE EFFECTS IN WAVEGUIDE SPASER

A. V. Shesterikov[a], M.Yu. Gubin[a], M. G. Gladush[b], A. V. Prokhorov[a]

Vladimir State University named after Alexander and Nikolay Stoletovs, Vladimir, Russia
**SBOCVR "State center", Vladimir, Russia*
e-mail: freeod@mail.ru

[a]*Alexandr and Nikolai Stoletovs Vladimir State University, Vladimir, 600000 Russia,*

e-mail: avprokhorov33@mail.ru

[b]*Institute of Spectroscopy, Russian Academy of Sciences, Troitsk, Moscow, 142190 Russia*

We consider theoretically cooperative effects in dense ensemble of semiconductor quantum dots (QDs) placed in a dielectric layer near a metal surface. Generation of plasmon pulses is due to collective excitation decay process in the QDs, similar to the effect superradiance (SR) in optics [1]. However, in contrast SR, the energy of QD collective excitations is not converted into an optical pulse, but provides near-field pumping of surface plasmon polaritons (SPPs).

The dynamics of the SPP pulse formation is described by self-consistent equations for the polarization, the population of the QD and Rabi frequency of plasmon field, similar to the model localized spaser [2]. A characteristic parameter of the problem is the time of formation of quantum correlations t_R between the individual QDs near the metal surface. The main criterion for realization of the spaser effect is a ratio between the time t_R and the plasmon decay time t_p.

In this work, we carried out a numerical simulation for the point-source model of QDs ensemble and compared different regimes of SPP mode formation on the gold / dielectric interface. It was calculated values of QD size and concentration, for which collective effects dominate over relaxation ones and lead to the Sub-picosecond SPP pulse formation on the metal/dielectric interface.

We showed that, using the mean-field approximation for the case $t_R \ll t_p$, and taking into account the local field corrections in a dense QDs ensemble, the self-consistent problem can be reduced to the nonlinear pendulum equation with an additional dissipative harmonic term. This term corresponds to the coherent energy exchange between the SPPs and QDs and can lead to the deformation of SPP profile.

Also, we carried out a numerical simulation of the SPP pulse propagation in 1D waveguide spaser. Significant increasing of the SPP pulse duration and significant broadening of SPP spectrum, due to local field nonlinearity, were demonstrated [3].

This work was supported by Russian Foundation for Basic Research Grant Nos. 17-42-330001 and the Ministry of Education and Science of the Russian Federation in the framework of the state task VlSU 2017 in the field of scientific research.

1. N. Skribanowitz, I.P. Hermann, J.C. MacGillivray, and M.S. Feld, “Observation of Dicke superradiance in optically pumped hf gas,”Phys. Rev. Lett. **30**, 309 (1973).
2. M.I. Stockman, “The spaser as a nanoscale quantum generator and ultrafast amplifier,” J. Opt. **12**, 024004 (2010).
3. A. V. Shesterikov, M. Yu. Gubin, M. G. Gladush, and A. V. Prokhorov “Formation of Plasmon Pulses in the Cooperative Decay of Excitons of Quantum Dots Near a Metal Surface”, JETP, 124, 18 (2017)

CONFERENCE INFORMATION AND CONCLUSION

ORGANIZERS

Stoletovs Vladimir State University, Vladimir, Russia

Institute of laser physics SB RAS, Novosibirsk, Russia

International Laser Center of M.V.Lomonosov Moscow State University, Moscow, Russia

SUPPORTED BY

Ministry of Education and Science of the Russian Federation

Russian Foundation for Basic Research

CONFERENCE CHAIRMAN

Bagaev Sergey - academician, President of the Institute of Laser Physics SB RAS, Novosibirsk

CHAIRMAN OF THE ORGANIZING COMMITTEE

Saralidze Anzor - Rector of Stoletovs Vladimir State University

Program Committee

Arakelian Sergey – Head of the Department of Physics and Applied Mathematics Vladimir State University, Dr.Sc., Prof, Chairman.

Kucherik Alexey – leading researcher of the Department of Physics and Applied Mathematics Vladimir State University, PhD, Scientific Secretary.

Tigran Vartanyan – Chief Researcher, University ITMO, Dr.Sc., Prof.

Veiko Vadim – Head of the Department of laser technology and laser technology ITMO University, Dr.Sc., Prof.

Garnov Sergey – Deputy Director of GPI RAS on scientific work, corresponding member of RAS, Dr.Sc., Prof.

Zadkov Viktor – Director of the Institute of Spectroscopy, RAS, Dr.Sc., Prof.

Kavokin Alexey – Chair of Nanophysics and Photonics, University of Southampton, Ph.D., Prof.

Makarov Vladimir – Head of the Department of General Physics and Wave Processes, Director of the ILC MSU. Dr.Sc., Prof.

Ryabtsev Igor – Head of the Laboratory of nonlinear resonant processes and laser diagnostics ISP SB RAS, corresponding member of RAS, Dr.Sc., Prof.

Taichenachev Alexey – Director ILP SB RAS,corresponding member of RAS, Dr.Sc., Prof.

Shkurinov Alexander – prof. Department of General Physics and Wave Processes MSU., Dr.Sc., Prof.

ORGANIZING COMMITTEE CONTACT ADDRESS

Vladimir State University

Gorky str., 87, Vladimir 600000, Russia

Tel./Fax: (4922)477796,

Fax: (4922)333369

e-mail: **laser@vlsu.ru**, **kucherik@vlsu.ru**

THE GOAL OF THE WORKSHOP

Getting together of young scientists (Master students, PhD students, postdocs) and leading researchersfor a joint discussion of actual research problems of modern fundamental and applied physics, modalities of training by research.

MAIN TOPICS OF THE CONFERENCE AND THE WORKSHOP

• The methods of synthesis and diagnostics of nanomaterials and nanostructures

Co-chairmen − Prof. T.Vartanyan, Prof. O.Karban'

• Nonlinear optics and spectroscopy

Chairman−Prof. V. Zadkov

• Quantum and atomic optics

Chairman − Prof. A. Taichenachev

• Laser and Plasma Nanotechnologies

Chairman − Prof. S.Arakelian

• New carbon materials and its application

Chairman–Dr. A. Kucherik

• Terahertz radiation sources and its application

Chairman −Prof. A. Shkurinov

• Nanophotonics and metamaterials

Chairman − Prof. A. Kavokin

LIST OF CONFIRMED INVITED AND PLENARY SPEAKERS

Alexey Kavokin (University of Southampton, UK),

Sven Hoefling (University of Wuerzburg, Germany),

Alexey Taichenachev (ILP RAS, Russia),

Ricardo Valentini (University of Tuscia, Italy),

Pavlos Savidis (FORTH, Greece),

Natalya Berloff (University of Cambridge, UK),

Yuri Kulchin (IASP SB RAS, Russia),

Giuseppe Eramo (MIFP, Italy),

Tien-Chang Lu (National Chiao Tung University, Taiwan).

Central part of Vladimir

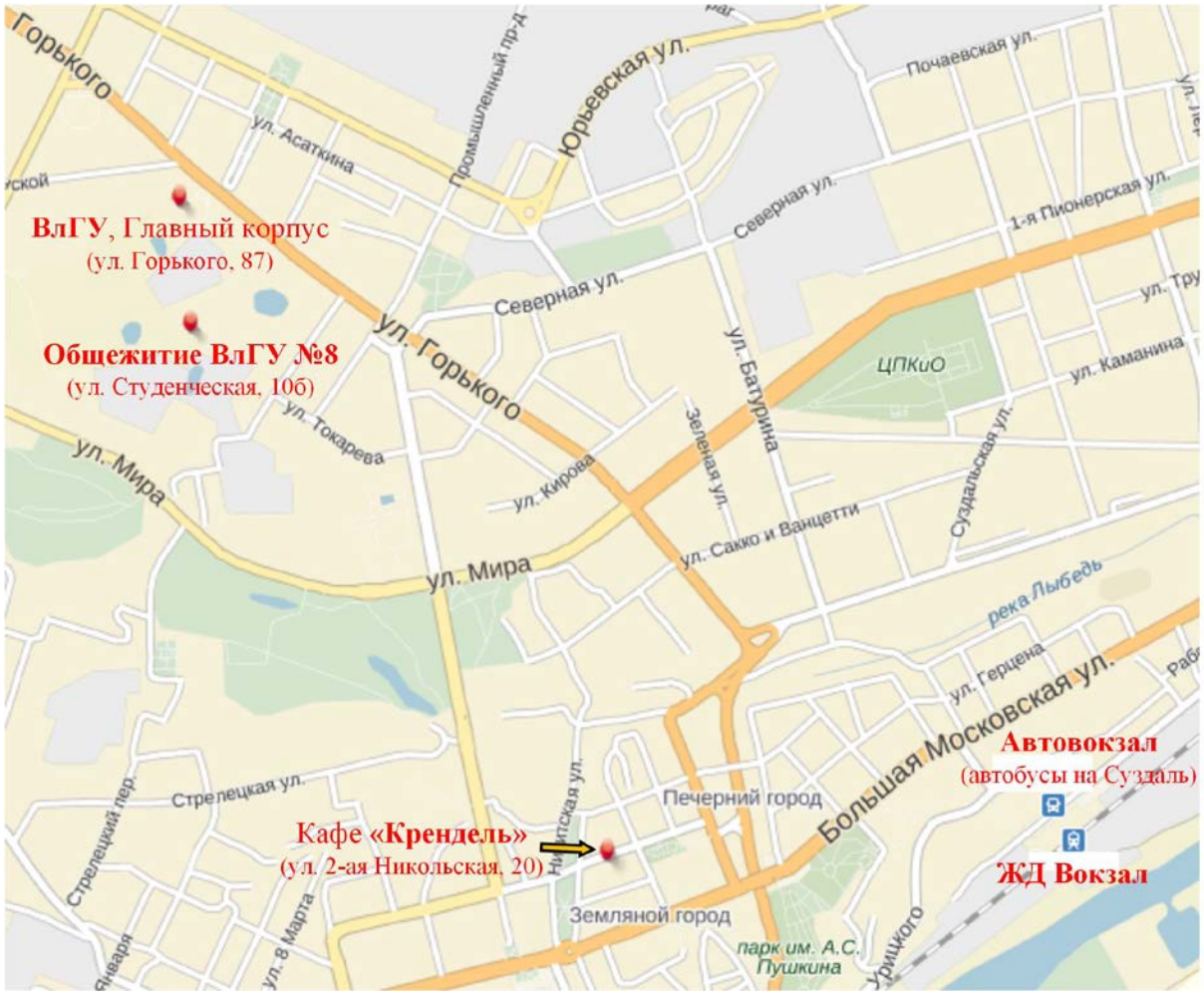

Suzdal

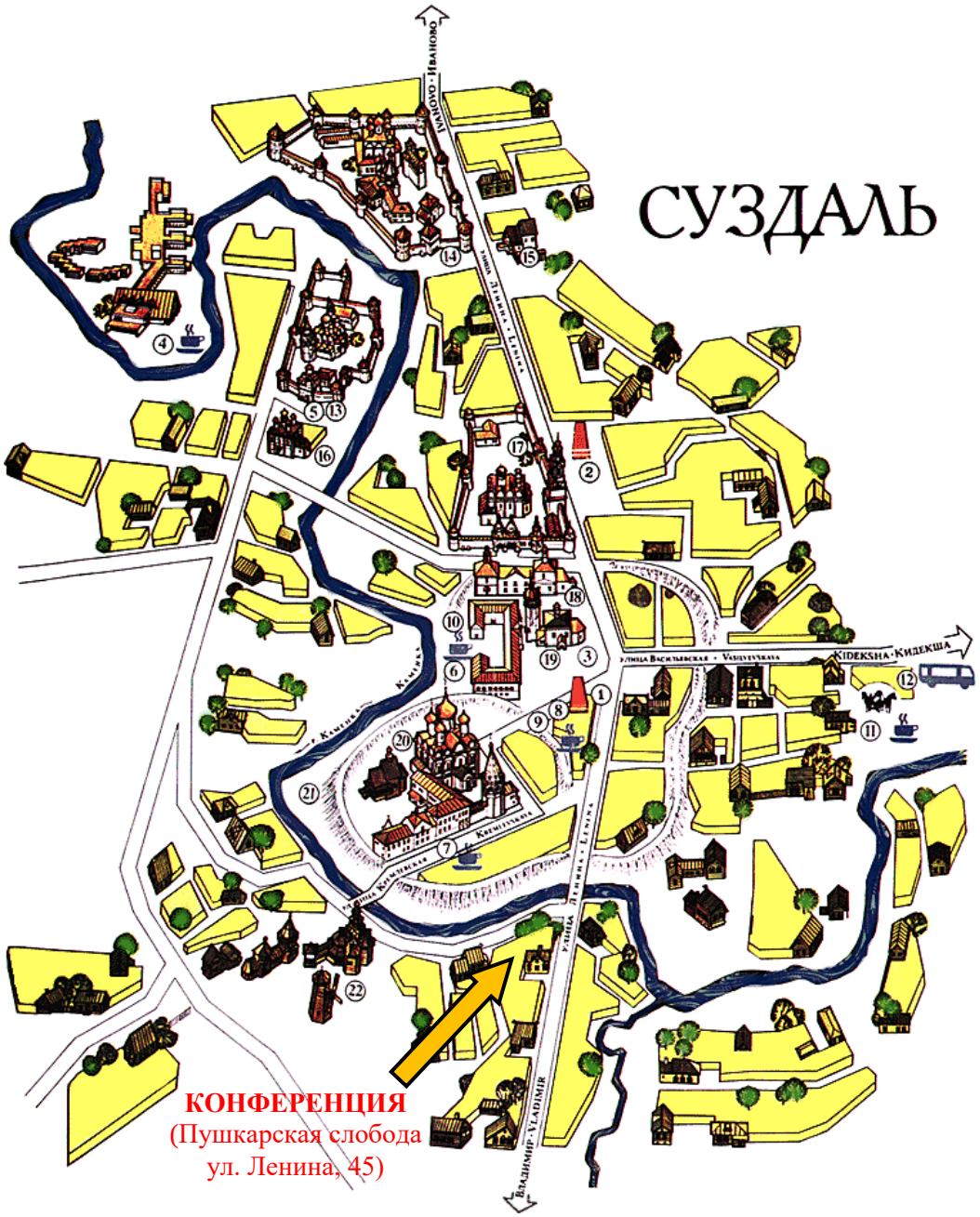

2. Suzdal City Council, Lenin monument
3. Monument to those fallen in World War II
4. Suzdal Tourist Centre. Hotel, motel, restaurant
5. Hotel on the grounds of the former Convent of the Intercession. The former convent refectory houses the restaurant Trapeznaya
6. Restaurant Gostiny Dvor
7. Restaurant Trapeznaya in Suzdal Kremlin
8. Restaurant Pogrebok (cellar)
9. Souvenirs' store Suzdalskaya Lavka
10. Arcade of shops (19th century)
11. Coachman's Inn
12. Bus station
13. The Convent of the Intercession (16th-18th cent.) Expositions: "From the History of the Convent", "Articles of Needlework", "Interior of the 17th-century Chancellor's House"
14. The Spaso-Yevfimievsky Monastery (16th-17th cent.) Museum of the Amateur Works of Art of the Peoples of the Russian Federation. Exposition: Gold Treasure Trove
15. The 17th-century townsman' house. The Interiors of Living Home Exposition.
16. The Church of St Peter and St Paul (17th century) Wood Painting Exposition
17. The Monastery of the Deposition of the Robe (16th-19th cent.)
18. The Church of St Nicholas and the Holy Cross (18th century). Peasant Clothing Exhibition
19. The Church of the Resurrection (18th century) Exposition: Folk Wood Carving
20. Suzdal Kremlin (13th-18th cent.). Expositions: "Leninist Policy of Protecting the Monuments of History and Culture", "Early Russian Painting", "The Cross Chamber Interior"
21. The earthen rampart surrounding the Kremlin (12th cent.)
22. The open-air Museum of Wooden Architecture and Peasants' Everyday Life.

CONCLUSION

Считать 6-ую международную конференцию/школу-семинар "Современные нанотехнологии и нанофотоника для науки и производства" состоявшейся, удовлетворяющей вопросам современных нанотехнологий и лазерной физике и запланировать проведение следующей конференцию на 2018г.

Научное издание

СОВРЕМЕННЫЕ НАНОТЕХНОЛОГИИ И НАНОФОТОНИКА ДЛЯ НАУКИ И ПРОИЗВОДСТВА

Материалы 6-й Международной конференции

9 – 13 ноября 2017 г.,
г. Владимир – г. Суздаль

Системные требования: Intel, AMD от 1,3 ГГц; Windows XP/Vista/7/8/10; Adobe Reader; CD-ROM; 6,5 Мб; Загл. с титула экрана.

Материалы представлены в авторской редакции

За содержание статей, точность приведенных фактов и цитирование несут ответственность авторы публикаций

Тираж 10 экз.

Владимирский государственный университет имени Александра Григорьевича и Николая Григорьевича Столетовых
Изд-во ВлГУ
rio.vlgu@yandex.ru
Кафедра физики и прикладной математики
laser@vlsu.ru